

b147 49014
copy 1

U.O.V.S. BIBLIOTHEEK

HIERDIE EKSEMPLAAR MAG ONDER
GEEN OMSTANDIGHEDEN UIT DIE
BIBLIOTHEEK VERWYDER WORD NIE

University Free State



34300002085748

Universiteit Vrystaat

**Synthesis, electrochemical and spectroscopic studies of
multidodecylated liquid crystalline phthalocyanine-
ferrocenylethoxide conjugates for biomedical applications**

A thesis submitted in fulfilment of the requirements for the degree

MAGISTER SCIENTIAE

in the

DEPARTMENT OF CHEMISTRY
FACULTY OF SCIENCE

at the

UNIVERSITY OF THE FREE STATE

by

WADE LUKE DAVIS

Supervisor: Prof. J.C. Swarts

February 2003

Universiteit van die
Oranje-Vrystaat
BLOEMFONTEIN

19 FEB 2004

UOVS SASOL BIBLIOTHEEK

Contents

Abstract	i
Opsomming	ii
List of abbreviations	iii
List of figures	iv
List of schemes	ix
List of tables	xi
Acknowledgements	xiii
CHAPTER 1	
INTRODUCTION AND AIMS	2
CHAPTER 2	
LITERATURE SURVEY	
2.1 History and structural determination	7
2.2 Applications of phthalocyanines	8
2.2.1 General	8
2.2.2 Photodynamic therapy (PDT)	8
2.2.2.1 Introduction	8
2.2.2.2 Mechanism of photosensitization	9
2.2.2.3 Porphyrins as photosensitizers in PDT	10
2.2.2.4 Phthalocyanines as photosensitizers in PDT	12
2.3 Synthesis of unsubstituted phthalocyanines	15
2.3.1 Metal-free phthalocyanine (2HPc)	15
2.3.2 Metallated phthalocyanines (MPc)	16
2.3.3 Mechanism of phthalocyanine formation	17
2.4 Synthesis of substituted phthalocyanines	18
2.4.1 Tetra-substituted phthalocyanines	19

2.4.2	Octa-substituted phthalocyanines	20
2.4.3	The synthesis of 3,6-disubstituted phthalonitriles	22
2.4.4	Synthesis of unsymmetrically substituted phthalocyanines	24
2.4.4.1	<i>The statistical condensation of two different phthalonitriles</i>	24
2.4.4.2	<i>Ring expansion of subphthalocyanines (SubPc)</i>	26
2.4.4.3	<i>Synthesis on a polymeric support</i>	28
2.5	Ferrocene compounds	30
2.5.1	Introduction	30
2.5.2	Ferrocene compounds as chemotherapeutic drugs	31
2.5.3	Synthesis of ferrocenyl derivatives	32
2.5.4	Synthesis of ferrocenyl-phthalocyanine conjugates	33
2.6	Electrochemical properties of ferrocene and phthalocyanine derivatives	34
2.6.1	Electrochemistry of ferrocene and its derivatives	34
2.6.2	Electrochemistry of phthalocyanines	36
2.6.3	Electrochemistry of ferrocene-phthalocyanine conjugates	37
2.7	UV-Visible spectroscopy of phthalocyanines	39
2.8	Phthalocyanines as discotic liquid crystals	42
2.8.1	General aspects of liquid crystals	42
2.8.1.1	<i>The influence of the number and type of flexible side-chains on mesophase behaviour</i>	46
2.8.1.2	<i>The influence of side-chain length on mesophase behaviour</i>	47
2.8.1.3	<i>The effects of the linking group and site of substitution on mesophase behaviour</i>	48
2.8.1.4	<i>The influence of the central metal ion on mesophase behaviour</i>	49
2.8.1.5	<i>The influence of side-chain branching on mesophase behaviour</i>	50
2.8.1.6	<i>The influence of unsymmetrical substitution on mesophase behaviour</i>	50
2.8.2	Thin films of phthalocyanines	52

CHAPTER 3

RESULTS AND DISCUSSION

3.1	Introduction	61
3.2	Synthesis of substituted phthalonitriles	61
3.2.1	Synthesis of 3,6-bis(dodecyl)phthalonitrile, (79)	62
3.2.1.1	<i>2,5-Bis(dodecyl)thiophene, (76)</i>	62
3.2.1.2	<i>2,5-Bis(dodecyl)thiophene-1,1-dioxide, (77)</i>	63
3.2.1.3	<i>3,6-Bis(dodecyl)phthalonitrile, (79)</i>	65
3.2.2	Synthesis of 4-(2'-ferrocenylethoxy)phthalonitrile, (81)	66
3.2.3	Synthesis of 2-ferrocenylethanol, (80)	67
3.3	Synthesis of substituted phthalocyanines	70
3.3.1	1,4,8,11,15,18,22,25-Oktakis(dodecyl)phthalocyanines, (83) and (84)	70
3.3.2	2,9,16,23-Tetrakis(2'-ferrocenylethoxy)phthalocyanine, (85)	72
3.3.3	Synthesis of ferrocene-phthalocyanine conjugates	73
3.4	Electrochemistry	81
3.4.1	Cyclic voltammetry of ferrocenyl derivatives	81
3.4.1.1	<i>Relationships between E^o and group 1H NMR peak positions (ppm)</i>	91
3.4.1.2	<i>Relationships between E^o and group electronegativities</i>	92
3.4.2	The cyclic voltammetry of phthalocyanine derivatives	97
3.4.2.1	<i>Cyclic voltammetry of a range of octa-alkylated metal-free and zinc-containing phthalocyanines</i>	97
3.4.2.2	<i>Cyclic voltammetry of ferrocenyl-phthalocyanine conjugates</i>	108
3.5	UV/VIS spectroscopy of selected phthalocyanine derivatives	112
3.6	Liquid crystalline properties of phthalocyanine derivatives	120
3.7	Visible region spectroscopy of spin-coated thin films of selected phthalocyanines	130

CHAPTER 4

EXPERIMENTAL

4	Equipment and chemicals	137
4.1	Chemicals	137
4.2	Techniques and apparatus	137
4.2.1	Spectroscopy	137
4.2.2	Electrochemistry	137
4.2.3	Differential scanning calorimetry (DSC)	138
4.2.4	Variable temperature microscope studies	138
4.2.5	Thin Film preparations	138
4.2.6	Microscope glass slide cleaning	138
4.3	Synthesis of 3,6-bis(dodecyl)phthalonitrile, (79)	139
4.3.1	2,5-Bis(dodecyl)thiophene, (76)	139
4.3.2	2,5-Bis(dodecyl)thiophene-1,1-dioxide, (77)	140
4.3.3	3,6-Bis(dodecyl)phthalonitrile, (79)	141
4.4	Synthesis of 4-(2'-ferrocenylethoxy)phthalonitrile, (81)	142
4.4.1	Dimethylaminomethylferrocene, (61)	142
4.4.2	<i>N,N</i> -Dimethylaminomethylferrocene methiodide, (62)	142
4.4.3	Ferrocenylacetonitrile, (63)	143
4.4.4	Ferrocenylacetic acid, (64)	143
4.4.5	2-Ferrocenylethanol, (80)	143
4.4.6	4-(2'-Ferrocenylethoxy)phthalonitrile, (81)	144
4.5	Synthesis of substituted phthalocyanines	144
4.5.1	1,4,8,11,15,18,22,25-Oktakis(dodecyl)phthalocyanine, (83)	144
4.5.2	2,9,16,23-Tetrakis(2'-ferrocenylethoxy)phthalocyanine, (85)	145
4.5.3	Statistical condensation of 3,6-bis(dodecyl)phthalonitrile and 4-(2'-ferrocenylethoxy)phthalonitrile (3:1 mole ratio) with lithium in pentanol	145

4.5.4	Statistical condensation of 3,6-bis(dodecyl)phthalonitrile and 4-(2'-ferrocenyl-ethoxy)phthalonitrile (9:1 mole ratio) with lithium in pentanol	147
4.5.5	Statistical condensation of 3,6-bis(dodecyl)phthalonitrile and 4-(2'-ferrocenyl-ethoxy)phthalonitrile (3:1 mole ratio) with zinc acetate dihydrate in dimethylaminoethanol	148
4.5.6	Complexation of Zn^{2+} with metal-free phthalocyanines	149

CHAPTER 5

CONCLUSIONS AND FUTURE PERSPECTIVES	152
--	------------

^1H NMR spectra

MALDI-tof spectra

DSC scans

Variable temperature UV/VIS spectra

ABSTRACT

This thesis is concerned with the synthesis and characterisation of some ferrocenyl and phthalocyanine derivatives. Symmetrically dodecylated phthalocyanines were obtained by the cyclisation of 3,6-bis(dodecyl)phthalonitrile. Unsymmetrically dodecyl-phthalocyanine-ferrocenylethoxide conjugates were obtained by the statistical condensation of 3,6-bis(dodecyl)-phthalonitrile and 4-(2'-ferrocenylethoxy)phthalonitrile. The anchoring of the ferrocenyl fragment, which itself is an antineoplastic entity, onto a phthalocyanine was accomplished utilising an ether bond.

The electrochemical behaviour of the ferrocenyl and selected phthalocyanine derivatives is reported. Most of the ferrocenyl compounds undergo a one-electron reversible process. Four ring-based electron transfer processes for the metal-free phthalocyanines were observed, whereas the ferrocenyl-phthalocyanine conjugate showed an additional, fifth, redox couple associated with the ferrocenyl moiety.

UV/VIS spectroscopy of the non-peripherally dodecyl substituted phthalocyanines showed a red shift in absorption Q_{\max} -band, which holds some advantages for irradiation with low-energy diode lasers during photodynamic cancer therapy. The new phthalocyanines also obeyed the Beer-Lambert law for the concentration range 78-163 μM (Q -band data) in THF, thus showing no aggregation.

The new symmetrical octadodecylated phthalocyanines as well as the hexadodecyl-phthalocyanine-ferrocenylethoxide conjugates exhibited liquid crystalline mesophase behaviour, which was studied using polarised light optical microscopy and differential scanning calorimetry. The zinc-containing ferrocenyl-phthalocyanine conjugate displayed mesophase behaviour over a larger temperature range (30.9-269.9°C) than the metal-free conjugate (30.4-185.3°C). Variable temperature UV/VIS spectra of thin films (*ca.* 1000 Å thick) of the phthalocyanine derivatives cast on glass is also reported for each mesophase.

Keywords: Ferrocene, phthalocyanine, dodecyl, electrochemistry, photodynamic cancer therapy, aggregation, mesophase, thin films.

OPSOMMING

Hierdie tesis behels die sintese en karakterisering van sekere ferroseen-en ftalosianienderivate. Simmetries dodesielgesubstitueerde ftalosianine is verkry deur die siklisering van 3,6-didodesielftalonitriël. Onsimmetriese dodesiel-ftalosianien-ferrosenietoksiedkonjugate is verkry deur die statistiese kondensasie van 3,6-didodesielftalonitriël en 4-(2'-ferrosenietoksie)ftalonitriël. Die koppeling van 'n ferrosenielfragment, wat self 'n neoplastiese fragment is, aan 'n ftalosianien is bereik deur van 'n eterbinding gebruik te maak.

Die elektrochemiese gedrag van die ferroseniel-en geselekteerde ftalosianienderivate is ook gerapporteer. Meeste van die ferroseenbevattende verbindings ondergaan 'n een-elektron omkeerbare proses. Vier ringgebaseerde elektronoordragprosesse vir die metaalvrye ftalosianien is waargeneem, terwyl die ferroseniel-ftalosianienkonjugate 'n addisionele, vyfde redokskoppel vertoon wat geassosieer word met die ferrosenielfragment.

UV/VIS spektroskopie van die nie-periferiese dodesielgesubstitueerde ftalosianiene het 'n verskuiwing na rooi in die absorpsie van die Q_{maks} -band getoon. Dit hou sekere voordele in vir die bestraling met lae-energie diode lasers tydens fotodinamiese kankerterapie. Die nuwe ftalosianiene gehoorsaam ook die Beer-Lambert wet vir die konsentrasiegebied 78-163 μM (Q -band data) in THF en vertoon dus geen aggregasie nie.

Die nuwe dodesielgesubstitueerde ftalosianiene asook die heksadodesiel-ftalosianien-ferrosenietoksiedkonjugate vertoon vloeikristal-mesofase gedrag wat deur middel van gepolariseerde lig optiese mikroskopie en differensiële skanderingskalorimetrie bestudeer is. Die sinkbevattende ferroseniel-ftalosianienkonjugaat vertoon mesofase gedrag oor 'n wyer temperatuurgebied (30.9-269.9°C) as die metaalvrye konjugaat (30.4-185.3°C). Veranderlike temperatuur UV/VIS spektrums van die ftalosianienderivate as dun films (*ca.* 1000 Å dik) op glas is ook gerapporteer vir elke mesofase.

Sleutelwoorde: Ferroseen, ftalosianien, dodesiel, elektrochemie, fotodinamiese kankerterapie, aggregasie, mesofase, dun films.

List of abbreviations

Å	angstrom units (10^{-10}m)
^1H NMR	proton nuclear magnetic resonance
b.p.	boiling point
cm^{-1}	wave number
CV	cyclic voltammogram
DBN	1,5-diazabicyclo[4.3.0]non-5-ene
DBU	1,8-diazabicyclo[5.4.0]undec-7-ene
DCE	dichloroethane
DCM	dichloromethane
DSC	differential scanning calorimetry
E_{pa}	peak anodic potential
E_{pc}	peak cathodic potential
ΔE_{p}	difference in peak anodic and peak cathodic potentials
$E^{\circ'}$	formal reduction potential
Fc	ferrocene
Fc^+	ferrocenium
HpD	hematoporphyrin derivative
i_{pa}	peak anodic current
i_{pc}	peak cathodic current
IR	infrared
m.p.	melting point
MPc	metallated phthalocyanine
Pc	phthalocyanine
PDT	photodynamic therapy
ppm	parts per million
SCE	saturated calomel electrode
$(^n\text{Bu})_4^+\text{NPF}_6^-$	tetra- <i>n</i> -butylammonium hexafluorophosphate
THF	tetrahydrofuran
UV/VIS	ultraviolet-visible
ε	molar extinction coefficient
λ	wavelength
χ_{R}	group electronegativity of group R

List of figures

Figure 2.1: Comparison of the phthalocyanine, (1) and porphyrin, (2) structures. The numbering system and substitution positions on phthalocyanines are also shown.	7
Figure 2.2: Structure of Photofrin®, (3) ranging from two to nine porphyrin units linked <i>via</i> ether bonds.	11
Figure 2.3: Disulphonated aluminium phthalocyanine, (4) and a tetrahydroxy ZnPc, (5).	13
Figure 2.4: Non-peripherally octadecyl substituted ZnPc, (6) and Silicon phthalocyanine, (7) designated as Pc-4.	14
Figure 2.5: Platinum-containing zinc phthalocyanine, (8).	15
Figure 2.6: The eclipsed and staggered conformations of ferrocene, (58).	30
Figure 2.7: Ferrocene-containing phthalocyanines, (66), (67) and (68).	33
Figure 2.8: Polymer bound ferrocenyl-phthalocyanine, (69) and ferrocenyl-Pc, (70).	34
Figure 2.9: Electron withdrawing (71) and electron donating (72) substituents on the ferrocene group.	35
Figure 2.10: CV of (71) in acetonitrile containing 0.1 M tetra- <i>n</i> -butylammonium hexafluorophosphate as supporting electrolyte at 25°C on a Pt working electrode, recorded at a scan rate of 50 mVs ⁻¹	35
Figure 2.11: Cyclic voltammogram of zinc(II)tertraneopentoxypthalocyanine in 1,2-dichlorobenzene containing 0.2 M tetrabutylammonium perchlorate (TBAP) <i>vs.</i> Ag/AgCl.	36
Figure 2.12: Redox processes associated with ring-based electron transfer couples and average formal reduction potentials, $E^{\circ'}$ for (C ₁₀ H ₂₁) ₈ -MPc (M = 2H or Zn) at a scan rate of 50 mV s ⁻¹ <i>vs</i> Ag/Ag ⁺	37
Figure 2.13: Structure of metal-free peripherally substituted tetraferrocenylphthalocyanine, (Fc) ₄ -2HPc, (73).	37
Figure 2.14: Cyclic voltammetry of (Fc) ₄ -2HPc, (73) in DCE containing 0.1 M (nBu) ₄ ⁺ NPF ₆ as supporting electrolyte on a platinum wire electrode at a scan rate of 200mV s ⁻¹	38
Figure 2.15: The visible absorption spectra of solutions of (a) 2HPc and (b) CuPc.	39
Figure 2.16: UV-Vis-near-IR absorption spectra of CoTAP, CoPc, CoNc and CoAc.	41
Figure 2.17: Schematic representation of the possible melting processes of mesogenic discotic materials.	42
Figure 2.18: Classification of mesophases.	43
Figure 2.19: Discotic mesophases: (a) – (e) columnar, (a) hexagonal (D _h), (b) + (c) rectangular (D _r), (d) oblique (D _{ob}), (e) rectangular face centered and (f) discotic nematic (N _D).	44
Figure 2.20: Left: (C ₉ H ₁₉) ₈ -ZnPc at the transition temperature between the two D _{hd} mesophases. The fan texture (of the high temperature mesophase) is being overlaid by the	

needle texture (of the lower temperature mesophase). **Right:** $(C_{10}H_{21})_8\text{-ZnPc}$ at the transition temperature D_{hd} mesophase and the D_{rd} mesophase (mosaic texture).45

Figure 2.21: Representation of the molecular structure and packing of non-peripheral octahexyl substituted metal-free phthalocyanine, $(C_6H_{13})_8\text{-2HPc}$45

Figure 2.22: A plot of side-chain length versus clearing temperature ($^{\circ}\text{C}$) for four different homologous series of mesogenic phthalocyanines.47

Figure 2.23: The influence of the central metal ion on the clearing point of the non-peripheral $(C_n)_8\text{-MPc}$ homologous series.49

Figure 2.24: A: UV/VIS spectra of spin coated films of non-peripherally octaoctyl substituted metal-free phthalocyanine, $(C_8H_{17})_8\text{-2HPc}$ at temperatures which corresponds to different phases: (a) 50°C , (b) 90°C , (c) 145°C , and (d) 160°C . **B:** Profile showing change of absorbance at 714 nm during heating of a spin-coated film of $(C_8H_{17})_8\text{-2HPc}$, (a)-(d) as in **A**.53

Figure 3.1: ^1H NMR spectra of 2,5-bis(dodecyl)thiophene, (**76**) and 2,5-bis(dodecyl)thiophene-1,1-dioxide, (**77**) in CDCl_3 . The position of the protons on the thiophene ring is highlighted. The signal at ≈ 1.6 ppm is that of water in the sample.64

Figure 3.2: Infrared spectra (in KBr, except for (**76**) which was recorded between NaCl discs) with assignments and structures of (**76**), (**77**) and (**79**). A water peak due to moisture in KBr is observable at ca. 3450 cm^{-1}65

Figure 3.3: Infrared spectra (in KBr, except for (**80**) which was recorded between NaCl discs) with assignments and structures of 4-nitrophthalonitrile, (**52**) and ferrocenyl derivatives (**63**), (**64**), (**80**) and (**81**). A water peak due to moisture in KBr is observable at ca. 3450 cm^{-1}69

Figure 3.4: Structures of phthalocyanhines **ABAB**, (**88a**) and **AABB**, (**88b**).75

Figure 3.5: MALDI-tof spectra 19 and 20 of fraction 4 (a mixture of metal-free phthalocyanines **AABB** and/or **ABAB**, (**88**) and **ABBB**) and zinc phthalocyanine (**84**) (with a single H_2O molecule coordinated axially to the zinc metal) respectively.76

Figure 3.6: ^1H NMR spectra of the ferrocene-containing phthalonitrile precursor (**81**) and phthalocyanines (**86**) and (**87**) in CDCl_379

Figure 3.7: Ferrocenyl derivatives that were studied by means of cyclic voltammetry.81

Figure 3.8: Cyclic voltammograms of ferrocene (1 mmol dm^{-3}), (**58**) in acetonitrile at 25°C on a platinum working electrode, recorded at scan rates of 50 (smallest voltammogram), 100, 150, 200 and 250 mV s^{-1} containing 0.2 mol dm^{-3} $(^n\text{Bu})_4\text{-}^+\text{NPF}_6$ as supporting electrolyte.82

Figure 3.9: Cyclic voltammograms of (a) ferrocenylacetonitrile, (**63**), (b) ferrocene, (**58**) and (c) (**63**) (0.001 mol dm^{-3} in acetonitrile) in the presence of ferrocene as an internal marker at 25°C on a platinum working electrode, recorded at a scan rate of 50 mV s^{-1} containing 0.2 mol dm^{-3} $(^n\text{Bu})_4\text{-}^+\text{NPF}_6$ as supporting electrolyte. The broken (-----) line shows the expected but inaccurately estimated decay currents of peaks 1 and 3, which imply peak currents, will not be accurate.83

Figure 3.10: A: Cyclic voltammograms of ferrocene, (**58**) and its derivatives (**61**), (**62**), (**63**), (**64**) and (**89**) (1 mmol dm^{-3}) in acetonitrile at 25°C on a platinum working electrode, recorded at a scan rate of 50 mV s^{-1} containing 0.2 mol dm^{-3} $(^n\text{Bu})_4\text{-}^+\text{NPF}_6$ as supporting electrolyte. **B:**

Osteryoung Square wave voltammogram of ferrocenylmethanol, (**89**) under the same conditions as for its CV recorded at scan rates of 1 (smallest voltammogram), 5, 15 and 50 mV s^{-1}84

Figure 3.11: ^1H NMR spectra of the quaternary ammonium salt, (**62**) in CDCl_3 at 25°C (top) and 50°C (bottom).85

Figure 3.12: Two possible positions of the iodide anion in *N,N*-dimethylaminomethylferrocene methiodide.86

Figure 3.13: Cyclic voltammograms and structures of diferrocenylmethane (left), ferrocenoylmethylamine (centre) and 2-ferrocenylmethanol (right) in acetonitrile, recorded at a scan rate of 50 mV s^{-1}89

Figure 3.14: Relationship between the formal reduction potential, $E^{\circ'}$, of the ferrocenyl group and ^1H NMR signal position (in ppm) of the ferrocyl fragment in CDCl_3 , of FcCH_2R with $\text{R} = ^+\text{N}(\text{CH}_3)_3$, CN, OH, COOH, $\text{N}(\text{CH}_3)_2$, CH_3 and NH_292

Figure 3.15: Linear relationship between the C_5H_5 ^1H NMR signal position of FcCH_2R and group electronegativity, χ_{R} . Points indicated with \circ were taken as calibration marks, points indicated with \diamond were fitted to the calibration line. **B:** Linear relationship between formal reduction potential, $E^{\circ'}$, of the ferrocenyl group and group electronegativity, χ_{R} , of the R-group in FcCH_2R . $\text{R} = ^+\text{N}(\text{CH}_3)_3$, CN, OH, COOH, $\text{N}(\text{CH}_3)_2$, CH_3 and NH_293

Figure 3.16: Cyclic voltammograms of ferrocene, (**58**), ferrocene-containing alcohols, (**80**), (**89**), (**90**) and (**91**) and phthalonitrile (**81**) at 25°C on a platinum working electrode, recorded at a scan rate of 50 mV s^{-1} containing 0.2 mol dm^{-3} $(n\text{-Bu})_4^+\text{NPF}_6^-$ as supporting electrolyte.94

Figure 3.17: The range of octa-alkyl substituted metal-free and zinc-containing phthalocyanines that were studied by means of cyclic voltammetry.97

Figure 3.18: **Above:** Cyclic voltammogram of $(\text{C}_{11}\text{H}_{23})_8\text{-2HPc}$ (1 mmol dm^{-3}) in dichloromethane at 25°C with 0.2 mol dm^{-3} $(n\text{-Bu})_4^+\text{NPF}_6^-$ as supporting electrolyte, on a platinum working electrode, at scan rates of 50, 100, 150, 200 and 250 mVs^{-1} . Four ring-centered redox processes **I**, **II**, **III** and **IV** are observable. The wave labelled **Fc** is that of free ferrocene (1 mmol dm^{-3}) in dichloromethane at 25°C. **Bottom:** Cyclic voltammogram of $(\text{C}_{11}\text{H}_{23})_8\text{-2HPc}$ under the same conditions as for the top CV but in the presence of ferrocene as internal standard. The shape of wave **IV** became distorted compared to the upper CV. This demonstrates *inter alia* the extreme sensitivity of good CV's for these compounds to minor impurities on the surface of the electrode.98

Figure 3.19: Redox couples and average formal reduction potentials, $E^{\circ'}$ for $(\text{C}_{11}\text{H}_{23})_8\text{-MPc}$ ($\text{M} = 2\text{H}$ or Zn) vs Ag/Ag^+99

Figure 3.20: Encapsulation of the phthalocyanine core by the alkyl side chains for the C_7 - and C_{15} - derivatives.99

Figure 3.21: Cyclic voltammograms (CV's) of a series of octa-alkyl substituted 2HPc (1 mmol dm^{-3} in DCM at 25°C, unless otherwise stated, with 0.2 mol dm^{-3} $(n\text{-Bu})_4^+\text{NPF}_6^-$ as supporting electrolyte) on a platinum working electrode, recorded at a scan rate of 100 mV s^{-1} . Four ring-based centered redox processes **I**, **II**, **III** and **IV** were observed. The similarity in shape of CV's (**b**) and (**c**) shows that temperature and solvent changes do not alter the CV's of the studied compounds. DCM = dichloromethane, DCE = dichloroethane and $n\text{-Bu} = n\text{-butyl}$100

Figure 3.22: Above: Cyclic voltammogram of $(C_5H_{11})_8\text{-ZnPc}$ (1 mmol dm^{-3}) in dichloroethane at 70°C with 0.2 mol dm^{-3} $(^n\text{Bu})_4\text{-}^+\text{NPF}_6$ as supporting electrolyte on a platinum working electrode, recorded at scan rates of 50, 100, 150, 200 and 250 mV s^{-1} . Bottom: The redox wave of free ferrocene (1 mmol dm^{-3}) in dichloroethane at 70°C recorded at a scan rate of 100 mV s^{-1} . ($E^\circ = 0.231 \text{ V}$ and $\Delta E_p = 0.097$).104

Figure 3.23: Cyclic voltammograms of a series of octa-alkylated zinc phthalocyanines (1 mmol dm^{-3} in dichloroethane at 70°C with 0.2 mol dm^{-3} $(^n\text{Bu})_4\text{-}^+\text{NPF}_6$ as supporting electrolyte) on a platinum working electrode, recorded at a scan rate of 100 mV s^{-1} . Poor solubility and extensive aggregation destroys meaningful CV's for (a) $(C_1H_3)_8\text{-2HPc}$. Poorly defined waves I and II are the result of solvent reduction that commences at *ca.* -1.8 V105

Figure 3.24: Relationship between ΔE_p and length of the alkyl chain (n) on the phthalocyanine macrocycles of general formula $(C_nH_{2n+1})_8\text{-MPc}$, where $M = 2\text{H}$ (left) or Zn (right). ΔE_p values for complexes with $n = 4, 6, 8, 10$ and 18 are from reference 14.107

Figure 3.25: Metal-free and zinc-containing ferrocenyl-phthalocyanine conjugates (86) and (87) that were studied by means of cyclic voltammetry.109

Figure 3.26: Cyclic voltammograms (CV's) of 1 mmol dm^{-3} ferrocenyl-free phthalocyanines (83) and (84) and ferrocenyl-phthalocyanine conjugates (86) and (87) in DCM at 25°C and DCE at 70°C respectively, with 0.2 mol dm^{-3} $(^n\text{Bu})_4\text{-}^+\text{NPF}_6$ as supporting electrolyte on a platinum working electrode, at a scan rate of 150 mV s^{-1} . Four redox processes I, II, III and IV on the phthalocyanine ring system and a fifth redox process FcPc at the anchored ferrocenyl group can be identified. The CV of free ferrocene, (58) (at 100 mV s^{-1}) is also shown and is labelled Fc_{free} . DCM = dichloromethane and DCE = dichloroethane.110

Figure 3.27: Redox couples and average formal reduction potentials, E° for $(C_{12}H_{25})_6\text{-MPc-O-(CH}_2)_2\text{-Fc}$, with $M = 2\text{H}$, (86) or Zn , (87) vs Ag/Ag^+110

Figure 3.28: Structures of the metal-free and zinc-containing octakis(dodecyl)phthalocyanines and ferrocenyl-phthalocyanine conjugates studied by UV/VIS spectroscopy.113

Figure 3.29: UV/VIS absorbance spectra in THF at 25°C for the indicated metal-free and zinc-containing phthalocyanines possessing dodecyl and/or ferrocenylethoxide groups, recorded at a concentration of approximately $80 \mu\text{mol dm}^{-3}$114

Figure 3.30: Graph of absorption *versus* concentration for the indicated 2H- and Zn-containing phthalocyanines in THF for the Soret and Q-bands. The graphs show a linear relationship between absorbance and concentration, implying that aggregation is absent in the concentration range studied.116

Figure 3.31: Aggregation data for compounds $(C_nH_{2n+1})_8\text{-ZnPc}$, $n = 5$ to 12 expressed as the concentration of the sample at which the Beer-Lambert plot for the Q-band absorption deviates from linearity.117

Figure 3.32: Extinction coefficient, ϵ , (in $\text{dm}^3 \text{mol}^{-1} \text{cm}^{-1}$) as a function of wavelength, for the indicated 2H- and Zn-containing phthalocyanines in THF possessing dodecyl and/or ferrocenylethoxide groups. Note ϵ was determined using a 1 mm path length cell, and then converted to units of $\text{dm}^3 \text{mol}^{-1} \text{cm}^{-1}$ by multiplying with 10.118

Figure 3.33: Relationship between λ_{\max} and the number of ferrocenylethoxide groups in the peripheral positions of the phthalocyanine macrocycle for the indicated dodecylated and ferrocenylethoxide-phthalocyanine conjugates.119

Figure 3.34: Octadodecylated phthalocyanines (83), (84) and ferrocenyl-phthalocyanine conjugates (86), (87) that were investigated for their liquid crystalline properties using differential scanning calorimetry as well as polarized light optical microscopy.120


Figure 3.35: Phthalocyanines tend to stack or aggregate on top of each other in a columnar fashion. The columnar stacking of symmetrical phthalocyanines such as (83) and (84) should be near perfect as indicated in the columnar stacking A. The ferrocenyl group in the unsymmetrical phthalocyanines (86) and (87) should impose many flaws on a columnar stacked liquid crystal. This is schematically shown in B.  = Phthalocyanine macrocycle.123

Figure 3.36: Differential scanning calorimetry (DSC) traces of heat flow vs temperature (left) and variable temperature UV/VIS spectra of spin coated thin films (right) for **A:** metal-free, (83) and **B:** zinc-containing phthalocyanines, (84) respectively. Temperatures corresponding to different phases of the bulk material for (83): (a) 35°C, (b) 60°C, (c) 80°C and (d) 100°C and for (84): (a) 30°C, (b) 80°C, (c) 130°C, (d) 80°C and (e) 230°C. The heating and cooling rate for the DSC apparatus was 10°C/min.125

Figure 3.37: Differential scanning calorimetry (DSC) traces of heat flow vs temperature (left) and variable temperature UV/VIS spectra of spin coated thin films (right) for **A:** metal-free, (86) and **B:** zinc-containing ferrocenyl-phthalocyanines, (87) respectively. Temperatures corresponding to different phases of the bulk material for (86): (a) 26°C, (b) 75°C, (c) 150°C and (d) 200°C and for (87): (a) 25°C, (b) 70°C and (c) 280°C. The heating and cooling rate for the DSC apparatus was 10°C/min.126

Figure 3.38: **Left:** Photograph showing simultaneously the fan (D_1 , majority of graph) and needle (D_2 , next to the yellow spot, needles are bundled together in the form of fibres) texture for $(C_{12}H_{25})_8$ -2HPc, (83). **Right:** Photograph showing simultaneously the blue crystalline solid (K) and the green D_2 mesophase with a mosaic pattern.129

Figure 3.39: Variable temperature UV/VIS spectra of spin-coated films (*ca.* 1000 Å thick) of zinc-containing non-peripherally octadodecyl substituted phthalocyanine, (84) on a glass slide at temperatures which correspond to different phases of the bulk material: (a) 30°C, crystalline solid phase K, (b) 80°C, mesophase D_3 , (c) 130°C, mesophase D_2 , (d) 180°C, mesophase D_1 and (e) 230°C, isotropic liquid phase I.131

Figure 3.40: Absorbance/Temperature profiles showing phase transitions as a function of absorbance changes at 780 nm for a spin coated film of (83), left and at 714 nm for a spin coated film of (84), right. The heating and cooling rates were 5°C/min.133

Figure 3.41: Absorbance/Temperature profiles showing phase transitions as a function of absorbance changes at 701 nm for a spin coated film of (86), left and at 690 nm for a spin coated film of (87), right. The heating and cooling rates were 5°C/min.133

Figure 4.1: Cleaning of glass slides used for thin film preparations.139

List of schemes

Schemes 2.1: Possible photosensitization processes in PDT.	10
Schemes 2.2: Synthetic routes to 2HPc, (1) from phthalonitrile, (9) as precursor. <i>Reagents and conditions:</i> (i) Lithium, refluxing pentanol, followed by aqueous hydrolysis. (ii) Fuse with hydroquinone. (iii) Heat with 1,8-diazabicyclo[4.3.0]non-5-ene (DBN) in a melt or in pentanol solution. (iv) NH ₃ , refluxing methanol, sodium methoxide. (v) Reflux in high boiling point alcohol.	15
Schemes 2.3: Synthetic routes to MPc, (11). <i>Reagents and conditions:</i> (i) Heat in a high-boiling-point solvent (e.g. quinoline) with metal salt. (ii) Heat in a high-boiling-point solvent with urea and metal salt. (iii) Heat in ethanol with metal salt. (iv) -15 to -20°C in DMF with metal salt.	16
Schemes 2.4: Role of the alkoxide anion in phthalocyanine formation.	17
Schemes 2.5: Four structural isomers of tetra-substituted MPc obtained during the condensation of a mono-substituted phthalonitrile.	19
Schemes 2.6: General synthetic route for preparing non-peripheral tetra-alkoxide substituted phthalocyanines.	20
Schemes 2.7: Synthesis of peripheral symmetrically octa-substituted phthalocyanines, Y = O or S, DBU = 1,8-diazabicyclo-[5.4.0]undec-7-ene.	21
Schemes 2.8: Synthetic routes to non-peripheral octa-alkyl substituted phthalocyanines. <i>Reagents and conditions:</i> (i) Acetone, 0°C. (ii) Lithium bis(trimethylsilyl)amide, THF, -78°C, aqueous work-up. (iii) Lithium, refluxing pentanol, aqueous hydrolysis. (iv) 3-Chloroperbenzoic acid, DCM. (v) 200°C.	22
Schemes 2.9: Synthesis of 3,6-dialkylphthalonitriles <i>via</i> furan route. <i>Reagents and conditions:</i> (i) BuLi, RBr. (ii) Fumaronitrile. (iii) LiN(SiMe ₃) ₂ , THF, -78°C.	22
Scheme 2.10: Synthesis of 3,6-dialkylphthalonitriles <i>via</i> thiophene route. <i>Reagents and conditions:</i> (i) BuLi, RBr. (ii) <i>m</i> -chloroperoxybenzoic acid (<i>m</i> -CPBA) or NaBO ₃ or dimethyldioxirane. (iii) Fumaronitrile, CHCl ₃ , 150°C, 18 h. (iv) -SO ₂ , -H ₂	23
Scheme 2.11: Six different unsymmetrically substituted phthalocyanines AAAA, AAAB, ABAB, etc. obtained when two different substituted phthalonitriles A and B are cyclotetramerized.	25
Scheme 2.12: Synthesis of a mono-functional phthalocyanine, (41) <i>via</i> ring expansion of SubPc, (39).	26
Scheme 2.13: Fragmentation of a subphthalocyanine to form all possible phthalocyanines. ...	26
Scheme 2.14: Synthesis of an unsymmetrical ZnPc, <i>via</i> ring expansion of a SubPc.	27
Scheme 2.15: Synthesis of a water-soluble unsymmetrical substituted phthalocyanine.	28

Scheme 2.16: Synthesis of an unsymmetrical phthalocyanine on a polymer support. O ⁱ Pr = isopropoxy, TrCl = trityl chloride, (P) = polymer, 2-DMAE = 2-dimethylaminoethanol and DMAP = <i>p</i> - <i>N,N</i> -dimethylaminopyridine.	29
Scheme 2.17: Reversible electrochemistry of ferrocene, (58).	30
Scheme 2.18: The synthesis of some ferrocenium salts from ferrocene.	31
Scheme 2.19: Synthesis of <i>N,N</i> -dimethylaminomethylferrocene methiodide, (62).	32
Scheme 2.20: Synthesis of ferrocenylacetonitrile, (63), ferrocenylacetic acid, (64) and ferrocenylethylamine, (65).	32
Scheme 2.21: Attachment of a ferrocenyl fragment onto a phthalocyanine macrocycle.	51
Scheme 2.22: Phase transitions for ferrocenyl-phthalocyanine, (67) compared to that of its parent phthalocyanine, (74). ΔH in kcal mol ⁻¹	51
Scheme 3.1: Synthesis of 3,6-bis(dodecyl)phthalonitrile, (79). <i>m</i> -CPBA = <i>m</i> -chloroperoxybenzoic acid. Oxone = the Aldrich trade name for 2KHSO ₅ ·KHSO ₄ ·K ₂ SO ₄	62
Scheme 3.2: Synthesis of 4-(2'-ferrocenylethoxy)phthalonitrile, (81).	66
Scheme 3.3: Synthesis of 2-ferrocenylethanol, (80).	67
Scheme 3.4: Synthesis of 1,4,8,11,15,22,25-octakis(dodecyl)phthalocyanine, (83).	71
Scheme 3.5: Synthesis of [1,4,8,11,15,22,25-octakis(dodecyl)phthalocyaninato]zinc(II).	71
Scheme 3.6: Synthesis of 2,9,16,23-tetrakis(2'-ferrocenylethoxy)phthalocyanine, (85).	73
Scheme 3.7: Synthesis of ferrocenyl-phthalocyanine conjugates, following a statistical condensation process, involving phthalonitriles (79), A and (81), B. The main products are (86) and (87) and can be abbreviated as AAAB. The symbols AAAA, AABB, ABAB, AB BB and BB BB represent additional products and product isomers that may be obtained when (79), A and (81), B are statistically condensed according to the guidelines in Chapter 2, page 25. DMAE = dimethylaminoethanol.	74
Scheme 3.8: Synthesis of (C ₁₂ H ₂₅) ₆ -ZnPc-O-(CH ₂) ₂ -Fc, (87) via the complexation of a metal-free ferrocene-containing phthalocyanine, (86) with zinc.	80
Scheme 3.9: The possible explanation of the broadening of the peaks of ferrocenylmethanol, (89) during oxidation-reduction processes.	90

List of tables

Table 2.1: Q-band positions in the visible absorption spectrum of Pcs in solution.	40
Table 2.2: The properties of linking groups.	48
Table 3.1: By reacting different ratios of 4-nitrophthalonitrile, (52) and 2-ferrocenylethanol, (80), different yields of the desired product, 4-(2'-ferrocenylethoxy)phthalonitrile, (81) were obtained.	67
Table 3.2: Proton assignment of signals (in ppm) of the ^1H NMR spectra of phthalonitrile (79) and phthalocyanines (83) and (84).	72
Table 3.3: The % yields, R_f values and MALDI-tof ms data of the fractions obtained from the statistical condensations of phthalonitriles (79), A and (81), B in a 3:1 ratio with lithium in pentanol <i>via route 1</i> in Scheme 3.7.	75
Table 3.4: The % yields, R_f values and MALDI-tof ms data of the fractions obtained from the statistical condensations of phthalonitriles (79) and (81) in the presence of zinc acetate dihydrate in a ratio of 3:1:4 as reactants <i>via route 2</i> in Scheme 3.7.	77
Table 3.5: Proton assignment of selected signals (in ppm) of the ^1H NMR spectra of phthalonitrile (81) and its corresponding phthalocyanines (86) and (87).	78
Table 3.6: Electrochemical data for ferrocene and the indicated ferrocenyl derivatives (1mmol dm^{-3}) in acetonitrile containing 0.2 mol dm^{-3} $(^t\text{Bu})_4\text{-}^+\text{NPF}_6$ as supporting electrolyte at 25°C vs Ag/Ag^+ at scan rates of 50, 100, 150, 200 and 250 mV s^{-1}	87
Table 3.7: Formal reduction potential, E^0 and ^1H NMR data of ferrocenyl derivatives of the type FcCH_2R	91
Table 3.8: Summary of group electronegativities, χ_R , obtained by electrochemical and ^1H NMR techniques.	93
Table 3.9: Electrochemical data for ferrocene, indicated ferrocene-containing alcohols and phthalonitrile (1 mmol dm^{-3}) in acetonitrile containing 0.2 mol dm^{-3} $(^t\text{Bu})_4\text{-}^+\text{NPF}_6$ as supporting electrolyte at 25°C vs Ag/Ag^+ at scan rates of 50, 100, 150, 200 and 250 mV s^{-1}	95
Table 3.10: Peak cathodic potentials (E_{pc}), difference in peak anodic and peak cathodic potentials (ΔE_p), formal reduction potentials (E^0), peak cathodic currents (i_{pc}) and peak current ratios (i_{pc}/i_{pa}) for the indicated 2H- and Zn- phthalocyanines. Potentials are versus Ag/Ag^+ . DCM = dichloromethane and DCE = dichloroethane.	101
Table 3.11: Peak cathodic potentials (E_{pc}), difference in peak anodic and peak cathodic potentials (ΔE_p), formal reduction potentials (E^0), peak cathodic currents (i_{pc}) and peak current ratios (i_{pc}/i_{pa}) for phthalocyanines (83), (84), (86) and (87). Potentials are versus Ag/Ag^+ . DCM = dichloromethane and DCE = dichloroethane.	111
Table 3.12: Extinction coefficients, ϵ for phthalocyanines (83), (84), (86), (87) and (88) at Q-band maximas and Soret band.	116
Table 3.13: Phase transition temperatures and transition energies (ΔH), observed during DSC and variable temperature optical microscopy studies of non-peripherally octadodecyl-substituted	

phthalocyanines, (83) and (84) as well as the ferrocenylethoxide-phthalocyanine conjugates, (86) and (87). The values in brackets were obtained from cooling cycles, while the others were from the heating cycles of DSC traces.128

Acknowledgements

I hereby wish to express my sincere gratitude towards the following people who all contributed directly or indirectly to the preparation of this thesis.

Prof J. C. Swarts, my promoter, for his leadership during this study and for introducing me to the very exciting applications of phthalocyanine molecules.

Collectively, all my post-graduate colleagues for their interest in my studies. I particularly want to thank Ina du Plessis for her help with the cyclic voltammetry, Dr. Conradie and Hardi Koortzen for the many NMR spectra they drew for me and especially Tessa Swarts for her support and motivation during sometimes difficult times.

Lastly, to my family for their support and showing a keen interest in my progress. This thesis is dedicated to my children Kim and Wayne.

For financial assistance during the course of my study I would like to thank the NRF and the Andrew Mellon Foundation.

Wade Luke Davis

February 2003.

CHAPTER 1

INTRODUCTION AND AIMS

In recent years a new dimension in cancer research has been introduced with the development of new and more effective chemotherapeutic agents to fight cancer. This was necessitated by the many negative side effects that cisplatin [*cis*-diamminedichloroplatinum(II)]¹ as a metal-containing chemotherapeutic agent and other drugs induce. In case of cisplatin, these negative side effects include *inter alia* exceptional high toxicity especially to the kidneys and bone marrow,² lack of aqueous solubility, loss of appetite and a high rate of excretion from the body.³ In addition, development of drug resistance with time after a continued drug dosage limits the long-term usage of the drug. Most chemotherapeutic drugs are themselves also carcinogenic. Cisplatin, for example, may cause lung cancer after a 15-year induction period.⁴ The most important problem in chemotherapy may be described as a lack of selectivity, which may be attributed to the inability of the drug to distinguish between healthy and cancerous cells, and thus exclusively destroying the latter. Certain phthalocyanines such as, aluminium, gallium and zinc phthalocyanines, that are photodynamically active,⁵ may play a significant role in this regard in future as they are found to be preferentially absorbed by cancer cells.⁶

To overcome the above-mentioned many negative side effects associated with chemotherapy of cancer, new antineoplastic drugs are continuously being synthesised and evaluated. New methods of delivering an active drug to a cancerous growth are being developed.⁷ Combination therapy (using more than one drug simultaneously) has been investigated in the hope of finding possible synergistic effects⁸ and even completely new methods of fighting cancer have been developed.

Photodynamic therapy of cancer where a photodynamically active drug is administered to the body and absorbed preferentially by the cancer cells is one such new method to treat cancer.⁹ The drug used in this procedure is totally inactive in the dark and is only activated when irradiated with normal visible light of the correct wavelength, usually around 630 nm or longer. The activated drug will then either destroy the cancer cells or activate a third party, normally oxygen to form singlet oxygen. Singlet oxygen then interacts with the cells leading to biological cell damage and ultimately cell death. This technique provides a unique way of introducing selective action in cancer therapy. The key to limited or no side effects during photodynamic cancer therapy is not as a result of drugs preferentially accumulated in the cancer cells, but is rather a function of the capability to irradiate cancerous growths without allowing irradiated light to fall on healthy surrounding cells.

Currently, porphyrins¹⁰ are mostly used in photodynamic cancer therapy studies because of their photo-optical properties. However, zinc, aluminium, gallium and some other phthalocyanines have produced some promising results recently.¹¹ One of the reasons being that phthalocyanines are better light scavengers than porphyrins (extinction coefficient, ϵ , of some of these phthalocyanines are $10^5 \text{ dm}^3 \text{ mol}^{-1} \text{ cm}^{-1}$ at 680 nm while ϵ of hematoporphyrin, a popular photodynamic cancer drug, is only $10^3 \text{ dm}^3 \text{ mol}^{-1} \text{ cm}^{-1}$ at 630 nm)^{11a} with stronger absorbances at longer wavelengths where tissue penetration by visible light is more superior. Commercial exploitation of phthalocyanines in photodynamic treatment is, however, still in its infancy because they are difficult to prepare and are mostly highly insoluble in most solvents due to excessive aggregation. Only a few derivatised phthalocyanines were found to be soluble. To this effect carboxylated, sulphonated and quaternary ammonium salts of phthalocyanines are only sparingly soluble in water while nitro phthalocyanines are only marginally soluble in warm concentrated sulphuric acid. In principle, bulky substituents like a ferrocenyl group or a tertiary butyl group on the phthalocyanine macrocycle tend to break this aggregation and enhance solubility in organic solvents.

Previous work in this laboratory found that the inclusion of a ferrocene moiety into rhodium complexes enhanced the chemotherapeutic effectiveness of these chemotherapeutic drugs due to synergistic effects.¹² By anchoring a ferrocene fragment onto a phthalocyanine we hope to find a synergistic effect in cancer therapy between the photodynamic phthalocyanine moiety and the chemotherapeutic ferrocene moiety. Preliminary results on a ferrocenylated phthalocyanine compound showed that this might be possible. A need now arises to increase the arsenal of available ferrocenylated phthalocyanines and hence, determine structural preferences in cancer therapy for this new class of photosensitisers/chemotherapeutic drugs.

With this background, the following goals were set for this study:

1. Synthesis of octadodecylated non-peripherally substituted phthalocyanines.

Non-peripheral substitution compared to peripheral substitution, causes the UV/VIS absorption maxima of phthalocyanines to shift more into the red-near infrared region, where tissue penetration by visible light is more superior. The long dodecyl substituents on the phthalocyanine macrocycle were chosen to investigate its influence on the liquid crystal properties of these phthalocyanines.

2. Synthesis of new ferrocenyl-phthalocyanine conjugates.

This goal was set because we hope to find a synergistic effect in cancer therapy between the photodynamic phthalocyanine moiety and the chemotherapeutic ferrocene moiety. The ferrocenyl substitution is specifically chosen to be on the peripheral position of the phthalocyanine macrocycle to investigate its influence on the shift in UV/VIS absorption peak maxima from the red to the blue light region or *vice versa*. The influence of ferrocene substituents on the liquid crystal properties of phthalocyanines is still unknown. This study represents therefore an ideal opportunity to also investigate the influence of the ferrocenyl group on the liquid crystal properties of the ferrocenyl-substituted phthalocyanines.

3. A comparative study of the electrochemical properties of ferrocene- and phthalocyanine derivatives.

The redox properties of some ferrocenyl derivatives, a series of octa-alkyl non-peripherally substituted phthalocyanines and the new ferrocene-containing phthalocyanines were investigated by means of cyclic voltammetry.

4. Thermodynamic investigations into the discotic liquid crystalline behaviour of the synthesised octadodecylated and the new ferrocene-containing phthalocyanines.

These included the determination of transition temperatures and enthalpies of each phase change of these compounds, utilising polarised light optical microscopy, differential scanning calorimetry (DSC) as well as variable temperature UV/VIS spectra of spin-coated thin films of the title compounds cast on glass.

- ¹ S.E. Sharman and S.J. Lippard, *Chem. Rev.*, 1987, **87**, 1153.
- ² J.M. Ward, M.E. Grabin, E. Berlin and D.M. Young, *Cancer Res.*, 1977, **37**, 1238.
- ³ (a) H.J. Wallace and D.J. Higby, *Platinum coordination complexes in cancer therapy*, eds. T.A. Connors and J.J. Roberts, Springer-Verlag Heidelberg, 1974, pp. 128, 167; (b) W. Wolf and R.C. Manaka, *J. Clin. Hemato. Oncol.*, 1977, **7**, 169.
- ⁴ W.R. Leopold, E.C. Miller and J.A. Miller, *Cancer Res.*, 1979, **39**, 913.
- ⁵ I. Rosenthal and E. Ben-Hur, *Phthalocyanines in Photobiology, Phthalocyanines: Properties and Applications*, eds. C.C. Leznoff and A.B.P. Lever, VCH: New York, 1989, pp. 397-399.
- ⁶ (a) C. Ometto, C. Fabris, C. Milanesi, G. Jori, M.J. Cook and D.A. Russell, *Br. J. Cancer*, 1996, **74**, 1891; (b) C. Fabris, C. Ometto, C. Milanesi, M.J. Cook and D.A. Russell, *J. Photochem. Photobiol., B: Biology*, 1997, **39**, 279.
- ⁷ G. Caldwell, E.W. Neuse, and C.E.J. van Rensburg, *J. Inorg. Organomet. Polym.*, 1999, **7**, 217.
- ⁸ G.R. Gale, L.M. Atkins, S.J. Meischen, A.B. Smith and E. Walker, *Cancer Treat. Rep.*, 1977, **61**, 445.
- ⁹ W.M. Sharman, C.M. Allen and J.E. van Lier, *Drug Discovery Today*, 1999, **44**, 507.
- ¹⁰ H. Ali and J.E. van Lier, *Chem. Rev.*, 1999, **99**, 2379.
- ¹¹ (a) C.M. Allen, W.M. Sharman and J.E. van Lier, *J. Porphyrins Phthalocyanines*, 2001, **5**, 161; (b) E.A. Lukyanets, *J. Porphyrins Phthalocyanines*, 1999, **3**, 424.
- ¹² J.C. Swarts, *Unpublished results, Provisional patent submitted*.

CHAPTER 2

LITERATURE SURVEY

2.1 History and structural determination

The first recorded observation of a phthalocyanine (Pc) occurred in 1907, during the synthesis of *o*-cyanobenzamide, from phthalimide and acetic anhydride when Braun and Tcherniac¹ observed the production of a highly coloured impurity of unknown structure. Comprehensive studies by Linstead² and co-workers lead to the determination of the phthalocyanine structure (Figure 2.1) in the early 1930's, which was later confirmed by Robertson³ *via* X-ray diffraction techniques.

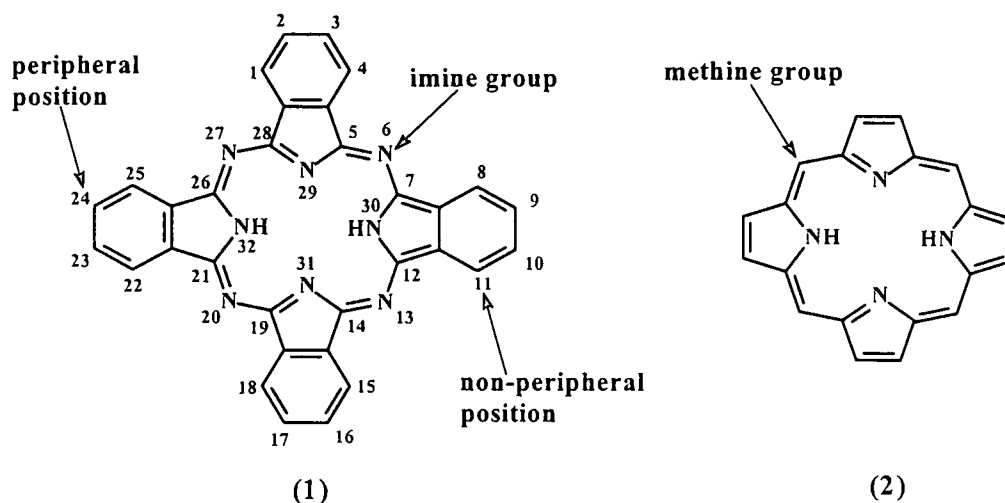


Figure 2.1: Comparison of the phthalocyanine, (1) and porphyrin, (2) structures. The numbering system and substitution positions on phthalocyanines are also shown.

Phthalocyanines, (1) are 18 π -electron aromatic macrocycles comprising four isoindole units linked together through their 1,3-positions by aza bridges with a central cavity of sufficient size to accommodate various metal ions. The central cavity of the phthalocyanine is more than half the width of the total molecule and contains either hydrogen (metal-free phthalocyanine, 2HPC) or a metal (metallophthalocyanine, MPC). The two-dimensional π -electron delocalisation over these macrocycles gives rise to unique physical properties. Thus, phthalocyanines are chemically and thermally stable compounds that exhibit exceptional optical and electrical behaviour. Other remarkable features that increase their usefulness are their versatility and tailorability; several chemical modifications can be made at the phthalocyanine ring, thereby allowing a fine-tuning of their physical properties. Phthalocyanines are capable of incorporating more than 70 different metallic and non-metallic cations in their ring cavity.⁴ It's also possible to attach a wide variety of substituents at the periphery of the macrocycle, which can alter the electronic structure of the system.

The similarity of the structure of phthalocyanine (1) and porphyrin (2), which forms the basis of many natural occurring compounds such as haemoglobin, is self-evident. The systems differ in that the 4-pyrrole units of a porphyrin are linked by methine groups, instead of the aza (imine) groups in a phthalocyanine.

2.2 Applications of phthalocyanines

2.2.1 General

Phthalocyanines have extensively been studied because of their many established uses and potentially new applications. They have long been used as blue and green dyes or colouring pigments⁵ because of their intense colours and stability towards heat, acids and alkalis. They have recently gained industrial applications as photoconducting agents in photocopying devices⁶ and as catalysts⁷ in numerous chemical reactions, including the selective hydrogenation of multiple bonds and oxidation of thiols.^{4,8} Phthalocyanines are able to form a wide range of condensed phases with controlled molecular structure, such as discotic liquid crystals⁹ and thin films. Notably, phthalocyanine-based thin films have found applications in a wide range of technological areas, such as gas sensors,¹⁰ electrochromic devices,¹¹ photovoltaic materials¹² and fuel cells.¹³ Other potential applications for phthalocyanines include solar energy conversion (to chemical and electrical energy),^{14,12} chemical sensors,¹⁰ optical storage devices^{15,5a} and non-linear optics.¹⁶ One of the most prominent new applications of phthalocyanine derivatives is their application in medicine as photosensitizers during photodynamic therapy (PDT)¹⁷ of cancer diseases. The aim of this study is set around the synthesis of new zinc-containing phthalocyanines for PDT and their characterisation in terms of electrochemical and liquid crystal properties.

2.2.2 Photodynamic therapy (PDT)

2.2.2.1 Introduction

This thesis does not primarily concern PDT. It provides however a contribution to an arsenal of new compounds by this laboratory submitted for PDT tests. The time span of this study is

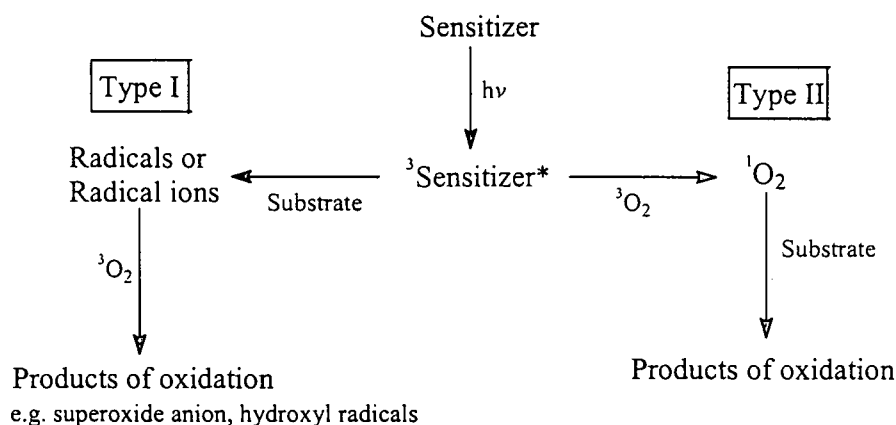
however of such a nature that PDT results could not be accommodated in this thesis.¹⁸ It is, however, appropriate to give a short introduction to PDT in general.

Traditional cancer therapies such as surgery, chemotherapy and radiation therapy involve a delicate balance between destroying diseased tissue while leaving surrounding healthy cells sufficiently undamaged that they can repair themselves. Chemotherapy and radiation therapy are associated with serious side effects while the location of a tumor may imply surgery is impossible. Photodynamic therapy, an emerging new bimodal strategy in cancer treatment, has been developed as an alternative for the treatment of cancer. PDT is a binary therapy that involves the combination of visible light and a photosensitizer. Each component is harmless by itself, but in combination with molecular oxygen, lead to the generation of a reactive oxygen specie, oxidative cell damage and cell death. The duality of this treatment leads to greater selectivity towards destroying diseased tissue since only cells that are exposed simultaneously to the photosensitizer, light and oxygen are subjected to the cytotoxic effects produced during PDT. This implies a possible two-fold selectivity, as there is often a preferential uptake of the photosensitizer by the diseased tissue as well as the technical capability of staff and equipment to confine activation of the photosensitizer to the tumor by restricting light illumination to the specific region where the tumor is located. As such, PDT allows for the exclusive eradication of tumor tissue while largely leaving surrounding healthy cells undamaged.

2.2.2.2 Mechanism of photosensitization

Upon illumination, the photosensitizer used in PDT is excited to its first excited singlet state. This excited state is far too short-lived (survival is in the *ns* region) to effectively interact with its surroundings and rapidly loses its energy *via* radiative and non-radiative decay. Rather an intersystem crossing of energy takes place to populate the much longer lived (μs -*ms* lifetime)¹⁹ triplet state of the photosensitizer. This photosensitizer in the excited state then interacts in one of two ways, defined as Type I and Type II mechanisms with oxygen in the ground state ($^3\text{O}_2$) during PDT (Scheme 2.1).

The Type I mechanism involves electron or hydrogen-atom transfer between the sensitizer and substrate molecules to yield radical ions and/or free radicals. The latter species react with molecular oxygen, inducing irreparable cellular damage and the production of reactive oxygen species, which can lead to further biological destruction.



Scheme 2.1: Possible photosensitization processes in PDT.

The Type II mechanism is defined as the interaction between the excited triplet state and ground state molecular oxygen ($^3\text{O}_2$), which also is in a triplet state.²⁰ The interaction involves energy transfer to yield singlet oxygen ($^1\text{O}_2$) that reacts rapidly with numerous biologically electron-rich substrates (e.g. cholesterol, unsaturated fatty acids, amino acid residues and nucleic acid bases of DNA) that again leads to extensive oxidative damage and ultimately cell death. It is generally accepted that the Type II mechanism dominates during PDT and that singlet oxygen is the most important cytotoxic species produced²¹ during PDT. The range of singlet oxygen translational movement in cellular media is limited to approximately 45 nm.²² With the diameter of human cells ranging from 10 to 100 μm , the site of primary generation of singlet oxygen consequently determines which subcellular target is attacked, either initiating an apoptotic or necrotic response. Type I reactions become more important at low oxygen concentrations or in polar environments²³ and produce reactive oxygen species such as the superoxide anion and hydroxyl radicals that has similar short ranges in cellular systems.

2.2.2.3 Porphyrins as photosensitizers in PDT

Various porphyrins, including hematoporphyrin (Hp) are selectively retained in tumors. The first photosensitizers accepted for clinical use in PDT are the first-generation hematoporphyrin derivatives (HpD), such as Photofrin®, (3), which is produced by the reaction of hematoporphyrin with 5% sulfuric acid in acetic acid followed by treatment with aqueous base and neutralization.²⁴ Photofrin® is a complex mixture of dimers and oligomers in which the most active component in the photodynamic action is described as the dihematoporphyrin ether (Figure 2.2).²⁵

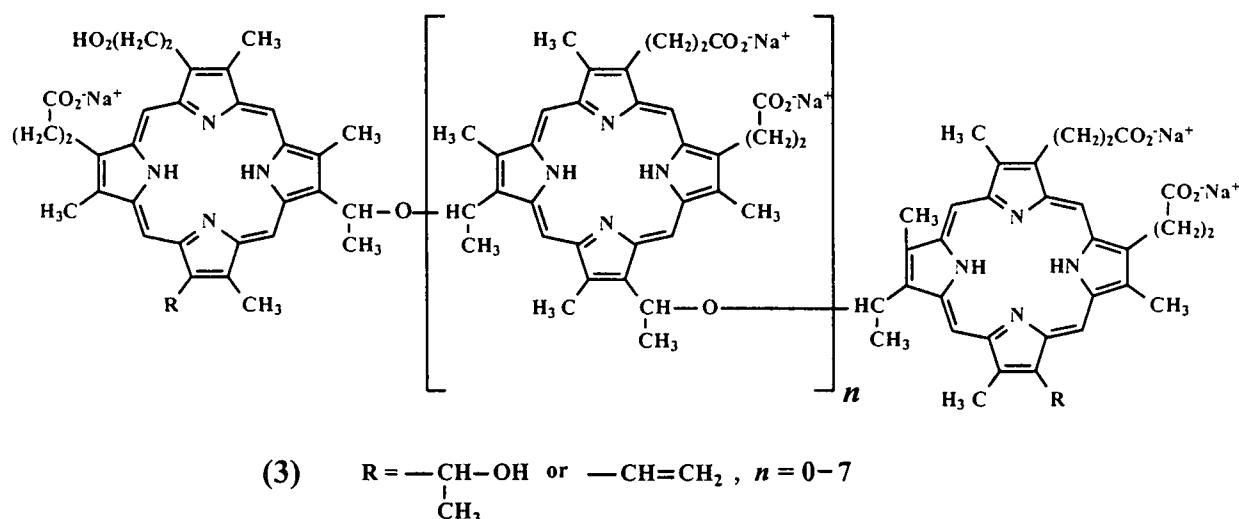


Figure 2.2: Structure of Photofrin®, (3) ranging from two to nine porphyrin units linked *via* ether bonds.

Despite the clinical success achieved using Photofrin®, it has several disadvantages, namely:

- a) It's a complex chemical mixture where the resulting dimers and oligomers, linked primarily with ester and ether bonds, may vary with different preparations and for storage times. Structure-activity relationships are therefore impossible to determine.²⁶
- b) It absorbs relatively weakly at the therapeutic wavelength of 630 nm. At this wavelength tissue penetration of light is not optimal, and tumor treatment is limited to depths of no more than 5 mm for a light source.²⁷
- c) Hematoporphyrin derivatives proved to be ineffective for cancers such as pigmented melanoma due to overlapping absorption of the photosensitizer and melanin in the malignant tissue.²⁸
- d) Most importantly, hematoporphyrin derivatives exhibit an extended retention in cutaneous tissue for up to 10 weeks post injection, resulting in a prolonged skin photosensitivity.^{23b}

While these disadvantages have not prevented Photofrin® from becoming a useful drug against cancer, the search for new second-generation photosensitizers with improved physical, chemical and spectral properties remains an important goal.^{29,17a} Phthalocyanines have emerged in recent years as one of the front-runners in the search for new photosensitizers. Ideal photosensitizers for PDT should meet certain criteria, namely:

- a) It should be chemically pure and maintain a constant composition throughout treatment, undergoing minimal photobleaching.³⁰
- b) It should have minimal dark toxicity.²⁴

- c) The photosensitizer should be preferentially retained by the target tumor tissue, so as to induce only marginal toxicity to surrounding healthy biological matter. In addition, the excess dye should be rapidly excreted from the body exhibiting low systematic toxicity.²⁷
- d) The dye should have high photochemical reactivity with a high quantum yield of long-lived triplet-states energetic enough to produce singlet oxygen.³¹
- e) The photosensitizer should have a strong absorption coefficient at a long wavelength (600-800 nm) where there is optimal tissue penetration by light with a low degree of attenuation by haemoglobin.³²

2.2.2.4 Phthalocyanines as photosensitizers in PDT

In the last few years, phthalocyanines have been intensively studied as second-generation photosensitizers for photodynamic antitumor therapy. They have been shown to be phototoxic against a number of cell types and tumor models.^{17b} These azaporphyrin derivatives have stronger absorbances at longer wavelengths than do porphyrins. Phthalocyanine derivatives have attractive photochemical and photophysical properties as compared to hematoporphyrin derivatives. These properties can be altered through the addition of substituents to the periphery of the macrocycle or axial ligands to the chelated central metal. Monomeric, unaggregated phthalocyanines have a strong, absorption peak in the far-red region (the so called 'therapeutic window')³³ of the visible spectra, (MPc $\lambda_{\max} \approx 680$ nm; HpD $\lambda_{\max} \approx 630$ nm), where tissue penetration by visible light is more efficient and are therefore less likely to induce skin photosensitivity upon radiation. Skin sensitivity to light is a major problem with HpD.³⁴ Metal-free and metallated phthalocyanines have an improved capacity to absorb light, by two orders of magnitude over that of the highest Q-band absorption of HpD (Pc molar extinction coefficient, $\epsilon \sim 10^5 \text{ M}^{-1}\text{cm}^{-1}$; HpD $\epsilon \sim 10^3 \text{ M}^{-1}\text{cm}^{-1}$).³⁵ The nature and presence of the central metal ion strongly influence the photophysical properties of the phthalocyanines. Complexation of phthalocyanines with open d shell or paramagnetic metal ions (Cu^{2+} , Co^{2+} , Fe^{2+} , Ni^{2+} , Cr^{3+} and Pd^{2+}) gives dyes with short triplet lifetimes (ns) while phthalocyanines with closed d shell or diamagnetic metal ions (Zn^{2+} , Al^{3+} and Ga^{3+}) are dyes producing high triplet yields with long lifetimes (μs).

Water-soluble sulpho-substituted zinc and aluminium phthalocyanine derivatives are the most studied as photosensitizers for PDT, with the majority of them more efficient than porphyrinic compounds such as Photofrin. The disulphonated AlPc with sulphonate groups on adjacent isoindole units (**4**) is the most potent photosensitizer of this class (Figure 2.3).³⁶

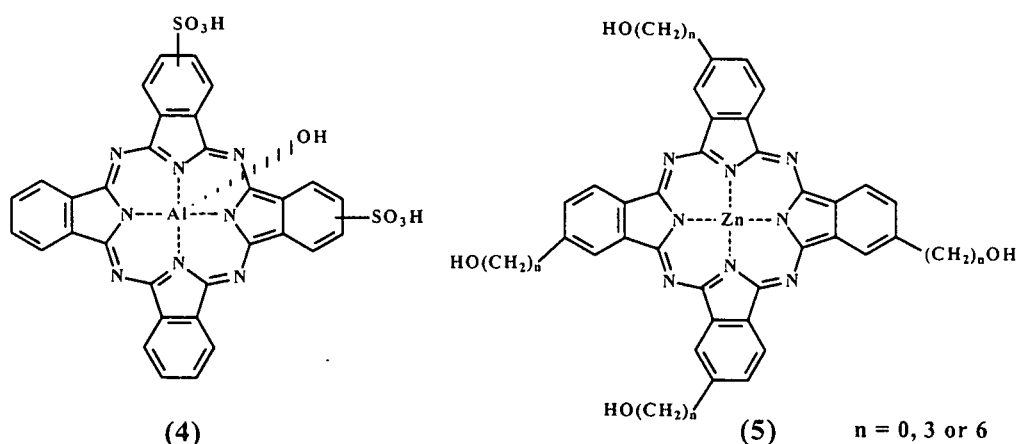


Figure 2.3: Disulphonated aluminium phthalocyanine, (4) and a tetrahydroxy ZnPc, (5).

The efficiency and mechanism of action in PDT of sulphonated phthalocyanines depend on the degree of sulphonation.³⁷ Van Lier and co-workers³⁸ showed that the cell uptake of the monomeric, non-aggregated (photoactive) compounds is optimal for sulphonated phthalocyanines, $\text{AlPc}(\text{SO}_3\text{H})_n$, $1 \leq n \leq 4$ preparations consisting of various regioisomers or of differently substituted compounds. PDT efficiency using a series of sulphonated phthalocyanines on vasculature can be ranked from high to low as $\text{AlPc}(\text{SO}_3\text{H})_2 \approx \text{ZnPc}(\text{SO}_3\text{H})_1 > \text{AlPc}(\text{SO}_3\text{H})_1 > \text{AlPc}(\text{SO}_3\text{H})_4 > \text{ZnPc}(\text{SO}_3\text{H})_2 > \text{ZnPc}(\text{SO}_3\text{H})_4$.³⁹

In 1993 Boyle and co-workers⁴⁰ tested ZnPcs (5) substituted with four hydroxyl groups attached to the macrocycle, either directly or via spacer chains of three or six carbon atoms (Figure 2.3) for their photodynamic potency *in vitro* against V-79 cells and *in vivo* on EMT-6 tumor bearing Balb/c mice. They found that both of the tetraalkylhydroxy substituted ZnPcs are effective photosensitizers *in vivo* with the tetrapropylhydroxy compound exhibiting about twice the activity of the tetrahexylhydroxy analogue. *In vitro*, these differences were accentuated by two orders of magnitude while the tetrahydroxy compound lacking spacer chains was inactive in both systems.

Ometto and co-workers⁴¹ in 1996 showed that a zinc containing octadecyl substituted phthalocyanine, $(\text{C}_{10}\text{H}_{21})_8\text{-ZnPc}$, (6) (Figure 2.4) has an unusually high affinity for serum low-density lipoprotein (LDL) and a high efficiency and selectivity of tumor targeting. In this study we concentrated on a C_{12} analogue. The maximum accumulation of phthalocyanine in the tumor occurred 24 h after injection. No detectable amount of phthalocyanine was recovered from the muscle between 1 h and 1 week after injection. At the same time, low amounts of phthalocyanines were recovered from the skin and then only at short times after injection, with

skin photosensitivity rapidly disappearing and the phthalocyanine present in the serum only. Tumor necrosis appears to be the consequence of both cell death and apoptosis.

In 1997 the same research group⁴² found that an analogous octapentylphthalocyanine, $(C_5H_{11})_8-ZnPc$ showed slightly poorer cytotoxic results and organ distributions to that found for the octadecyl derivative, whereas unsubstituted $ZnPc$ showed a lower efficiency and selectivity of tumor targeting than both octaalkyl substituted phthalocyanines. The use of axial ligated phthalocyanines in PDT studies rather than periphery-substituted phthalocyanines have some advantages, namely that the axial ligand impart greater solubility and prevent aggregation. Additionally these compounds do not exist as isomers, which implies purification procedures are much more simplified. One of these phthalocyanines receiving a great deal of attention in PDT is the silicon phthalocyanine, denoted as Pc-4, (7), bearing a long-chain amino axial ligand $(HOSiPcOSi(CH_3)_2(CH_2)_3N(CH_3)_2)$ (Figure 2.4).

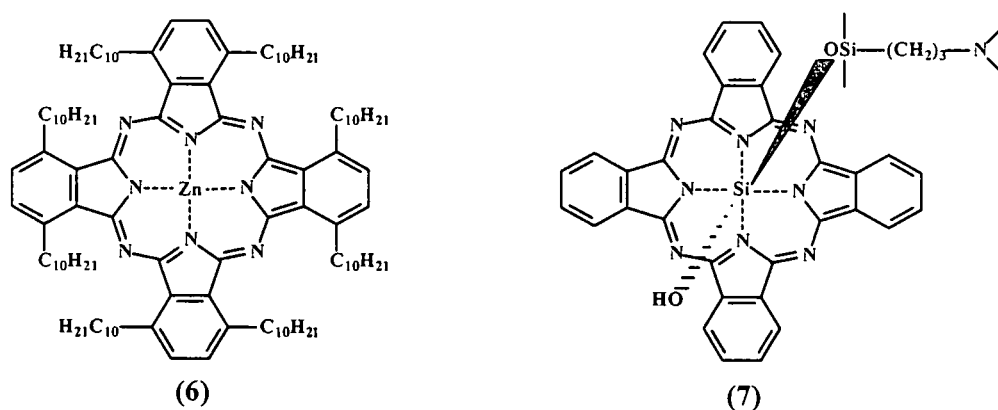


Figure 2.4: Non-peripherally octadecyl substituted $ZnPc$, (6) and Silicon phthalocyanine, (7) designated as Pc-4.

This SiPc showed promising results both *in vitro* and *in vivo*.^{43,44} Kenney and co-workers⁴³ showed that a three-fold increase in Pc-4 cytotoxicity as compared to a reference AlPc was found in V-79 Chinese hamster cells.

Kobayashi and co-workers⁴⁵ synthesised the first examples of second-generation photosensitizers, platinum-containing $ZnPcs$, (8) (Figure 2.5) with cytotoxic peripheral groups. A potentially high antitumor activity, reflecting the combined effect of the photodynamic activity of the phthalocyanine and the cytotoxicity of the platinum-containing fragments as in the case of platinum-containing porphyrins is expected.⁴⁶

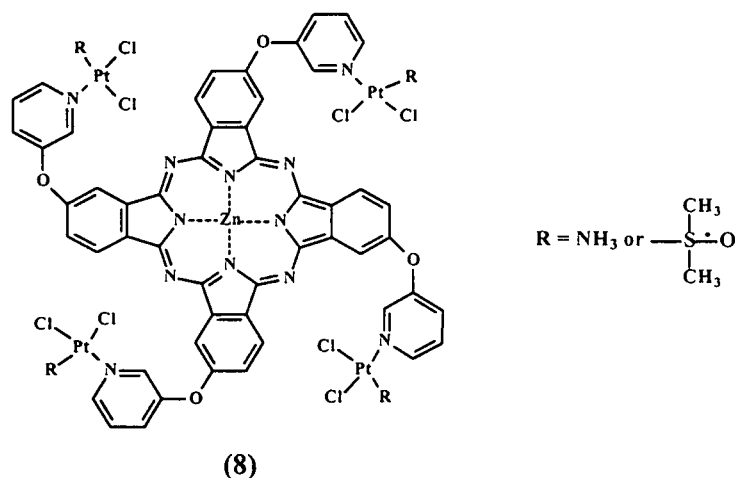
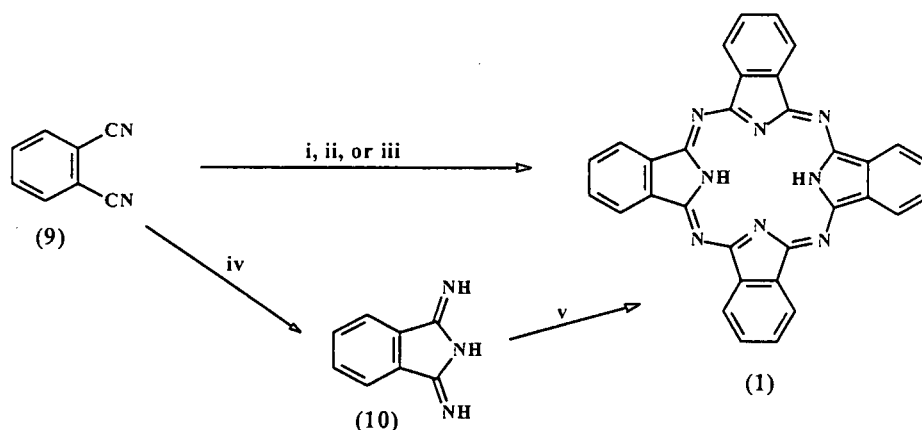


Figure 2.5: Platinum-containing zinc phthalocyanine, (8).

2.3 Synthesis of unsubstituted phthalocyanines

2.3.1 Metal-free phthalocyanine (2HPc)

One of the aims of this study includes the synthesis of phthalocyanine derivatives. Metal-free phthalocyanines can be synthesised from a wide range of *ortho*-disubstituted benzene derivatives, but for most laboratory syntheses phthalonitrile (1,2-dicyano benzene), (9) is used (Scheme 2.2).



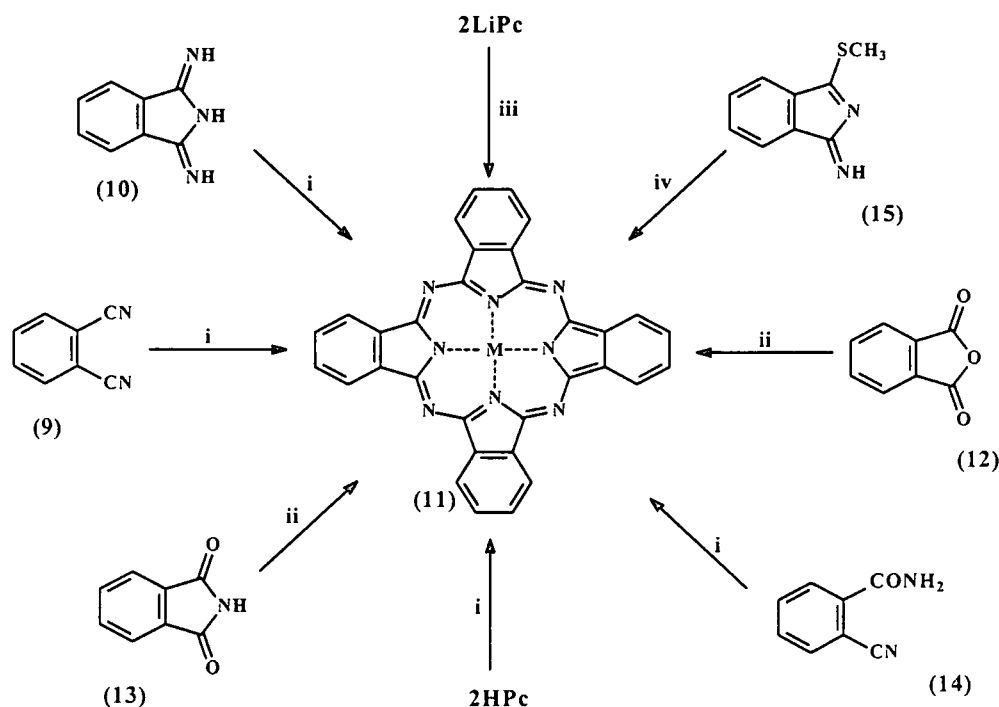
Scheme 2.2: Synthetic routes to 2HPc, (1) from phthalonitrile, (9) as precursor. *Reagents and conditions:* (i) Lithium, refluxing pentanol, followed by aqueous hydrolysis. (ii) Fuse with hydroquinone. (iii) Heat with 1,8-diazabicyclo[4.3.0]non-5-ene (DBN) in a melt or in pentanol solution. (iv) NH_3 , refluxing methanol, sodium methoxide. (v) Reflux in high boiling point alcohol.

There are several methods of cyclotetramerisation of phthalonitrile, (9) to form 2HPc, (1). The first include the initial formation of diiminoisoindoline, (10) by the reaction of phthalonitrile with ammonia.⁴⁷ Diiminoisoindoline condenses under relatively mild conditions to form 2HPc.

In addition, diiminoisoindoline in dimethylaminoethanol (DMAE) in the absence of a metal salt⁴⁸ condense to produce 2HPc. Cyclotetramerization of phthalonitrile, (9) in a melt with hydroquinone as reducing agent also allows preparation of 2HPc in the absence of any metal ions.⁴⁹ A non-nucleophilic hindered base such as 1,8-diazabicyclo-[4.3.0]non-5-ene (DBN) is another efficient reagent for cyclotetramerization of (9) in a melt or pentanol solution.⁵⁰ In addition, 2HPc is conveniently prepared from (9) using a refluxing solution of lithium metal dissolved in pentanol (to *in situ* form lithium pentyloxide) to form 2LiPc, which can readily undergo demetallation using dilute aqueous acid.⁵¹

2.3.2 Metallated phthalocyanines (MPc)

Phthalocyanines can be synthesised from a wide range of precursors, all derived from phthalic anhydride. The more general methods leading to metallophthalocyanines are illustrated in Scheme 2.3. Most MPcs, (11) are prepared directly from phthalonitrile, (9) with a base such as 1,8-diazabicyclo[4.3.0]non-5-ene and a metal salt in a high boiling solvent such as pentanol or quinoline.⁵² If an alcohol is used as solvent, the metal alkoxide formed *in situ* serves as both the base and metal salt.

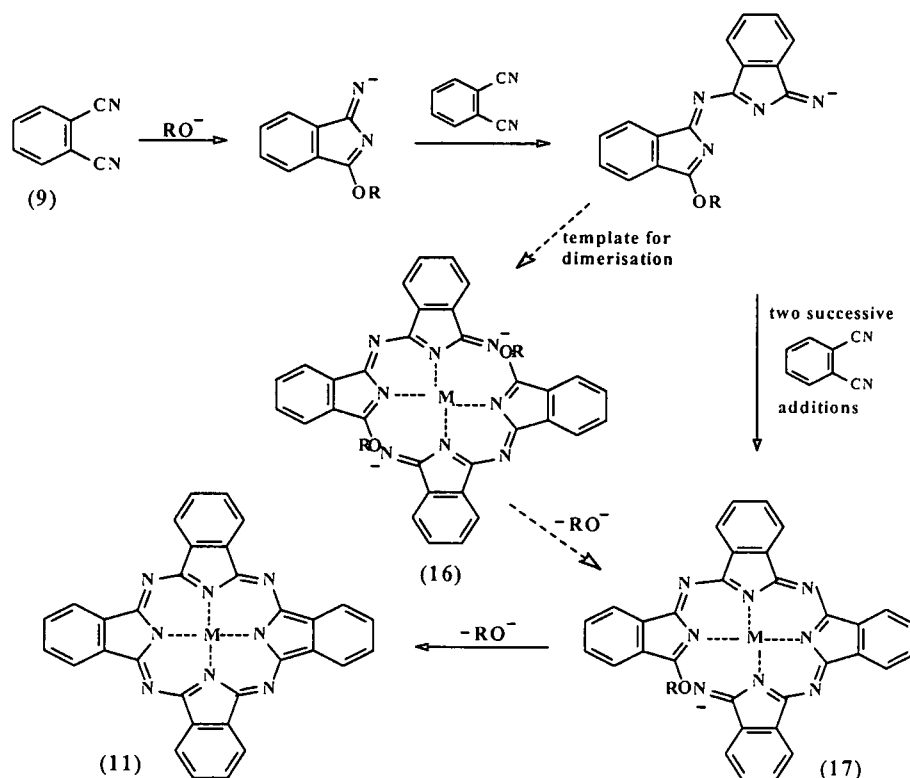


Scheme 2.3: Synthetic routes to MPc, (11). *Reagents and conditions:* (i) Heat in a high-boiling-point solvent (e.g. quinoline) with metal salt. (ii) Heat in a high-boiling-point solvent with urea and metal salt. (iii) Heat in ethanol with metal salt. (iv) -15 to -20°C in DMF with metal salt.

Further variations include using 1,8-diazabicyclo-[5.4.0]undec-7-ene (DBU) as base.⁵³ Diiminoisoindoline, (10) in the presence of a metal salt and a solvent such as dimethylaminoethanol is a very mild route to MPc.⁴⁸ In addition, phthalic anhydride, (12) or phthalimide, (13) can be used as precursors in the presence of a metal salt and a source of nitrogen (urea).⁵² Alternatively, the reaction between 2HPc or 2LiPc and an appropriate metal salt produces most MPcs.⁵² Finally, *o*-cyanobenzamide, (14) in the presence of a high boiling solvent and metal salt as well as 1-amino-3-methylthioisoindolenine, (15) in DMF at -20°C in the presence of a metal salt can also be used as precursors to produce MPc.⁵⁴

2.3.3 Mechanism of phthalocyanine formation

The formation of phthalocyanine from phthalonitrile has been shown to proceed through reactive precursors condensing reactive oligomeric intermediates, which, as a result of ring-closure reactions, cyclise to conjugated macrocyclic product. In 1987 Oliver and co-worker⁵⁵ described the role of the alkoxide anion in a reaction scheme, leading to phthalocyanine formation (Scheme 2.4).



Scheme 2.4: Role of the alkoxide anion in phthalocyanine formation.

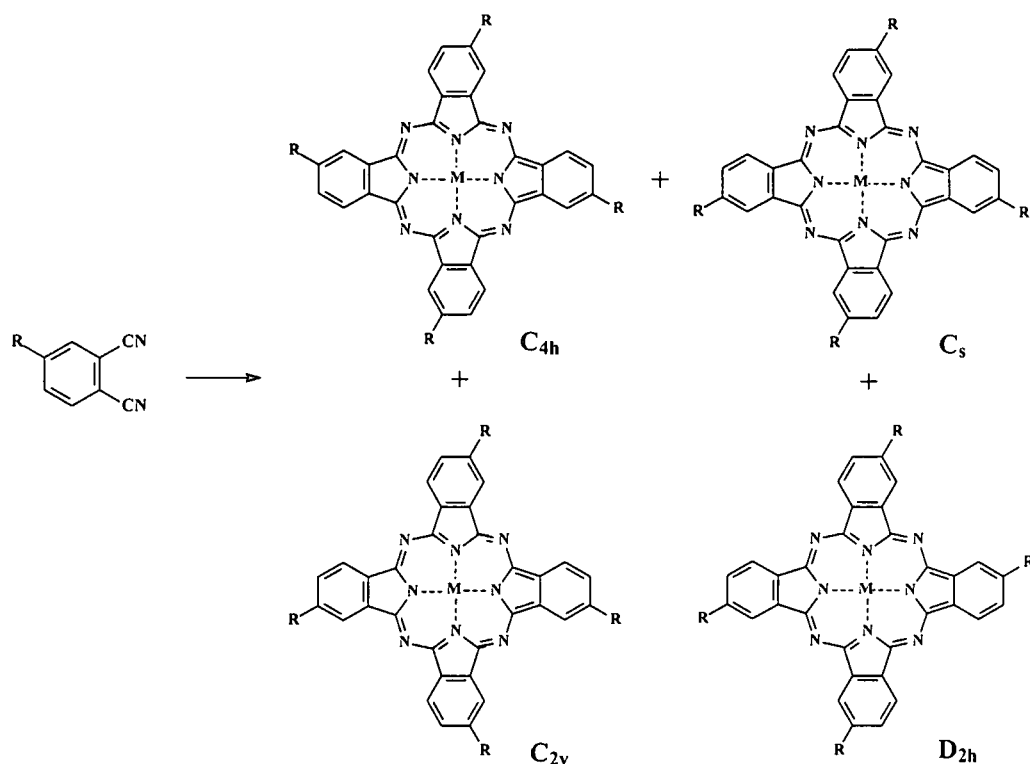
Only one alkoxide per macrocycle is necessary for initiation and reduction: the other reagent necessary is a base to react with hydrogen ions resulting from the formation of aldehyde. The described⁵⁵ elimination of an aldehyde is somewhat dubious. Rather than an aldehyde, an alkoxide would be eliminated. Usually two moles of alkoxide per macrocycle are added, which satisfies both requirements. Presumably this also facilitates the reaction by initial formation of an intermediate, (16), which then displaces an alkoxide in a template-assisted reaction leading to (17). Alkoxides are quite reactive and there is a possibility that the alkoxide anions may react with intermediate condensation products so as to diminish the yield of the conjugated macrocycle product. Therefore, substitution of the alkoxide by hydroxide (after the initial reactions have taken place) may increase the yield. Since the reactions occurring after the reaction of lithium alkoxide with phthalonitrile proceed rapidly, the influence of the alkoxide anion on reaction steps beyond that required for forming the initial reactive intermediate is difficult to measure. Ring closure would be assisted by the presence of a metal cation coordinated to the nitrogen donor atoms of structure (17) or (11) as a result of positioning the terminal functional groups for reaction.

2.4 Synthesis of substituted phthalocyanines

The incorporation of substituents onto the ring system greatly expands the range of available phthalocyanines and their applications of possible phthalocyanines. There are 16 available sites on the benzenoid rings where substituents may be placed. These fall into two categories, the so-called peripheral (2,3,9,10,16,17,23,24) and non-peripheral (1,4,8,11,15,18,22,25) positions (Figure 2.1, page 7).⁵⁶ Substituents are introduced either by substitution reactions on the preformed macrocycle or, more commonly, through the use of appropriately substituted precursors, especially phthalonitrile derivatives.⁵⁷ Unsubstituted phthalocyanines generally show poor solubility in common organic solvents, while an important effect of substituents is to assist solubilisation of the macrocyclic phthalocyanine ring system in either aqueous media or organic solvents. They are important in modifying the wavelength of the visible region absorption band, the Q-band. Importantly, certain substituents, particularly long aliphatic chains, can promote discotic liquid-crystal behaviour.⁵⁸ They can also affect the packing of the phthalocyanines in the solid state,⁵⁶ which plays a major role in the overall conductivity of for example thin films.⁵⁹

2.4.1 Tetra-substituted phthalocyanines

Pure substituted phthalocyanines are prepared by cyclotetramerization of substituted phthalonitriles or 1,3-diaminoisindolines. If mono-substituted phthalonitriles are employed as precursors, tetra-substituted phthalocyanines with a mixture of four regioisomers with C_{4h} , C_s , C_{2v} and D_{2h} symmetries are obtained (Scheme 2.5).⁵⁷



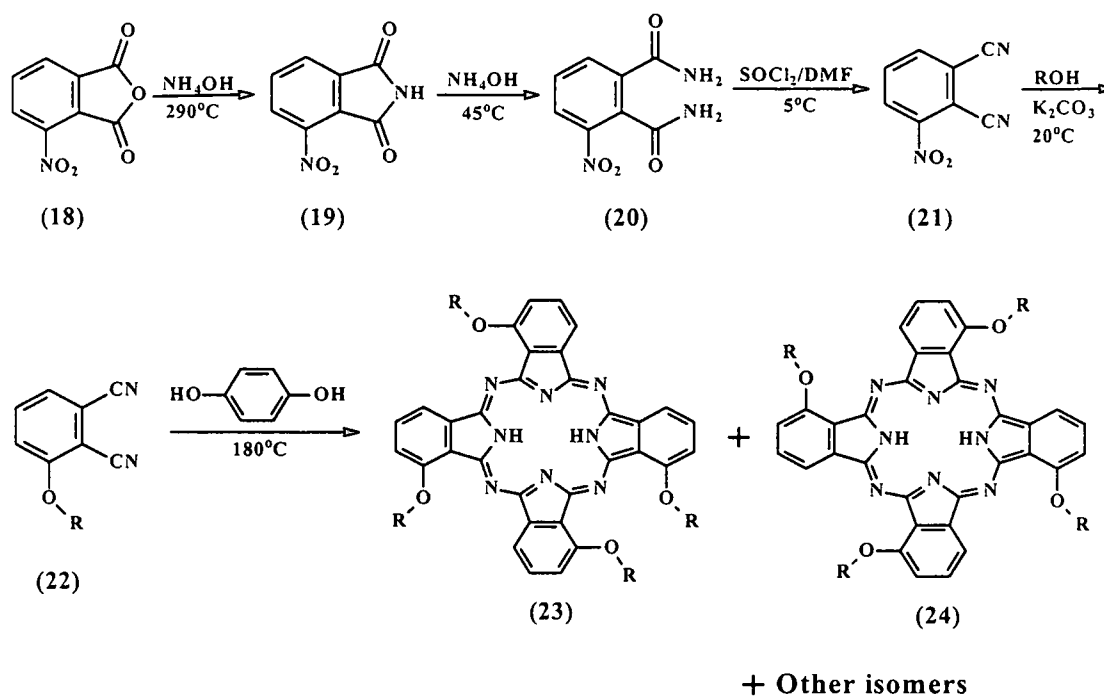
Scheme 2.5: Four structural isomers of tetra-substituted MPc obtained during the condensation of a mono-substituted phthalonitrile.

The presence of a mixture of isomers has the positive effect of disrupting crystalline order and thus enhancing solubility. It's, however, a disadvantage if a highly ordered bulk material or thin film is required. Phthalocyanines with substituents located on the inner, sterically crowded non-periphery positions of the benzo rings of the macrocycle exhibit different electronic properties than Pcs with substituents attached at the outer periphery carbons of the benzo ring.

In 1995 George and Snow⁶⁰ developed a stepwise method for the synthesis of non-peripherally tetra-alkoxide substituted phthalocyanines (Scheme 2.6).

Commercially available 3-nitrophthalic anhydride, (18) was first reacted with ammonium hydroxide to yield 3-nitrophthalimide, (19). This compound was isolated and reacted with ammonium hydroxide under mild conditions to produce the diamide derivative, (20). The amide was subsequently dehydrated, using SOCl_2 , to yield 3-nitrophthalonitrile, (21). Nitro

displacement with an alcohol or phenol to give an aryl-ether phthalonitrile precursor was finally followed by cyclotetramerisation to the corresponding phthalocyanine, (23).



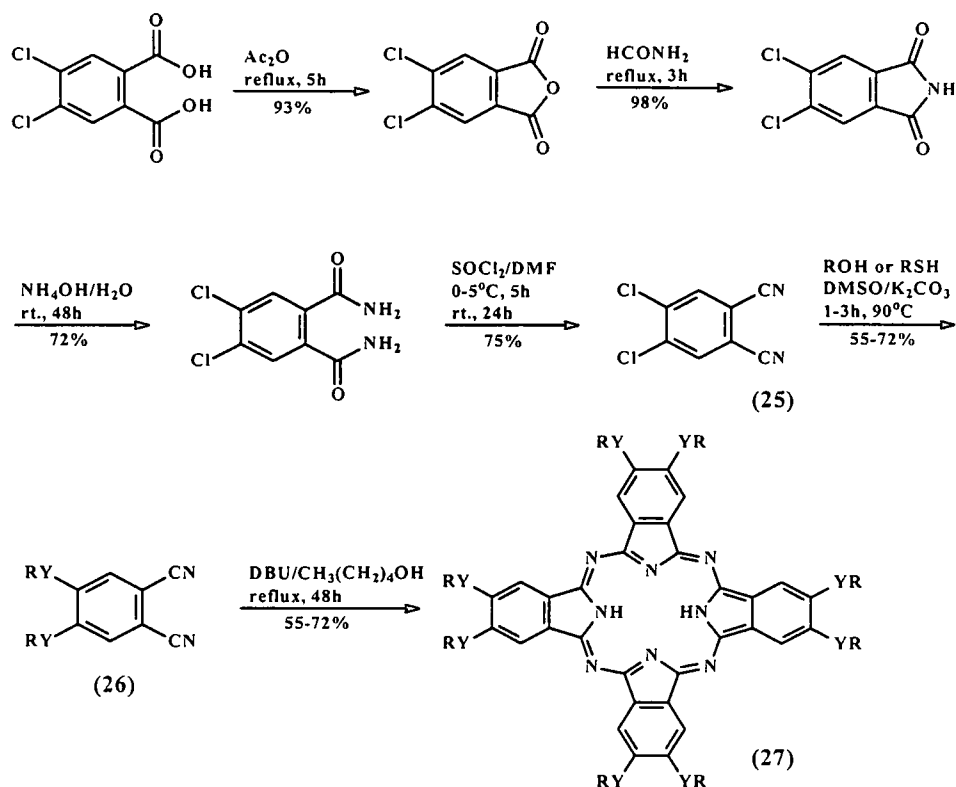
Scheme 2.6: General synthetic route for preparing non-peripheral tetra-alkoxide substituted phthalocyanines.

The 3-nitrophthalonitrile intermediate is a key reagent for synthesis of many alkoxy- and aryloxyphthalonitrile precursors, (22) for the preparation of non-peripheral tetra-substituted phthalocyanines. From statistical considerations, the product is again a mixture of four geometric isomers, however with bulky R groups the isomer (24) tends to dominate for steric reasons. The availability of 3-nitrophthalonitrile as a synthetic precursor provides a means by which many direct structure-property comparisons can be made with derivatives of 4-nitrophthalonitrile.

2.4.2 Octa-substituted phthalocyanines

In contrast to the tetra-substituted phthalocyanines, it is possible to synthesise octa-substituted phthalocyanines as a single isomer with comparative ease. A single-isomer of 2,3,9,10,16,17,23,24 identically substituted phthalocyanine was prepared from appropriate 4,5-disubstituted phthalonitriles by Wöhrle and co-workers.⁶¹ They described an elegant way for the synthesis of 2,3,9,10,16,17,23,24-octa-substituted phthalocyanines by reacting 4,5-dichloro-

phthalonitrile, (25) with O- and S-nucleophiles to obtain the corresponding 4,5-disubstituted phthalonitriles, (26) (Scheme 2.7).

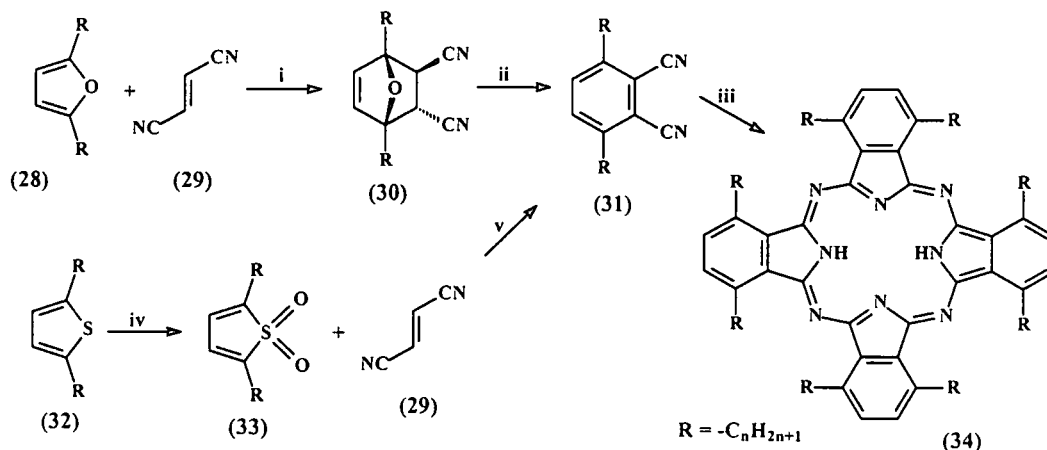


Scheme 2.7: Synthesis of symmetrically peripheral octa-substituted phthalocyanines, Y = O or S, DBU = 1,8-diazabicyclo-[5.4.0]undec-7-ene.

The precursors (26) were then converted into the symmetrically octa-substituted phthalocyanines, (27). These compounds contain free phenolic function or the alkyl chains R (Scheme 2.7). They could be manufactured or processed into thin films by the Langmuir-Blodgett^{57,62} technique, showed mesomorphic liquid crystalline properties⁶³ and zinc complexes may be prepared for PDT.⁶⁴

The synthesis of precursors to non-peripheral substituted phthalocyanines is generally much more difficult and the corresponding yields are lower than phthalocyanines with substituents at the outer, less crowded, peripheral positions of the benzoid rings. Cook and co-workers⁵¹ developed two synthetic routes to non-peripheral octaalkyl substituted phthalocyanines, (34). The required precursors, 3,6-dialkylphthalonitriles, (31), are synthesised from the appropriate 2,5-dialkylfuran, (28) or 2,5-dialkylthiophene, (32) (Scheme 2.8). The reaction to obtain phthalonitrile (31) involves a Diels-Alder cycloaddition reaction between the five membered heterocycles (28) or (33) and fumaronitrile, (29). The thiophene route is more efficient for

simple non-peripheral MPc derivatives but the furan route is more flexible, allowing the preparation of phthalonitriles that contain different R-substituents with greater ease. The same research group found an efficient route to 1,4,8,11,15,18,22,25-octaalkoxy substituted MPcs from the readily available starting material 2,3-dicyanobenzoquinone.⁶⁵

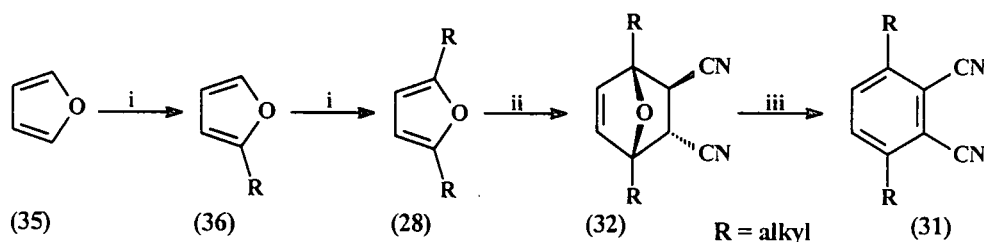


Scheme 2.8: Synthetic routes to non-peripheral octa-alkyl substituted phthalocyanines. *Reagents and conditions:* (i) Acetone, 0°C. (ii) Lithium bis(trimethylsilyl)amide, THF, -78°C, aqueous work-up. (iii) Lithium, refluxing pentanol, aqueous hydrolysis. (iv) 3-Chloroperbenzoic acid, DCM. (v) 200°C.

2.4.3 The synthesis of 3,6-disubstituted phthalonitriles

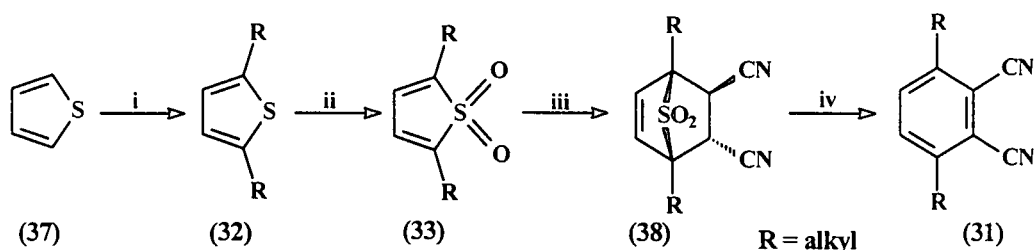
Numerous examples of substituted phthalocyanines appear in the literature. Undoubtedly the challenge of their synthesis lies in the preparation of the appropriately substituted phthalonitrile precursor, rather than the cyclisation into the phthalocyanine. A brief review of the preparation for 3,6-disubstituted phthalonitriles follows.

The potential ease of preparing 2,5-dialkylfurans, (28) and 2,5-dialkylthiophenes, (32), *via* lithiation of the aromatic rings, led to the investigation of the chemistry depicted in Scheme 2.9 and Scheme 2.10.⁵¹



Scheme 2.9: Synthesis of 3,6-dialkylphthalonitriles *via* furan route. *Reagents and conditions:* (i) BuLi, RBr. (ii) Fumaronitrile. (iii) LiN(SiMe₃)₂, THF, -78°C.

The alkylation of furan, (35) was achieved using butyl-lithium in THF initially to deprotonate the furan ring followed by reaction with a bromoalkane. The two-step procedure that gave first the monoalkyl, (36) and then the dialkyl, (28) derivatives was preferred over a one-step dialkylation which invariably gave a mixture of (36) and (28).



Scheme 2.10: Synthesis of 3,6-dialkylphthalonitriles via thiophene route. *Reagents and conditions:* (i) BuLi, RBr. (ii) *m*-chloroperoxybenzoic acid (*m*-CPBA) or NaBO₃ or dimethyldioxirane. (iii) Fumaronitrile, CHCl₃, 150°C, 18 h. (iv) -SO₂, -H₂.

The chemistry in Scheme 2.10 proved technically simpler to undertake once optimum conditions had been established. Chadwick and Willbe⁶⁶ achieved dilithiation of thiophene, (37) within half an hour using two equivalents of butyllithium and *N,N,N',N'*-tetramethylenediamine (TMEDA) in refluxing hexane.

Cook and co-workers^{51,67} found that near-complete disubstitution could be achieved in one step using 2.5 equivalents of butyl-lithium in hexane-THF and longer reaction times. Yields of 94% for 2,5-dialkylthiophene, (32) can be achieved by carrying out the alkylation under argon, and performing the addition of the alkyl halide to the dianion at -78°C. Langner demonstrated that oxidation of (32) to the sulphone derivative can be performed virtually quantitatively with dimethyldioxirane. Other oxidants, such as *m*-chloroperoxybenzoic acid and NaBO₃ invariably gave lower yields.⁶⁸ Solutions of dimethyldioxirane are prepared by oxidising acetone with Oxone® (the Aldrich trade name for 2KHSO₅·KHSO₄·K₂SO₄) in the presence of a base such as potassium bicarbonate.⁶⁹

The Diels-Alder reaction, well suited for synthesising multiply substituted six-membered rings, has been used previously⁷⁰ for the synthesis of 3,6-disubstituted phthalonitriles. In particular, fumaronitrile, (29) has been used as a dienophile in reactions with various conjugated dienes,⁷⁰ the products being subsequently dehydrogenated over sulphur. Alternatively, dicyanoacetylene has been added across both furans⁷¹ and thiophenes.⁷² The Diels-Alder reaction of furans with dienophiles is reversible and adduct formation is encouraged using high pressure or, for reactions performed under normal pressure, low temperature. For the purpose of this study the

Diels-Alder reaction of 2,5-bis(dodecyl)thiophene-1,1-dioxide, (**33**) with fumaronitrile, extrusion of SO₂, and dehydrogenation of the intermediate to give the phthalonitrile derivative (**31**), all of which proceeded in a one-pot sealed-tube reaction are important. The thiophene route is high yielding and is used in the synthesis of straight alkyl chain derivatives, whereas the inclusion of sensitive functionalities in the side chain R, such as bis-orthoester groups, requires the use of the lower yielding furan route.

2.4.4 Synthesis of unsymmetrically substituted phthalocyanines

Phthalocyanines with lower symmetry show interesting properties in non-linear optics⁷³ and are important materials for Langmuir-blodgett films,⁵⁶ ladder polymers⁷⁴ and liquid crystals.⁹ Recently, a great deal of attention has been paid to the preparation of low-symmetry phthalocyanines and phthalocyanine-related systems,⁷⁵ obtained either by introducing different substituents on the macrocycle ring or by formal substitution of some isoindoline units. For example, such noncentrosymmetric systems can exhibit second-order non-linear optical properties whereas unsubstituted or symmetrical substituted phthalocyanines usually only give rise to third-order responses.⁷⁶ To obtain unsymmetrical substituted phthalocyanines several synthetic strategies can be applied:

- i. The statistical condensation of two different phthalonitriles;
- ii. Ring expansion of subphthalocyanines;
- iii. Synthesis on a polymeric support.

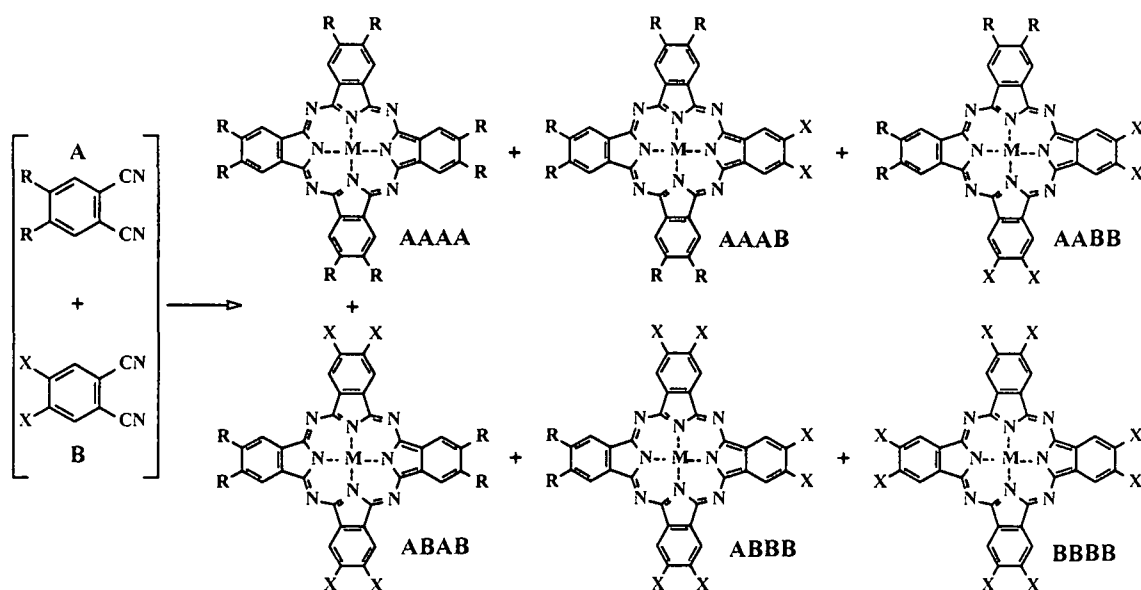
Other less utilised methods include the Meerwein procedure,⁷⁷ the condensation of two different phthalyl precursors⁷⁸ and stepwise synthetic procedures.⁷⁹

2.4.4.1 The statistical condensation of two different phthalonitriles

The most common route to unsymmetrical substituted phthalocyanines involves cyclotetramerisation of a mixture of two (or more) different phthalonitriles (or diiminoisoindolines).⁵¹ Theoretically, for two different phthalonitriles, **A** and **B**, there are six possible products (Scheme 2.11).^{80,81}

To some extent, a reasonable yield of a particular unsymmetrical phthalocyanine can be obtained by controlling the relative amount of the two precursors **A** and **B**. However, in

practice mixed phthalonitrile reactions always lead to significant quantities of at least two phthalocyanines that require separation.



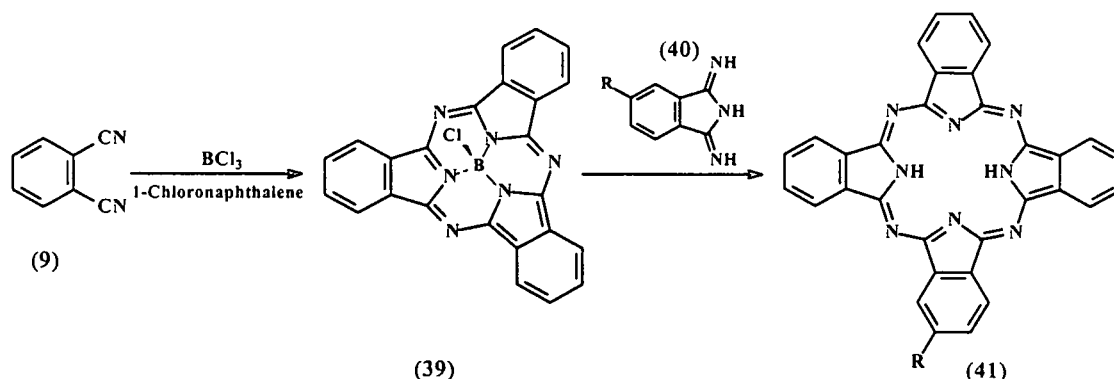
Scheme 2.11: Six different unsymmetrically substituted phthalocyanines **AAAA**, **AAAB**, **ABAB** etc. obtained when two different substituted phthalonitriles **A** and **B** are cyclotetramerized.

When the two types of substituents X and R of the precursors **A** and **B** (Scheme 2.11) are sufficiently different in polarity (*e.g.* R = alkyl, X = alkoxide),⁸⁰ the resulting phthalocyanines will possess different chromatographic properties that will allow easy separation.

In order to favour the formation of the **A₃B** derivative for example, an appropriate stoichiometric ratio of the two reactants **A** and **B** have to be chosen. Statistical considerations⁷⁷ predict that the reaction of two different phthalonitrile derivatives of the same reactivity in a 3:1 ratio will afford a mixture of products in the following percentages: **A₄** (33%), **A₃B** (44%) and other cross-condensations products (23%). When precursors **A** and **B** are mixed and reacted in a 9:1 ratio, product distribution is 66% **A₄**, 29% **A₃B** and only 5% of the other isomers, thus the mixture of products can more easily be separated to produce pure **A₃B**. This 9:1 stoichiometry is also useful when **B** is much more reactive than **A**, because it reduces the yields of products with more than one **B** subunit.^{73c} A procedure that reduces the number of possible phthalocyanines and also suppresses the aggregation between them involves the use of a phthalonitrile (**A**) bearing bulky and rigid groups, *e.g.* tert-butyl, in the 3,6-positions, in conjunction with another phthalonitrile lacking bulky substituents (**B**).⁸²

2.4.4.2 Ring expansion of subphthalocyanines (SubPc)

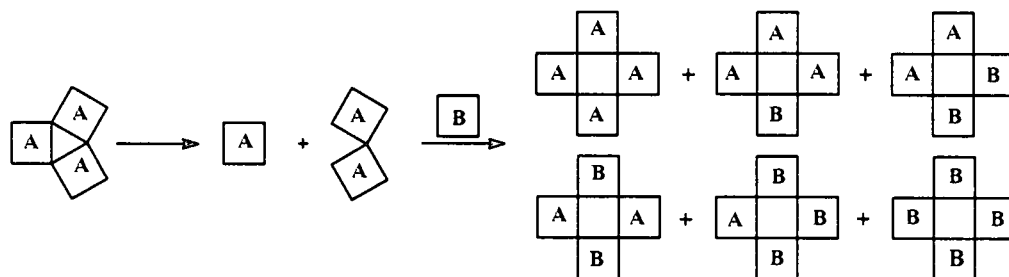
The second method for the synthesis of unsymmetrically substituted phthalocyanines involves a ring expansion reaction of a subphthalocyanine,⁸³ (39) by treating it with a mono-substituted diiminoisoindoline, (40) derivative to yield (41) (Scheme 2.12).



Scheme 2.12: Synthesis of a mono-functional phthalocyanine, (41) *via* ring expansion of SubPc, (39).

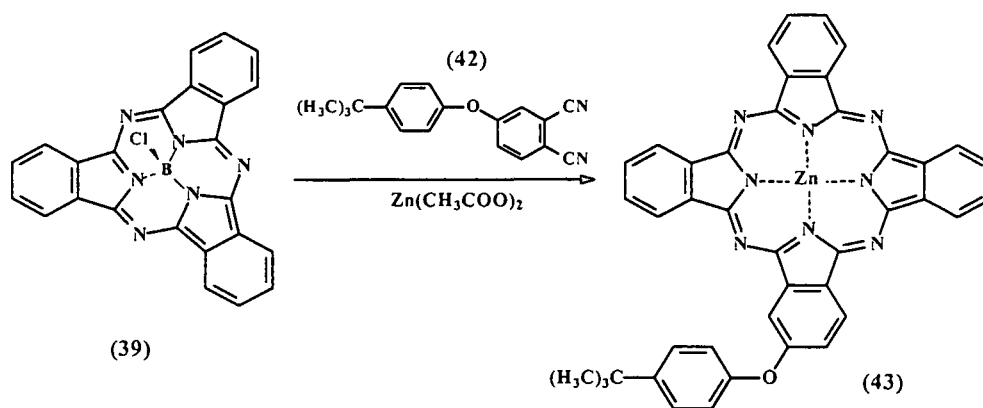
The geometrically constrained subphthalocyanine core is readily cleaved in the presence of a diiminoisoindoline unit, which is then incorporated into its framework so as to form a phthalocyanine derivative of type A_3B .^{84,85,86} The outcome of this synthetic method depends very much on the reaction conditions and on the characteristics of the starting material.

In 1995 Torres and co-workers⁸⁵ suggested that the reaction proceeds through partial or total fragmentation of a subphthalocyanine followed by statistical ring closure, giving rise to a mixture of all possible phthalocyanines containing all the combination of diiminoisoindoline units present in the starting materials (Scheme 2.13).



Scheme 2.13: Fragmentation of a subphthalocyanine to form all possible phthalocyanines.

Wöhrle and co-workers⁸⁴ showed that the addition of a metal template to the reaction mixture increases the yield of the products and that the subphthalocyanines can react with the less reactive phthalonitrile (rather than isoindoline) derivatives in the presence of a strong base such as DBU, giving rise to good yields of the A_3B phthalocyanine (Scheme 2.14).

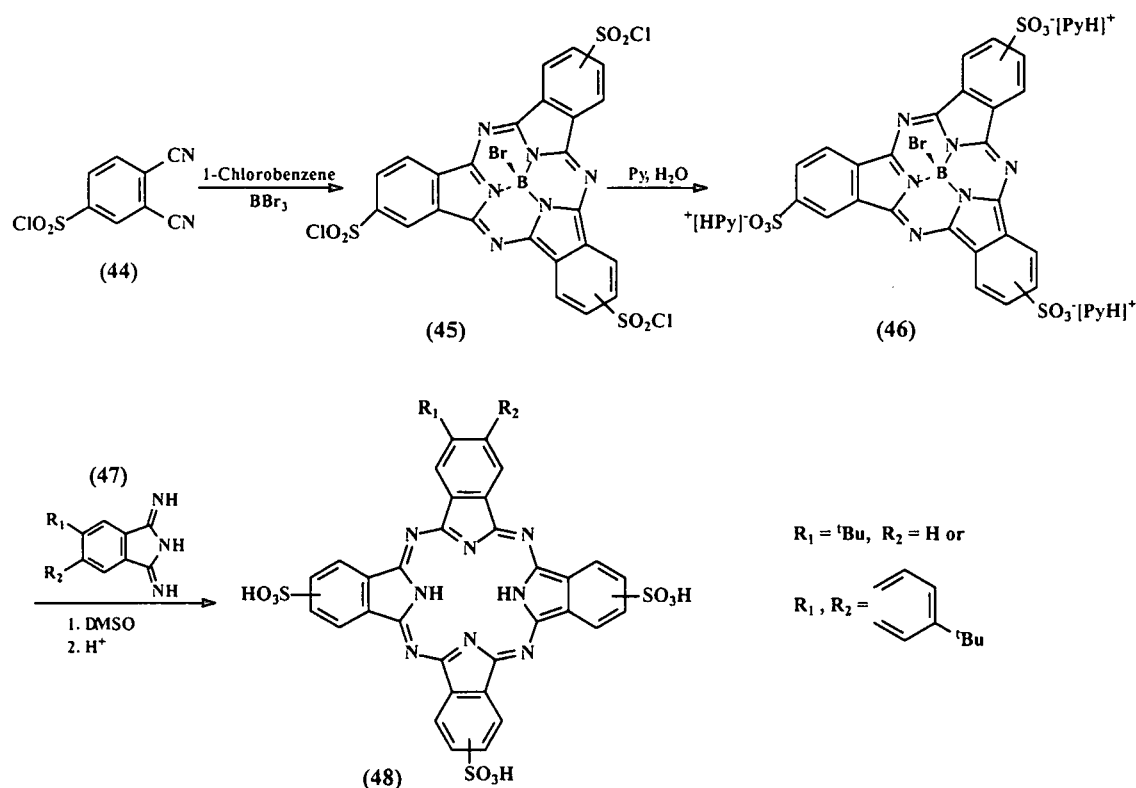


Scheme 2.14: Synthesis of an unsymmetrical substituted ZnPc, (43) *via* ring expansion of a SubPc.

The reaction was carried out in the presence of zinc acetate dihydrate as template in order to provide selectivity for the formation of mono-substituted phthalocyanines and to get a metallated phthalocyanine in a one-step procedure. The reaction of subphthalocyanines with substituted diiminoisoindolines in the presence of a zinc salt results in higher percentages of tetra-substituted phthalocyanines because diiminoisoindolines undergo cyclotetramerization with the salt. The reaction of (39) with (42) in the presence of a zinc salt leads to much higher yields of phthalocyanines in total (40%), but also to a relative high amount of di-, tri-, and tetra-substituted phthalocyanines. Their formations can be reduced by catalytic amounts of DBU and pentanol and higher reaction temperatures because this increased the rate of the ring-opening reaction of (39). By this procedure the best yields of the mono-substituted ZnPc, (43) in the product mixture as determined by HPLC was obtained.

Recently, Kudrevich and co-workers⁸⁷ synthesised a water-soluble unsymmetrical substituted phthalocyanine using a subphthalocyanine intermediate (Scheme 2.15).

They synthesised tris(4-chlorosulphonyl)SubPcB(Br) (>60% yield), (45) from the reaction of 4-(chlorosulphonyl)phthalonitrile, (44) and commercially available BBr_3 in DCM. The chlorosulphonyl moieties were protected from hydrolysis by dissolving it in a mixture of water/pyridine (2:1) and converted to the pyridinium salt (46). The reaction of (46) with diiminoisoindoline derivative, (47) occurred at temperatures lower than those required for similar ring expansions reported earlier^{83,84,85} to form the unsymmetrical mono-substituted metal-free phthalocyanine, (48).



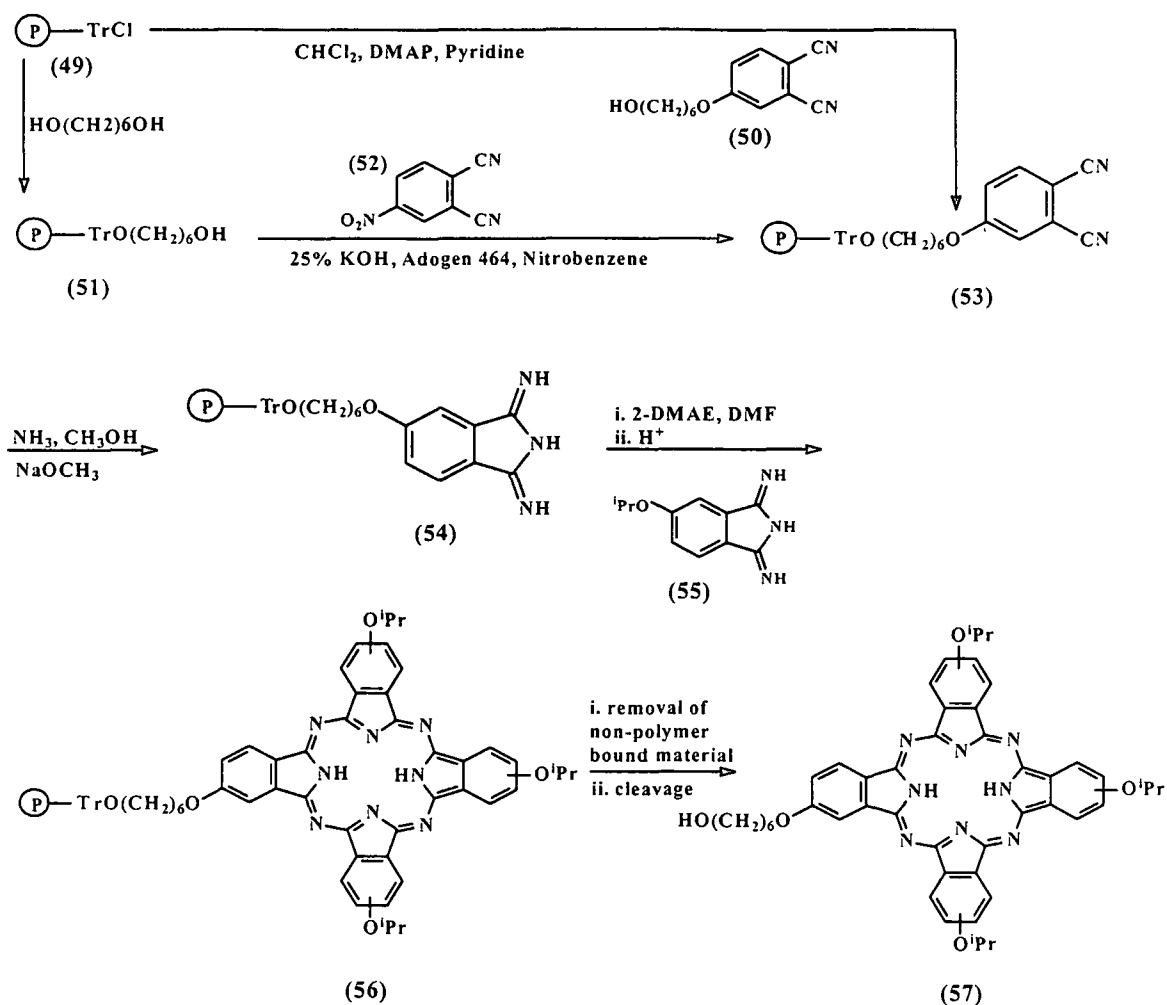
Scheme 2.15: Synthesis of a water-soluble unsymmetrical substituted phthalocyanine, (48).

2.4.4.3 Synthesis on a polymeric support

Another approach for the preparation of unsymmetrically substituted phthalocyanines, mainly developed by Leznoff, is the solid phase polymer support synthesis.^{47,88} This method involves the attachment of an appropriate substituted phthalonitrile (**B**) to a polymeric support. This insoluble polymer-bound precursor can then be treated with another different substituted unbound phthalonitrile (**A**) giving rise to a polymer-bound A_3B phthalocyanine. This can be easily separated from the A_4 macrocycle since the symmetrical phthalocyanine can be washed away. The desired A_3B phthalocyanine is subsequently liberated from the polymer support by chemical cleavage.

Leznoff et al. used polymers with pendant alcohol groups and has treated these with 4-nitrophthalonitriles. Further cleavage at the pendant chain furnishes the unsymmetrical phthalocyanine in yields of around 20-25%. For example, in 1982 Leznoff and co-worker⁴⁷ synthesised a soluble, unsymmetrical phthalocyanine on a polymer support (Scheme 2.16).

They used a 1% crosslinked divinyl benzene-styrene copolymer, (49) in the preparation of the unsymmetrical 2-(6'-hydroxyhexoxy)-9,16,23-triisopropoxyphthalocyanine, (57), which are soluble in common organic solvents.



Scheme 2.16: Synthesis of an unsymmetrical phthalocyanine on a polymer support. O^iPr = isopropoxy, TrCl = trityl chloride, P = polymer, 2-DMAE = 2-dimethylaminoethanol and DMAP = *p*-*N,N*-dimethylaminopyridine.

The polymer-bound phthalonitrile, (53) was first prepared and reacted with an excess of a substituted diiminoisoindoline, (55). The dark green-black insoluble reaction residue, which *inter alia* contains (56) was extracted with DCM to remove any absorbed tetra-isopropoxy-phthalocyanine. The insolubility of the polymer, (56) allowed the authors to 'fish out' the unsymmetrical phthalocyanine bound to the polymer from a sea of polysubstituted phthalocyanines in solution. After hydrolyses of the isolated polymer, (56) and extraction of the polymer with DCM, (57) was obtained as a deep blue solid, in 24% yield. This approach is restricted to the use of phthalonitriles bearing functional groups that can be bound to the polymer and subsequently cleaved from it.

2.5 Ferrocene compounds

2.5.1 Introduction

One of the goals of this study is to synthesise a ferrocene/phthalocyanine conjugate to obtain a compound consisting of a ferrocenyl fragment and phthalocyanine fragment covalently linked to each other. It is anticipated that potential synergistic antineoplastic effects may be obtained as a result of the chemotherapeutic action of the ferrocenyl group,⁸⁹ and the photodynamic activity of the phthalocyanine moiety. Ferrocene (Fc) is an organometallic compound of exceptional chemical and thermal stability. Ferrocene, (58) has a remarkable geometry in that it possesses a sandwich structure in which the two cyclopentadienyl rings lie parallel to one another and the iron cation is buried in the π -electron cloud between them. Two conformations (Figure 2.6) are possible for ferrocene, one in which the cyclopentadienyl rings (Cp rings) are in the eclipsed (D_{5h} symmetry) conformation and the other in the staggered (D_{5d} symmetry) conformation. Although the energy to cyclopentadienyl ring rotation is less than 4 KJ mole⁻¹, many substituted ferrocene derivatives are in the eclipsed conformation.

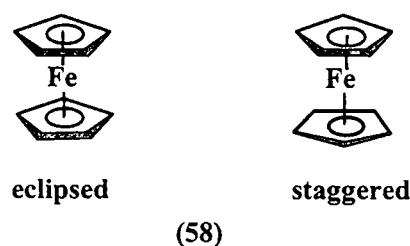
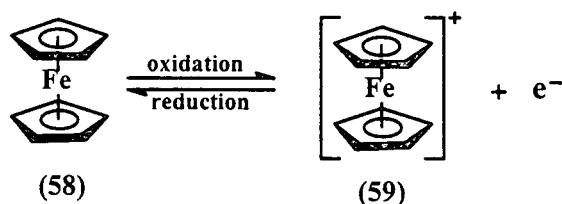


Figure 2.6: The eclipsed and staggered conformations of ferrocene, (58).

The iron nucleus of ferrocene is involved in reversible electrochemical processes (Scheme 2.17).



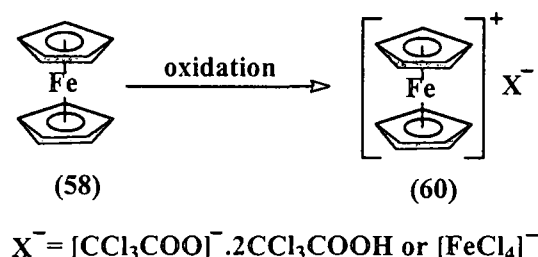
Scheme 2.17: Reversible electrochemistry of ferrocene, (58).

Compound (59) represents an oxidised Fe^{III} complex with an overall charge of +1. It actually represents an inorganic radical species that has appreciable activity in terms of electron-transfer processes.

Some applications of ferrocene include the following: It can be used as high burning rate catalysts in solid propellants,⁹⁰ yellow and orange pigments,⁹¹ smoke depression additives,⁹² catalysts in conjunction with, for example, palladium in C-C bond formation⁹³ and as chemotherapeutic drugs.⁸⁹

2.5.2 Ferrocene compounds as chemotherapeutic drugs

In 1984 Köpf-Maier was the first to report on the antineoplastic activity of some ferrocenium salts against Ehrlich ascites tumor (EAT) cell lines, which are resistant to classical antitumor agents.⁸⁹ The ferrocenium salts, (60) were obtained *via* the oxidation of ferrocene, (58) according to Scheme 2.18.



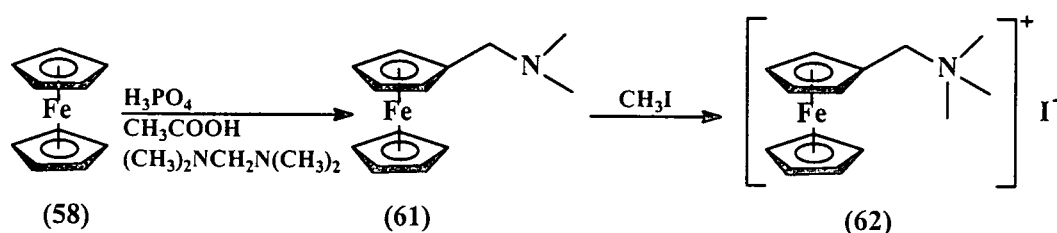
Scheme 2.18: The synthesis of some ferrocenium salts from ferrocene.

It was shown that trichloroacetate gave the best pharmaceutical results of all the ferrocenium salts used, with a 50% lethal dosage (LD_{50}) value of 480 mg/kg tested animal (mice) and a therapeutic index (TI) value of 2.0. Cisplatin also has a TI value of 2.0. Unsubstituted ferrocene does not display any anti tumor inhibiting activity, presumably due to its total lack of aqueous solubility.

In the earlier parts of this chapter the mechanism of action of the phthalocyanine moiety in PDT has been elucidated. The chemotherapeutic mechanism of action of the ferrocenyl moiety has been well described by Osella et al.⁹⁴ and involves the generation of a hydroxyl radical by the action of *in situ* generated ferrocenium cation radical on oxygen and water. The hydroxyl radical leads to irreparable DNA damage (cutting) and ultimately cell death.

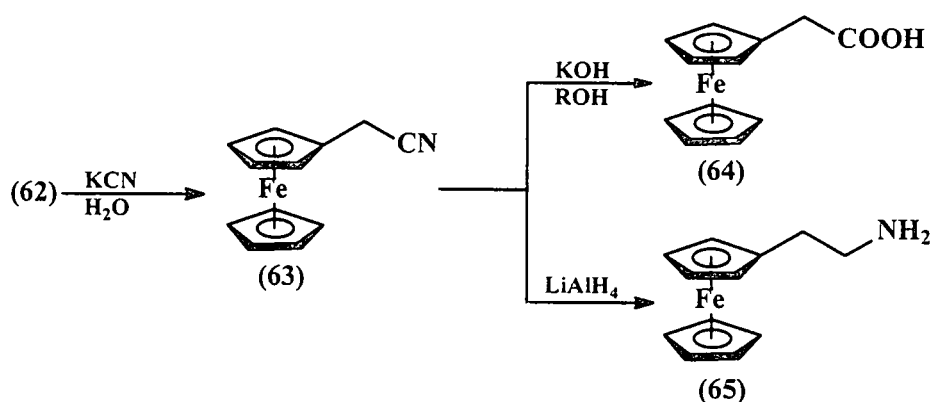
2.5.3 Synthesis of ferrocenyl derivatives

One of the goals of this study is to synthesise a ferrocenyl-phthalocyanine conjugate. In order for ferrocene to be anchored onto a phthalocyanine macrocycle, a suitably functionalised ferrocenyl derivative has to be synthesised. There are several extensive reviews on the general organic chemistry of ferrocene available.⁹⁵ With regard to this thesis, the aminomethylation of ferrocene to form *N,N*-dimethylaminomethylferrocene, (61)⁹⁶ is a particularly important reaction. Methylation of the amino group of (61) with methyl iodide to form the quaternary ammonium salt (62),⁹⁷ a compound that contains a good leaving group, trimethylamine, that can be displaced by the attack of many nucleophiles (Scheme 2.19).



Scheme 2.19: Synthesis of *N,N*-dimethylaminomethylferrocene methiodide, (62).

One such an example is the cyanation of *N,N*-dimethylaminomethylferrocene methiodide, (62) with potassium cyanide to generate the ferrocenylacetonitrile, (63) which can either be reduced to ferrocenylethylamine, (65) with LiAlH_4 or saponified (hydrolysed) to ferrocenylacetic acid, (66) (Scheme 2.20).⁹⁸



Scheme 2.20: Synthesis of ferrocenylacetonitrile, (63), ferrocenylacetic acid, (64) and ferrocenylethylamine, (65).

For the purpose of this study ferrocenylacetic acid, (64) was synthesised with the view to investigate the reduction of this acid to obtain a ferrocene-containing alcohol. This alcohol may then be anchored to a phthalonitrile and used as a precursor in the synthesis of ferrocene-containing phthalocyanines.

2.5.4 Synthesis of ferrocenyl-phthalocyanine conjugates

The strategy employed in this thesis to obtain a ferrocenylated phthalocyanine is based on the known reaction between alcohols and nitrated aromatic compounds.⁹⁹

As far as known ferrocenyl-phthalocyanines are concerned (Figure 2.7), the ferrocenylated phthalocyanine (66) was synthesised in moderate yield but further studies on this compound were hampered due to their poor solubility.¹⁰⁰

Cook and co-workers synthesised ferrocenyl-phthalocyanine (67), which was better soluble with non-periphery substituents and a functional group that connected the phthalocyanine and ferrocenyl moieties by making use of an ester bond¹⁰¹ rather than an amide bond as in (66).

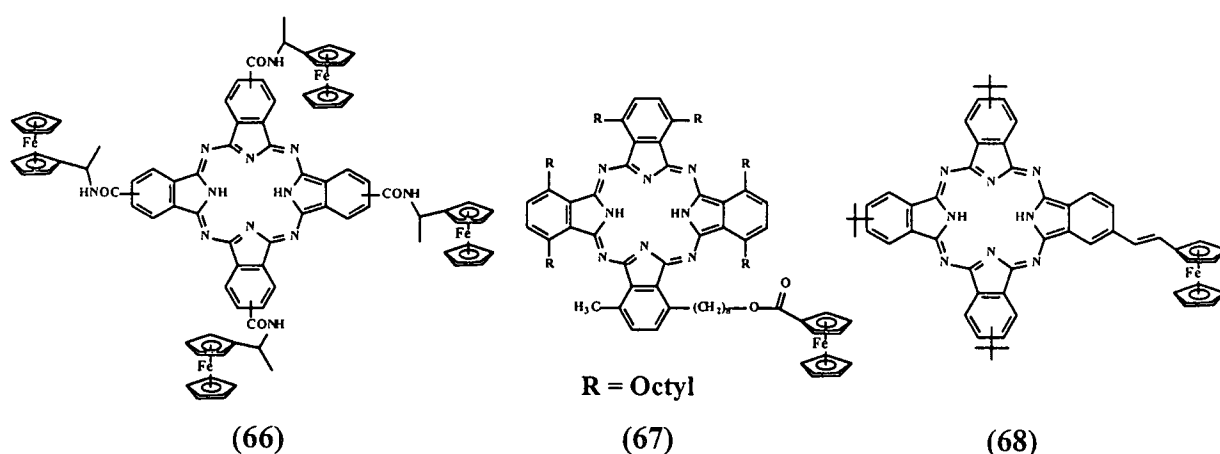


Figure 2.7: Ferrocene-containing phthalocyanines, (66), (67) and (68).

Compound (67) is the first ferrocenyl-phthalocyanine derivative found that display liquid crystalline properties.

Torres and co-workers synthesised ferrocenyl-phthalocyanine (68) with the view of synthesising the first homo-dimetallic ferrocenyl-bridge phthalocyanine.¹⁰²

To enhance the aqueous solubility of compounds resembling (66) Maree¹⁰⁰ synthesised a polymer bound phthalocyanine derivative, (69) (Figure 2.8).

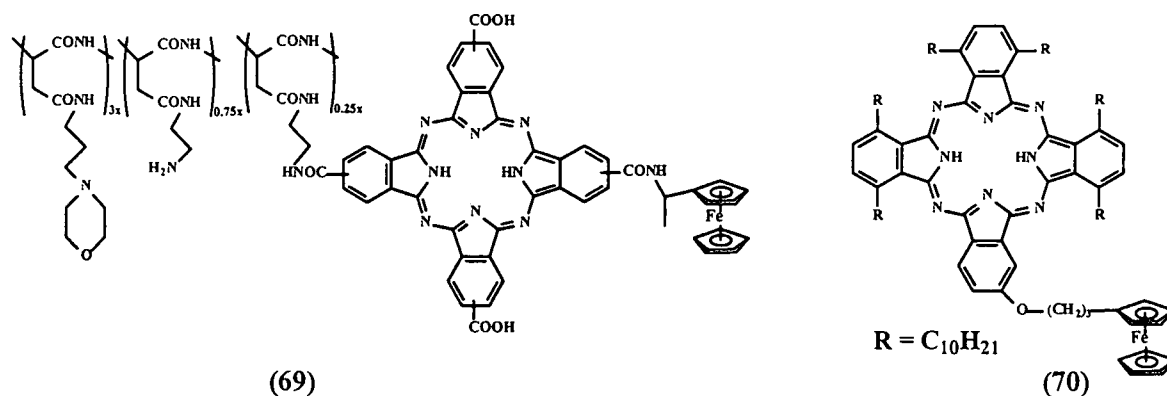


Figure 2.8: Polymer bound ferrocenyl-phthalocyanine, (69) and ferrocenyl-phthalocyanine, (70).

Compound (70) synthesised by Langner is structurally related to the compound that was set as target for this study, except that the substituent chain length is different.¹⁰³ This was done to comply with the goals described in Chapter 1 of this study: to increase the arsenal of available ferrocenylated drugs to determine structural preferences in cancer therapy for this new class of photosensitizer/chemotherapeutic drugs.

2.6 Electrochemical properties of ferrocene and phthalocyanine derivatives

A considerable part of this study concerns the electrochemistry (by means of cyclic voltammetry) of selected and newly synthesised phthalocyanine and ferrocene derivatives. Cyclic voltammetry has established itself as a standard method to investigate the redox properties of electro-active compounds. It is extremely useful in detecting electrochemical reversibility in redox processes.

2.6.1 Electrochemistry of ferrocene and its derivatives

Since the mechanism of action of both the ferrocenyl and phthalocyanine moiety is intimately associated with electron transfer processes, an electrochemical discussion of these two classes of compounds is of importance for this research program. In addition, ferrocene is used as a marker for comparing the electrochemistry of different compounds in different solvents and using different reference electrodes.¹⁰⁴ The electrochemical behaviour of ferrocene and its

derivatives have been reported by many researches. Most of these studies have been examined in organic solvents owing to their poor aqueous solubility. The electrochemistry of the ferrocenyl group is simple and straightforward. The ferrocenyl group can be electrochemically oxidised in a reversible one-electron transfer process to the ferrocenium group. The reduction potential at which this happens depends on the substituents on the cyclopentadienyl rings of the ferrocenyl group. Ferrocene itself is oxidised at 0.077 V vs. a Ag/Ag^+ reference electrode¹⁰⁵ and at 0.365 V vs. an aqueous SCE¹⁰⁶ at 25 °C in acetonitrile.

Electron withdrawing substituents on ferrocene increase the value of the formal reduction potential in the positive direction while electron donating substituents on the ferrocenyl group lead to less positive formal reduction potentials. To demonstrate these phenomena, du Plessis¹⁰⁵ showed that the formal reduction potential of ferrocenyltrifluoroacetone, (71) is 240 mV more positive than that of ferrocene, while Ogata and co-workers¹⁰⁶ demonstrated that the formal reduction potential of [4](1,1')[4](2,2')[4](4,4')- ferrocenophane, (72) is 262 mV less positive than that of free ferrocene (Figure 2.9).

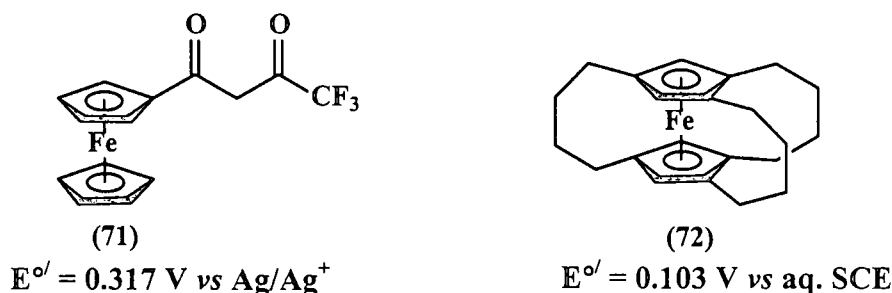


Figure 2.9: Electron withdrawing (71) and electron donating (72) substituents on the ferrocene group.

The cyclic voltammogram of ferrocene-containing β -diketone (71) in acetonitrile is shown in Figure 2.10.

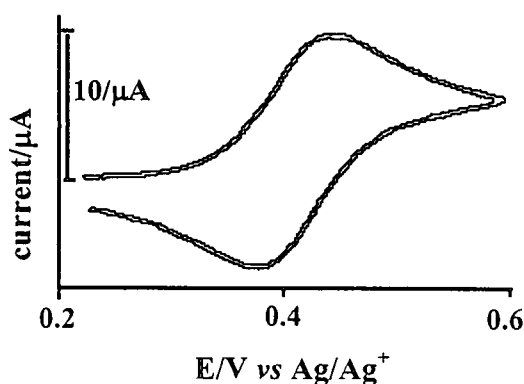


Figure 2.10: CV of (71) in acetonitrile containing 0.1 M tetra-*n*-butylammonium hexafluorophosphate as supporting electrolyte at 25°C on a Pt working electrode, recorded at a scan rate of 50 mVs⁻¹.

In aqueous solutions, ferrocenes are also oxidised to ferrocenium ions. Electrochemistry of ferrocenes solubilised in micellar solution showed that ferrocene molecules are incorporated as micelles that readily transfer electrons with platinum electrode. Cyclic voltammetric data indicate that the electron-transfer is also reversible.¹⁰⁷

2.6.2 Electrochemistry of phthalocyanines

The electrochemistry of phthalocyanines is very rich with as many as six ring-based redox processes. Incorporation of different metals into the core of the phthalocyanine ring and variations in the substituents on the periphery of the ring result in complexes with different properties.¹⁰⁸ Redox processes occurring in metal-phthalocyanine complexes may be centered at the phthalocyanine ring or at the central metal and are effected by several factors¹⁰⁹ such as:

- i) the nature of the substituents on the phthalocyanine ring;
- ii) the nature and oxidation state of the central metal and
- iii) the nature of the axial ligands and/or solvents co-ordinated to the central metal.

To illustrate a typical ring based redox process the cyclic voltammogram of zinc(II)tetraneopentoxypthalocyanine (ZnTnPc)¹¹⁰ in 1,2-dichlorobenzene is shown in Figure 2.11.

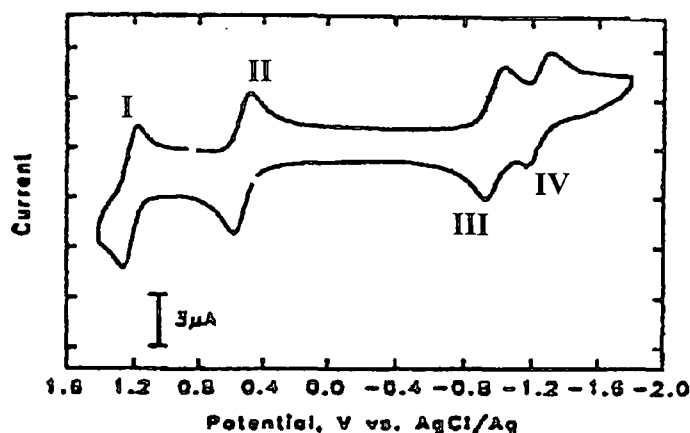


Figure 2.11: Cyclic voltammogram of zinc(II)tetraneopentoxypthalocyanine in 1,2-dichlorobenzene containing 0.2 M tetrabutylammonium perchlorate (TBAP) vs. Ag/AgCl.

Four ring-based redox processes were observed. Two oxidation couples at 1.23 V and 0.55 V that correspond to two one-electron removals from the phthalocyanine macrocycle and thus the formation of the π -cation species, $[\text{ZnTnPc}]^{+•}/[\text{ZnTnPc}]^{2+}$ (couple I) and $[\text{ZnTnPc}]/[\text{ZnTnPc}]^{+•}$ (couple II) respectively. The two reduction couples at -0.98 V and -1.24 V correspond to two one-electron additions to the phthalocyanine macrocycle and thus the formation of the π -anion species, $[\text{ZnTnPc}]^{-•}/[\text{ZnTnPc}]$ (couple III) and $[\text{ZnTnPc}]^{2-}/[\text{ZnTnPc}]^{-•}$ (couple IV) respectively.

Langner found that the metal-free and zinc-containing phthalocyanines with octadecyl substituents on the non-peripheral positions exhibited four ring-based redox processes in the potential range -1.8 to 1.2 V vs. a Ag/Ag^+ electrode in dichloromethane or 1,2-dichloroethane.⁶⁸ The redox processes of the zinc complexes were not as well defined as those of the metal-free phthalocyanines. The redox processes of these phthalocyanines are demonstrated in the equation in Figure 2.12.

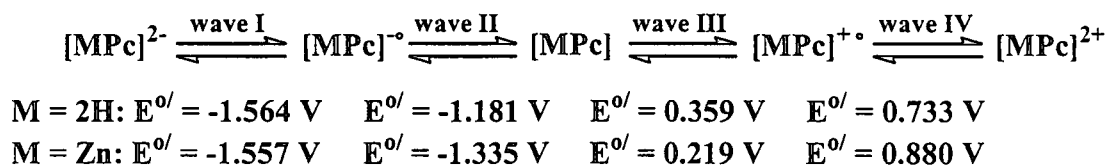


Figure 2.12: Redox processes associated with ring-based electron transfer couples and average formal reduction potentials, E° for $(\text{C}_{10}\text{H}_{21})_8\text{-MPc}$ ($\text{M} = 2\text{H}$ or Zn) at a scan rate of 50 mV s^{-1} vs Ag/Ag^+ .

Zinc is a redox inactive metal. Redox active metals can display additional redox processes in this region. For cobalt complexes for example the position of the metal redox processes is dependent whether the solvent is coordinated or not to the metal. The oxidation of cobalt in cobalt(II) tetrasulphonated phthalocyanine occurs at lower potentials than the oxidation of the phthalocyanine macrocycle¹¹¹ in the MPc^+/MPc couple.

2.6.3 Electrochemistry of ferrocenyl-phthalocyanine conjugates

In 1994 Jin and co-workers¹¹² investigated the electrochemical properties of metal-free peripherally substituted 2, 9,16,23-tetraferrocenylphthalocyanine, $(\text{Fc})_4\text{-2HPc}$, (73).

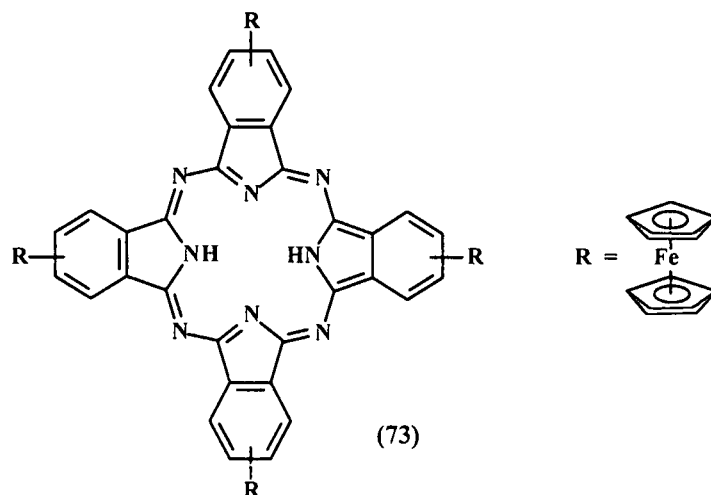


Figure 2.13: Structure of metal-free peripherally substituted tetraferrocenylphthalocyanine, $(\text{Fc})_4\text{-2HPc}$, (73).

The cyclic voltammogram, with a table of assignments for redox couples, of (Fc)₄-2HPc, (**73**) in dichloroethane is shown in Figure 2.14.

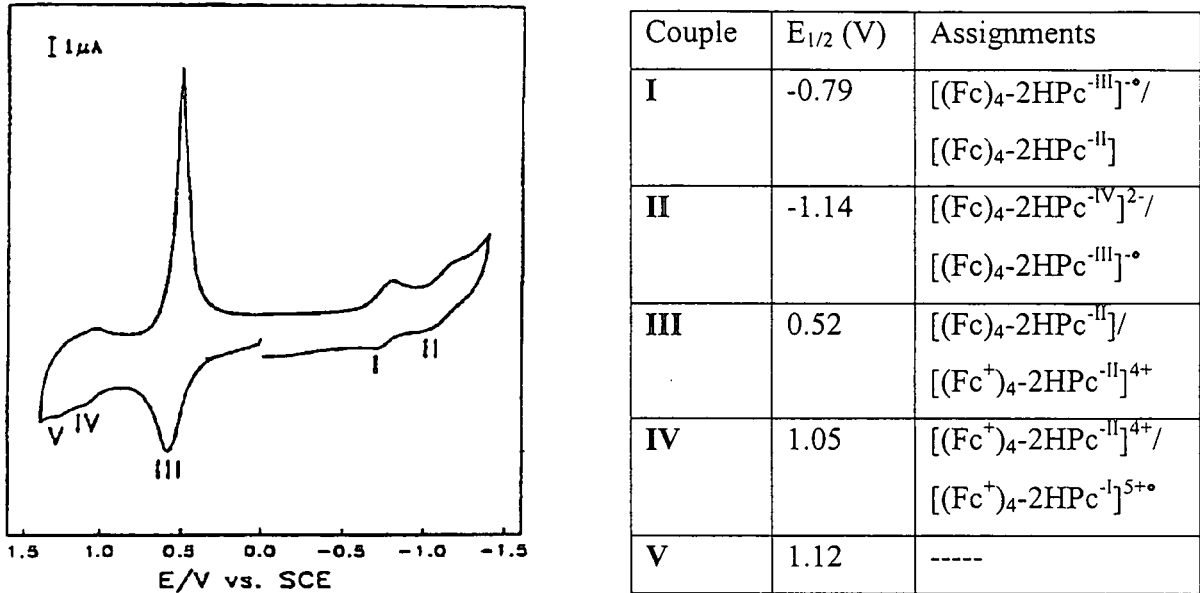


Figure 2.14: Cyclic voltammetry of (Fc)₄-2HPc, (**73**) in DCE containing 0.1 M (tBu)₄⁺NPF₆ as supporting electrolyte on a platinum wire electrode at a scan rate of 200mV s⁻¹.

Two reversible reductions (couples **I** and **II**) are observed at E_{1/2} = -0.79 and -1.14 vs. SCE (Figure 2.14). The difference between the first and second reductions of (**73**) is 0.35 V, which compares to an average separation of 0.35 ± 0.05 V for the first and second reduction processes metal-free phthalocyanine¹¹³ at the phthalocyanine π-ring system. These two couples are unequivocally assigned to successive ring reduction processes, namely, couple **I**, [(Fc)₄-2HPc^{-III}]^{•-}/[(Fc)₄-2HPc^{-II}] and couple **II**, [(Fc)₄-2HPc^{-IV}]²⁻/[(Fc)₄-2HPc^{-III}]^{•-} respectively (see Table in Figure 2.14). The first reduction potential lies between that of unsubstituted metal-free phthalocyanine (2HPc) and that of tetraneopentoxypthalocyanine (TN2HPc) suggesting that the effect of the ferrocene units is to transfer some small amount of additional charge density to the ring, relative to a hydrogen atom. (Fc)₄-2HPc, (**73**) displays one prominent oxidation couple (**III**), with a sharp cathodic component, E_{pc} 0.49 V, and a well defined anodic component, E_{pa} = 0.57 V. The cathodic wave for **III** has a shape clearly indicative of a desorption wave. Evidently the oxidation product at couple **III** is insoluble in dichloroethane and deposits on the electrode. The insolubility of species containing multi-Fc⁺ units has been previously noted.¹¹⁴ There are additionally, two redox couples, (**IV** and **V**) between 1.0 V and 1.4 V. The difference between **IV** and **I** is 1.84 V, which compares to the difference of 1.80 V between the first-step reduction and the first-step oxidation for metal-free tetraneopentoxypthalocyanine.¹¹⁵ Therefore it is reasonable to assign **IV** to the first-step

oxidation of phthalocyanine ring,¹¹³ forming $[(\text{Fc}^+)_{4-2\text{HPc}}^{-1}]^{5+}$. There is no coupling between the ferrocene units in the ground state of (73) present, and the four ferrocene units are oxidised at the same potential. The difference between IV and V is only 0.07 V, so V cannot be the second-step phthalocyanine ring oxidation to Pc^0 .^{113,115} Ring oxidised Pc^{-1} species are known to dimerise,¹¹⁶ and hence oxidation of mononuclear and binuclear species is probably observed.

Ng and co-workers¹¹⁷ have studied the electrochemistry of a series of phthalocyanines containing 4 and 8 (non-peripheral) as well as 16 (both peripheral and non-peripheral) 2-ferrocenylethoxy moieties. These ferrocenyl-phthalocyanine conjugates revealed that all the ferrocenyl redox centers attached to the macrocyclic core are electrochemically independent and undergo an oxidation at the same potential. All the cyclic voltammograms of these ferrocenyl-phthalocyanine conjugates showed a quasi-reversible oxidation attributed to the ferrocenyl units together with one to two quasi-reversible oxidations and up to three quasi-reversible reductions due to the phthalocyanine π system.

2.7 UV-Visible spectroscopy of phthalocyanines

The remarkably strong absorption of light by phthalocyanines to give clear blue and green colours led to their use as pigments and dyes soon after their discovery and is still of immense commercial importance. Phthalocyanines show strong absorption in the visible region (Q-band) for metal-free (2HPc) and metal-containing (*e.g.* CuPc) phthalocyanines (Figure 2.15).

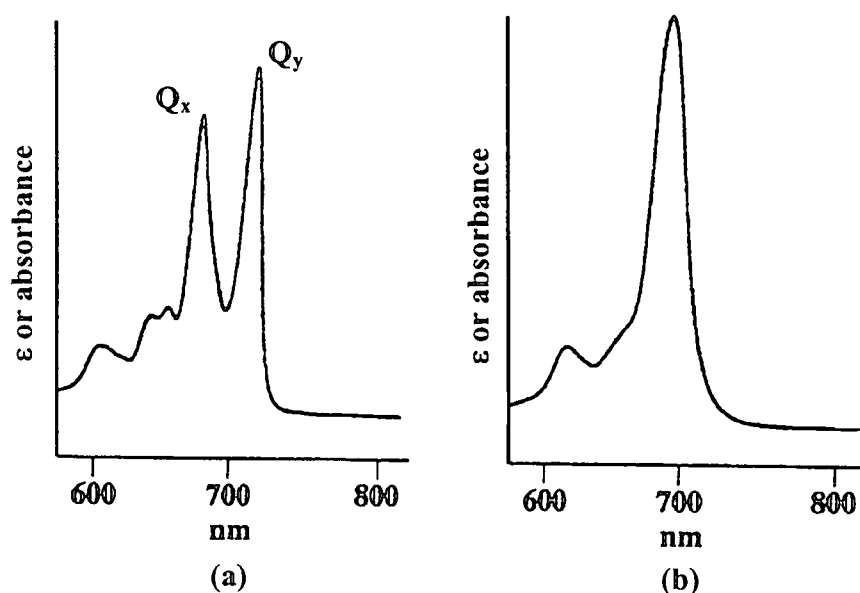


Figure 2.15: The visible absorption spectra of solutions of (a) 2HPc and (b) CuPc.

In both cases there is a strong absorption between 670 and 690 nm (Q-band). In addition there is a strong absorption band in the ultra-violet (UV) region between 320 and 370 nm (not shown in Figure 2.15), denoted as the Soret band. The former, Q-band, absorption is responsible for the characteristic intense blue (or blue-green) colour of the compound. The Q-band is particularly sensitive to substitution and environment of the phthalocyanine macrocycle. The low intensity bands at shorter wavelengths than the Q-band, *ca.* 600 nm are vibrational overtones of the Q-band. It is known that aggregation of phthalocyanines in solution significantly lowers the extinction coefficients, ϵ of solutions of these compounds.^{51,67,118} A typical value for the extinction coefficient of the intense Q-band is around $1 \times 10^5 \text{ dm}^3 \text{ mol}^{-1} \text{ cm}^{-1}$.

Metal-free and metal-containing phthalocyanines differ in having D_{2h} and D_{4h} symmetry respectively and this is manifested in differences especially in the Q-band region. Metallated phthalocyanines show a single intense maximum at about 700 nm. However, degeneracy of the lowest energy singlet state of the metallated derivatives is lifted in the metal-free derivatives. This leads to a splitting of the Q-band into a Q_x and Q_y component. The splitting of the Q-band of 2HPc is lost on deprotonation, using a strong base to form the Pc^{2-} anion, which also has D_{4h} symmetry. In addition, the position of the Q-band in the absorption spectrum of phthalocyanines is modified to some extent by the central metal ion. Distinct metal-to-ligand charge-transfer (MLCT) bands owing to excitation from the atomic orbitals of the metal ion to the ligand's molecular orbitals, or *vice versa*, is also possible.¹¹⁹ Non-peripheral substitution,¹²⁰ in particular, can influence greatly the energy levels of the molecular orbital and hence the absorption spectrum (Table 2.1).

Table 2.1: Q-band positions in the visible absorption spectrum of phthalocyanines in solution.

No.	Phthalocyanine (Pc)	λ_{max} (nm)	Reference
1	2HPc	699, 655	Sharp and Lardon (1968) ¹²¹
2	(C ₁₆ H ₃₃) ₈ -2HPc, peripheral	704, 668	Clarkson <i>et al.</i> (1995) ⁸⁰
3	(C ₆ H ₁₃) ₈ -2HPc, non-peripheral	725, 695	McKeown <i>et al.</i> (1990) ⁵¹
4	CuPc	678	Stillman and Noyokong (1989) ¹¹⁹
5	(OC ₁₂ H ₂₅) ₈ -CuPc, peripheral	675	Van der Pol <i>et al.</i> (1989) ¹²²
6	(OC ₈ H ₁₇) ₈ -CuPc, non-peripheral	752	Cook <i>et al.</i> (1988) ⁶⁵
7	PbPc	702	Stillman and Noyokong (1989) ¹¹⁹

For example, electron-donating groups such as alkoxy moieties (e.g. $\text{OC}_n\text{H}_{2n+1}\text{-CuPc}$) on the non-peripheral positions cause a 70 nm red shift of the Q-band.⁶⁵ In contrast, most peripheral substitutions have very little effect on the Q-band's position (see numbers 4 and 5 in Table 2.1). An exception is when the substituents result in an extension of the π -orbital system by benzoannulation. Thus, the Q-band of naphthalocyanines (Nc) and anthracocyanines (Ac) are shifted to the red light region by approximately 90 and 170 nm respectively.¹²³ Kobayashi and co-workers¹²⁴ showed a good spectroscopic comparison between the absorption spectra of benzoannulated macrocycles (Figure 2.16).

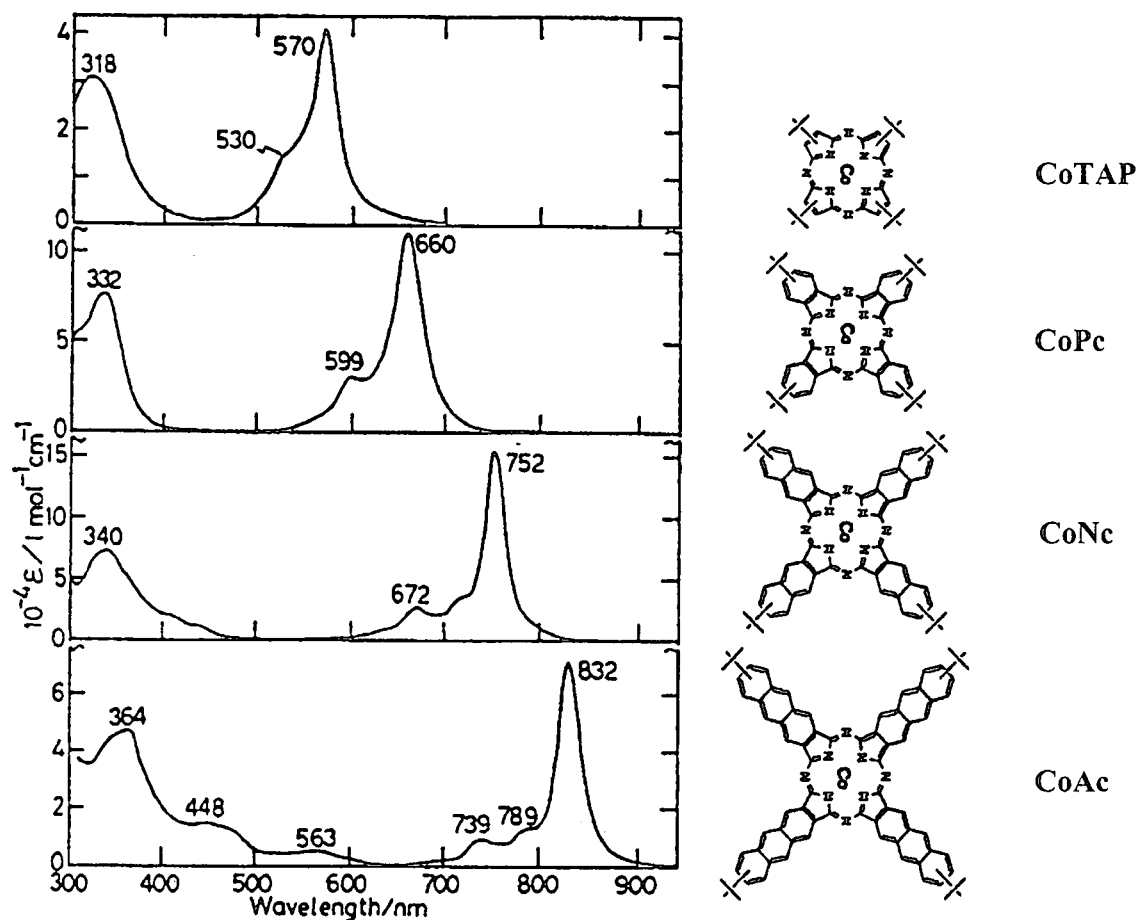


Figure 2.16: UV-Vis-near-IR absorption spectra of CoTAP, CoPc, CoNc and CoAc in pyridine.

Although the Q-band shifts to longer wavelength with expansion of the π -conjugated system, the extent of the shift becomes smaller the larger the size of the macrocyclic ligand. The combination of benzoannulation and non-peripheral alkoxy substituents (e.g. $\text{OC}_n\text{-CuNc}$) pushes the Q-band firmly into the infra-red (IR) region of the spectrum.⁶⁵ Stable IR-absorbing dyes such as these are both rare and of technological importance owing to their ability to absorb

light from compact, cheap semiconductor lasers that produce light of wavelengths in the range 800-1100 nm.

In addition Torres and co-workers have also shown that the position of the Q-band of phthalocyanines changes according to the kind of central metal atom and the type, number and positions of the peripheral substituents.¹²⁵

2.8 Phthalocyanines as discotic liquid crystals

2.8.1 General aspects of liquid crystals

The melting of most crystalline solids involves the abrupt collapse of the positional and orientational order of the lattice array, which marks the onset of essentially free movement of molecules in the isotropic liquid phase. In contrast, for many compounds that have rod-like or disc-like shapes, this process occurs by way of one or more intermediate phases as the temperature is increased (Figure 2.17). This intermediary state is called the liquid crystal state or the mesomorphic state and compounds exhibiting mesophases are called mesogens.

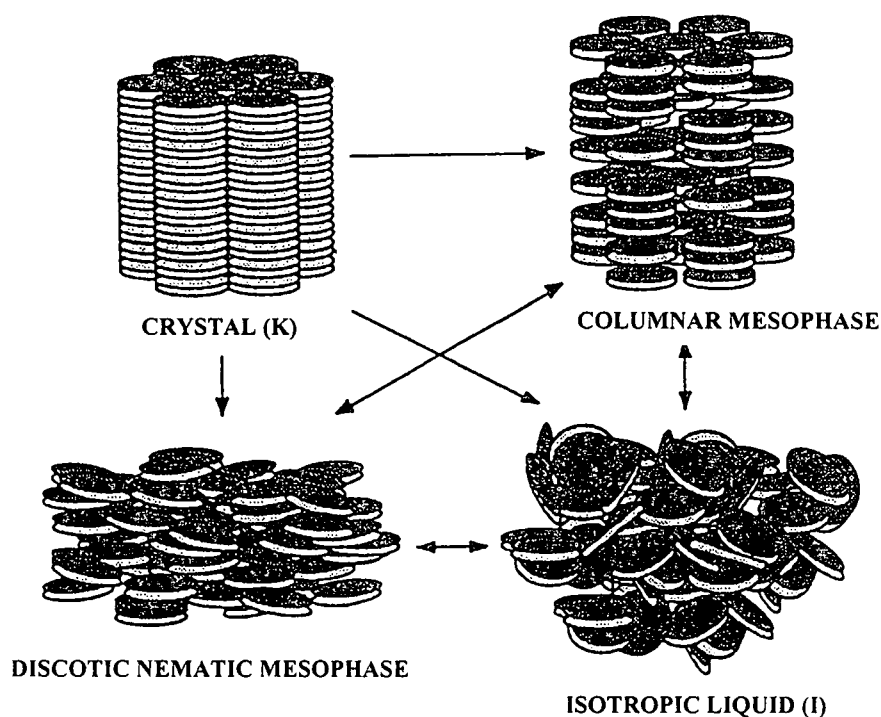


Figure 2.17: Schematic representation of the possible melting processes of mesogenic discotic materials.

In these mesophases, varying degrees of molecular order are retained. Mesophases have properties, which are intermediate between those of the fully ordered crystalline solid and an isotropic liquid. These mesophases can be divided into two main groups: (i) those which are produced by the action of heat on the crystal or cooling to the isotropic liquid are called Thermotropic Mesophases and (ii) those that are generated by the action of a solvent on the solid crystal are called Lyotropic Mesophases. The latter type of mesophases falls outside the scope of this thesis.

Thermotropic mesophases can be further divided and are summarised in Figure 2.18.¹²⁶

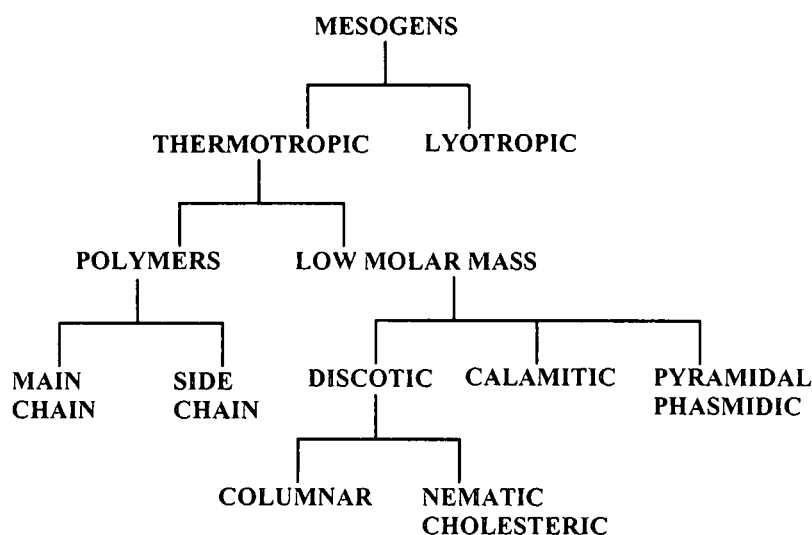


Figure 2.18: Classification of mesophases.

Studies by Destradé have indicated that the structural requirements for a discotic mesophase include a rigid core (generally aromatic) surrounded by flexible side-chains.¹²⁷ In the simplest form the emergence of a mesophase from the crystal can be attributed to the melting of the side-chains, which yield an array of core discs that orient themselves with respect to each other, generating the discotic liquid crystalline state. The degree of order of the molecules within the columns, and the symmetry of the resulting two-dimensional lattice are indicative of the type of columnar discotic mesophases (Figure 2.19). The discotic nematic phase is devoid of any two-dimensional ordering, but the molecules are arranged so that on average the aromatic cores are parallel. Such phases arise when bulky substituents or branched side-chains are introduced to a phthalocyanine macrocycle.

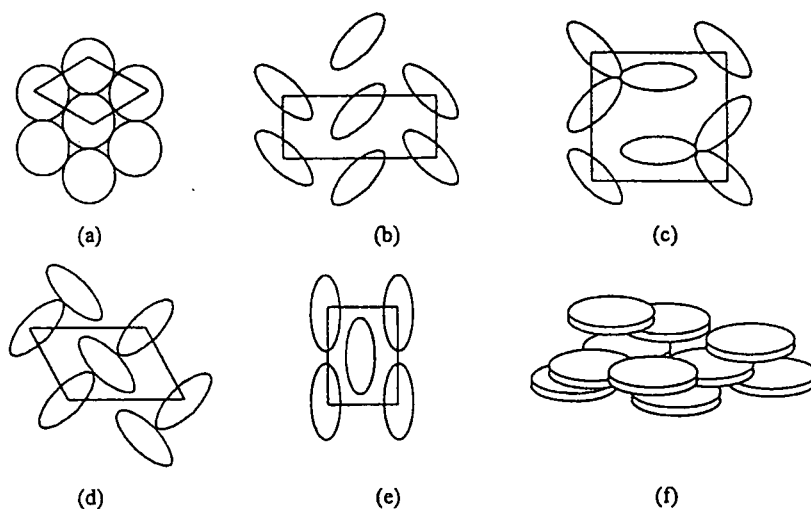


Figure 2.19: Discotic mesophases: (a) – (e) columnar, (a) hexagonal (D_h), (b) + (c) rectangular (D_r), (d) oblique (D_{ob}), (e) rectangular face centered and (f) discotic nematic (N_D).

The first thermotropic discotic liquid crystalline phthalocyanine was reported by Piechocki et al in 1982,¹²⁸ for a peripherally substituted $(CH_2OC_{12}H_{25})_8-CuPc$. This compound displays a mesophase with such a remarkably large thermal range (from $53^\circ C$ to $> 300^\circ C$) that it decomposes before reaching its clearing point (the temperature of the mesophase/isotropic liquid transition). Since this initial discovery, many examples of mesogenic phthalocyanines have been prepared with variations in the number, length and position of flexible substituents. In addition, the linking group attaching the side-chain to the phthalocyanine core and the central metal ion all have a strong influence on the structure and thermal stability of the resultant mesophase.¹²⁹

Ring substituted phthalocyanines, especially those derivatives that bear long aliphatic chains, are of interest because many are thermotropic liquid crystals. On heating, these compounds undergo a transition from the crystal state into a discotic columnar mesophase. Examples include a number of 1,4,8,11,15,18,22,25-octaalkylphthalocyanines, where the alkyl groups are hexyl or longer.^{130,131,132} The C_{15} -ZnPc and C_{18} -ZnPc derivatives are the first examples of this class of phthalocyanines to show three observable mesophases, D_1 , D_2 and D_3 , between the crystalline and isotropic liquid states.

Langner⁶⁸ found that the texture observed under the microscope was very much a function of the rate of cooling or heating. In the case of $(C_{15}H_{31})_8-2HPc$ it was found that a fast cooling rate ($10^\circ C\ min^{-1}$) resulted in a needle-like texture upon cooling from the isotropic liquid at $94^\circ C$. A slow cooling rate ($2^\circ C\ min^{-1}$) resulted in a texture that resembled the fan for the same transition. However on heating the needle-like texture from 90 to $92^\circ C$, it slowly converted in appearance

from the needle texture to the fan-like texture. Different textures observed under the polarising microscope is shown in Figure 2.20 for the indicated zinc phthalocyanines.

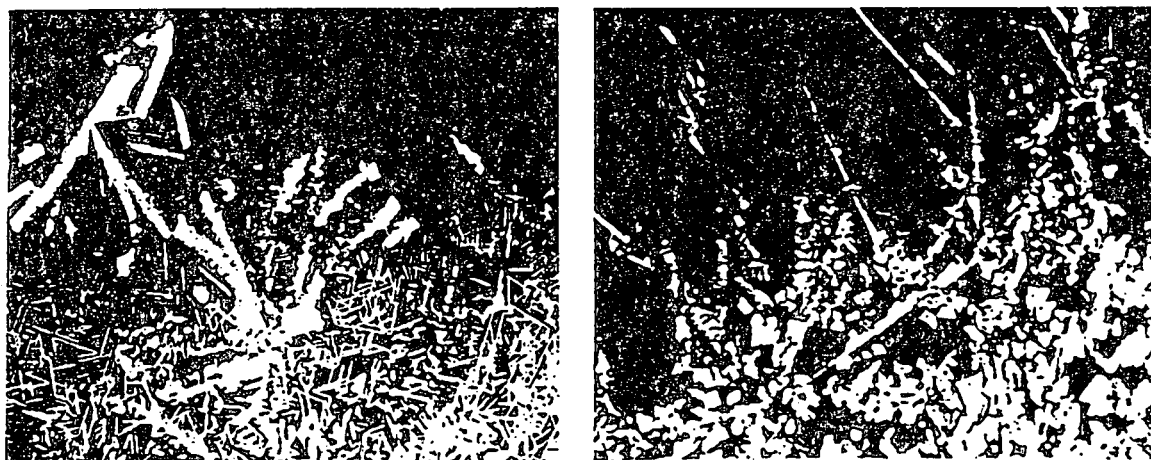


Figure 2.20: Left: $(C_9H_{19})_8\text{-ZnPc}$ at the transition temperature between the two D_{hd} mesophases. The fan texture (of the high temperature mesophase) is being overlaid by the needle texture (of the lower temperature mesophase). Right: $(C_{10}H_{21})_8\text{-ZnPc}$ at the transition temperature D_{hd} mesophase and the D_{rd} mesophase (mosaic texture). hd = hexagonal disordered, rd = rectangular disordered.

Chambrier and co-workers¹³³ reported the crystal structure of the octahexyl compound of this series. A problem they met with those compounds is that they tend to recrystallise as fibrous needles⁵¹ that are difficult to handle for diffraction work. However, recrystallisation of $(C_6H_{13})_8\text{-2HPc}$ from tetrahydrofuran afforded small blue plates, which proved to be single crystals of rather small dimensions. The packing of these unit cells, each containing one phthalocyanine molecule, is shown in Figure 2.21.

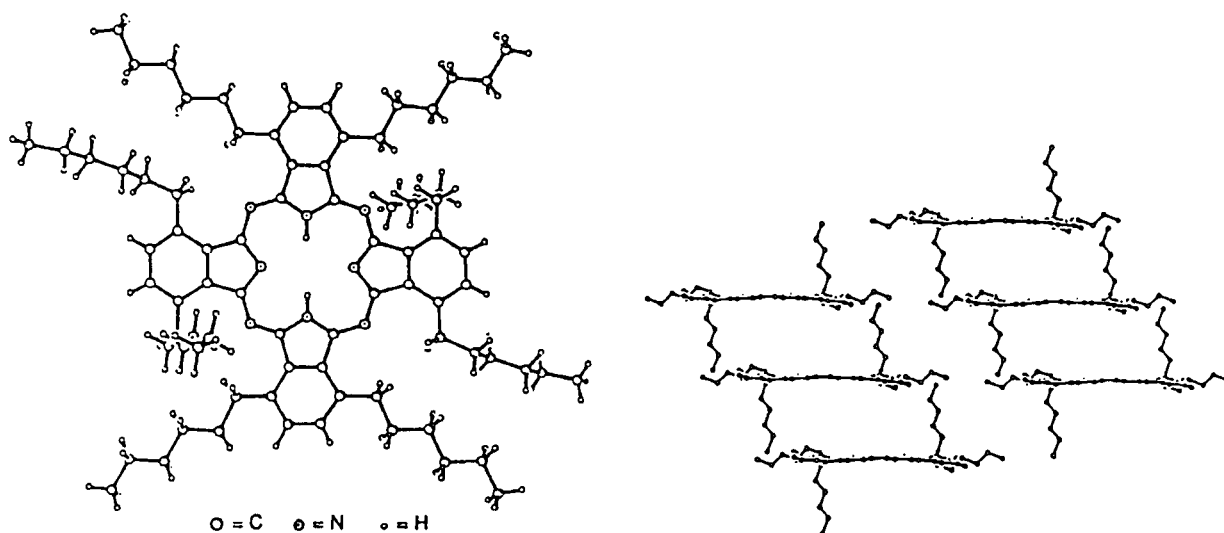


Figure 2.21: Representation of the molecular structure and packing of non-peripheral octahexyl substituted metal-free phthalocyanine, $(C_6H_{13})_8\text{-2HPc}$.

Six of the alkyl chains are approximately in the plane of the ring with four having their C-C bonds staggered in the plane and two staggered out of the plane. The remaining two alkyl chains act as spacers between molecules in the packing (stack). At 159°C, the compound undergoes a transition into a discotic columnar mesophase, which had earlier been identified as hexagonal, *i.e.* columnar stacks of cofacial molecules arranged such that a cross section shows a classical two-dimensional hexagonal lattice symmetry.^{51,132,133} An X-ray diffraction study of the mesophase exhibited by the octa-octyl homologue, (C₈H₁₇)₈-2HPc suggested that the distance between molecules within a column is *ca.* 4.4 Å.¹³² A similar distance is likely for the present compound. The implication is that upon transition from the liquid crystal phase there is a significant increase in core-core interactions, which becomes possible once the alkyl groups become mobile and no longer act as spacers. This presumed change in spacing, which occurs during the transition, can be expected to have significant effect on properties such as the semi-conductivity of the system.

2.8.1.1 The influence of the number and type of flexible side-chains on mesophase behaviour

The ability to form thermotropic columnar liquid crystals can be induced by the peripheral (2,3,9,10,16,17,23,24) substitution of phthalocyanines with eight alkyl,¹³⁴ alkoxy,¹³⁵ alkoxymethyl¹²⁸ or oligo(ethyleneoxy)¹³⁶ side-chains. Similar behaviour is demonstrated by derivatives with eight alkyl¹³⁰ or methyleneoxy¹³⁷ substitution at the non-peripheral (1,4,8,11,15,18,22,25) sites. A direct comparison between alkyl and oligo(ethyleneoxy) substituted phthalocyanines that differ only in the type of side-chain indicates that the peripheral substituted (OC₁₀H₂₁)₈-2HPc derivative has a crystal/mesophase transition that is 75°C higher and a clearing point (mesophase/isotropic liquid transition) that is 50°C higher than are those of its oligo(ethyleneoxy)-substituted analogue.¹²⁹ The former difference reflects the higher melting points of alkyl compared with oligo(ethyleneoxy) chains (the equilibrium melting temperature of polyethylene is 135°C whereas that of poly(ethyleneoxy) is 60°C); the latter difference is probably related to the greater rigidity of the alkyl chains, which would enhance the disc-shape anisotropy and hence extend their thermal stability of the mesophase. The incorporation of oligo(ethyleneoxy) in place of alkoxy side-chains of similar length results in a marked reduction of the crystal/mesophase transition temperatures but has very little effect on the clearing temperatures.⁸⁰ In addition, a number of unsymmetrically substituted phthalocyanines have been shown to form thermotropic liquid crystals.¹³⁸

2.8.1.2 The influence of side-chain length on mesophase behaviour

Generally, phthalocyanines with straight alkyl side-chains with a length of four or fewer atoms do not possess a mesophase and melt directly from their crystalline state into an isotropic liquid (or sublime) at high temperatures. For moderate alkyl side-chain lengths of four to eight atoms, the initial melting temperatures are very dependent on the chain length; longer chains reduce the temperatures of crystal-mesophase transitions considerably. However, for phthalocyanines with side-chain containing more than nine atoms there are no clearly defined relationship between the side-chain length and the temperature of the initial melting transition.

Remarkably linear relationships exist between the clearing point and the side-chain length for homologous series of phthalocyanine mesogens whose mesophase/isotropic transitions temperatures are below their decomposition temperatures (Figure 2.22).¹²⁹

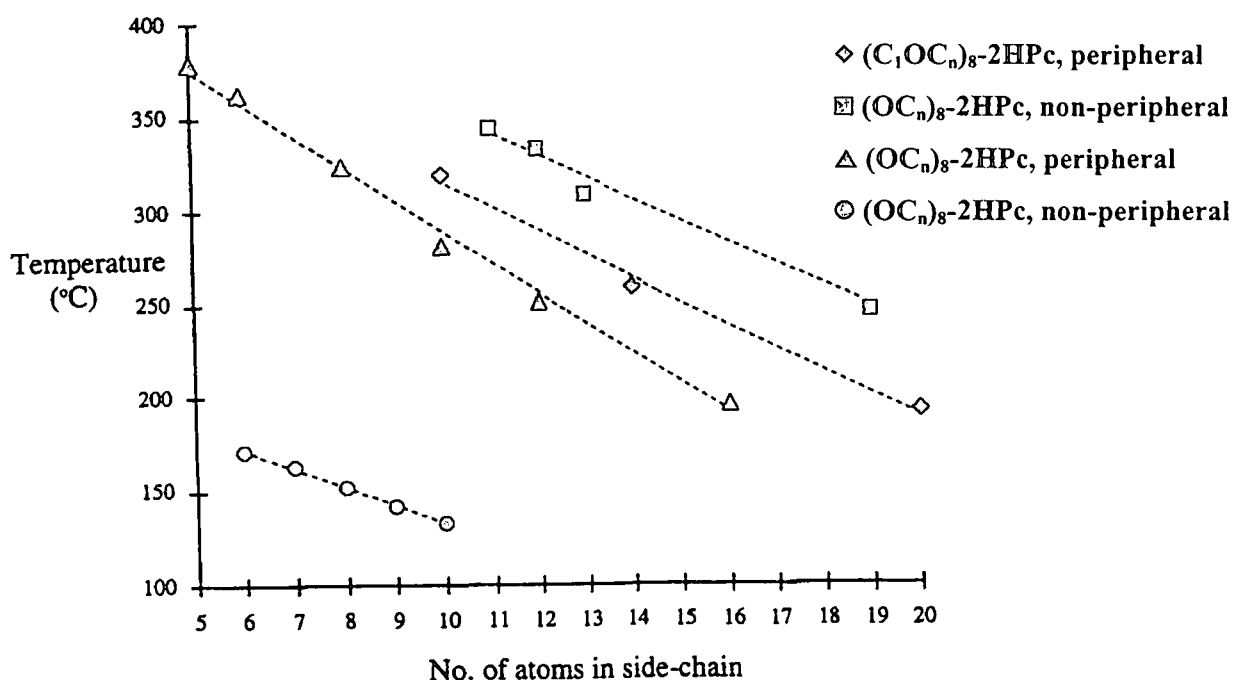


Figure 2.22: A plot of side-chain length versus clearing temperature (°C) for four different homologous series of mesogenic phthalocyanines.

On average, an extra methylene unit in each alkyl side-chain reduces the clearing point by 13°C. It has been shown by Cook and co-workers¹³⁰ that increasing the length of alkyl substituents on the phthalocyanine ring results in a decrease in the clearing temperature. Later the same group¹³⁹ showed that upon cooling of the isotropic liquid, the first mesophase, D₁, is formed. On further cooling, the mesophase undergoes a transition either directly to the crystal state or into one of the two alternative mesophases depending upon chain length and the central atom. For example, non-peripherally substituted (C₆H₁₃)₈-2HPc crystallises on cooling whereas

(C₇H₁₅)₈-2HPc, (C₆H₁₃)₈-CuPc, (C₇H₁₅)₈-CuPc and (C₈H₁₇)₈-CuPc first form a mesophase, D_{hd}, with a needle like texture. On the other hand, (C₈H₁₇)₈-2HPc, (C₉H₁₉)₈-2HPc and (C₉H₁₉)₈-CuPc undergo transition into a mesophase which is characterised by a mosaic texture. X-ray examination reveals that the symmetry of the latter is rectangular and the mesophase is assigned as D_{rd}.

2.8.1.3 The effects of the linking group and site of substitution on mesophase behaviour

The steric and electronic effects of the group that links the alkyl chains to the macrocycle strongly influence the transition temperatures and types of mesophase exhibited by the phthalocyanine. The linking groups are defined, for this discussion, as the first two atoms in the chain next to the phthalocyanine ring and are listed in Table 2.2 together with a crude description of their electronic and steric properties.

Table 2.2: The properties of linking groups.

Side chain (R)	Linking group	Properties
Alkyl (C _n)	Pc-CH ₂ CH ₂ -alkyl	Bulky and weakly electron-donating
Alkoxy (OC _n)	Pc-OCH ₂ -alkyl	Non-bulky and strongly electron donating
Methyleneoxy (C ₁ OC _n)	Pc-CH ₂ O-alkyl	Bulky and electron-withdrawing
Alkyl-ester (CO ₂ C _n)	Pc-CO ₂ -alkyl	Strongly electron-withdrawing

For the peripherally octa-substituted phthalocyanine mesogens, the mutual steric interactions of the neighboring linking groups and the effect that this has on the orientation of the disordered side-chains relative to the plane of the phthalocyanine ring are of prime importance. Molecular modeling calculations suggest that the relatively small -O-CH₂- linking group allow the side-chains to sit comfortably in the plane of the phthalocyanine ring, whereas the steric crowding of the alkyl (CH₂CH₂) and methyleneoxy (-CH₂O-) linking groups results in a side-chain conformation at a 35°C angle to the plane of the phthalocyanine ring.¹⁴⁰ The steric crowding at the peripheral sites of octa-substitution for the alkyl and methyleneoxy linking groups in the C_n-MPc and C₁OC_n-MPc series is responsible for their lower clearing temperatures, compared with those of members of the OC_n-MPc homologous series. The hexagonal columnar mesophase with no strong periodicity of ordering along the axis of the column (D_{hd}) is predominant among these phthalocyanines. The strongest steric interactions for non-peripheral side chains are those between chains situated on neighbouring benzo-moieties. These

interactions are likely to result in the displacement of some of the side-chains from the plane of the phthalocyanine ring. The effect is clearly evident in the molecular structures of the non-peripheral $(C_6H_{13})_8$ -2HPc and $(OC_5)_8$ -2HPc (octa-*iso*-pentoxy) derivatives.¹³⁹ This steric effect, therefore, appears to be completely independent of the linking group. The weakly electron-donating alkyl groups of the non-peripheral series $(C_n)_8$ -MPc induce columnar mesophases of moderate thermal ranges with clearing points about 170°C less than those of the isomeric peripherally substituted series $(C_n)_8$ -MPc, on average. Remarkably, the non-peripheral substitution of phthalocyanines with strongly electron-donating peripheral alkoxy side-chains, $(OC_n)_8$ -MPc, results in phthalocyanines that melt directly from the crystal to the isotropic liquid without the formation of any columnar mesophase.^{65,139}

2.8.1.4 The influence of the central metal ion on mesophase behaviour

The central metal ion exerts a strong influence on the thermal range of the columnar mesophase. The most complete study of this effect involves the homologous non-peripheral $(C_n)_8$ -MPc series and revealed that the magnitude of the increase (ΔT) in the clearing point, compared with that of the metal-free series,¹³¹ is in the following order: Zn^{2+} ($\Delta T \approx 100^\circ C$) > $Co^{2+} \approx Cu^{2+}$ ($\Delta T \approx 60^\circ C$) > Ni^{2+} ($\Delta T \approx 2^\circ C$) > $(H^+)_2$ (Figure 2.23).

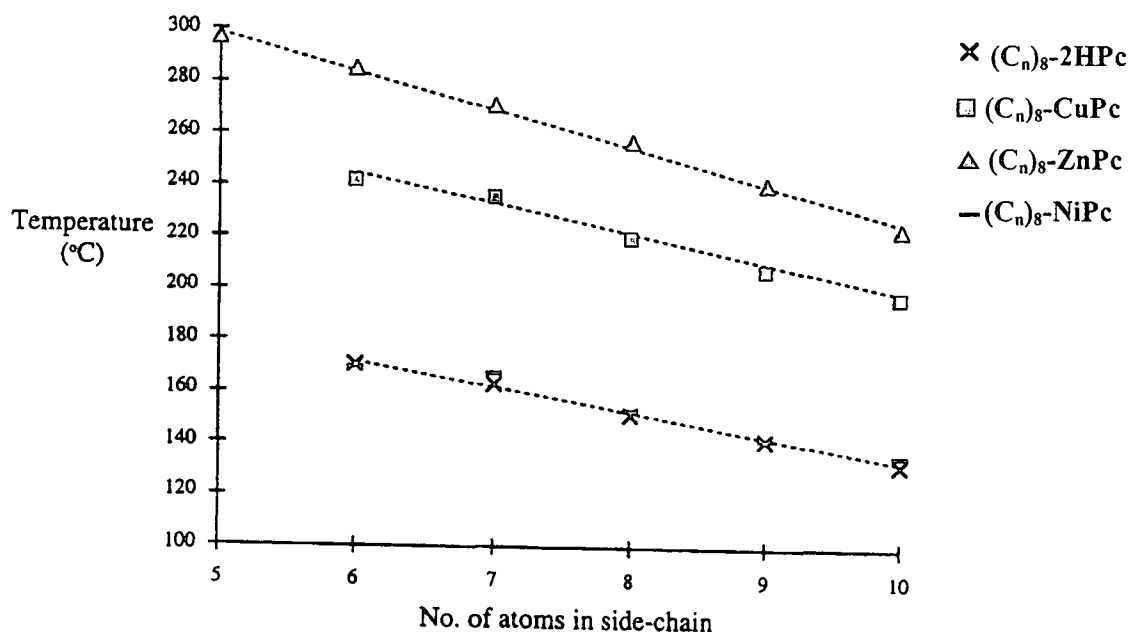


Figure 2.23: The influence of the central metal ion on the clearing point of the non-peripheral $(C_n)_8$ -MPc homologous series.

The crystal/mesophase transitions are relatively unaffected. These data are consistent with less systematic studies of other phthalocyanine systems and confirm that metal ions (*e.g.* Zn^{2+}) with

a propensity for penta-coordination help to stabilise the columnar structure. Metal ions that favour planar tetra-coordination (*e.g.* Ni^{2+}) do not greatly improve the thermal stability of the mesophase compared with that of the metal-free phthalocyanine. Large ions such as Pb^{2+} ¹⁴¹ and $[\text{Si}(\text{OH})_2]^{2+}$,¹⁴² which are not wholly accommodated in the central cavity, sterically destabilise the cofacial columnar structure and dramatically reduce both crystal-to-mesophase and mesophase-to-isotropic transition temperatures.

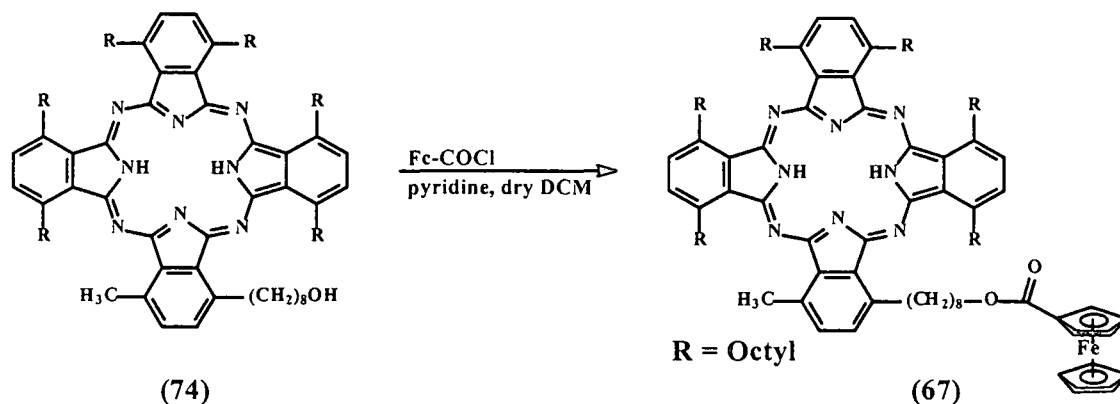
2.8.1.5 The influence of side-chain branching on mesophase behaviour

Increasing the steric bulk of the side-chain with short methyl or ethyl branches result in phthalocyanines that possess mesophases with reduced thermal range and order compared with those of straight-chain analogues. Thus members of the peripheral octa-substituted $\text{OC}_n\text{-MPc}$ series containing branched side-chains tend to give the D_{hd} ¹⁴³ or even the rare non-columnar N_D ,¹⁴⁴ rather than the hexagonal ordered, D_{ho} , mesophase encountered for the straight-chained phthalocyanines of this series. The presence of branched side-chains in the non-peripheral octa-substituted $\text{C}_1\text{OC}_n\text{-MPc}$ series results in materials that possess a clearing point below their decomposition temperature, which is in contrast to the behaviour of the unbranched derivatives of the same series.¹³⁷

2.8.1.6 The influence of unsymmetrical substitution on mesophase behaviour

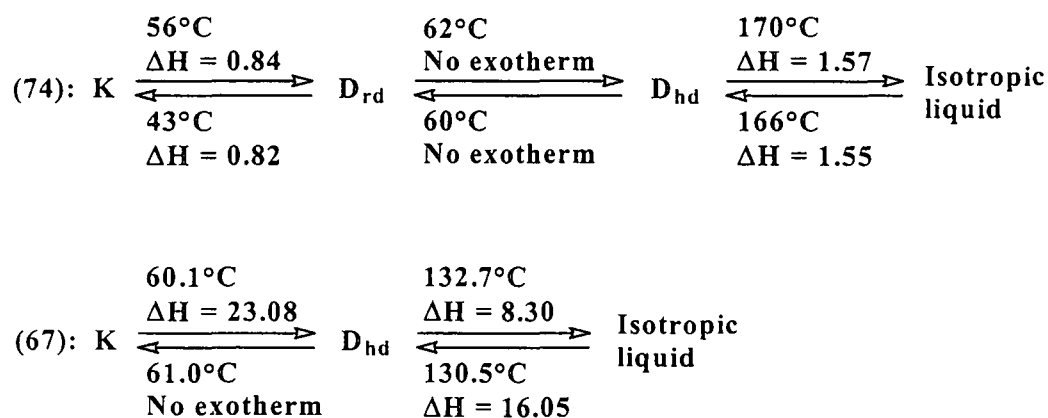
Many studies have shown that non-uniform substitution of the phthalocyanine ring need not preclude mesophase behaviour. Combinations of flexible alkyl, alkoxy or alkoxymethyl side-chains with nitrile,¹³⁸ oligo- or poly(ethyleneoxy) side-chains,^{80,145} redox-active hindered phenols¹⁴⁶ or hydroxyalkyl¹⁴⁷ chains are compatible with mesogenicity and give additional functionality. An investigation¹³⁹ has been undertaken of related structures, namely the isopropylidene derivatives, $\text{ipR}_6\text{-2HPcs}$, the mono-hydroxy and bis-hydroxy derivatives, $\text{R}_7\text{-2HPc-(OH)}$ and $\text{R}_6\text{-2HPc-(OH)}_2$ respectively. These derivatives are of lower symmetry than the octaalkyl substituted phthalocyanines but this does not preclude them from developing a mesophase, although examples of the bis-hydroxy series, $\text{R}_6\text{-2HPc-(OH)}_2$ showed monotropic behaviour, *i.e.* the compounds only exhibited a mesophase during the cooling cycle. Secondly, the inclusion of oxygen functionality, at least in the peripheral positions, did not inhibit mesophase behaviour. Finally, the lower symmetry of the heptaalkyl series, $\text{R}_7\text{-2HPc-(OH)}$ appears to disorganise the crystal and mesophase states, resulting in lower transition temperatures compared to their octaalkyl analogues.

Cook and co-workers¹⁰¹ have attached a ferrocenyl fragment to a liquid crystalline phthalocyanine to afford a ferrocenyl-phthalocyanine, (67) according to Scheme 2.21. The dimensions of the ferrocene molecule suggest that its attachment to structures giving rise to discotic columnar mesophase behaviour, *e.g.* octa-substituted phthalocyanines, might have one of two effects. The bulky unit could severely disrupt columnar packing to the extent that the new material would exhibit no mesophase behaviour. Alternatively, because the distance of *ca.* 3.3 Å between the two cyclopentadienyl rings is close to the intermolecular spacing of phthalocyanine molecules within mesophase stacks, a purpose designed derivative might allow the ferrocenyl unit to be readily accommodated into mesophase packing. In fact, compound (67) displayed mesophase behaviour as it was observed using polarised light microscopy and differential scanning calorimetry (DSC), thus making it the first example of a liquid crystalline ferrocenyl-phthalocyanine derivative.



Scheme 2.21: Attachment of a ferrocenyl fragment onto a phthalocyanine macrocycle.

Scheme 2.22 summarises phase transition data for the ferrocenyl-phthalocyanine system (67). This data is compared with those for the parent phthalocyanine (74).



Scheme 2.22: Phase transitions for ferrocenyl-phthalocyanine, (67) compared to that of its parent phthalocyanine, (74). ΔH in kcal mol^{-1} . K = crystalline solid.

2.8.2 Thin films of phthalocyanines

While substituents on the phthalocyanine ring can advantageously tune some of the system's electronic characteristics, they may also lead to new types of packing. This in turn expands the range and variety of properties of the macrocycle in the solid state. However there is sometimes a price to pay in that the extraordinary thermal stability of the unsubstituted ring compounds may, in part, be sacrificed. Indeed, few substituted phthalocyanines have been satisfactorily sublimed without decomposition. On the other hand, the solubility in organic solvents conferred by substituents opens the way for the deposition of phthalocyanines as films by methods very different from sublimation. Three developments are being considered for this purpose:

- (i) The application of the Langmuir-Blodgett (LB) technique,⁵⁶ which is a method of obtaining highly ordered thin films of suitable organic compounds by the sequential deposition of a monolayer adsorbed at an air-water interface.¹⁴⁸
- (ii) The spin-coating method⁵⁶ was utilised in this study, which is a straightforward and fast technique for organic film fabrication. It involves the rapid drying of a drop of solution containing the organic compound as it rotates and spreads under centrifugal forces on a substrate revolving at high speeds ($(2-4) \times 10^3$ rpm). The thickness of the resultant films is controlled by both the concentration of the solution and by the rate of rotation of the substrate.¹⁴⁹ This procedure is much simpler and more convenient than the LB method, but there is less control over film thickness.
- (iii) The third development, one which gives ultrathin films (one molecule thick), is the newest and involves generating a self assembled monolayer (SAM) chemically bonded to a substrate surface.¹⁵⁰ These films are thus potentially more robust than LB and spin-coated films.

Major challenges in these areas are the reproducible deposition of well ordered films and the design and development of derivatives, which lead to different types of molecular packing.

It was shown by Cook and co-workers⁵⁶ that the visible region spectra of spin-coated films of examples of non-peripherally octa-substituted R_8 -MPcs, R_8 -2HPcs and the R_6 -2HPc-(OH)₂, (R= alkyl) series undergo sharp changes at or close to the mesophase transition temperatures of the bulk material. These are fully reversible provided the films are not heated into the liquid phase where evenness is lost. As an example the UV/VIS spectra of a spin-coated film of $(C_8H_{17})_8$ -2HPc, at temperatures corresponding to different phases: (a) 50°C, crystal state;

(b) 90°C, the columnar mesophase of rectangular symmetry; (c) 145°C, the columnar mesophase of hexagonal symmetry, and (d) 160°C, the isotropic liquid phase are shown in Figure 2.24 A.

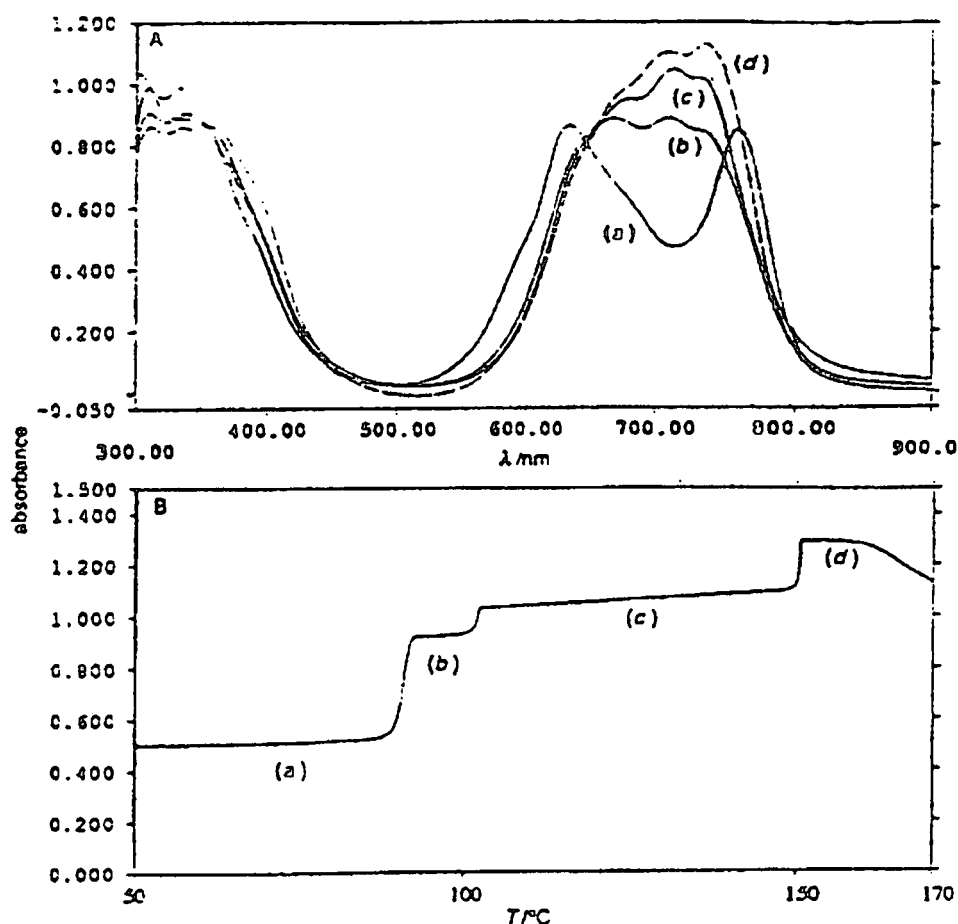


Figure 2.24: A: UV/VIS spectra of spin coated films of non-peripherally octaoctyl-substituted metal-free phthalocyanine, $(C_8H_{17})_8-2HPc$ at temperatures which corresponds to different phases: (a) 50°C, (b) 90°C, (c) 145°C, and (d) 160°C. B: Profile showing change of absorbance at 714 nm during heating of a spin-coated film of $(C_8H_{17})_8-2HPc$, (a)-(d) as in A.

It is important to note that the spectra varied as the temperature of the film was increased. On the basis of these results a wavelength of 714 nm was chosen to monitor the change in absorbance with temperature (Figure 2.24 B). Three transitions leading to an increase in absorbance were apparent. The first transition at 85°C corresponds to the $K \rightarrow D_3$ transition (from the crystal state, (a) to the first mesophase, (b)) observed for the bulk material. That at 105°C corresponds to the $D_3 \rightarrow D_1$ transition (from the first mesophase, (b) to the second mesophase, (c)). The third transition at 151°C corresponds to the $D_1 \rightarrow I$ transition (from the second mesophase, (c) to the isotropic liquid phase, (d)). The fall in absorbance on heating the material in the liquid state is due to material flowing down the slide. These spectral changes are

assigned to molecular reorganisations within the films that occur over relatively narrow temperature ranges of *ca.* 0.5-3°C.

- ¹ A. Braun and J. Tcherniac, *Chem. Ber.*, 1907, **40**, 2709.
- ² (a) R.P. Linstead, *J. Chem. Soc.*, 1934, 1016; (b) R.P. Linstead and A.R. Lowe, *J. Chem. Soc.*, 1934, 1031; (c) C.E. Dent, R.P. Linstead and A.R. Lowe, *J. Chem. Soc.*, 1934, 1033.
- ³ (a) J.M. Robertson, *J. Chem. Soc.*, 1935, 615; (b) J.M. Robertson, *J. Chem. Soc.*, 1936, 1195.
- ⁴ F.H. Moser and A.L. Thomas, *The Phthalocyanines*, CRC Press, Boca Raton, FL., 1983, vol. 1 and 2.
- ⁵ (a) R. Ao, L. Kilmmert and D. Haarer, *Adv. Mater.*, 1995, **7**, 495; (b) D. Birkett, *Chem. Ind.*, 2000, 178.
- ⁶ P. Gregory, *High-Technology Applications of Organic Colrants*, Plenum Press: New York, 1991, Chapter 7, p. 59.
- ⁷ O.L. Kaliya, E.A. Lukyanets and G.N. Vorozhtsov, *J. Porphyrins Phthalocyanines*, 1999, **3**, 592.
- ⁸ (a) T. Buck, D. Wöhrle, G. Schulz-Ekloff and A. Andreef, *J. Mol. Catal.*, 1991, **70**, 259; (b) D. Wöhrle and M. Kaneto, *J. Synth. Org. Chem.*, 1987, **45**, 837.
- ⁹ (a) C. Piechocki and J. Simon, *Nouv. J. Chim.*, 1985, **9**, 159; (b) J. Simon and C. Sirlin, *Pure Appl. Chem.*, 1989, **61**, 1625; (c) M.J. Cook, G. Cooke and A. Jaferi-Fini, *Chem. Commun.*, 1996, 1925.
- ¹⁰ (a) A.W. Snow and W.R. Barger, *Phthalocyanines: Properties and Applications*, eds. C.C. Leznoff and A.B.P. Lever, VCH: New York, 1989, vol. 1, p. 341; (b) J.D. Wright, *Prog. Surf. Sci.*, 1989, **31**, 1.
- ¹¹ (a) C.S. Frampton, J.M. O'Connor, J. Peterson and J. Silver, *Displays*, 1988, 174; (b) M.M. Niccholson, *Phthalocyanines: Properties and Applications*, eds. C.C. Leznoff and A.B.P. Lever, VCH: Weinheim, 1993, vol. 3, p. 75.
- ¹² D. Wöhrle and D. Meissner, *Adv. Mater.*, 1991, **3**, 129.
- ¹³ A.B.P. Lever, M.R. Hempstead, C.C. Leznoff, W. Lui, M. Melnik, W.A. Nevin and P. Seymour, *Pure Appl. Chem.*, 1986, **58**, 1467.
- ¹⁴ (a) D. Wöhrle, D. Schlettwein, M. Kirschenmann, M. Kaneto and A. Yamada, *J. Macromol. Sci. Chem.*, 1990, **A27**, 1239; (b) H. Eichhorn, *J. Porphyrins Phthalocyanines*, 2000, **4**, 88.
- ¹⁵ J.E. Kuder, *J. Imaging Sci.*, 1988, **32**, 51.
- ¹⁶ (a) A. Grund, A. Kaltbeitzel, A. Mathy, R. Schwarz, C. Bubeck, P. Vermehren and M. Hanack, *J. Phys. Chem.*, 1992, **96**, 7450; (b) G. de la Torre, T. Torres and F. Agulló-López, *Adv. Mater.*, 1997, **9**, 265.
- ¹⁷ (a) H. Ali and J.E. van Lier, *Chem. Rev.*, 1999, **99**, 2379; (b) C. M. Allen, W.M. Sharman and J.E. van Lier, *J. Porphyrins Phthalocyanines*, 2001, **5**, 161.
- ¹⁸ J.C. Swarts and J.E. van Lier, *Unpublished results*.
- ¹⁹ M. Oschner, *J. Photochem. Photobiol., B: Biol.*, 1997, **39**, 1.
- ²⁰ C.S. Foote, *Photochem. Photobiol.*, 1991, **54**, 659.
- ²¹ (a) D.P. Valenzo, *Photochem. Photobiol.*, 1987, **46**, 147; (b) J. Fuchs and J. Thiele, *Free Radical Biol. Med.*, 1998, **24**, 835; (c) W.M. Sharman, C.M. Allen and J.E. van Lier, *Methods Enzymol.*, 2000, **319**, 376.
- ²² J. Moan, *J. Photochem. Photobiol., B: Biol.*, 1990, **6**, 343.
- ²³ (a) I. Rosenthal and E. Ben Hur, *Int. J. Radiat. Biol.*, 1995, **67**, 85; (b) D. Philips, *Prog. Reaction Kinetics*, 1997, **22**, 175.
- ²⁴ R. Bonnett, *Chem. Soc. Rev.*, 1995, **24**, 19.
- ²⁵ D. Phillips, *Science Progress*, 1993/94, **77**, 300.
- ²⁶ S.B. Brown and T.G. Truscott, *Chem. Ber.*, 1993, **29**, 955.
- ²⁷ D. Wöhrle, A. Hirth, T. Bogdahn-Rai, G. Schnurpfeil and M. Shopova, *Russ. Chem. Bull.*, 1998, **47**, 807.

- 28 M. Peeva, M. Shopova, N. Stoichkova, N. Michailov, D. Wöhrle and S. Müller, *J. Porphyrins Phthalocyanines*, 1999, **3**, 380.
- 29 W.M. Sharman, C.M. Allen and J.E. van Lier, *Drug Discovery Today*, 1999, **4**, 507.
- 30 R. Bonnett, *Rev. Contemp. Pharmacother.*, 1999, **10**, 1.
- 31 J.E. van Lier, *Light in Biology And Medicine*, eds. R.H. Douglas, J. Moan and F. Dall'Acqua, Plenum: New York, 1988, p. 133.
- 32 A.J. MacRoberts, S.G. Brown and D. Philips, *Photosensitising Compounds: Their Chemical, Biological and Clinical Use*, eds. G. Bock and S. Harnett, Wiley: Chichester, 1989, p. 4.
- 33 M.L. Yarmush, W.P. Thorpe, L. Strong, S.L. Rakestraw, M. Toner and R.G. Tompkins, *Crit. Rev. Therapeut. Drug Carrier Syst.*, 1993, **10 (3)**, 197.
- 34 R.W. Boyle and J.E. van Lier, *Synthesis*, 1995, 1079.
- 35 J.E. van Lier and J. Spikes, *Photosensitising compounds: Their Chemical, Biological and Clinical Use*, eds. G. Bock and S. Harnett, Wiley: Chichester, 1989, p. 95.
- 36 S.M. Bishop, B.J. Knoo, A.J. MacRobert, M.S.C. Simpson, D. Phillips and A. Beeby, *J. Chromatogr.*, 1993, **646**, 345.
- 37 Q. Peng and J. Moan, *Br. J. Cancer*, 1995, **72**, 565.
- 38 R. Edrei, V. Gottfreid, J.E. van Lier and S. Kimel, *J. Porphyrins Phthalocyanines*, 1998, **2**, 191.
- 39 H.L. van Leengoed, N. van der Veen, A.A. Versteeg, R. Ouellet, J.E. van Lier and W. M. Star, *Photochem. Photobiol.*, 1993, **58**, 575.
- 40 R.W. Boyle, C.C. Leznoff and J.E. van Lier, *Br. J. Cancer*, 1993, **67**, 1177.
- 41 C. Ometto, C. Fabris, C. Milanese, G. Jori, M.J. Cook and D.A. Russell, *Br. J. Cancer*, 1996, **74**, 1891.
- 42 C. Fabris, C. Ometto, C. Milanese, G. Jori, M.J. Cook and D.A. Russell, *J. Photochem. Photobiol., B: Biol.*, 1997, **39**, 279.
- 43 N.L. Oleinick, A.R. Antunez, M.E. Clay, B.D. Ruther and M.E. Kenney, *Photochem. Photobiol.*, 1993, **57**, 242.
- 44 S. Rywkin, E. Ben-Hur, Z. Malik, A.M. Prince, Y-S. Li, M.E. Kenney, N.L. Oleinick and B. Horowitz, *Photochem. Photobiol.*, 1994, **60**, 165.
- 45 V.N. Nemykin, V.M. Mytsyk, S.V. Volkov and N. Kobayashi, *J. Porphyrins Phthalocyanines*, 2000, **4**, 551.
- 46 (a) H. Brunner, F. Maiterth and B. Treitinger, *Chem. Ber.*, 1994, **127**, 2141; (b) H. Brunner, H. Obermeier, and R-M. Szeimies, *Chem. Ber.*, 1995, **128**, 173.
- 47 C.C. Leznoff and T.W. Hall, *Tetrahedron Lett.*, 1982, **23**, 3023.
- 48 E.V. Maya, P. Haisch, P. Vázquez and T. Torres, *Tetrahedron*, 1998, **54**, 4397.
- 49 J.A. Thompson, K. Murata, D.C. Miller, J.L. Stanton, W.E. Broderick, B.M. Hoffman and J.A. Ibers, *Inorg. Chem.*, 1993, **32**, 3546.
- 50 D. Wöhrle, M. Eskes, K. Shigehara and A. Yamada, *Synthesis*, 1993, 194.
- 51 N.B. McKeown, I. Chambrier and M.J. Cook, *J. Chem. Soc., Perkin Trans. 1*, 1990, 1169.
- 52 N.B. McKeown, *Phthalocyanine materials: Synthesis, Structure and Function*, University Press, Cambridge, 1998, p. 14.
- 53 H. Tomoda, S. Saito and S. Shiraishi, *Chem. Lett.*, 1983, 313.
- 54 C.C. Leznoff, *Phthalocyanines: Properties and Applications*, eds. C.C. Leznoff and A.B.P. Lever, VCH: New York, 1989, vol. **1**, pp. 6, 18.
- 55 S.T. Oliver and T.D. Smith, *J. Chem. Soc., Perkin Trans. 2*, 1987, 1579.
- 56 M.J. Cook, *J. Mater. Chem.*, 1996, **6(5)**, 677.
- 57 C.C. Leznoff, *Phthalocyanines: Properties and Applications*, eds. C.C. Leznoff and A.B.P. Lever, VCH: New York, 1989, vol. **1**, p. 1.

- 58 J. Simon and P. Bassoul, *Phthalocyanines: Properties and Applications*, eds. C.C. Leznoff and A.B.P. Lever, VCH: New York, 1993, vol. 2, p. 223.
- 59 M. Hanack and M. Lang, *Adv. Mater.*, 1994, 6, 819.
- 60 R.D. George and A.W. Snow, *J. Heterocycl. Chem.*, 1995, 495.
- 61 D. Wöhrle, M. Eskes, K. Shigehara and A. Yamada, *Synthesis*, 1993, 194.
- 62 M.A. Mohammad, P. Ottenbreit, W. Prass, G. Schurpfeil and D. Wöhrle, *Thin Solid Films*, 1992, 213, 285.
- 63 (a) J.F. van der Pol, E. Neeleman, J.C. van Miltenburg, J.W. Zwikker, R.J.M. Nolte and W. Drenth, *Macromolecules*, 1990, 23, 155; (b) A-M. Giroud-Godquin, and P.M. Maitlis, *Angew. Chem.*, 1991, 30, 375.
- 64 D. Wöhrle, N. Iskandar, G. Grashew, H. Sinn and E.A. Friedrich, *Photobiol.*, 1990, 51, 351.
- 65 M.J. Cook, A.J. Dunn, S.D. Howe, A.J. Thomson and K.J. Harrison, *J. Chem. Soc., Perkin Trans. 1*, 1988, 2453.
- 66 D.J. Chadwick and C. Willbe, *J. Chem. Soc., Perkin Trans. 1*, 1977, 887.
- 67 I. Chambrier, M.J. Cook, S. Cracknell and J. McMurdo, *J. Mater. Chem.*, 1993, 3, 841.
- 68 J.C. Swarts, E.H.G. Langner, N. Krokeide-Hove and M.J. Cook, *J. Mater. Chem.*, 2001, 11, 434.
- 69 Y. Miyahara and T. Inazu, *Tetrahedron Lett.*, 1990, 31, 5955.
- 70 A. Mukoh, T. Kitamura, M. Kaneko and T. Ozawa, *Chem. Abs.*, 1984, 100, 15417.
- 71 H. Hogeveen and T.B. Middelkoop, *Tetrahedron Lett.*, 1973, 3671.
- 72 R. Helder and H. Wynberg, *Tetrahedron Lett.*, 1972, 605.
- 73 (a) M. Tian, T. Wada, H. Kimura-Suda and H. Sasabe, *J. Mater. Chem.*, 1997, 7, 861; (b) G. de la Torre and T. Torres, *J. Porphyrins Phthalocyanines*, 1997, 1, 221; (c) T. Torres, G. de la Torre and J. García-Ruiz, *Eur. J. Org. Chem.*, 1999, 2323.
- 74 C. Feucht, T. Linßen and M. Hanack, *Chem. Ber.*, 1994, 127, 113.
- 75 F. Fernández-Lázaro, E.M. Maya, N. Nicolau and T. Torres, *Advanced Porphyrin Chemistry*, ed. O. A. Golubtchikov, IS-UCT Press, St. Petersburg, 1999.
- 76 G. de la Torre, P. Vázquez, F. Agulló-López and T. Torres, *J. Mater. Chem.*, 1998, 8, 1671.
- 77 S.V. Kudrevich, H. Ali and J.E. van Lier, *J. Chem. Soc., Perkin Trans. 1*, 1994, 2767.
- 78 J.G. Young and W. Onyebuagu, *J. Org. Chem.*, 1990, 55, 2155.
- 79 B. Cbezoin, S. Rodrgues-Morgade and T. Torres, *J. Org. Chem.*, 1995, 60, 1872.
- 80 G.J. Clarkson, N.B. McKeown and K.E. Treacher, *J. Chem. Soc., Perkin Trans. 1*, 1995, 1817.
- 81 *Phthalocyanines: Properties and Applications*, eds. C.C. Leznoff and A.B.P. Lever, VCH: New York, 1996, vol.4, p. 83.
- 82 T.G. Linßen and M. Hanack, *Chem. Ber.*, 1994, 127, 2051.
- 83 (a) N. Kobayashi, R. Kondo, S. Nakajima and T. Osa, *J. Am. Chem. Soc.*, 1990, 112, 9640; (b) K. Kasuga, T. Idehara M. Handa and K. Isa, *Inorg. Chim. Acta*, 1992, 196, 127.
- 84 A. Weitemeyer, H. Kliesch and D. Wöhrle, *J. Org. Chem.*, 1995, 60, 4900.
- 85 A. Sastre, T. Torres and M. Hanack, *Tetrahedron Lett.*, 1995, 36, 8501.
- 86 S. Dabak, A. Gül and Ö. Bekarolu, *Chem. Ber.*, 1994, 127, 2009.
- 87 S.V. Kudrevich, S. Gilbert and J.E. van Lier, *J. Org. Chem.*, 1996, 61, 5706.
- 88 C.C. Leznoff, P.I. Svirskaya, B. Khouw, R.L. Cerny, P. Seymour and A.B.P. Lever, *J. Org. Chem.*, 1991, 56, 82.
- 89 (a) P. Köpf-Maier, H. Köpf and E.W. Neuse, *Cancer Res. Clin. Oncol.*, 1984, 108, 336. (b) E.W. Neuse and Kanzawa, *Appl. Organomet. Chem.*, 1990, 4, 19.
- 90 P.J. Swarts (Snr.), M. Immelman, G.J. Lamprecht, S.E. Greyling and J.C. Swarts, *S. Afr. J. Chem.*, 1997, 50(4), 208.
- 91 A.N. Nesmeyanov and N.S. Kochetkova, *Russ. Chem. Rev.*, 1974, 43, 710.

- ⁹² E.W. Neuse, J.R. Woodhouse, G. Montaudo and C. Puglisi, *Appl. Organomet. Chem.*, 1988, **2**, 53.
- ⁹³ G. Wagner and R. Herrmann, *Ferrocenes: Homogeneous Catalysis, Organic Synthesis, Materials Science*, eds. A. Togni and T. Hayashi, VCH: Weinheim, New York, 1995, p. 212.
- ⁹⁴ D. Osella, M. Ferrali, P. Zanello, F. Laschi, M. Fontani, C. Nervi and G. Cavignoli, *Inorg. Chim. Acta*, 2000, **306**, 42.
- ⁹⁵ (a) A. Haaland and J. Nilsson, *J. Chem. Soc., Chem. Commun.*, 1968, 88; (b) *Comprehensive Organometallic Chemistry*, ed. G. Wilkinson, Pergamon Press, Oxford, 1982, vol. 4, chapter 31 and vol. 8, chapter 59. (c) G. Wagner and R. Herrmann, *Ferrocenes: Homogeneous Catalysis, Organic Synthesis, Materials Science*, eds. A. Togni and T. Hayashi, VCH: Weinheim, New York, 1995, p. 173.
- ⁹⁶ J.K. Lindsay and C.R. Hauser, *J. Org. Chem.*, 1957, **22**, 355.
- ⁹⁷ D. Lednicher and C.R. Hauser, *Org. Synth.*, 1961, **40**, 31.
- ⁹⁸ D. Lednicher, J.K. Lindsay and C.R. Hauser, *J. Org. Chem.*, 1958, **23**, 653.
- ⁹⁹ H. Kliesch, A. Weitemeyer, S. Müller and D. Wöhrle, *Liebigs Ann. Chem.*, 1995, 1272.
- ¹⁰⁰ M.D. Maree and J.C. Swarts, *Unpublished results*.
- ¹⁰¹ M.J. Cook, G. Cooke and A. Jafari-Fini, *J. Chem. Soc., Chem. Commun.*, 1995, 1715.
- ¹⁰² A. González, P. Vázquez and T. Torres, *Tetrahedron Lett.*, 1999, **40**, 3263.
- ¹⁰³ E.H.G. Langner and J.C. Swarts, *Unpublished results*.
- ¹⁰⁴ R.R. Gagne, C.A. Koval and G.C. Lisensky, *Inorg. Chem.*, 1980, **19**, 2854.
- ¹⁰⁵ W.C. (Ina) du Plessis, J.C. Erasmus, G.J. Lamprecht, J. Conradie, T.S. Cameron, M.A.S. Aquino and J.C. Swarts, *Can. J. Chem.*, 1999, **77**, 378.
- ¹⁰⁶ T. Ogata, K. Oikawa, T. Fujisawa, S. Motoyama, T. Izumi, A. Kasahara and N. Tanaka, *Bull. Chem. Soc. Jpn.*, 1981, **54**, 3723.
- ¹⁰⁷ T. Saji, *Phthalocyanines: Properties and Applications*, eds. C.C. Leznoff and A.B.P. Lever, VCH: New York, 1993, vol. 2, chapter 4, p. 170.
- ¹⁰⁸ T. Nyokong, *S. Afr. J. Chem.*, 1995, **48**, 23.
- ¹⁰⁹ T. Nyokong, *Polyhedron*, 1993, **12**, 375.
- ¹¹⁰ Y. Fu, G. Fu and A.B.P. Lever, *Inorg. Chem.*, 1994, **33**, 1038.
- ¹¹¹ M.D. Maree and J.C. Swarts, *Unpublished results*.
- ¹¹² Z. Jin, K. Nolan, C.R. McArthur, A.B.P. Lever and C.C. Leznoff, *J. Organomet. Chem.*, 1994, **468**, 205.
- ¹¹³ C.C. Leznoff and A.B.P. Lever, *Phthalocyanines: Properties and Applications*, eds., VCH: New York, 1993, vol. 3, p. 1.
- ¹¹⁴ E.S. Schmidt, T.S. Calderwood and T.C. Bruice, *Inorg. Chem.*, 1986, **25**, 3718.
- ¹¹⁵ G. Fu, Y. Fu, K. Jayaraj and A.B.P. Lever, *Inorg. Chem.*, 1990, **29**, 4090.
- ¹¹⁶ Y. H. Tse, A. Goel, M. Hu, C.C. Leznoff, J.E. van Lier and A.B.P. Lever, *Can. J. Chem.*, 1993, **71**, 742.
- ¹¹⁷ K-W. Poon, Y. Yan, X-y. Li and D.K.P. Ng, *Organometallics*, 1999, **18**(17), 3528.
- ¹¹⁸ M.J. Cook, I. Chambrier, S.J. Cracknell, D.A. Mayes and D.A. Russell, *Photochem. Photobiol.*, 1995, **62**, 542.
- ¹¹⁹ M.J. Stillman and T. Nyokong, *Phthalocyanines: Properties and Applications*, eds. C.C. Leznoff and A.B.P. Lever, VCH: New York, 1989, vol. 1, pp.133-257.
- ¹²⁰ N.B. McKeown, *Phthalocyanine materials: Synthesis, Structure and Function*, University Press, Cambridge, 1998, p. 90.
- ¹²¹ J.H. Sharp and M. Lardon, *J. Phys. Chem.*, 1968, **72**, 3230.
- ¹²² J.F. Van der Pol, E. Neeleman, J.W. Zwikker, R.J.M. Nolte, W. Drenth, J. Aerts, R. Visser and S.J. Picken, *Liq. Cryst.*, 1989, **6**, 577.
- ¹²³ T. Kobayashi and S. Isoda, *J. Mater. Chem.*, 1993, **3**, 1.

- ¹²⁴ N. Kobayashi, S. Nakajima and T. Osa, *Inorg. Chim. Acta*, 1993, **210**, 131.
- ¹²⁵ T. Torres, G. de la Torre and J. Garcia-Ruiz, *Eur. J. Org. Chem.*, 1999, 2323.
- ¹²⁶ M.J. Cook, *Phthalocyanines: Introduction to Liquid Crystals-UEA Report*, 1992.
- ¹²⁷ (a) C. Destrade, H. Gasparoux, A. Babeau, N.H. Tinh and J. Malthete, *J. Mol. Cryst. :Liq. Cryst.*, 1981, **67**, 37. (b) L. Lamlok, J. Malthete, N.H. Tinh, C. Destrade and A.M. Levelut, *J. Phys. Lett.*, 1982, **43**, 641.
- ¹²⁸ C. Piechocki, J. Simon, A. Skoulios, D. Guillon and P. Weber, *J. Am. Chem. Soc.*, 1982, **104**, 5245.
- ¹²⁹ N.B. McKeown, *Phthalocyanine materials: Synthesis, structure and Function*, University Press, Cambridge, 1998, 65.
- ¹³⁰ M.J. Cook, M.F. Daniel, K.J. Harrison, N.B. McKeown and A.J. Thomson, *J. Chem. Soc., Chem. Commun.*, 1987, 1086.
- ¹³¹ M.J. Cook, S.J. Cracknell and K.J. Harrison, *J. Mater. Chem.*, 1991, **1**, 703.
- ¹³² A.S. Cherodian, A.N. Davies, R.M. Richardson, M.J. Cook, N.B. McKeown, A.J. Thomson, J. Feijoo, G. Ungar and K.J. Harrison, *Mol. Cryst. Liq. Cryst.*, 1991, **196**, 103.
- ¹³³ I. Chambrier, M.J. Cook, M. Helliwell and A.K. Powell, *J. Chem. Soc., Chem. Commun.*, 1992, 444.
- ¹³⁴ K. Ohta, L. Jacquemin, C. Sirlin, L. Bosio and J. Simon, *Nouv. J. Chim.*, 1988, **12**, 751.
- ¹³⁵ D. Masurel, C. Sirlin and J. Simon, *Nouv. J. Chim.*, 1987, **11**, 455.
- ¹³⁶ D. Guillon, A. Skoulios, C. Piechocki, J. Simon and P. Weber, *Mol. Cryst. Liq. Cryst.*, 1983, **100**, 275.
- ¹³⁷ A.N. Cammidge, M.J. Cook, K.J. Harrison and N.B. McKeown, *J. Chem. Soc., Perkin Trans. I*, 1991, 3053.
- ¹³⁸ C. Piechocki and J. Simon, *J. Chem. Soc., Chem. Commun.*, 1985, 259.
- ¹³⁹ M.J. Cook, *J. Mater. Sci.: Mater. In Electronics*, 1994, **5**, 117.
- ¹⁴⁰ J.F. Van der Pol, E. Neeleman, J.W. Zwikker, R.J.M. Nolte and W. Drenth, *Recueil des Travaux Chimiques des Pays-Bas*, 1988, **107**, 615.
- ¹⁴¹ P. Weber, D. Guillon and A. Skoulios, *J. Phys. Chem.*, 1987, **91**, 2242.
- ¹⁴² T. Sauer and G. Wegner, *Mol. Cryst. Liq. Cryst.*, 1988, **162**, 97.
- ¹⁴³ P.G. Schouten, J.F. Van der Pol, J.W. Zwikker, W. Drenth and S.J. Picken, *Mol. Cryst. Liq. Cryst.*, 1991, **195**, 291.
- ¹⁴⁴ D. Lelievre, M.A. Petit and J. Simon, *Liq. Cryst.*, 1989, **4**, 707.
- ¹⁴⁵ G.J. Clarkson, A. Cook, N.B. McKeown, K.E. Treacher and Z. Ali-Adib, *Macromolecules*, 1996b, **29**, 913.
- ¹⁴⁶ P. Humberstone, G.J. Clarkson, N.B. McKeown and K.E. Treacher, *J. Mater. Chem.*, 1996, **6**, 315.
- ¹⁴⁷ G.C. Bryant, M.J. Cook, T.G. Ryan and A.J. Thorne, *Tetrahedron*, 1996, **52**, 809.
- ¹⁴⁸ (a) A. Ulman, *An Introduction to Ultrathin Organic Films: From Lanmuir-Blodgett to Self-assembly*, San Diego: Academic Press, 1991. (b) R.H. Tredgold, *Order in Thin Organic Films*, Cambridge: Cambridge University, 1994.
- ¹⁴⁹ N.B. McKeown, *Phthalocyanine materials: Synthesis, structure and Function*, University Press, Cambridge, 1998, p. 58.
- ¹⁵⁰ R.H. Tredgold, *J. Mater. Chem.*, 1995, **5**, 1095.

CHAPTER 3

RESULTS AND DISCUSSION

3.1 Introduction

In this chapter, research results are ordered to discuss the synthesis of mono- and disubstituted phthalonitriles first. These phthalonitriles and their precursors were characterised using ^1H NMR, IR spectroscopy and elemental analysis. The resulting phthalonitriles were then used to synthesise metal-free and zinc-containing non-peripherally octadodecyl substituted phthalocyanines and new ferrocenyl-phthalocyanine conjugates as discussed in section two. Most of these phthalocyanines were characterised using ^1H NMR, matrix-assisted laser desorption/ionisation time of flight mass spectrophotometry (MALDI-tof ms) and solution phase electronic (UV-VIS) spectroscopy. The third section involves the discussion of the electrochemical properties of the synthesised ferrocenyl derivatives and some of the phthalocyanines by using cyclic voltammetry. This discussion is then followed by the UV spectroscopic properties of these synthesised phthalocyanines. The final section is devoted to the liquid crystalline properties of the synthesised octadodecylated phthalocyanines and hexadodecylated-phthalocyanine-ferrocenyl conjugates. The liquid crystalline properties were investigated using polarised light optical microscopy, differential scanning calorimetry (DSC) and variable temperature UV-VIS spectroscopy of thin films of these synthesised phthalocyanines cast on glass. The numbers used to identify compounds in this chapter were, where possible, chosen to correspond with numbers in Chapter 2.

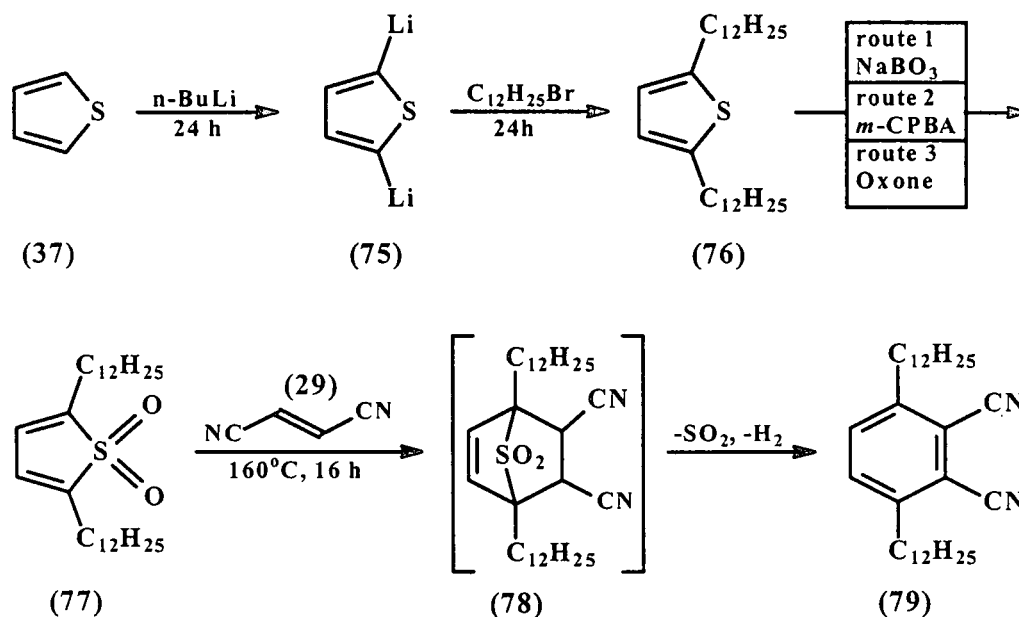
3.2 Synthesis of substituted phthalonitriles

The challenge of synthesising substituted phthalocyanines lies in the preparation of an appropriately substituted phthalonitrile precursor, rather than the cyclisation of the precursor into the phthalocyanine. Two different types of phthalonitriles were targeted for synthesis in this study:

- (i) 3,6-Bis(dodecyl)phthalonitrile, (**79**) was synthesised according to Scheme 3.1 to be used as a precursor for the synthesis of symmetrically non-peripherally octadodecyl as well as mixed ferrocenyl-dodecyl substituted phthalocyanines.
- (ii) A new compound, 4-(2'-ferrocenylethoxy)phthalonitrile, (**81**) was prepared to be used as a precursor for the synthesis of unsymmetrically substituted ferrocenyl-phthalocyanine conjugates. This precursor was obtained by nitro displacement of 4-nitrophthalonitrile, (**52**) with 2-ferrocenylethanol, (**80**) according to Scheme 3.2 (page 66).

3.2.1 Synthesis of 3,6-bis(dodecyl)phthalonitrile, (79)

The synthesis of 3,6-bis(dodecyl)phthalonitrile involves firstly the dilithiation of thiophene, (37), to give the 2,5-dilithiated product, (75) followed by the didodecylation of (75) to yield the dialkylated product (76).



Scheme 3.1: Synthesis of 3,6-bis(dodecyl)phthalonitrile, (79). *m*-CPBA = *m*-chloroperoxybenzoic acid. Oxone = the Aldrich trade name for 2KHSO₅·KHSO₄·K₂SO₄.

The resulting 2,5-bis(dodecyl)thiophene, (76) was subsequently oxidised to the corresponding 2,5-bis(dodecyl)thiophene-1,1-dioxide, (77), followed by a Diels-Alder addition with fumaronitrile, (29) to produce the desired 3,6-bis(dodecyl)phthalonitrile, (79) (Scheme 3.1) after *in situ* SO₂ and H₂ elimination.

3.2.1.1 2,5-Bis(dodecyl)thiophene, (76)

Lithiation of thiophene, (37) to the dilithiated specie (75), followed by dialkylation of the intermediate to the dialkylated thiophene were found to be high yielding (>80%) reactions. Precooled to -80°C under a nitrogen atmosphere, over 24 h reaction times for both the lithiation and alkylation steps, 2,5-bis(dodecyl)thiophene, (76) was obtained in a yield of 76%. Crude (76), a dark brown oil, was purified via fractional distillation under reduced pressure (1-1.5 mmHg) and the pure, light yellow 2,5-bis(dodecyl)thiophene, (76) collected from 175-190°C. The didodecylation of thiophene was confirmed by IR, ¹H NMR as well as elemental analysis. The infrared spectrum (Figure 3.2, page 65) showed strong, sharp peaks at 2860 and 1464 cm⁻¹ which are associated with the aromatic proton, C-H stretch and alkyl chains on the thiophene

ring respectively. The ^1H NMR (spectrum 1) of **(76)** showed *inter alia* a signal at $\delta 6.57$ representing the 2 aromatic protons on the thiophene ring and a triplet at $\delta 0.90$ corresponding to the six methyl protons ($2 \times -\text{CH}_3$) at the end of the two alkyl chains which is consistent with the structure of **(76)**.

3.2.1.2 2,5-Bis(dodecyl)thiophene-1,1-dioxide, **(77)**

Three oxidation routes were followed to obtain the dioxide **(77)** in this study:

(i) Oxidation of 2,5-bis(dodecyl)thiophene, **(76)** with sodium perborate¹ (Scheme 3.1, **route 1**) afforded the lowest yield of 17% for 2,5-bis(dodecyl)thiophene-1,1-dioxide. The poor solubility of 2,5-bis(dodecyl)thiophene in the solvent of choice for sodium perborate induced oxidations, glacial acetic acid, probably contributes much to the observed low yield. The reaction is temperature dependent and should be controlled at *ca.* 50°C. Lower temperatures lead to incomplete oxidation while higher temperatures caused excessive degradation. Recrystallisation of the crude product from hexane gave 2,5-bis(dodecyl)thiophene-1,1-dioxide, **(77)**.

(ii) Oxidation of 2,5-bis(dodecyl)thiophene with *m*-chloroperoxybenzoic acid (*m*-CPBA)² (Scheme 3.1, **route 2**) in dichloromethane increased the yield of 2,5-bis(dodecyl)thiophene-1,1-dioxide, **(77)** to 40% after 19 h of reaction time and recrystallisation from ethanol. Due to the instability of the oxidising agent (an explosive hazard exists), the heterogeneous reaction mixture had to be kept between 0 and 5°C. An excess of sodium bicarbonate was required for this reaction to ensure the neutralisation of *m*-chlorobenzoic acid, which is always present in commercial *m*-chloroperoxybenzoic acid.

(iii) Oxidation of **(76)** with dimethyldioxirane³ (Scheme 3.1, **route 3**), proved to be most efficient, in that a substantially higher yield of 82% of 2,5-bis(dodecyl)thiophene-1,1-dioxide, **(77)** was obtained. Near qualitative oxidation was observed provided stirring of the heterogeneous reaction mixture was efficient. We found that dimethyldioxirane need not be isolated by distillation prior to thiophene oxidation as described by Miyahara and co-workers.⁴ In our modification of Miyahara's method, dimethyldioxirane was generated *in situ* in the reaction mixture already containing the thiophene derivative that is to be oxidised, by reacting acetone with Oxone® (the Aldrich trade name for $2\text{KHSO}_5 \cdot \text{KHSO}_4 \cdot \text{K}_2\text{SO}_4$) in the presence of potassium hydrogen carbonate. A large CO_2 /acetone-condenser was used to avoid the

evaporation of *in situ* prepared dimethyldioxirane (b.p. = 8°C) at room temperature. An ice-bath was also used to absorb the heat released during the slow addition of oxone. Though the concentration of the generated dimethyldioxirane varies, good results in our one-pot procedure were obtained by assuming a concentration of 0.08 mol dm^{-3} . This concentration is the average of concentrations found when the generated dimethyldioxirane is distilled from sulfide-free generation vessels.⁴

Elemental analysis and ^1H NMR are consistent with the structure of 2,5-bis(dodecyl)thiophene-1,1-dioxide, (**77**). The ^1H NMR (spectrum 2) of (**77**) showed an interesting observation compared to the ^1H NMR (spectrum 1) of 2,5-bis(dodecyl)thiophene, (**76**) as can be seen in Figure 3.1.

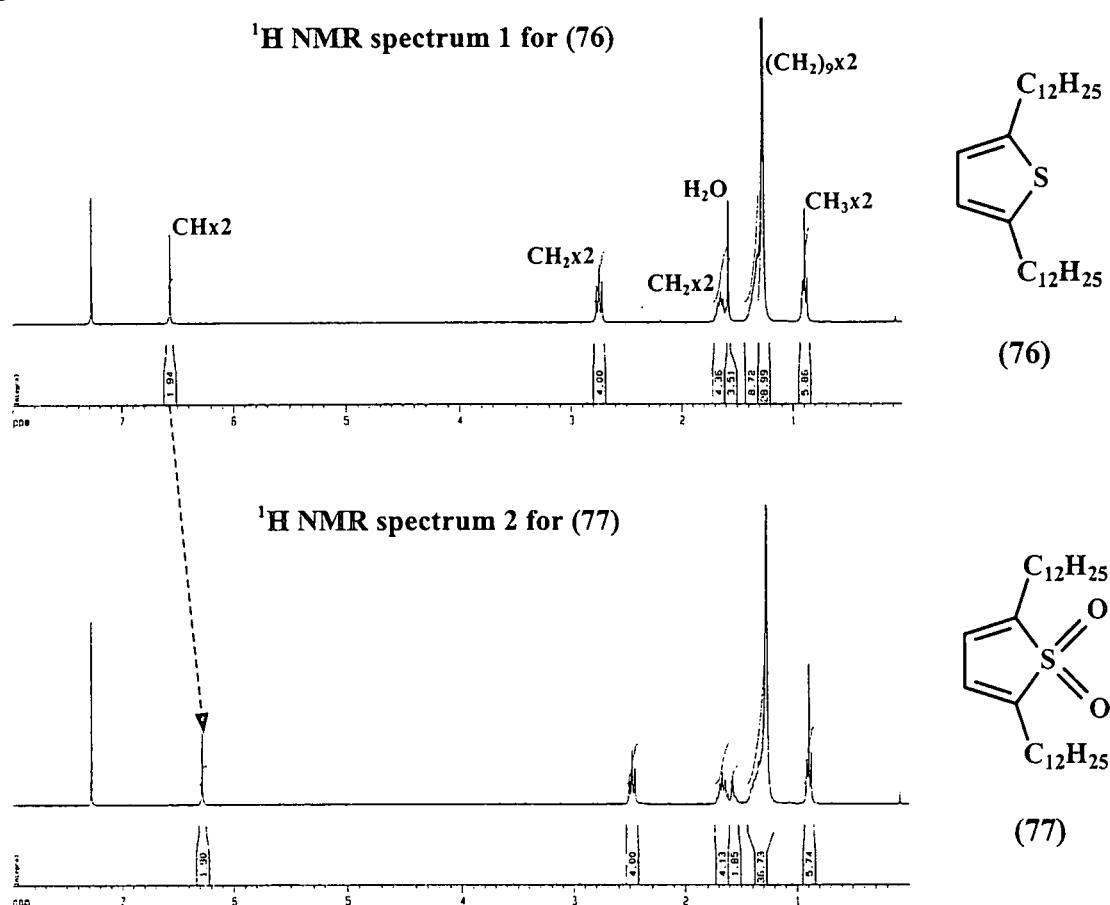


Figure 3.1: ^1H NMR spectra of 2,5-bis(dodecyl)thiophene, (**76**) and 2,5-bis(dodecyl)thiophene-1,1-dioxide, (**77**) in CDCl_3 . The position of the protons on the thiophene ring is highlighted. The signal at ≈ 1.6 ppm is that of water in the sample.

The position of the thiophene-1,1-dioxide protons ($\text{C}_4\text{H}_2\text{SO}_2$) of (**77**) is at $\delta 6.28$, which is 0.29 ppm more upfield than the position of the same protons of 2,5-bis(dodecyl)thiophene, (**76**). This chemical shift is due to the fact that (**76**) is aromatic while (**77**) is not. The presence of the SO_2 -group was also confirmed by infrared spectroscopy (Figure 3.2, page 65) by virtue of two strong peaks at 1284 and 1137 cm^{-1} .

3.2.1.3 3,6-Bis(dodecyl)phthalonitrile, (79)

The Diels-Alder addition between fumaronitrile and 2,5-bis(dodecyl)thiophene-1,1-dioxide, (77), followed by subsequent *in situ* SO₂ extrusion and dehydrogenation of the intermediate (78) gave the desired phthalonitrile (79) in 44% yield. These reactions proceeded simultaneously in a sealed glass tube over 16 h at 160°C in the presence of a minimal quantity chloroform (1.0-1.5 cm³ for 6.5 mmol fumaronitrile), which is the volume needed to wash the reactants through the nozzle of the tube. Larger quantities of chloroform reduced the yield of the desired phthalonitrile (79) dramatically. Elemental analysis and an infrared transmission peak at 2228 cm⁻¹, confirmed the presence of the nitrile (C≡N) groups in (79). The ¹H NMR (spectrum 3) of (79) is also consistent with its structure.

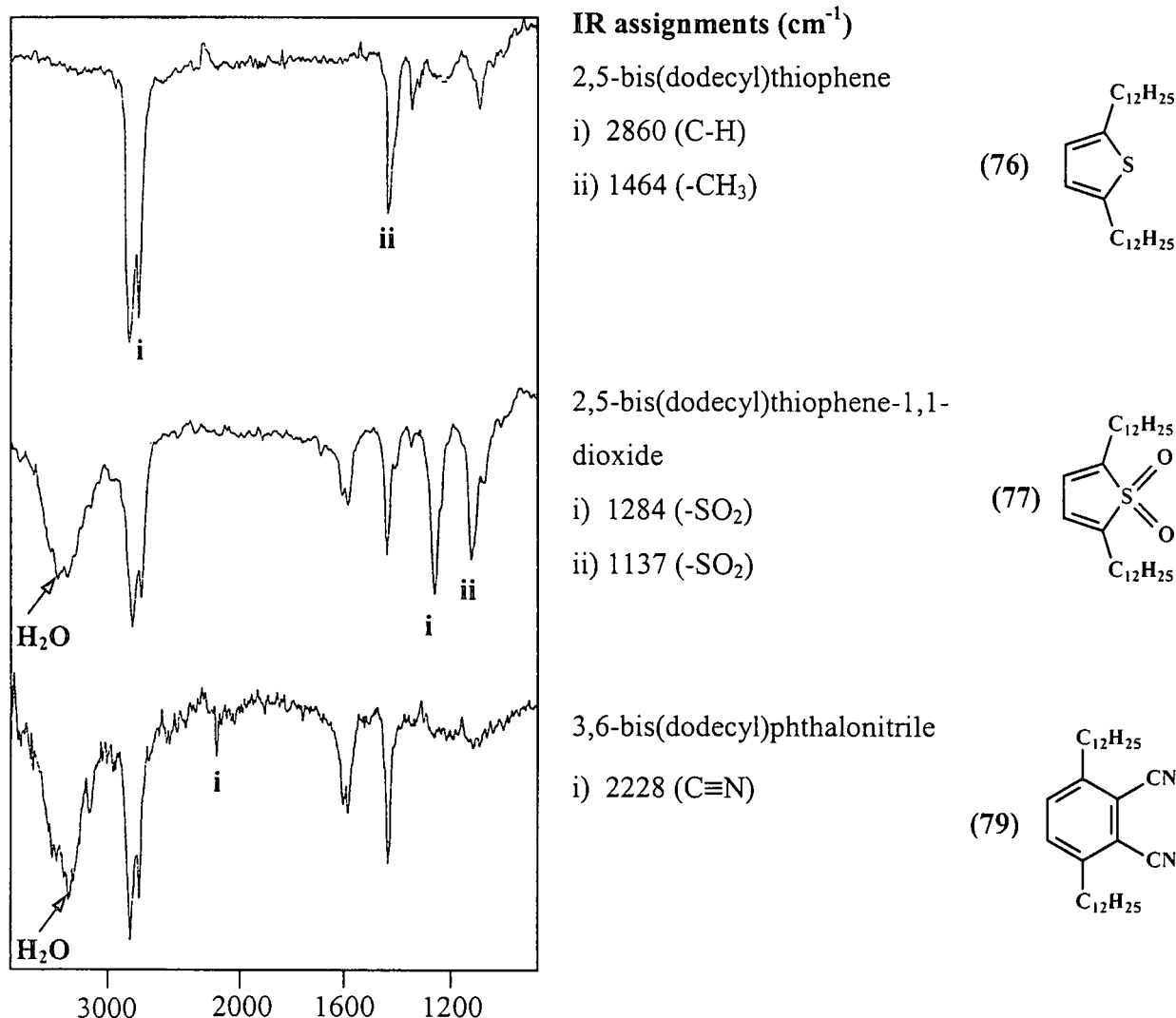
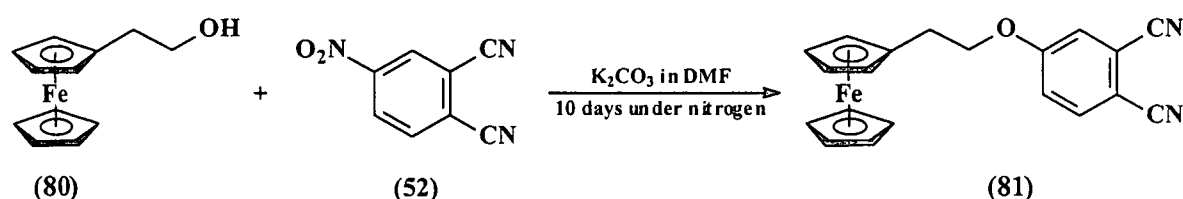


Figure 3.2: Infrared spectra (in KBr, except for (76) which was recorded between NaCl discs) with assignments and structures of (76), (77) and (79). A water peak due to moisture in KBr is observable at ca. 3450 cm⁻¹.

3.2.2 Synthesis of 4-(2'-ferrocenylethoxy)phthalonitrile, (81)

One of the goals of this study is to prepare a ferrocene/phthalocyanine conjugate linked by means of an ether bridge. In order to anchor a ferrocenyl fragment onto a phthalocyanine macrocycle, a suitably functionalised ferrocenyl derivative had to be synthesised first. For this purpose, 4-(2'-ferrocenylethoxy)phthalonitrile, (81) was prepared by a nucleophilic substitution reaction (via nitro displacement) between 4-nitrophthalonitrile and an alcohol forming an ether linkage. Nitro displacement by alcohols is generally a slow reaction: a long reaction time of 10 days was required for the linking of 2-ferrocenylethanol, (80) to 4-nitrophthalonitrile, (52) according to Scheme 3.2.



Scheme 3.2: Synthesis of 4-(2'-ferrocenylethoxy)phthalonitrile, (81).

The nitro group in (52) is activated by the presence of two strongly electron withdrawing cyano groups enhancing its behaviour as a good leaving group under the specified conditions. The excess potassium carbonate used in the reaction seemed to facilitate to a small extent cyclotetramerisation of the phthalonitriles present. As a result, a green precipitate in the aqueous layer during work-up indicated trace amounts of phthalocyanines formed. The crude residue containing the ether (81) was chromatographed on silica to afford the desired product (81) as well as a substantial amount of the unreacted 2-ferrocenylethanol, (80). The ¹H NMR (spectrum 9) of 4-(2'-ferrocenylethoxy)phthalonitrile, (81) showed characteristic signals at δ2.85 (triplet, Fc-CH₂-) and δ4.12 (multiplet, -CH₂-O-)[†] for the two methylene protons in the side chain, respectively. The infrared spectrum of (81) also showed a sharp peak at 2228 cm⁻¹ and a strong peak at 1254 cm⁻¹ confirming the presence of the nitrile (C≡N) and ether linkage (Ar-O-R) respectively.

The above reaction was repeated using different ratios of 4-nitrophthalonitrile, (52) and 2-ferrocenylethanol, (80) with the yields obtained for product (81) compared in Table 3.1.

[†] This peak should be a triplet, but a multiplet is observed because it overlaps with ferrocenyl signals.

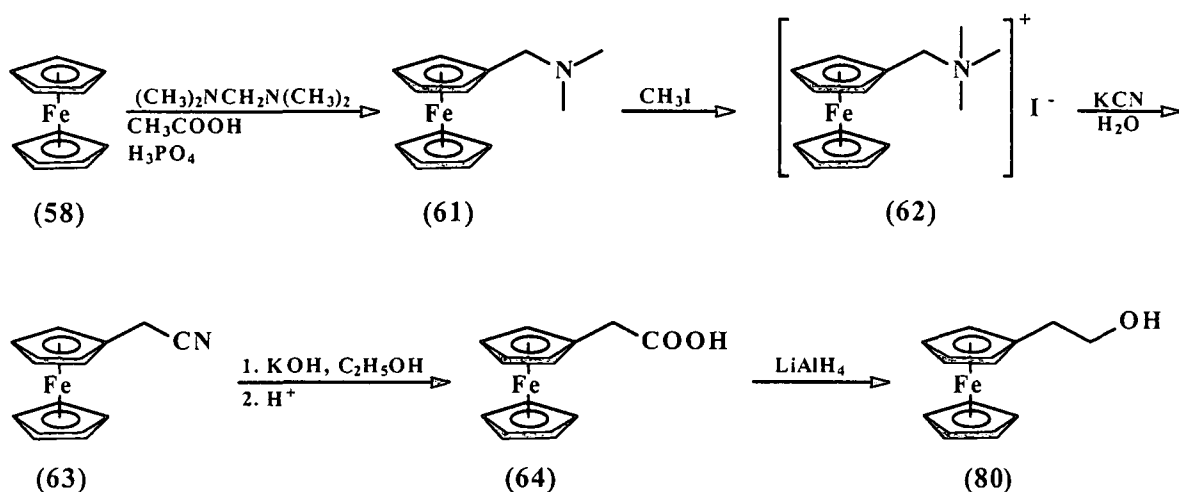
Table 3.1: By reacting different ratios of 4-nitrophthalonitrile, (52) and 2-ferrocenylethanol, (80), different yields of the desired product, 4-(2'-ferrocenylethoxy)phthalonitrile, (81) were obtained.

Ratio of precursors (52):(80)	% yield of phthalo- nitrile (81)	% alcohol (80) recovered
1:3	65.6	59.5
1:2	79.0	42.2

From these results it can be concluded that large excesses of alcohol nucleophiles impair formation of 4-(2'-ferrocenylethoxy)phthalonitrile, (81).

3.2.3 Synthesis of 2-ferrocenylethanol, (80)

The synthesis was directed at synthesising a suitable ferrocene-containing alcohol that could be used as a precursor in the synthesis of 4-(2'-ferrocenylethoxy)phthalonitrile, (81). The desired alcohol, 2-ferrocenylethanol, (80) was synthesised in five steps from ferrocene, (58) according to Scheme 3.3.



Scheme 3.3: Synthesis of 2-ferrocenylethanol, (80).

The initial step involves the preparation of dimethylaminomethylferrocene, (61) via the dimethylaminomethylation of ferrocene, (58) with bis(dimethylamino)methane under an inert atmosphere, to minimise air oxidation of ferrocene and its derivatives in the presence of acids (Scheme 3.3). Slow addition (dropwise) of the amine with stirring on an ice-bath controls the very exothermic reaction between the amine and acids. After sodium hydroxide workup the tertiary amine separates from the alkaline solution as oil in the presence of some black tar. Vacuum distillation of the crude amine gave dimethylaminomethylferrocene, (61) as a dark-red liquid. This compound was characterised by ^1H NMR (spectrum 4), where signals at δ 2.18 and

δ 3.29 represents 6 protons of the two methyl groups and 2 protons of the methylene group in the side chain, respectively.

Thereafter, *N,N*-dimethylaminomethylferrocene methiodide, (**62**) was prepared by methylation of the tertiary amine (**61**) with methyl iodide to give the quaternary ammonium salt in 72% yield as a yellow powder. The methiodide, which separated as oil, crystallised on being scratched. The melting point of this compound is ill-defined because it darkens considerably upon heating as well as shrinking that starts at 173°C. The crude precipitate (**62**) thus obtained was analysed by ^1H NMR (spectrum 5) and was sufficiently pure for further reactions. A signal at δ 3.32 integrating for 9 protons indicates the three methyl groups ($3 \times -\text{CH}_3$) present in (**62**). A second signal in approximately 14% population percentage as per integral ratio is observed at 3.24 ppm. This is explained under the electrochemical section of (**62**) on page 85.

Ferrocenylacetonitrile, (**63**) was then prepared by refluxing the quaternary ammonium salt, (**62**) with sodium cyanide for 2.5 h under nitrogen. Following workup and recrystallisation from hexane the acetonitrile was obtained as yellow crystals in 59% yield. Evolution of trimethylamine was observed during this displacement reaction. Ferrocenylacetonitrile was characterised by both infrared spectrum and ^1H NMR (spectrum 6). A signal at δ 3.45 integrating for 2 protons is assigned to the methylene group in the side chain. The disappearance of the trimethyl signal, which is present in the precursor, (**62**) is also evident. A transmission peak in the infrared spectrum of (**63**) at 2248 cm^{-1} confirmed the presence of the nitrile ($\text{C}\equiv\text{N}$) group (See Figure 3.3). This product is unstable and decomposes with time, therefore it was used immediately after it was prepared.

The saponification (hydrolysis) of (**63**) to liberate ferrocenylacetic acid, (**64**) as orange-brown crystals was a high yielding (86%) reaction. Hydrolysis of (**63**) was achieved by refluxing in ethanol in the presence of potassium hydroxide. After the evolution of ammonia has ceased the alkaline solution was acidified with 85% phosphoric acid to obtain flaky crystals, which after isolation was identified as the desired acid (**64**). The acid was characterised by both IR and ^1H NMR (spectrum 7). Compared to the infrared spectrum of (**63**), the spectrum of (**64**) shows no trace of the nitrile ($\text{C}\equiv\text{N}$) group at 2248 cm^{-1} but instead the appearance of two transmission peaks for (**64**) at 3088 and 1710 cm^{-1} confirmed the presence of the $-\text{OH}$ and $\text{C}=\text{O}$ groups respectively (See Figure 3.3).

Finally, acid (64) was reduced by an excess of lithiumaluminiumhydride in dry ether to give after 3 h of reflux the desired 2-ferrocenylethanol, (80) in a high yield of 93 % as a red-brown viscous oil. The oil is a solid at room temperature with a very low melting point of 32°C. The reduction of the acid (64) was confirmed by the absence of the carbonyl (C=O) peak in the infrared spectrum (See Figure 3.3) of (80) and also by ^1H NMR (spectrum 8) where a triplet confirms the presence of an additional CH_2 group ($-\text{CH}_2-\underline{\text{CH}_2}-\text{OH}$) in the structure of (80) compared to the acid (64) (spectrum 7).

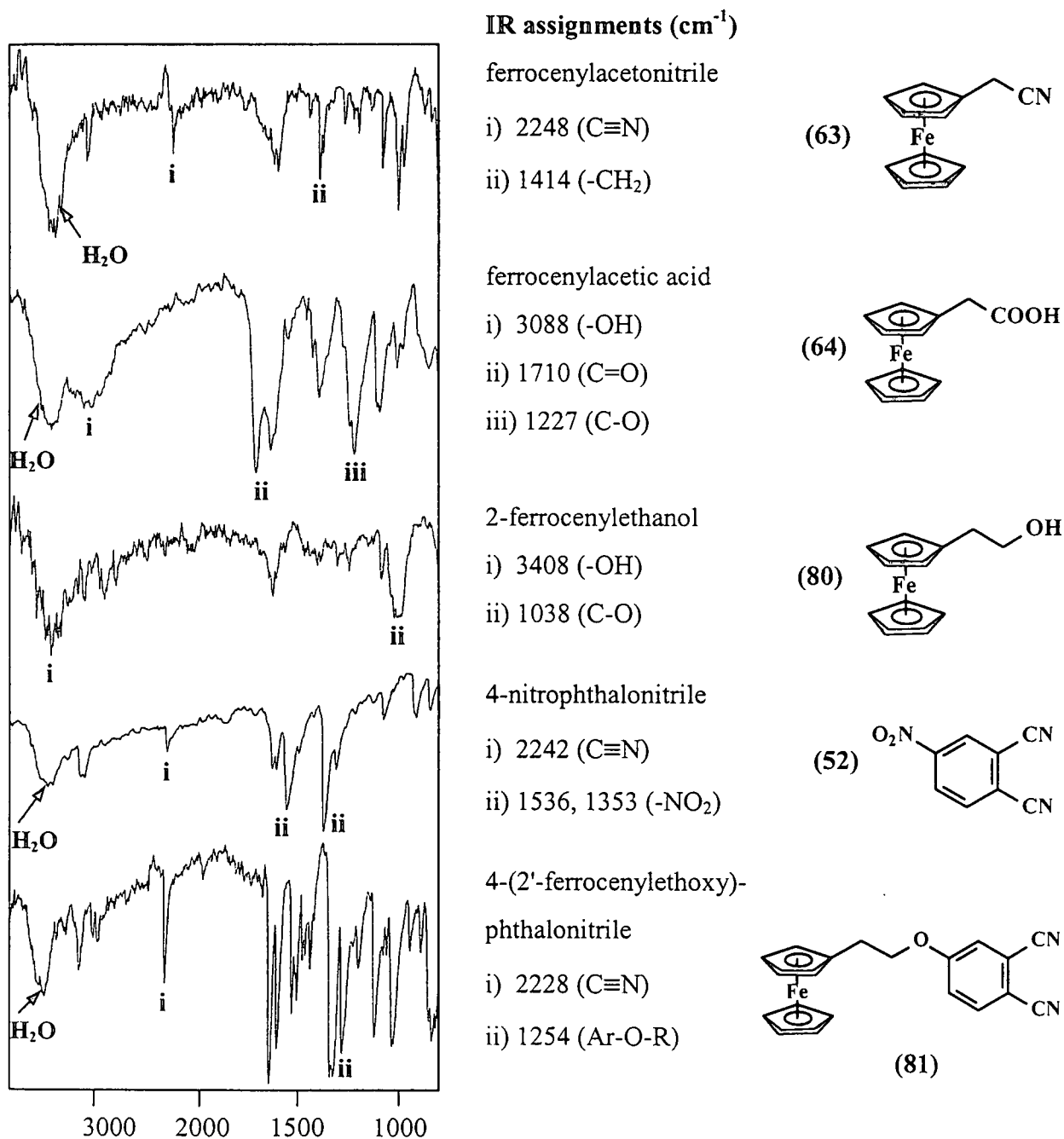


Figure 3.3: Infrared spectra (in KBr, except for (80) which was recorded between NaCl discs) with assignments and structures of 4-nitrophthalonitrile, (52) and ferrocenyl derivatives (63), (64), (80) and (81). A water peak due to moisture in KBr is observable at $\text{ca. } 3450 \text{ cm}^{-1}$.

3.3 Synthesis of substituted phthalocyanines

Having synthesised the 3,6-didodecylated-and 4-(2'-ferrocenylethoxy)phthalonitriles, (79) and (81) respectively, attention was focussed on phthalocyanine synthesis. Two types of phthalocyanines were targeted for synthesis in this study:

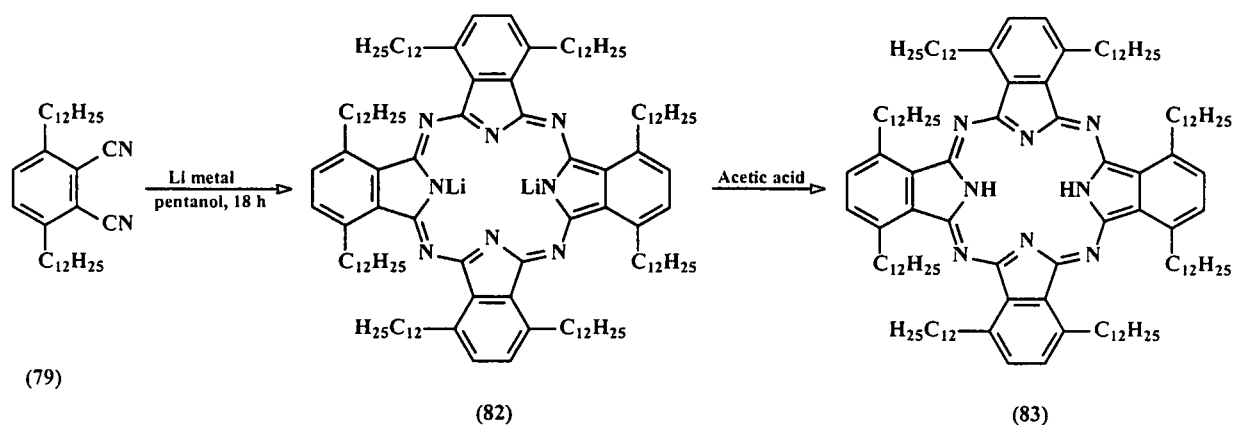
- (i) The first consisted of symmetrically non-peripherally octadodecyl substituted phthalocyanines.
- (ii) The second consisted of unsymmetrically dodecyl-ferrocenylethoxide substituted phthalocyanine conjugates, whereby a 2-ferrocenylethoxy group on the peripheral position via a statistical condensation between two different phthalonitriles took the place of two dodecyl chains on the non-peripheral positions.

In the synthesis of these phthalocyanines, the lithium alkoxide-catalysed procedure was selected using the method of Cook.⁵ This two step procedure is preferred to existing direct metallation procedures due to higher expected yields. All reaction mixtures and stock solutions of phthalocyanines were kept in the dark as far as possible, since all phthalocyanines were regarded as light sensitive in the presence of oxygen. Reaction times of 18 h proved to be more efficient than shorter (~ 5 h) reaction times, because the latter resulted in a decrease in yield of the desired phthalocyanines. All crude phthalocyanine products obtained after work-up were recrystallised from THF/methanol, which proved to be a procedure requiring a fine technique, since the rate of crystallisation depended strongly on the THF/methanol ratio. Fast recrystallisation resulted in co-precipitation of impurities or incorporation of solvent molecules. This led to a phthalocyanine of lower purity and smaller particle size, which made filtration difficult. Purification difficulties of the phthalocyanines of this study are in part attributed to the long dodecyl side chains, wherein impurities can be trapped or entangled, and also to aggregation. Purification via column chromatography on silica was used in cases where mixtures of phthalocyanines or isomers were obtained. The TLC plates used before chromatography discoloured within a day confirming the light sensitivity of the product mixture.

3.3.1 1,4,8,11,15,18,22,25-Octakis(dodecyl)phthalocyanines, (83) and (84)

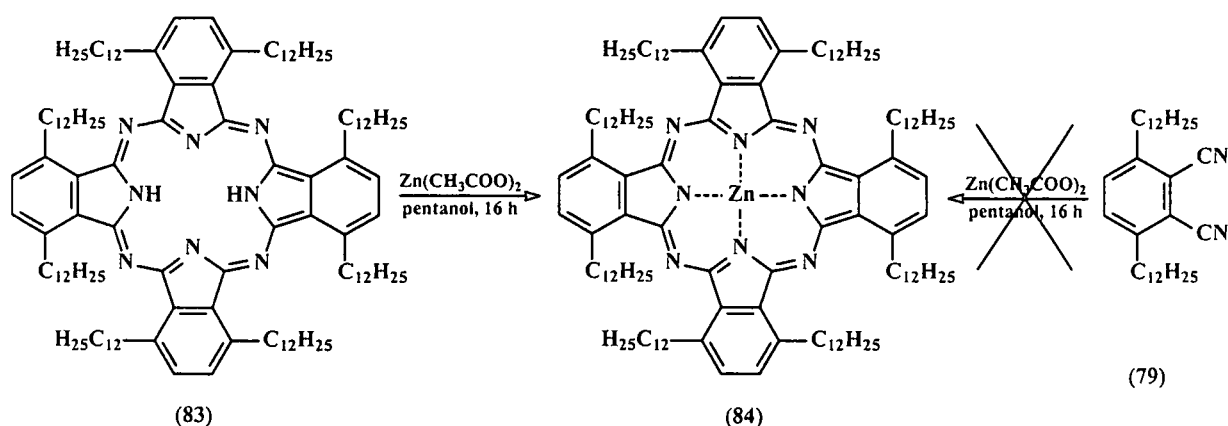
The first phthalocyanine to be synthesised was the non-peripheral octadodecyl substituted metal-free phthalocyanine, (83) in 20% yield by the cyclisation of phthalonitrile (79) in

refluxing pentanol between 110-115°C in the presence of lithium metal according to Scheme 3.4. Lithium pentoxide is formed *in situ* and the formation of a green solution of the dilithium phthalocyanine, (82) species is almost instantaneous. Delithiation of the formed 2LiPc, (82) to liberate the metal-free derivative, (83) is achieved by acid work-up.



Scheme 3.4: Synthesis of 1,4,8,11,15,22,25-octakis(dodecyl)phthalocyanine, (83).

Metallation of the metal-free phthalocyanine, (83) to the corresponding ZnPc, (84) is a very efficient reaction. Yields of 83% by the reaction of (83) with zinc(II)acetate dihydrate in refluxing pentanol over 16 h (Scheme 3.5) was obtained. An attempt to obtain phthalocyanine (84) directly by reacting phthalonitrile (79) with zinc(II)acetate dihydrate in refluxing pentanol, failed. Only the metal-free phthalocyanine was obtained following work-up with acetic acid.



Scheme 3.5: Synthesis of [1,4,8,11,15,22,25-octakis(dodecyl)phthalocyaninato]zinc(II), (84).

Phthalocyanines (83) and (84) were characterised by elemental analyses and ¹H NMR spectroscopy. Assignments of selected ¹H NMR signals are summarised in Table 3.2.

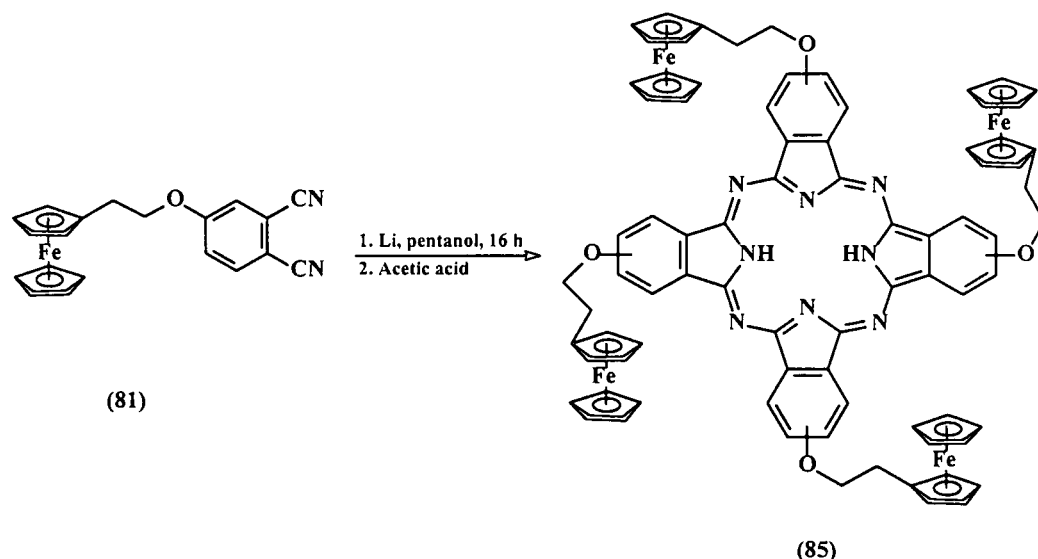
Table 3.2: Proton assignment of signals (in ppm) of the ^1H NMR spectra of phthalonitrile (**79**) and phthalocyanines (**83**) and (**84**).

Compound	Spectrum number	Proton type				
		-CH ₃	-(CH ₂) ₉ -CH ₃	Ar-CH ₂ -CH ₂ -	Ar-CH ₂ -CH ₂ -	Ar-H
Phthalonitrile (79)	3	0.87 6H, t	1.28 36H, s	1.65 4H, m	2.83 4H, t	7.44 2H, s
(C ₁₂ H ₂₅) ₈ -2HPc (83)	10	0.86 24H, t	1.21-1.35 144H, m	2.06 16H, m	4.41 16H, t	7.82 8H, s
(C ₁₂ H ₂₅) ₈ -ZnPc (84)	11	0.85 24H, t	1.12-1.40 144H, m	2.04 16H, m	4.28 16H, t	7.64 8H, s

An interesting observation is the huge downfield shift of the triplet for the benzylic protons (Ar-CH₂-) from phthalonitrile (**79**) to the phthalocyanines (**83**) and (**84**). This shift is from 2.83 ppm for (**79**) to 4.41 and 4.28 ppm for (**83**) and (**84**) respectively. The NMR's also shows a slightly downfield shift in the positions of the aromatic protons (Ar-H) from 7.44 ppm for (**79**) to 7.87 and 7.64 ppm for (**83**) and (**84**) respectively. The huge downfield shift is mostly attributed to the larger deshielding effect the large aromatic phthalocyanine ring has on the benzylic protons (Ar-CH₂-) compared to a simple phenyl ring in Ph-CH₂-. A similar effect was also observed for the ferrocenyl substituted phthalonitrile (**81**) and its corresponding phthalocyanines, which is discussed on pages 78 and 79.

3.3.2 2,9,16,23-Tetrakis(2'-ferrocenylethoxy)phthalocyanine, (**85**)

One of the goals of this study was to prepare a conjugate of a ferrocene and a phthalocyanine moiety by means of an ether linkage. Before the statistical condensation between phthalonitriles (**79**) and (**81**) was considered, the peripherally tetraferrocenyl substituted phthalocyanine, (**85**) was synthesised according to Scheme 3.6 via the lithium alkoxide-catalysed reaction of 4-(2'-ferrocenylethoxy)phthalonitrile, (**81**) in refluxing pentanol at 110°C over 16 h. This mono-substituted phthalonitriles, (**81**) underwent cyclisation to afford the tetraferrocenyl substituted phthalocyanine, (**85**) (Scheme 3.6) as a mixture of four constitutional isomers, which can be separated to some extent by extraction with chloroform (see Chapter 2, page 19).



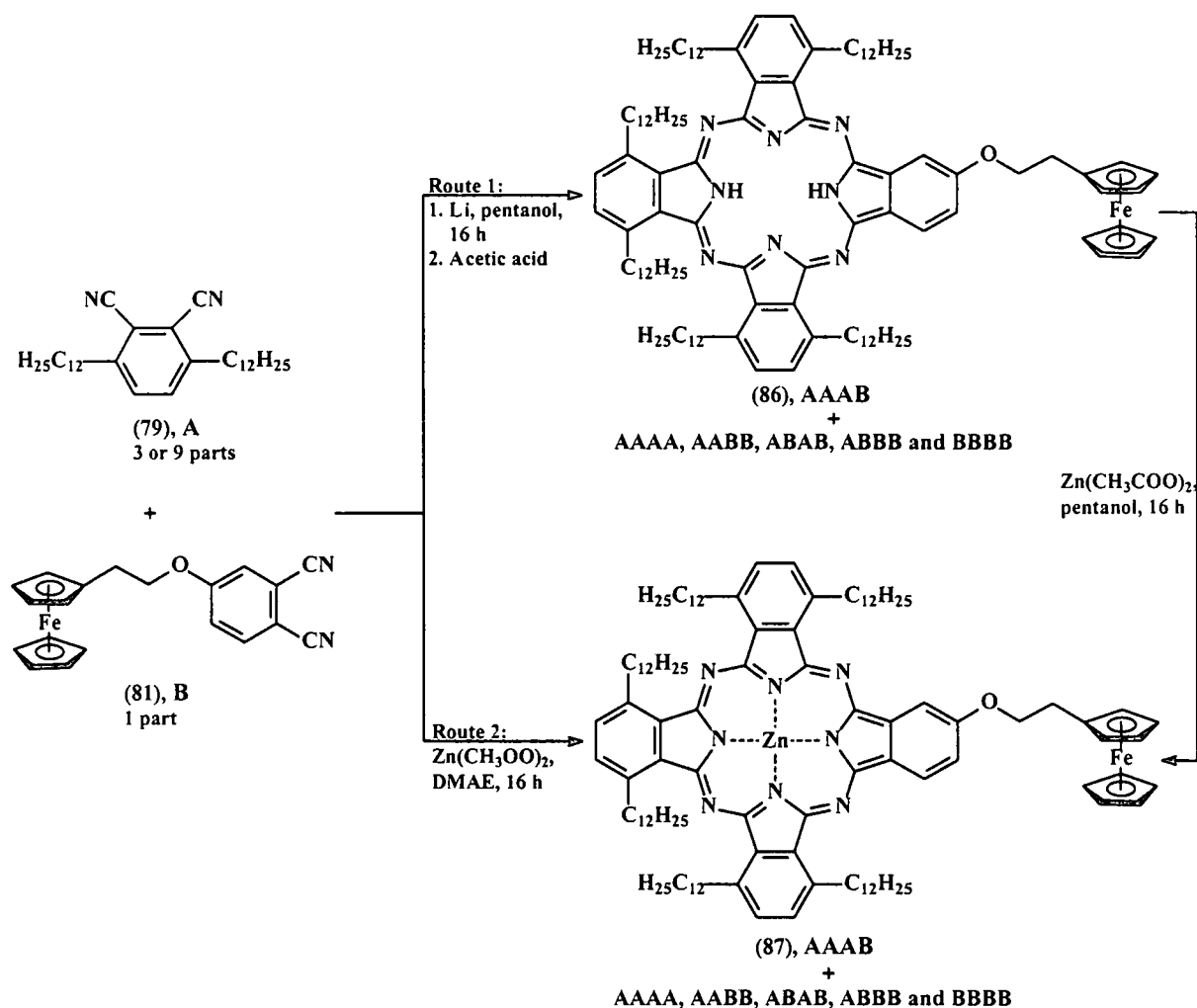
Scheme 3.6: Synthesis of 2,9,16,23-tetrakis(2'-ferrocenylethoxy)phthalocyanine, (85).

The extracted fraction was chromatographed to afford two fractions. The first was positively characterised by ^1H NMR (spectrum 12) as the desired tetraferrocenyl substituted phthalocyanine, (85) in approximately 5% yield. This low yield is attributed to the decomposition of the compound on the silica column. The ^1H NMR spectrum showed multiplets at $\delta 3.16$ and 4.52 ppm that represents 8 protons of the methylene groups in the ferrocenyl side chains ($4 \times \text{Fc}-\text{CH}_2-$) and ($4 \times -\text{O}-\text{CH}_2-$) respectively. Another multiplet at 4.36 ppm which corresponds to the ferrocenyl group's ^1H NMR signal, representing 36 protons of the 4 ferrocenyl groups ($4 \times \text{C}_{10}\text{H}_9$) and a multiplet at 7.05 - 8.60 ppm that corresponds to the 12 phenyl protons ($4 \times \text{Ar}-\text{H}_3$) on the phthalocyanine ring is consistent with the structure of (85). The second fraction from the column could not be identified unambiguously by ^1H NMR.

3.3.3 Synthesis of ferrocene-phthalocyanine conjugates

The next step in the development of phthalonitrile (81) as a phthalocyanine precursor was to utilise it in a reaction to obtain mixed dodecyl-ferrocenyl substituted phthalocyanines. Two different routes were followed to obtain the ZnPc (87) according to Scheme 3.7.

Both routes produced, apart from a large percentage of the non-peripherally octadodecylated phthalocyanines (83) and (84), AAAA, also the desired phthalocyanines (86) and (87), consisting of six non-peripheral dodecyl chains and one 2-ferrocenylethoxy moiety, *i.e.* the AAAB product. Other products and product isomers were also obtained, which are abbreviated as AABB, ABAB, AB BB and BBBB.



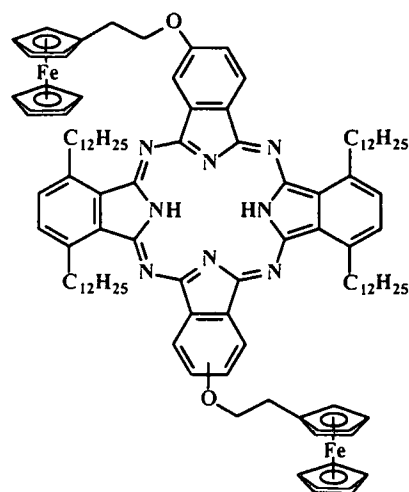
Scheme 3.7: Synthesis of ferrocenyl-phthalocyanine conjugates, following a statistical condensation process, involving phthalonitriles (79), A and (81), B. The main products are (86) and (87) and can be abbreviated as AAAB. The symbols AAAA, AABB, ABAB, AB BB and BBBB represent additional products and product isomers that may be obtained when (79), A and (81), B are statistically condensed according to the guidelines in Chapter 2, page 25. DMAE = dimethylaminoethanol.

The first method (**route 1**) involves the statistical condensation of phthalonitriles (79), A and (81), B in a 3:1 ratio with lithium in pentanol. The reaction mixture was refluxed for 16 h to obtain after acid workup a crude metal-free mixture that *inter alia* contained ferrocenyl-phthalocyanine mixtures. The crude product mixture was initially chromatographed over silica with hexane-toluene (20:1) as eluent, but the toluene gradient was increased gradually with time. This led to the isolation of four fractions, while a fifth fraction was washed from the silica with THF. Some of these fractions were characterised by MALDI-tof mass spectrometry and ^1H NMR, with results of the first four fractions summarised in Table 3.3. The fifth fraction could not be identified due to an unsatisfactory ^1H NMR.

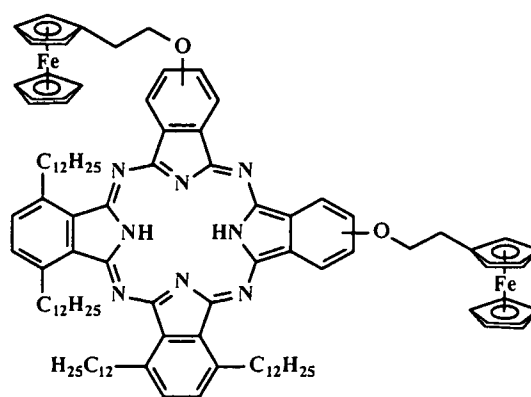
Table 3.3: The % yields, R_f values and MALDI-tof ms data of the fractions obtained from the statistical condensation of phthalonitriles (79), **A** and (81), **B** in a 3:1 ratio with lithium in pentanol *via* route 1 in Scheme 3.7.

Fraction	2HPc as assigned in Scheme 3.7	% yield	R_f in hexane-toluene (20:1)	Ms(MALDI-tof) m/z: position of the $[M+1]^+$ isotopic cluster	ms(MALDI-tof) spectrum nr.	^1H NMR spectrum nr.
1	AAAA, (83)	17.6	0.97	----	----	10
2	AAAB, (86)	12.8	0.59	1752.5	17	13
3	AABB / ABAB, (88)	6.2	0.11	1644.1	18	14
4	AABB / ABAB, (88) and ABBB	5.1	0.06	1644.1 and 1535.4	19	15

The MALDI-tof (spectrum 17, found at the end of this thesis) of fraction 2 shows a narrow peak distribution of isotopic $[M+1]$ peaks centred around 1752.5, which compares well with the formula mass of $1752.3 \text{ g mol}^{-1}$ for 8,11,15,18,22,25-hexakis(dodecyl)-2-(2'-ferrocenylethoxy)phthalocyanine, (86), AAAB. This result was supported by ^1H NMR spectroscopy (spectrum 13, page 79), which shows peaks integrated for 9 aromatic protons (Ar-H) in a 1:1:6:1 ratio between 7.66-9.14 ppm. The 18 protons at 0.85 ppm represents the six methyl groups at the end of the dodecyl chains and the 23 protons between 4.20-4.66 ppm represents –O-CH₂, C₅H₄, C₅H₅ and 6(Ar-CH₂) (See Figure 3.6, page 79). The ratio between these 9, 18 and 23 protons is consistent with the structure of (C₁₂H₂₅)₆-2HPc-O-(CH₂)₂-Fc, (86).



(88a): Two possible isomers



(88b): Three possible isomers

(88)

Figure 3.4: Structures of phthalocyanines ABAB, (88a) and AABB, (88b).

The MALDI-tof (spectrum 18) of fraction 3 shows a narrow distribution of peaks at 1644.1 $m/z = [M+1]$, and correspond to different isotopes of 8,11,22,25-tetrakis(dodecyl)-2,9-bis(2'-ferrocenylethoxy)phthalocyanine, (**88**), **AABB** and/or **ABAB** ($M_r = 1644$ g mol^{-1} , Figure 3.4). This result was also supported by ^1H NMR spectroscopy (spectrum 14), where the peaks at 7.2-8.6 ppm are those of the 10 aromatic protons of this compound. The ratio between the 10 aromatic protons, the 12 protons representing the four methyl groups at the end of the dodecyl chain and the 30 protons representing $2(-\text{O}-\text{CH}_2)$, $2(\text{C}_5\text{H}_4)$, $2(\text{C}_5\text{H}_5)$ and $4(\text{Ar}-\text{CH}_2)$, is consistent with the structure of $(\text{C}_{12}\text{H}_{25})_4\text{-2HPc-[O-(CH}_2)_2\text{-Fc]}_2$, (**88**).

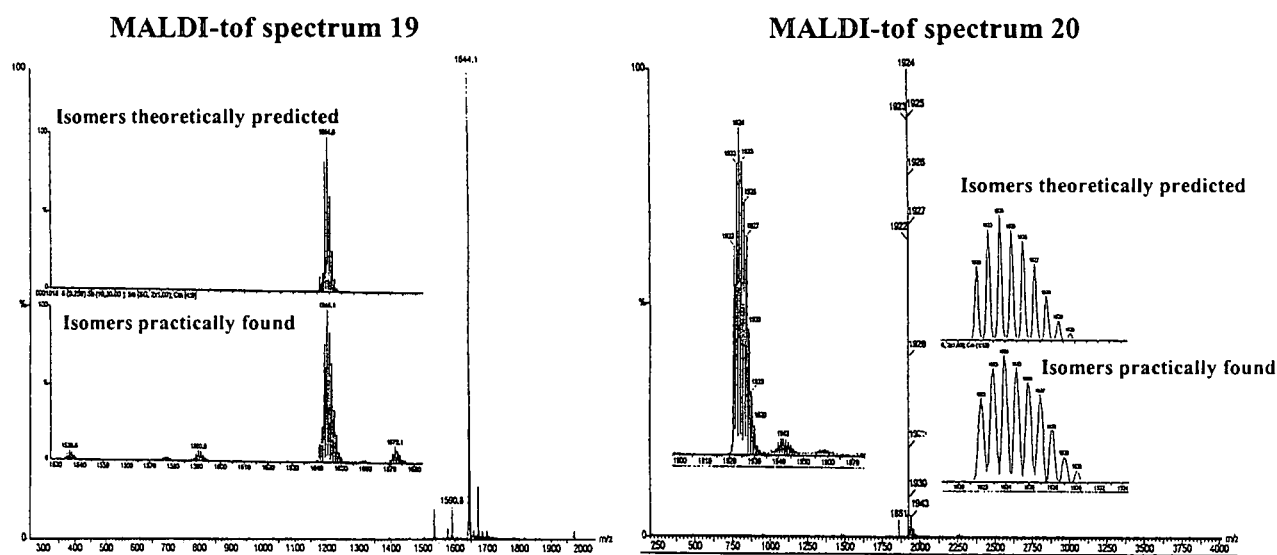


Figure 3.5: MALDI-tof spectra 19 and 20 of fraction 4 (a mixture of metal-free phthalocyanines **AABB** and/or **ABAB**, (**88**) and **ABBB**) and zinc phthalocyanine (**84**) (with a single H_2O molecule coordinated axially to the zinc metal) respectively.

Fraction 4 showed one major isotopic cluster of peaks on its MALDI-tof (spectrum 19, Figure 3.5) at 1644.1 and two minor isotopic clusters of peaks at 1535.8 and 1590 . The first cluster of peaks corresponds to the formula mass of 1644 g mol^{-1} for 8,11,22,25-tetrakis(dodecyl)-2,9-bis(2'-ferrocenylethoxy)phthalocyanine, (**88**), **AABB** and/or **ABAB**. The second cluster of peaks correspond to the formula mass of 1535.4 g mol^{-1} for 22,25-bis(dodecyl)-2,9,16-tris(2'-ferrocenylethoxy)phthalocyanine, **ABBB** and the third some sort of impurity.

A possible explanation of why fraction 4 was not a single compound may be found in a higher tendency to aggregation of the products containing less than six dodecyl chains on the phthalocyanine macrocycle. One may conclude that the non-peripheral dodecyl moieties on the phthalocyanine are much more effective in preventing aggregation than the mono-ferrocenyl fragment in the peripheral position.

This reaction was repeated with a different ratio (9:1) of phthalonitriles (**79**) and (**81**), using the same procedure as for the just described reaction that used a 3:1 ratio. After chromatography four fractions were obtained ($R_f = 0.96$, $R_f = 0.58$, $R_f = 0.10$ and a spot at the origin) and characterised by ^1H NMR. Fraction 1 was positively identified as phthalocyanine (**83**), **AAAA** in 49.9% yield and fraction 2 as the desired ferrocenyl-phthalocyanine (**86**), **AAAB** in 9.6% yield. Fraction 3 was identified as phthalocyanine (**88**), **AABB** and/or **ABAB** in 3.5% yield and fraction 4 as a mixture of phthalocyanines (**AABB** and/or **ABAB** and **ABBB**) in 2.1 % yield. Results obtained in this study are in accordance with what theory predicts. It was shown elsewhere,⁶ that, on the assumption that phthalonitriles (**79**) and (**81**) are equally reactive towards cyclisation, a 3:1 ratio should give 44% of **AAAB**, (**86**) while a 9:1 ratio give 29% of **AAAB**, (**86**). The 9:1 ratio decreases therefore, the yield of (**86**) 34% over a 3:1 ratio. The 9:1 reactant ratio, however, has an advantage over the 3:1 ratio in that **AAAA** and **AAAB** are the major products and only 5% other products and product isomers (**AABB**, **ABAB**, **ABBB** and **BBBB**) are formed, compared to 23% at the 3:1 ratio. The latter makes purification or retrieving of the desired (**86**), **AAAB** more difficult. In the hands of the author, the 9:1 ratio (9.8% of **AAAB**) decreases, the yield of (**86**) 25% over a 3:1 ratio (12.8% yield of **AAAB**). This low yield is attributed to the decomposition of the compound on the silica column.

The zinc-containing ferrocenyl-phthalocyanine, (**87**) can be obtained directly via **route 2** (Scheme 3.7), by the statistical condensation of phthalonitriles (**79**) and (**81**) in dimethylaminoethanol, in the presence of zinc acetate dihydrate in a ratio of 3:1:4 as reactants. After recrystallisation from THF/methanol the crude product was chromatographed on silica with hexane-toluene (2:1) as eluent, to obtain two fractions while a third was washed out of the silica with toluene. A summary of the results of the first two fractions appears in Table 3.4.

Table 3.4: The % yields, R_f values and MALDI-tof ms data of the fractions obtained from the statistical condensation of phthalonitriles (**79**) and (**81**) in the presence of zinc acetate dihydrate in a ratio of 3:1:4 as reactants *via route 2* in Scheme 3.7.

Fraction	2HPc as assigned in Scheme 3.7	% yield	R_f in hexane- toluene (2:1)	Ms(MALDI-tof) m/z: position of the $[M+1]^+$ isotopic cluster	ms(MALDI-tof) spectrum nr.	^1H NMR spectrum nr.
1	AAAA , (84)	7.2	0.97	1924	20	11
2	AAAB , (87)	5.8	0.81	1815	21	16

The third fraction could not be identified due to unsatisfactory ^1H NMR data. The MALDI-tof (spectrum 20 in Figure 3.5, page 76) of fraction 1 shows a narrow distribution of isotopic $[\text{M}+1]$ peaks centred around 1924, which represents different isotopic products of 1,4,8,11,15,18,22,25-octakis(dodecyl)phthalocyaninatozinc(II), **(84)**, **AAAA** ($1924.5 \text{ g}\cdot\text{mol}^{-1}$). A small peak distribution observed at $1942 \text{ m/z} = [\text{M}+1]^+$ indicate the presence of a single water molecule coordinated axially to the zinc metal in the centre of the phthalocyanine macrocycle. The MALDI-tof (spectrum 21) of fraction 2 shows a narrow distribution of peaks at $1815 \text{ m/z} = [\text{M}+1]$ and correspond well with the formula mass for [8,11,15,18,22,25-hexakis-(dodecyl)-2-(2'-ferrocenyl-ethoxy)phthalocyaninato]zinc(II), **AAAB**, **(87)** ($1815.9 \text{ g}\cdot\text{mol}^{-1}$). The ^1H NMR spectrum (spectrum 16) is also consistent with the structure of **(87)**. Important ^1H NMR signals of the ferrocene-containing phthalonitrile precursor **(81)** and phthalocyanines **(86)** and **(87)**, (Figure 3.6, page 79) are summarised in Table 3.5.

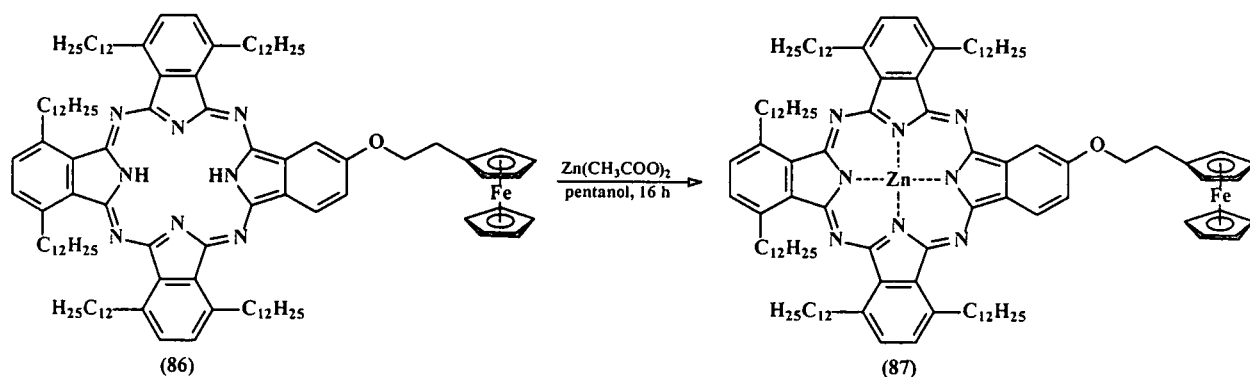
Table 3.5: Proton assignment of selected signals (in ppm) of the ^1H NMR spectra of phthalonitrile **(81)** and its corresponding phthalocyanines **(86)** and **(87)**.

Compound	Spectrum number	Proton type			
		-CH ₃	Ar-CH ₂ - <u>CH₂</u> - and/or - <u>CH₂</u> -Fc	Fc-, -O-CH ₂ - and/or Ar- <u>CH₂</u> -	Ar-H
Phthalonitrile (81)	9	-----	2.85 2H, t, - <u>CH₂</u> -Fc	4.12 11H, m, Fc, -O-CH ₂ -	7.10-7.70 3H, m
(C ₁₂ H ₂₅) ₈ -2HPc- [O-(CH ₂) ₂ -Fc], (86)	13	0.85 18H, t	2.18 12H, m, Ar-CH ₂ - <u>CH₂</u> 3.15 2H, t, - <u>CH₂</u> -Fc	4.20-4.66 23H, m, Fc, -O-CH ₂ - and Ar- <u>CH₂</u>	7.66-9.14 9H, m
(C ₁₂ H ₂₅) ₈ -ZnPc- [O-(CH ₂) ₂ -Fc], (87)	16	0.86 18H, t	2.17 12H, m, Ar-CH ₂ - <u>CH₂</u> 3.10 2H, t, - <u>CH₂</u> -Fc	3.89-4.50 23, m, Fc-, -O-CH ₂ - and Ar- <u>CH₂</u> -	7.33-8.58 9H, m

The cluster of peaks indicated with (\downarrow) in the spectrums in Figure 3.6 clearly indicates the presence of the ferrocenyl group in phthalonitrile **(81)** at $\delta = 4.12 \text{ ppm}$ and at 4.28 ppm for the desired phthalocyanines **(86)** and **(87)**. A marked (\downarrow) downfield shift is observed in the position of the two aliphatic protons (Fc-CH₂-) in moving from 2.85 ppm for phthalonitrile **(81)** to 3.15 and 3.10 ppm for the ferrocene-containing phthalocyanines **(86)** and **(87)** respectively. This downfield shift is mostly attributed to the larger deshielding effect the large aromatic

Likewise, there is a downfield shift in the resonating positions of aromatic protons in moving from (81) to (86), which is again ascribed to the larger deshielding effect of the phthalocyanine macrocycle compared to a phenyl ring. There is also an upfield shift observed in the positions of the 9 aromatic protons (Ar-H) of the phthalocyanine macrocycle in moving from 7.66 - 9.14 ppm for (86) to 7.33 - 8.58 for (87). This upfield shift is attributed to the stronger electron-donating properties of zinc in the phthalocyanine core of (87) compared to the poorer electron-donating properties of the two hydrogen cations, in (86). To quantify this it is instructive to note that zinc in (87) is less electronegative ($\chi_{\text{Zn}}=1.7$) than the protons in (86), ($\chi_{2\text{H}}=2.2 \times 2=4.4$), which implies one zinc cation is on a relative scale more electron donating than two protons and therefore induces an upfield chemical shift of aromatic protons when moving from (86) to (87).

The zinc-containing ferrocenyl-phthalocyanine, (87) can also be obtained by the complexation of Zn^{2+} with the metal-free phthalocyanine, (86). This was achieved in 86% yield by reacting phthalocyanine (86) with zinc(II)acetate dihydrate in refluxing pentanol over 16 h at 110°C (Scheme 3.8).



Scheme 3.8: Synthesis of $(\text{C}_{12}\text{H}_{25})_6\text{-ZnPc-O-(CH}_2)_2\text{-Fc}$, (87) via the complexation of a metal-free ferrocene-containing phthalocyanine, (86) with zinc.

This reaction held several advantages over the direct route shown in Scheme 3.7, page 74, especially because (86) is much easier to purify from **AABB** isomers than (87) due to better solubility properties. This meant that (87) obtained from the route shown in Scheme 3.8 is more pure due to the purity of (86) as compared to (87) obtained from Scheme 3.7. The high yield of metallation according to Scheme 3.8 (86%) is also very attractive from a synthetic point of view.

3.4 Electrochemistry

The third aim of this study (Chapter 1) was to investigate the electron transfer properties of some ferrocene derivatives, as well as the ferrocene-free and ferrocene-containing phthalocyanines by means of cyclic voltammetry.

3.4.1 Cyclic voltammetry of ferrocenyl derivatives

The cyclic voltammetry study on the ferrocenyl derivatives were carried out at 25°C in argon purged acetonitrile in the presence of tetra-*n*-butylammonium hexafluorophosphate, (${}^n\text{Bu}$) $_4^+\text{NPF}_6^-$ as supporting electrolyte. The three-electrode system used, consisted of a platinum auxiliary electrode, a platinum working electrode and a Ag/Ag^+ (0.01 mol dm $^{-3}$ in acetonitrile) non-aqueous reference electrode. Scan rates varied over the range 50-250 mV s $^{-1}$.

The structures of the ferrocenyl derivatives that were considered for an electrochemical investigation in this study are shown in Figure 3.7.

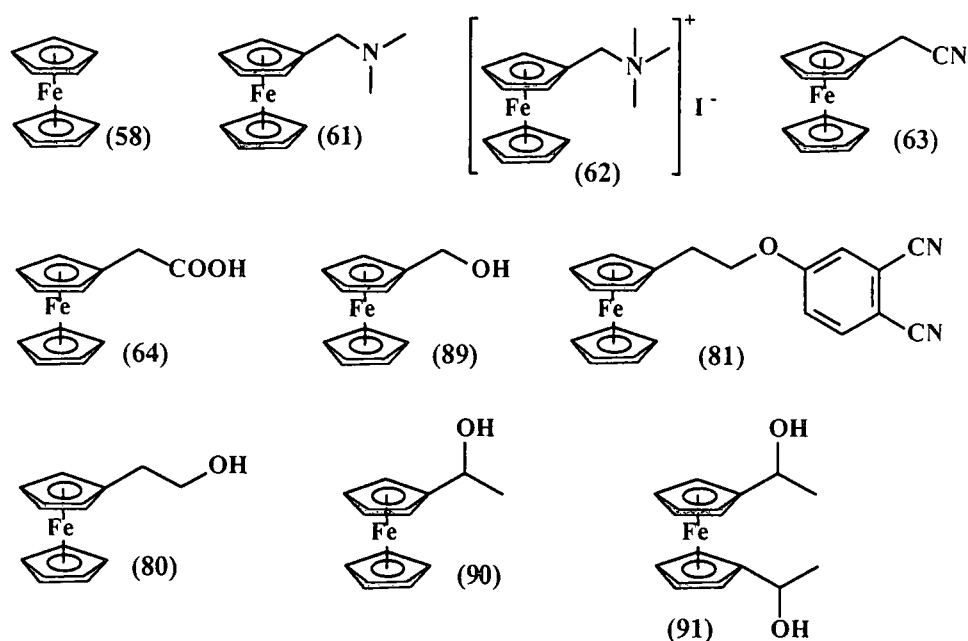


Figure 3.7: Ferrocenyl derivatives that were studied by means of cyclic voltammetry.

Voltammograms of ferrocene, (58) at various scan rates are shown in Figure 3.8. Peak anodic (E_{pa}) and peak cathodic (E_{pc}) potentials (referenced against Ag/Ag^+) as well as their differences, $\Delta E_{\text{p}} = E_{\text{pa}} - E_{\text{pc}}$, and the ratio of peak anodic and peak cathodic currents, $i_{\text{pa}}/i_{\text{pc}}$, were determined by reading off the appropriate values on the cyclic voltammogram as shown in Figure 3.8 for the 250 mV s $^{-1}$ scan rate. The formal reduction potentials, $E^{\circ'} = (E_{\text{pa}} + E_{\text{pc}})/2$ of each compound were also calculated. Results are summarised in Table 3.6, page 87 and Table 3.9, page 95.

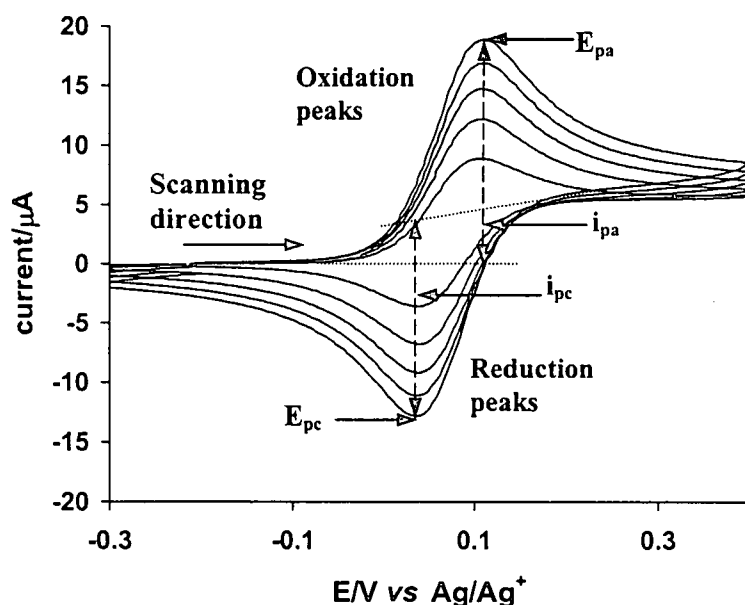


Figure 3.8: Cyclic voltammograms of ferrocene (1 mmol dm^{-3}), (58) in acetonitrile at 25°C on a platinum working electrode, recorded at scan rates of 50 (smallest voltammogram), 100, 150, 200 and 250 mV s^{-1} containing $0.2 \text{ mol dm}^{-3} (\text{tBu})_4\text{NPF}_6$ as supporting electrolyte.

It is normal under IUPAC convention to report potentials referenced to the Fc/Fc^+ couple where ferrocene is used as an internal standard as described by Gagny.⁷ However, for the present study it is an improper approach for the simple reason that when ferrocene is added as an internal standard to a solution, the peak potentials are so close that poor resolution (*i.e.* peak separation) is obtained. This is demonstrated for the compound ferrocenylacetonitrile, (63) in Figure 3.9.

The CV labelled (a) is that of pure FcCH_2CN , the CV labelled (b) is that of pure ferrocene, $\text{FcC}_{10}\text{H}_{10}$, and the CV labelled (c) is that of FcCH_2CN in the presence of the internal marker, ferrocene. The closeness of the Fc/Fc^+ couple to that of the ferrocenyl couple of FcCH_2CN tend to distort both the expected peaks maximas for these two compounds (CV (c)) and slightly alter the observed formal reduction potential (E°) because accurate measurements of peak potentials is not possible. In this case, E° of (63) changed from 0.176 V to 0.173 V in the presence of ferrocene, while E° for free ferrocene itself is 0.073 V and in the presence of (63) as internal marker E° changed to 0.077 V . Furthermore, the uncertainty of the decay current for peaks 1 and 3 shown in CV (c), will lead to inaccuracies in the reported peak current values. The i_{pa}/i_{pc} ratios of (63) were estimated from superimposing the decay current of peak 2 on peak 1 and the decay current of peak 4 on peak 3. Hence, in this study all potentials are given referenced against Ag/Ag^+ . An interested reader can convert to potentials referenced against Fc/Fc^+ by

subtracting the formal reduction potential of ferrocene, 0.072 V vs. Ag/Ag^+ (in acetonitrile) from reported E° values listed in Table 3.6.

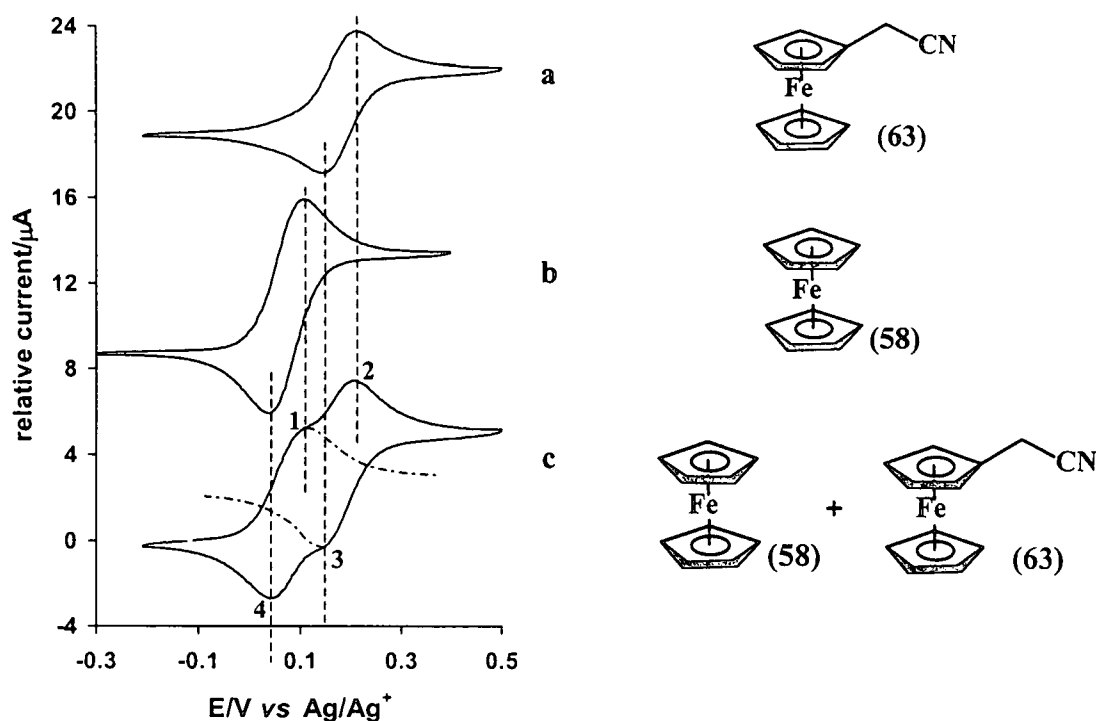


Figure 3.9: Cyclic voltammograms of (a) ferrocenylacetonitrile, (63), (b) ferrocene, (58) and (c) (63) ($0.001 \text{ mol dm}^{-3}$ in acetonitrile) in the presence of ferrocene as an internal marker at 25°C on a platinum working electrode, recorded at a scan rate of 50 mV s^{-1} containing 0.2 mol dm^{-3} $(^t\text{Bu})_4^+\text{NPF}_6^-$ as supporting electrolyte. The broken (----) line shows the expected but inaccurately estimated decay currents of peaks 1 and 3, which imply peak currents, will not be accurate.

Differences in peak anodic (E_{pa}) and peak cathodic (E_{pc}) potentials, ΔE_p , for all the ferrocenyl derivatives of Figure 3.7 except for alcohol (89) were below 80 mV and indicate reasonable electrochemical reversibility. Electrochemical reversibility implies that peak potential differences, ΔE_p of a one-electron process at 25°C should in theory be 0.059 V and is independent of scan rates. However, in practice the value of ΔE_p seldom reaches exactly 0.059 V. In practice, factors such as overvoltage and internal resistance cause ΔE_p values in acetonitrile to be somewhat larger. For the purposes of this thesis, any ΔE_p value smaller than 0.080 V at the slowest scan rate employed (50 mV s^{-1}) is taken to imply electrochemical reversibility for the investigated compound. The $i_{\text{pa}}/i_{\text{pc}}$ ratios for all compounds except couple I of (62) approached 1.

The first important interpretation from the electrochemical study involves the influence of the group electronegativity, which is a measure of electron withdrawing power of this group, on the formal reduction potential of the ferrocenyl group in compounds of the type $\text{Fc}-(\text{CH}_2)_n\text{-R}$, $n = 1$

or 2. In this study, for compounds with $n = 1$, $R = N(CH_3)_2$, (61), $^+N(CH_3)_3$, (62), CN, (63), COOH, (64), or OH, (89) (compound (89) was provided by Prof. J.C. Swarts).

Voltammograms of ferrocene, (58), and the derivatives (61), (62), (63), (64) and, (89) are shown in Figure 3.10 at a scan rate of 50 mV s^{-1} .

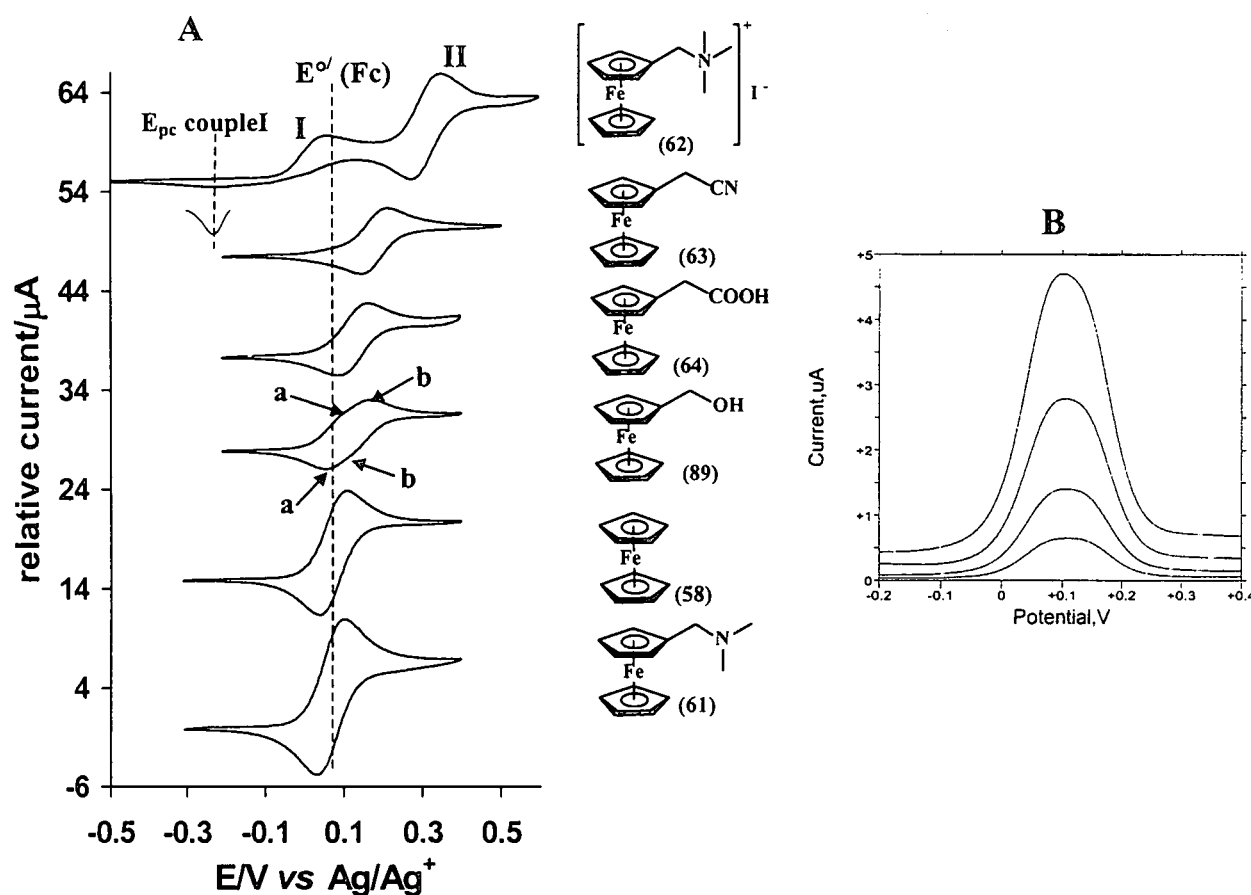


Figure 3.10: A: Cyclic voltammograms of ferrocene, (58) and its derivatives (61), (62), (63), (64) and (89) (1 mmol dm^{-3}) in acetonitrile at 25°C on a platinum working electrode, recorded at a scan rate of 50 mV s^{-1} containing 0.2 mol dm^{-3} $(^n\text{Bu})_4\text{-}^+\text{NPF}_6$ as supporting electrolyte. B: Osteryoung Square wave voltammogram of ferrocenylmethanol, (89) under the same conditions as for its CV recorded at scan rates of 1 (smallest voltammogram), 5, 15 and 50 mV s^{-1} .

When one considers the average formal reduction potentials, E° , tabulated in Table 3.6, page 87, it becomes apparent that the redox properties of each compound are manipulated by the side-chain bound to the ferrocyl moiety (ferrocyl = $\text{Fc-CH}_2\text{-}$, whereas ferrocenyl = Fc-).

Firstly, introduction of the dimethylaminomethyl side-chain in (61) resulted in a formal reduction potential of $0.066 \text{ V vs Ag/Ag}^+$. This is 0.007 V more negative than E° of ferrocene (0.073 V) itself. This small shift implies the $\text{CH}_2\text{-N(CH}_3)_2$ substituent may have electron donating properties which only slightly increase the electron density on the iron centre of the ferrocenyl group. Methylation of (61) to give the quaternary ammonium salt, (62) resulted in a

compound which showed in its cyclic voltammogram two peaks, indicated by couples I ($E_{pc} = -0.273$ at $v = 50 \text{ mV s}^{-1}$, an irreversible wave) and II ($E^{0'} = 0.308$, a reversible wave) in Figure 3.10. These two peaks were still present even after extensive hexane washing of the finely powdered solid (**62**) to remove any non-methylated starting material, (**61**), or by carrying the CV out at a higher temperature of 70°C . This implies that both waves I and II in the CV of (**62**) are an intrinsic part of the electrochemical fingerprint of this compound.

The ^1H NMR spectrum of (**62**) (Figure 3.11) shows that this compound is clean in the sense that there are no impurities. However, it does detect the presence of a second, probably conformational species of $\text{Fc-CH}_2\text{-}^+\text{N}(\text{CH}_3)_3$ in approximately 14% population percentage as per integral ratios. It is difficult to establish a clear-cut reason for this observation, but a Dreiding model of this compound showed that a rotational conformation where free rotation of all side groups is severely hampered exists. If this is the case, it follows that in this particular conformational configuration, free rotation may be slowed down to the point where two conformations of the same compound, here (**62**), is observable on the ^1H NMR time scale. If this is indeed the case, then it will also explain the observation of couples I and II in the CV of compound (**62**).

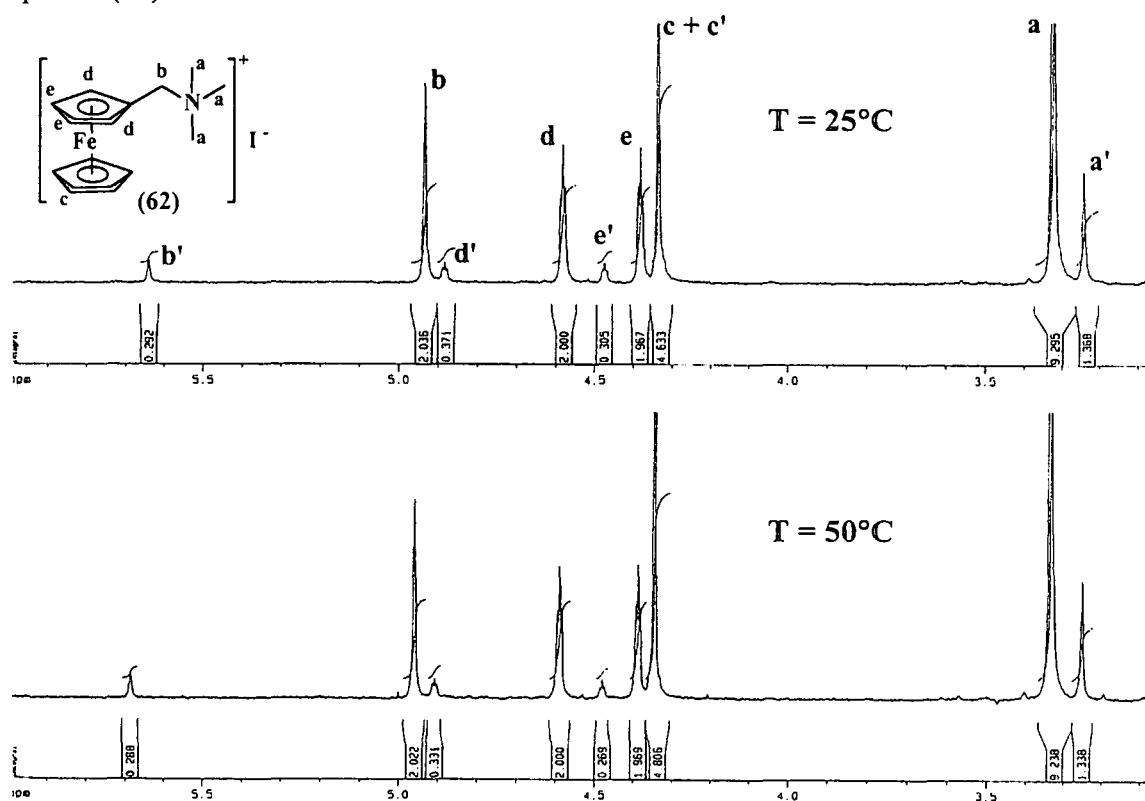


Figure 3.11: ^1H NMR spectra of the quaternary ammonium salt, (**62**) in CDCl_3 at 25°C (top) and 50°C (bottom).

A variable temperature ^1H NMR study of (62) in CDCl_3 showed a 15% (at 25°C) and 13% (at 50°C) population percentage as per integral ratios for the signals at 4.49 and 4.52 ppm (Figure 3.11).

The low boiling point of the solvent, CDCl_3 , prevented us to increase the temperature to higher values. The integral ratio decrease of 2% from 25°C to 50°C is too small, to read any meaning into it. One would, however, expect to see at least the beginning of a possible merge of the peaks of the two species over this temperature range. On this evidence we concede that rotational isomerisation, as the main cause of the second species of (62) is a small possibility. As an alternative possible explanation, it may be possible that the iodide anionic species, (62a) exist parallel with (62) (Figure 3.12). If (62a) is stable on the NMR and CV time scale, it may account for the presence of couple I in the CV shown in Figure 3.10, as well as for the isomer peaks labelled with a prime (*i.e.* a', b', c', d' and e') in the ^1H NMR shown in Figure 3.11.

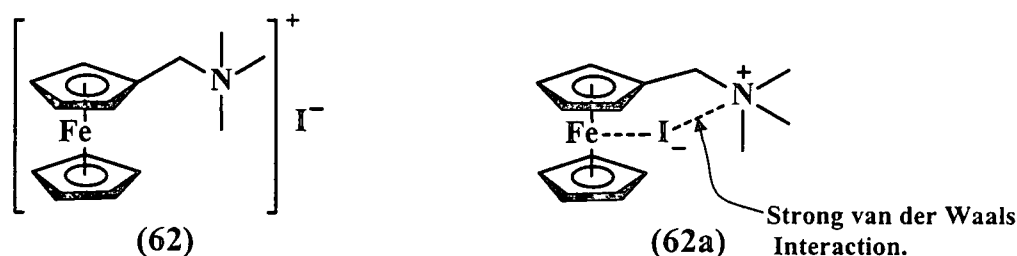
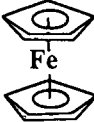
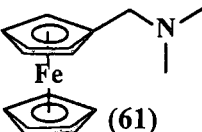
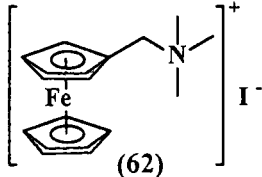
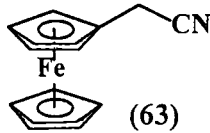
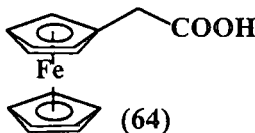
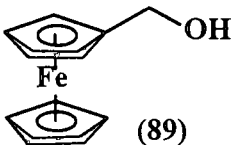


Figure 3.12: Two possible positions of the iodide anion in *N,N*-dimethylaminomethylferrocene methiodide.

It must be stressed, however, that further research is required, which may include quantum chemical calculations, to clearly establish an unambiguous explanation for the observation of couple I in the CV and the second structural isomer of (62) in its ^1H NMR.

In contrast to couple I, couple II is associated with a well electrochemically reversible process by virtue of $\Delta E_p = 68$ mV and $i_{pa}/i_{pc} = 1.03$ at a scan rate of 50 mV s^{-1} . This couple is therefore assumed to be the principally important redox process associated with $\text{Fc-CH}_2\text{-}^+\text{N}(\text{CH}_3)_3$ (*i.e.* structure (62) in Figure 3.12) and is thus used for comparison with formal reduction potentials of other complexes in this study. Couple II implies a formal reduction potential, E° of 0.308 V. This E° of (62) is 235 mV more positive than E° of ferrocene, (58) and 242 mV more positive than E° of the free base $\text{FcCH}_2\text{N}(\text{CH}_3)_2$, (61), which implies that the electron withdrawing capabilities of $\text{-CH}_2\text{-}^+\text{N}(\text{CH}_3)_3$ exceeds that of $\text{-CH}_2\text{-N}(\text{CH}_3)_2$ by far.

Table 3.6: Electrochemical data for ferrocene and the indicated ferrocenyl derivatives (1mmol dm⁻³) in acetonitrile containing 0.2 mol dm⁻³ (nBu)₄⁺NPF₆⁻ as supporting electrolyte at 25°C vs Ag/Ag⁺ at scan rates of 50, 100, 150, 200 and 250 mV s⁻¹.

Compound	v/ mV.s ⁻¹	E _{pa} / V	ΔE _p / mV	E ^o / V	i _{pa} / μA	i _{pa} /i _{pc}
 (58)	250	0.109	73	0.073	17.19	1.02
	200	0.108	71	0.073	15.44	1.01
	150	0.106	68	0.072	13.66	1.00
	100	0.105	65	0.073	11.29	1.00
	50	0.103	62	0.072	8.36	1.00
	Average			0.073		1.01
 (61)	250	0.103	77	0.065	21.39	1.11
	200	0.102	74	0.065	19.43	1.11
	150	0.101	72	0.065	16.99	1.12
	100	0.100	68	0.066	14.13	1.11
	50	0.099	64	0.067	10.46	1.11
	Average			0.066		1.11
COUPLE I  (62)	250	0.068	410	-0.342 ^a	8.55	4.19
	200	0.064	395	-0.331 ^a	7.69	4.63
	150	0.061	381	-0.320 ^a	6.84	4.88
	100	0.057	366	-0.309 ^a	5.64	4.41
	50	0.051	344	-0.293 ^a	4.24	3.86
	Average : Couple I					
	250	0.348	80	0.308	13.40	1.07
	200	0.347	78	0.308	12.26	1.04
	150	0.346	76	0.308	10.95	1.02
	100	0.344	72	0.308	9.17	1.02
	50	0.342	68	0.308	6.89	1.03
	Average : Couple II			0.308		1.04
 (63)	250	0.212	74	0.175	9.05	1.11
	200	0.211	71	0.176	8.06	1.10
	150	0.210	69	0.176	7.07	1.09
	100	0.209	67	0.176	5.88	1.09
	50	0.208	63	0.177	4.23	1.05
	Average			0.176		1.09
 (64)	250	0.162	79	0.123	10.22	1.09
	200	0.161	77	0.123	9.17	1.07
	150	0.160	75	0.123	7.89	1.03
	100	0.159	73	0.123	6.47	1.06
	50	0.158	69	0.124	4.75	1.04
	Average			0.123		1.06
Couple a  (89)	250	0.050 ^c	- ^b	0.089 ^d	- ^b	- ^b
	200	0.052 ^c	- ^b	0.089 ^d	- ^b	- ^b
	150	0.053 ^c	- ^b	0.088 ^d	- ^b	- ^b
	100	0.054 ^c	- ^b	0.088 ^d	- ^b	- ^b
	50	0.055 ^c	- ^b	0.088 ^d	- ^b	- ^b
	Average : Couple a			0.088 ^d		
	250	0.169	- ^b	0.132 ^d	- ^b	- ^b
	200	0.168	- ^b	0.132 ^d	- ^b	- ^b
	150	0.168	- ^b	0.133 ^d	- ^b	- ^b
	100	0.167	- ^b	0.133 ^d	- ^b	- ^b
	50	0.166	- ^b	0.133 ^d	- ^b	- ^b
	Average : Couple b			0.133 ^d		

^aE_{pc} instead of E^o values due to the irreversibility of couple I. ^bPoorly defined oxidation wave of couple a and reduction wave of couple b made current and ΔE_p measurements impossible. ^cE_{pc} value. ^dE^o were obtained by assuming ΔE_p = 66 mV, the average of ΔE_p values for (58), (61), (63) and (64) at a scan rate of 50 mV s⁻¹.

The cyclic voltammogram of ferrocenylacetonitrile, (63) exhibited good electrochemical reversibility with $E^{\circ'} = 0.176$ V. This implies that although the nitrile substituent removes electron density from the ferrocenyl group, it is not as strong an electron withdrawing group as $\text{CH}_2\text{-}^+\text{N}(\text{CH}_3)_3$. The carboxylic acid $\text{Fc-CH}_2\text{-COOH}$, (64), exhibits $E^{\circ'} = 0.123$ which implies the carboxylic acid group is even less electron withdrawing than a nitrile group.

The last compound investigated in this series is $\text{Fc-CH}_2\text{-OH}$, (89). The introduction of a methanol side-chain in ferrocene to give (89) resulted once again in complex electrochemical behaviour as with $\text{Fc-CH}_2\text{-}^+\text{N}(\text{CH}_3)_3$, (62). Two poorly resolved redox processes labelled **a** and **b** respectively were observed in the voltammogram (Figure 3.10). Only the peak cathodic potential for couple **a** and the peak anodic potential for couple **b** could be accurately measured. These were $E_{\text{pc}} = 0.055$ V and $E_{\text{pa}} = 0.166$ V respectively at a scan rate of 50 mV s^{-1} . Formal reduction potentials listed in Table 3.6 were on the assumption that ΔE_{p} was 66 mV, the average ΔE_{p} values for (58), (61), (63), (64) at a scan rate of 50 mV s^{-1} . The peak shape for (89) on normal cyclic voltammetry was repeated in acetonitrile under neutral conditions, in acetonitrile containing $0.001 \text{ mol dm}^{-3}$ NaOH and in acetonitrile containing $0.001 \text{ mol dm}^{-3}$ H_2SO_4 . In the alkaline environment (solution containing $0.001 \text{ mol dm}^{-3}$ NaOH) the observed formal reduction potentials for these two peaks were $E^{\circ'} = 0.065$ and 0.135 V, while in the presence of $0.001 \text{ mol dm}^{-3}$ H_2SO_4 they were $E^{\circ'} = 0.062$ and 0.133 V at a scan rate of 50 mVs^{-1} . This indicated that protonation or deprotonation of the alcohol $\text{Fc-CH}_2\text{-OH}$ had no significant effect on the two observed formal reduction potentials. In the hope of resolving peaks **a** and **b** for (89) the Osteryoung Square wave voltammetric technique was used on (89). However, only a very broad peak was observed (**B** in Figure 3.10). It follows that the $E^{\circ'}$ values for peaks **a** and **b** are too close to each other to be resolved, even for the Osteryoung Square wave technique. Another technique is required to improve the resolution in such a way that the peaks can be separated. One such a technique may be voltammetry with a microelectrode, but due to the unavailability of this technique, we've not been able to pursue it yet.

To explain the observed pattern of two peaks for (89) it is necessary to first consider two previous cyclic voltammetry studies on a β -diketone, diferrocenoylmethane⁸ and ferrocenylmethylamine.⁹ Cyclic voltammograms for these two compounds are shown in Figure 3.13.

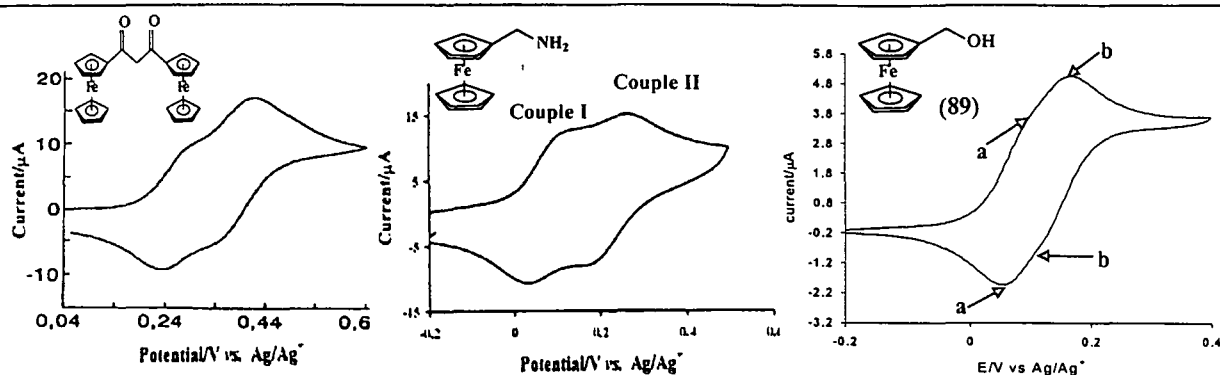


Figure 3.13: Cyclic voltammograms and structures of diferrocenylmethane (left), ferrocenylmethanamine (centre) and 2-ferrocenylmethanol (right) in acetonitrile, recorded at a scan rate of 50 mV s^{-1} .

The similarity of the first two cyclic voltammograms in Figure 3.13 is obvious. By allowing for the poor resolution of the two peaks *a* and *b* for (89), basically the third voltammogram in Figure 3.13, tells the same story: There are two peaks associated with ferrocenyl redox processes in each voltammogram. Upon considering the first voltammogram in Figure 3.13 the two peaks observed for diferrocenylmethane were explained by observing that the two ferrocenyl groups are not oxidised simultaneously at the surface electrode. The first ferrocenyl (Fc) group is oxidised in the reaction:

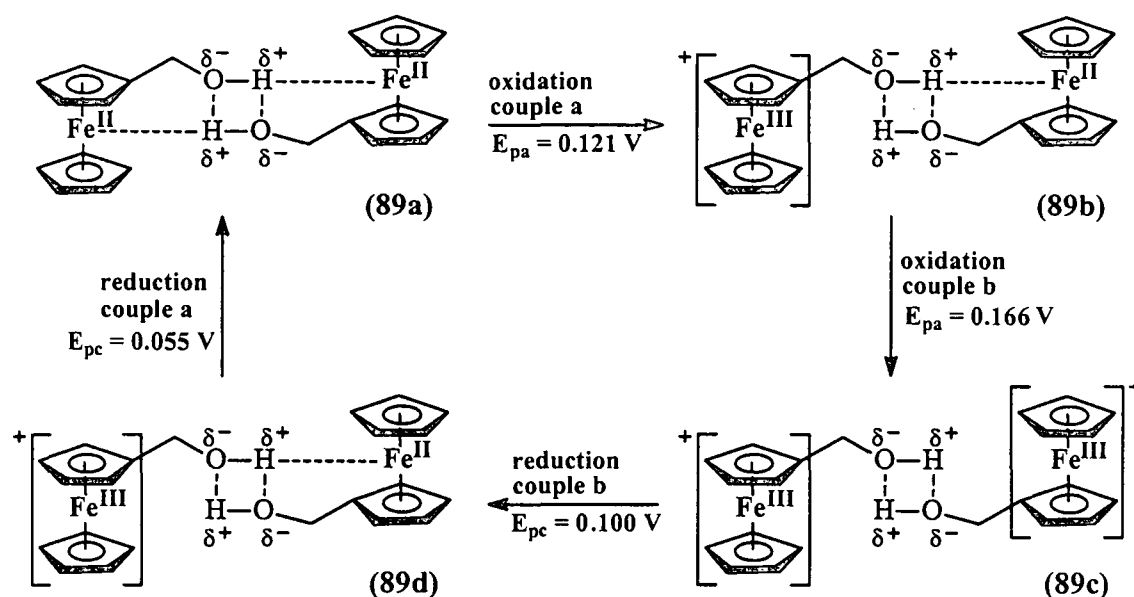


The group electronegativity of the oxidised ferrocenium group, Fc^+ ($\chi_{\text{Fc}^+} = 2.82$) is, however, much more than that of a Fc group ($\chi_{\text{Fc}} = 1.87$).⁸ This meant that the second Fc group that still has to be oxidised in $\text{FcCOCH}_2\text{COFc}^+$ is now, by means of conjugation, experiencing the rather strong electron withdrawing properties of the Fc^+ group. This makes the second ferrocenyl group of diferrocenylmethane much more difficult to oxidise and oxidation for this Fc group therefore takes place at a more positive formal reduction potential:



It is proposed that a similar process is taking place in ferrocenylmethanamine and ferrocenylmethanol, (89) when electrochemically oxidised. However, unlike the situation for diferrocenylmethane, there is no direct communication via conjugation between two ferrocenyl groups possible in FcCH_2NH_2 or FcCH_2OH , (89). Communication here must be restricted to a thorough-space, inductive field effect in hydrogen bonded dimers. The hydrogen bonded dimeric network may result in the observed two ferrocenyl based couples. It is known that the

iron (II) nucleus of ferrocene can interact with H^+ .¹⁰ Making use of this property one may conceive a hydrogen bonding network for alcohol (89) as proposed in structure (89a) in Scheme 3. 9.



Scheme 3. 9: The possible explanation for the broadening of the peaks of ferrocenylmethanol, (89) during oxidation-reduction processes.

Structure (89a) proposes that (89) actually exists as a stable dimer in acetonitrile solutions. When the dimer (89a) is oxidised in couple a, we propose that (89b) with only one Fc^+ group is formed. The remaining unoxidised ferrocenyl group of (89b) is now experiencing through the hydrogen bonds and also thorough space the strong electron withdrawing properties of the Fc^+ group, as was described for diferrocenoylmethane. The oxidation of (89b) to give the double oxidised ferricenium dimer (89c) therefore takes place at a more positive potential than was necessary to oxidise (89a) to (89b). However, the effect is not as dramatic as for diferrocenoylmethane, because "thorough space" or through σ -bond communication is not as effective as communication in the pseudo aromatic β -diketone. Hence the resolution of the two peaks for diferrocenoylmethane is much better than for (89).

In the cathodic cycle, the above two processes are reversed. The overall effect formation of a stable dimer would therefore be two redox couples in the cyclic voltammogram of (89). The formal reduction potentials of couples a and b were observed at 0.088 V and 0.133 V respectively. A similar scheme to Scheme 3. 9 can be written for $FcCH_2NH_2$ and it is adequately described elsewhere.⁹

3.4.1.1 Relationship between $E^{o'}$ and group ^1H NMR peak positions (ppm)

The relationship between the formal reduction potential, $E^{o'}$ and ^1H NMR chemical shifts (in ppm) of peak positions of protons of the ferrocyl fragment for compounds of the type FcCH_2R with $\text{R} = ^+\text{N}(\text{CH}_3)_3$, CN , OH , COOH , $\text{N}(\text{CH}_3)_2$, CH_3 and NH_2 were investigated. Data for these parameters are summarised in Table 3.7.

Table 3.7: Formal reduction potential, $E^{o'}$ and ^1H NMR data (in ppm) of ferrocenyl derivatives of the type FcCH_2R .

R-group	$E^{o'}$	^1H NMR signals of ferrocenyl fragment in ppm			
		2H, $\text{Fc}-\underline{\text{CH}_2}-$	5H, C_5H_5	2H, C_5H_4	2H, C_5H_4
$^+\text{N}(\text{CH}_3)_3$	0.308	4.38	4.34	4.57	4.92
CN	0.176	3.45	4.25	4.19	4.27
COOH	0.123	3.42	4.16	4.16	4.24
OH (couple a)	0.088	4.28	4.13	4.15	4.25
NH_2 (couple I) ^a	0.078	3.54	4.14	4.13	4.18
$\text{N}(\text{CH}_3)_2$	0.066	3.29	4.12	4.12	4.18
CH_3 ^b	0.020	2.32	4.05	4.10	4.15

^aData from reference 9.

^bData from reference 11.

The graphical relationship between, $E^{o'}$ and the ^1H NMR peak positions of ferrocyl protons, $\text{Fc}\underline{\text{CH}_2}$, C_5H_5 , C_5H_4 (two sets of signals, each corresponding to 2 protons) are shown in Figure 3.14. No clear-cut trend could be observed utilising the position of the ^1H NMR signal of $\text{Fc}\underline{\text{CH}_2}$, because data points were exceptionally scattered. However, there is a definite linear relationship between $E^{o'}$ and the ^1H NMR position of the C_5H_5 signal. This may well be a consequence of the remoteness of the C_5H_5 group from the $\text{CH}_2\text{-R}$ substituent. Any effect that the C_5H_5 group experience from the side chain must purely be due to electronic effects whereas the position of the $\text{Fc}\underline{\text{CH}_2}\text{R}$ ^1H NMR signal will also be determined by anisotropic deshielding effects induced by the ferrocenyl and R groups. The relationship between $E^{o'}$ and each of the two C_5H_4 ferrocenyl signals were reasonably linear provided the compound with $\text{R} = ^+\text{N}(\text{CH}_3)_3$ were ignored (bottom two graphs of Figure 3.14). The deviation of the ^1H NMR signal position of the $^+\text{N}(\text{CH}_3)_3$ derivative is attributed to a deshielding effect that the bulky, positively charged, $^+\text{N}(\text{CH}_3)_3$ group may induce on the C_5H_4 group in terms of ^1H NMR peak positions.

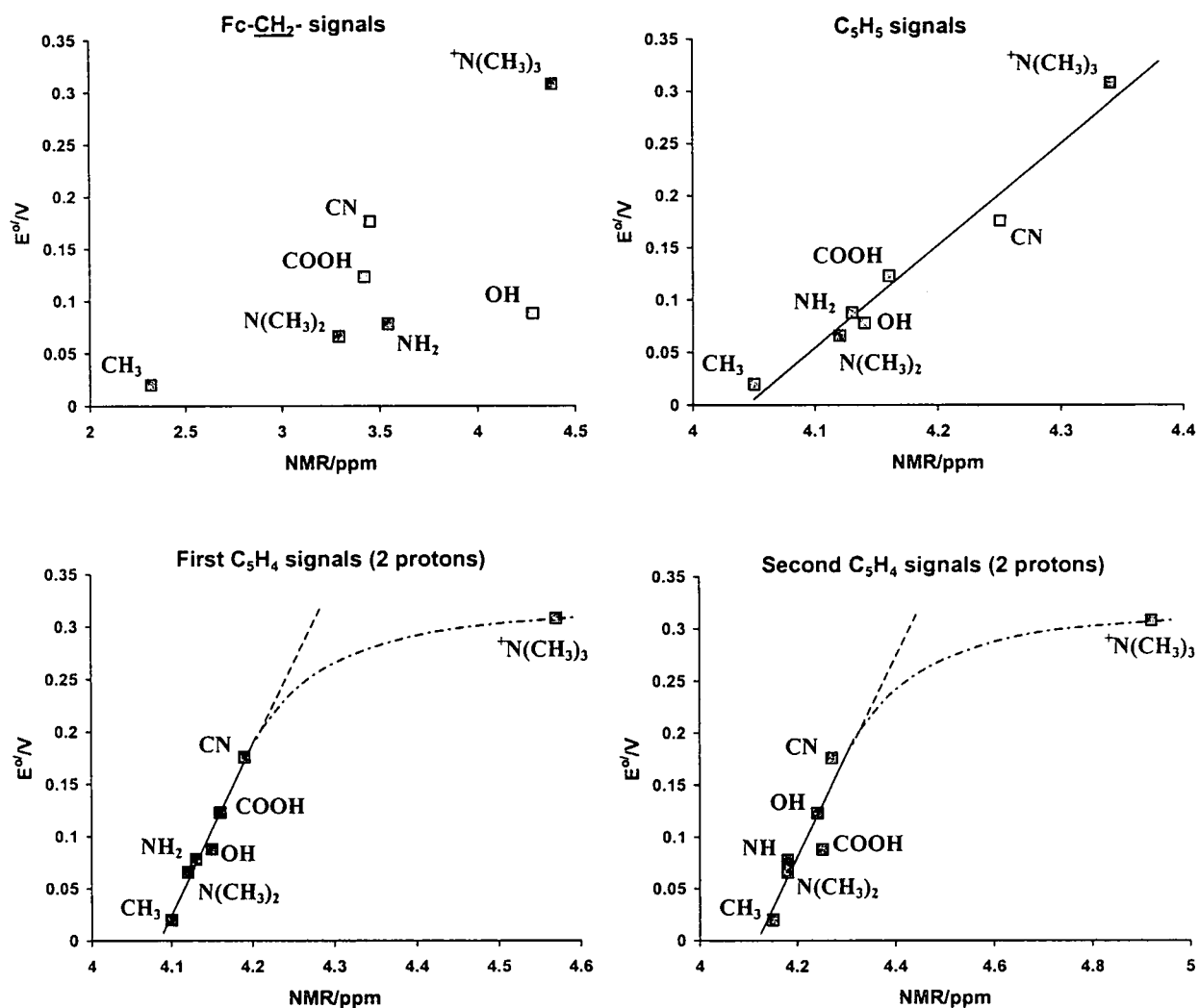


Figure 3.14: Relationship between the formal reduction potential, E° , of the ferrocenyl group and 1H NMR signal position (in ppm) of the ferrocyl fragment in $CDCl_3$, of $FcCH_2R$ with $R = ^+N(CH_3)_3$, CN, OH, COOH, $N(CH_3)_2$, CH_3 and NH_2 .

3.4.1.2 Relationship between E° and group electronegativities

It was previously established that there exists a linear relationship between E° and group electronegativities, χ_R , of a series of β -diketones of the type $FcCOCH_2COR$, with $R = Fc$, Ph, CH_3 , CF_3 , and CCl_3 .⁸ This relationship was explored during this study for compounds of the type $FcCH_2R$ with $R = ^+N(CH_3)_3$, CN, OH, COOH, $N(CH_3)_2$, CH_3 and NH_2 . 1H NMR data of the C_5H_5 signal of Fc in the 4.10 – 4.33 ppm region were chosen for this purpose. Utilising previously determined empirical group electronegativity values¹² of $\chi_{CH_3} = 2.34$, $\chi_{COOH} = 2.85$ and $\chi_{OH} = 2.71$ a calibration line was drawn by plotting the 1H NMR signal position (ppm) of the C_5H_5 group (Y-axis) against χ_R ($R = CH_3$, OH and COOH). This graph is shown in Figure 3.15, A. The 1H NMR signal position of the C_5H_5 group of compounds with $R = NH_2$, $N(CH_3)_2$, CN and $^+N(CH_3)_3$ was then fitted to this line and the group electronegativity, χ_R , of

each group read off on the X-axis. Results are summarised in Table 3.8. The ^1H NMR obtained χ_R -values was then tested for their accuracy utilising the formal reduction potentials obtained in this study. For this purpose a graph of $E^{o'}$ of each compound against χ_R were drawn. This is shown in Figure 3.15, right. The linearity of this plot is strikingly evident and is proof that the apparent group electronegativities determined by ^1H NMR are reasonably accurate.

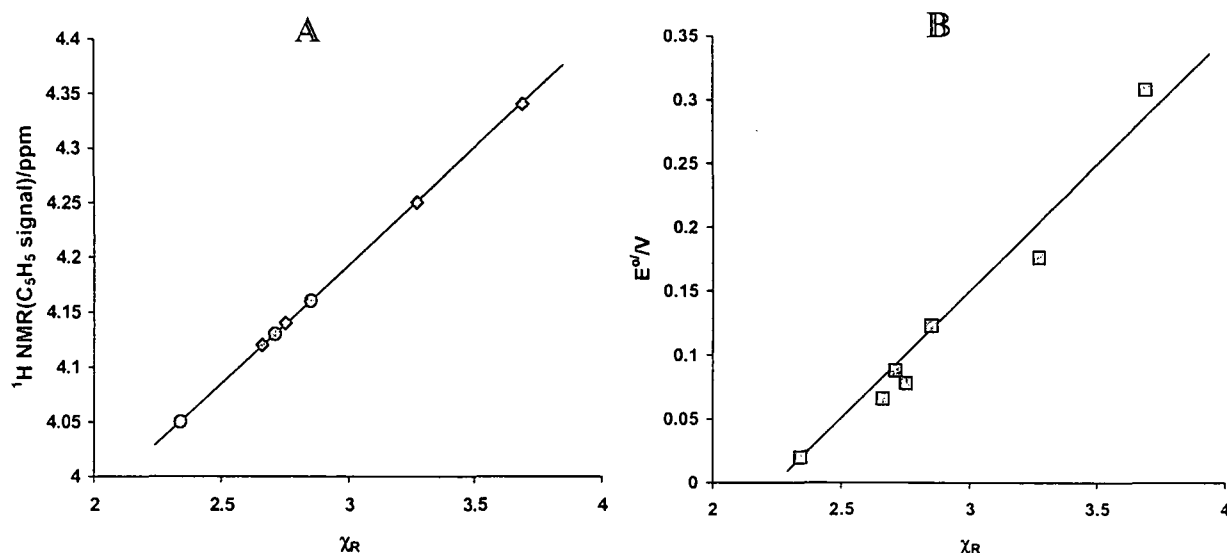


Figure 3.15: A: Linear relationship between the C_5H_5 ^1H NMR signal position of FcCH_2R and group electronegativity, χ_R . Points indicated with ○ were taken as calibration marks, points indicated with ◇ were fitted to the calibration line. **B:** Linear relationship between formal reduction potential, $E^{o'}$, of the ferrocenyl group and group electronegativity, χ_R , of the R-group in FcCH_2R . $\text{R} = ^+\text{N}(\text{CH}_3)_3$, CN, OH, COOH, $\text{N}(\text{CH}_3)_2$, CH_3 and NH_2 .

Upon actually fitting $E^{o'}$ to the observed linear graph of Figure 3.15, **B**, more accurate χ_R values for each R group is obtained, and these values are also summarised in Table 3.8.

Table 3.8: Summary of group electronegativities, χ_R , obtained by electrochemical and ^1H NMR techniques.

R-group	^1H NMR signal position for C_5H_5 (in ppm)	$E^{o'}$ (V)	χ_R (from ^1H NMR)	χ_R (from $E^{o'}$)
$^+\text{N}(\text{CH}_3)_3$	4.34	0.308	3.69	3.80
CN	4.25	0.176	3.27	3.15
COOH	4.16	0.123	2.85	2.85
OH (couple a)	4.13	0.088	2.71	2.71
NH_2 (couple I)	4.14	0.078	2.75	2.66
$\text{N}(\text{CH}_3)_2$	4.12	0.066	2.66	2.60
CH_3	4.05	0.020	2.34	2.34

To convert group electronegativities obtained in this study to more reliable and accurate χ_R -values, it is evident that the family of compounds having the general structure FcCH_2R should be expanded to include especially more known χ_R -values on the calibration curve.

The final part of the electrochemical investigation of this study involves a comparative electrochemical study on ferrocene alcohols FcCH_2OH , (89), $\text{FcCH}(\text{CH}_3)\text{OH}$, (90), $\text{Fc}[\text{CH}(\text{CH}_3)\text{OH}]_2$, (91), and $\text{FcCH}_2\text{CH}_2\text{OH}$, (80) (compounds (90) and (91) were provided by Prof. J.C. Swarts for this electrochemical study). The cyclic voltammetry behaviour of these ferrocenyl alcohols is shown in Figure 3.16 at a scan rate of 50 mV s^{-1} . Electrochemical results are summarised in Table 3.9, page 95.

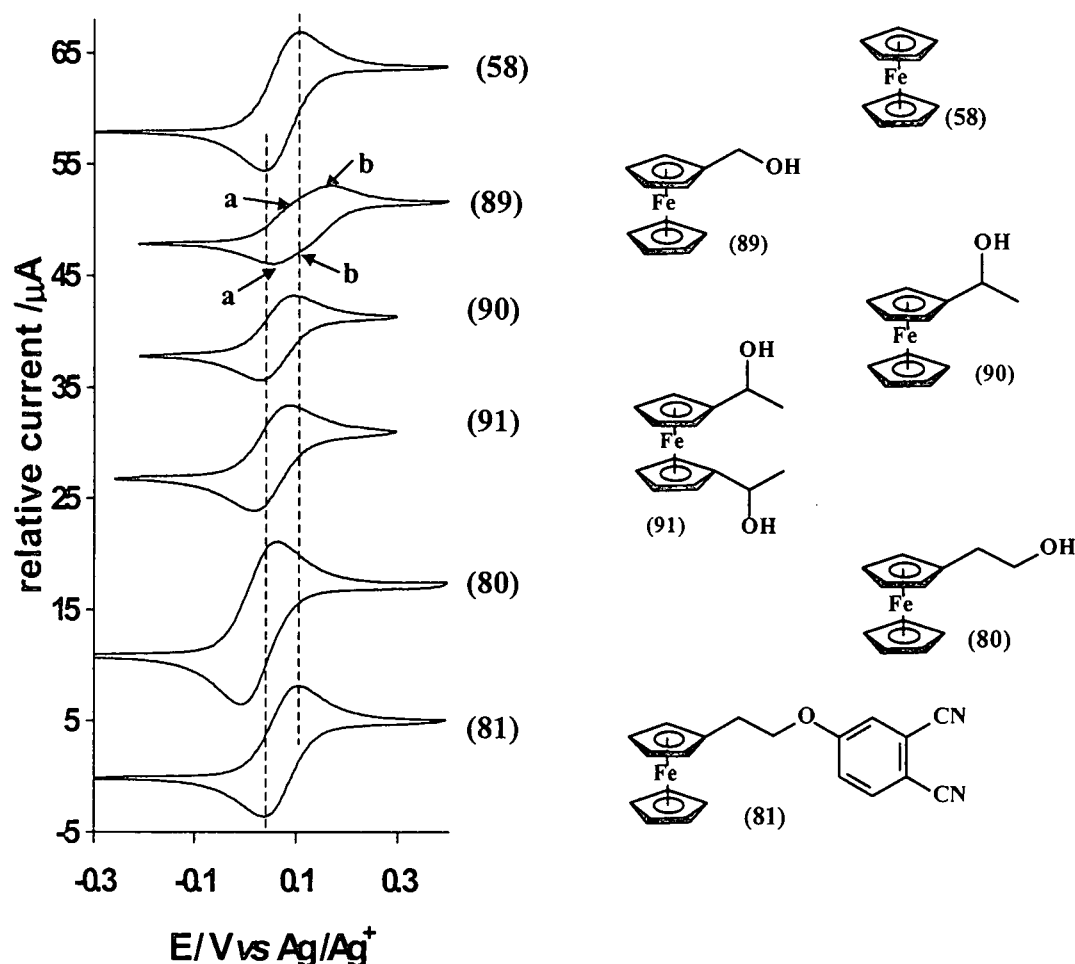
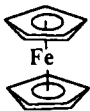
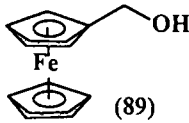
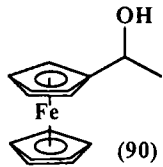
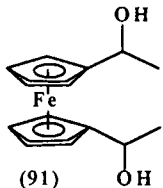
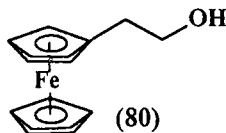
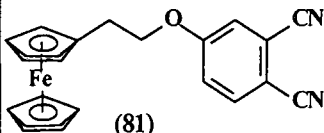


Figure 3.16: Cyclic voltammograms of ferrocene, (58), ferrocene-containing alcohols, (80), (89), (90) and (91) and phthalonitrile (81) at 25°C on a platinum working electrode, recorded at a scan rate of 50 mV s^{-1} containing $0.2 \text{ mol dm}^{-3} (\text{nBu})_4^+\text{NPF}_6^-$ as supporting electrolyte.

The first observation from the electrochemical data, summarised in Table 3.9 is that ΔE_p for all the ferrocenyl alcohols, (except for (89)) are below 80 mV and thus indicate reasonable electrochemical reversibility.

Table 3.9: Electrochemical data for ferrocene, indicated ferrocene-containing alcohols and phthalonitrile (1 mmol dm⁻³) in acetonitrile containing 0.2 mol dm⁻³ (nBu)₄⁺NPF₆ as supporting electrolyte at 25°C vs Ag/Ag⁺ at scan rates of 50, 100, 150, 200 and 250 mV s⁻¹.

Compound	v/ mV.s ⁻¹	E _{pa} / V	ΔE _p / mV	E ^o / V	i _{pa} / μA	i _{pa} /i _{pc}
 (58)	250	0.109	73	0.073	17.19	1.02
	200	0.108	71	0.073	15.44	1.01
	150	0.106	68	0.072	13.66	1.00
	100	0.105	65	0.073	11.29	1.00
	50	0.103	62	0.072	8.36	1.00
	Average			0.073		1.01
Couple a^a  (89)	250	0.050 ^c	- ^b	0.089 ^d	- ^b	- ^b
	200	0.052 ^c	- ^b	0.089 ^d	- ^b	- ^b
	150	0.053 ^c	- ^b	0.088 ^d	- ^b	- ^b
	100	0.054 ^c	- ^b	0.088 ^d	- ^b	- ^b
	50	0.055 ^c	- ^b	0.088 ^d	- ^b	- ^b
	Average			0.088^d		
 (90)	250	0.098	73	0.062	9.99	1.08
	200	0.097	71	0.062	9.00	1.06
	150	0.096	68	0.062	7.83	1.03
	100	0.095	66	0.062	6.47	1.02
	50	0.092	62	0.061	4.68	0.99
	Average			0.062		1.04
 (91)	250	0.090	77	0.052	12.53	1.11
	200	0.088	73	0.052	11.26	1.11
	150	0.087	71	0.051	9.81	1.07
	100	0.085	68	0.052	8.23	1.05
	50	0.083	65	0.051	5.96	1.04
	Average			0.052		1.08
 (80)	250	0.066	79	0.027	20.34	1.02
	200	0.065	76	0.027	18.26	1.00
	150	0.064	74	0.027	15.95	0.99
	100	0.062	70	0.027	13.18	0.98
	50	0.060	66	0.027	9.60	0.98
	Average			0.027		0.99
 (81)	250	0.110	77	0.072	16.06	1.03
	200	0.108	73	0.072	14.42	1.01
	150	0.107	72	0.072	12.80	1.01
	100	0.105	68	0.071	10.56	1.00
	50	0.103	65	0.071	7.81	1.00
	Average			0.072		1.01

^aOnly data for couple **a** are shown. Data for couple **b** may be found in Table 3.6. ^bPoorly defined oxidation wave of couple **a** made current and ΔE_p measurements impossible. ^cE_{pc} value. ^dE^o were obtained by assuming ΔE_p = 66 mV, the average of ΔE_p values for (58), (61), (63) and (64) at a scan rate of 50 mV s⁻¹.

The i_{pa}/i_{pc} ratios for compounds (80), (89) and (90) approached 1, while that of (91) did not deviate enough from 1 to read any meaning into it. Details of the electrochemistry of (89) were already described in section 3.4.1, page 88. Elongation of the spacer group between the Fc and OH moieties from CH₂ to CH₂-CH₂ led to a decrease of 61 mV in formal reduction potential, E^o from 0.088 (couple **a**) to 0.027V. This value is also 96 mV more negative than the formal reduction potential of the parent acid (64) and 46 mV more negative than E^o of ferrocene itself.

This result clearly indicates that there is much less communication between the hydroxyl group and the ferrocenyl moiety of **(80)** than in **(89)**. In particular, for $E^{\circ'}$ of **(80)** to be 46 mV more negative than $E^{\circ'}$ of ferrocene itself, the side-chain of **(80)**, $\text{CH}_2\text{CH}_2\text{OH}$ has to become electron-donating relative to a H-atom. This is consistent with a conclusion that CH_2CH_2 alkyl spacers effectively isolates the OH group from the ferrocenyl group, but that the CH_2 group does not. This also means that electron-donating properties of the CH_2CH_2 part of the side-chain in **(80)** dominates over the electron-withdrawing properties of the $-\text{OH}$ moiety of **(80)**.

The $E^{\circ'}$ of alcohol **(90)** (0.062 V) is 26 mV more negative than $E^{\circ'}$ of **(89)** and 11 mV more negative than $E^{\circ'}$ of ferrocene itself, however its $E^{\circ'}$ is 35 mV more positive than $E^{\circ'}$ of **(80)**. This is because **(90)** has an additional electron-donating methyl group in the side-chain in the place of a H-atom as in **(89)**. Alcohol **(91)** with $E^{\circ'}$ of 0.052 V is some 10 mV more negative than $E^{\circ'}$ of **(90)** and 36 mV more negative than $E^{\circ'}$ of **(89)**, and is consistent with what is expected in a compound with two electron donating side chains, here two $\text{CH}(\text{CH}_3)\text{OH}$ groups. It is instructive to observe that **(80)**, **(90)** and **(91)** do not show the double peak that **(89)** had. This implies that the structural effects that was discussed and interpreted above as dimerisation for **(89)** is absent in **(80)**, **(90)** and **(91)**. This observation is consistent with the fact that the longer chain of **(80)** introduces so much flexibility in **(80)** compared to what is expected for **(89)**, that a dimeric product may not be stable enough to allow its detection in noticeable amounts. As for **(90)** and **(91)**, it is conceivable that the methyl groups in the side chain is bulky enough to impose so much steric constraints on the molecules that dimerisation as it is realised for **(89)** is not any more feasible in **(90)** and **(91)**.

The $E^{\circ'}$ of phthalonitrile **(81)** (Table 3.9, Figure 3.16) is almost the same as that of ferrocene itself, (only 1 mV more negative), but 45 mV more positive than $E^{\circ'} = 0.027$ V for the alcohol **(80)**. The closeness of the value of $E^{\circ'}$ for phthalonitrile **(81)** to that of pure ferrocene again demonstrates the effective isolation capabilities of the $\text{CH}_2\text{-CH}_2\text{-}$ spacer group as the strong electron-withdrawing properties of the CN groups does not influence the formal reduction potential of the ferrocenyl moiety of this compound much. The slightly larger $E^{\circ'}$ value as compared with the alcohol $\text{Fc-CH}_2\text{-CH}_2\text{-OH}$ is attributed to a "thorough-space" field effect that the cyanide-containing phthalonitrile moiety may have on the ferrocenyl group.

3.4.2 The cyclic voltammetry of phthalocyanine derivatives

The cyclic voltammetry of the phthalocyanine derivatives in this study was investigated in either dichloromethane at 25°C or dichloroethane at 70°C. The choice of solvent and temperature was determined by the solubility of the compound under investigation. The phthalocyanine-based analytes were prepared in *ca.* 1 mmol dm⁻³ argon purged solutions containing 0.2 mol dm⁻³ (nBu)₄⁺NPF₆ as supporting electrolyte. The three-electrode system used, consisted of a platinum wire electrode, a platinum working electrode and a Ag/Ag⁺ non aqueous reference electrode.

3.4.2.1 Cyclic voltammetry of a range of octa-alkylated metal-free and zinc-containing phthalocyanines

The octakis(dodecyl)phthalocyanines (83) and (84), synthesised in this study are part of a range of octa-alkylated phthalocyanine derivatives that were now or before synthesised in this laboratory. The entire range shown in Figure 3.17 was subjected to an electrochemical investigation during the course of this study.

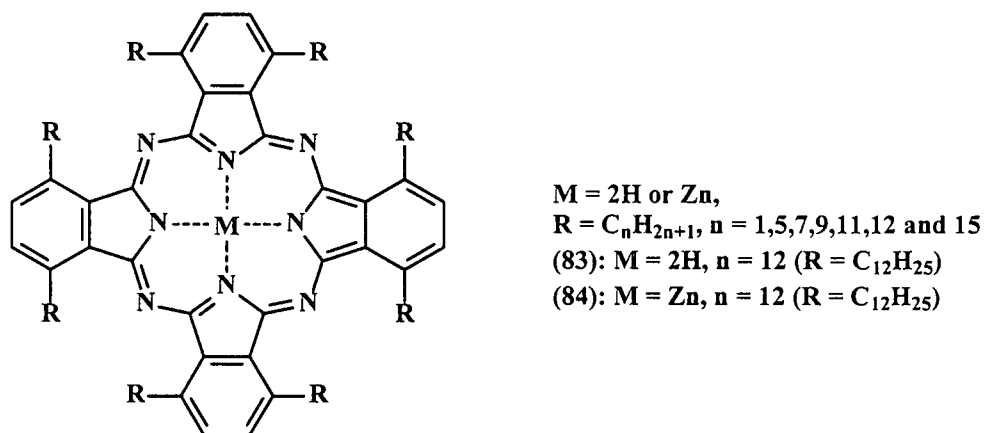


Figure 3.17: The range of octa-alkyl substituted metal-free and zinc-containing phthalocyanines that were studied by means of cyclic voltammetry.

Cyclic voltammetry of all the metal-free phthalocyanines,[†] except the C₁₅-2HPc derivative, were studied in dichloromethane at 25°C, while the latter and all the zinc-containing phthalocyanines of this range were investigated in dichloroethane at 70°C because of their insolubility in dichloromethane. Four ring-based redox processes were identified for all the complexes in the

[†] The phthalocyanines with $n = 1, 5, 7, 9, 11$ and 15 were provided by Prof. J. C. Swarts for this electrochemical study.

potential range -2 to 1.5 V vs Ag/Ag^+ but all of them were not always well defined in the cyclic voltammogram. These redox processes were more ideal for the metal-free phthalocyanines, 2HPc than for the zinc derivatives, ZnPc, but neither exhibited fully reversible behaviour for all four electron transfer processes. (Electrochemical reversibility for one-electron process at 25°C is theoretically characterised by peak potential differences of 59 mV and is independent of scan rate; in this study an *experimental* result of $\Delta E_p \leq 80$ mV is considered as indicative of an electrochemical reversible process.)

A representative example of a cyclic voltammogram (top CV) of a metal-free octa-undecylated phthalocyanine, $(\text{C}_{11}\text{H}_{23})_8\text{-2HPc}$, is shown in Figure 3.18.

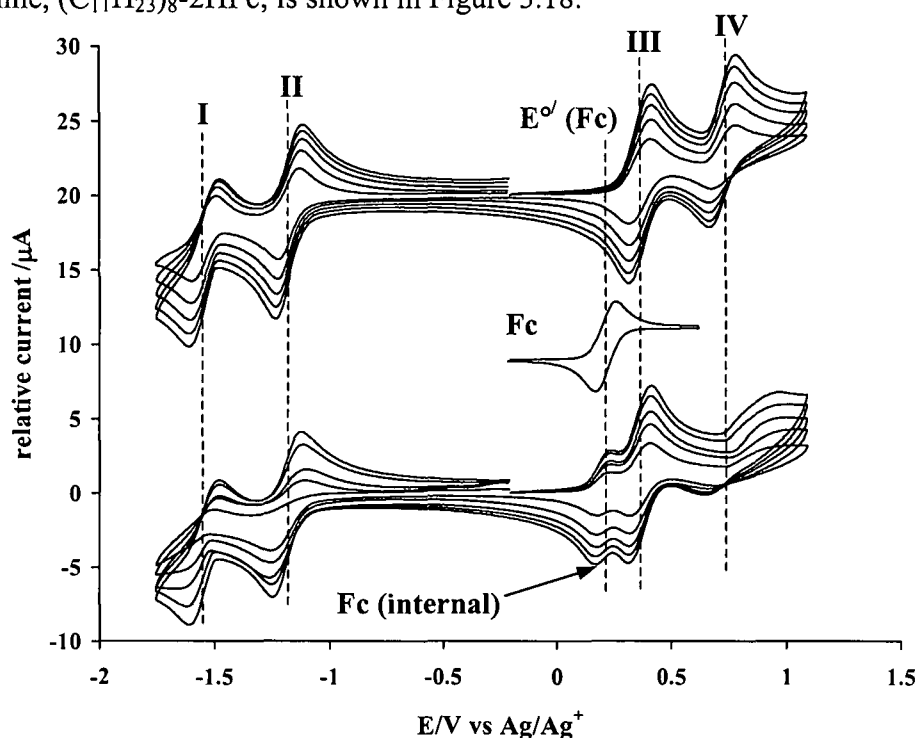


Figure 3.18: Top: Cyclic voltammogram of $(\text{C}_{11}\text{H}_{23})_8\text{-2HPc}$ (1 mmol dm^{-3}) in dichloromethane at 25°C with 0.2 mol dm^{-3} $(\text{tBu})_4\text{-NPF}_6$ as supporting electrolyte, on a platinum working electrode, at scan rates of 50 , 100 , 150 , 200 and 250 mVs^{-1} . Four ring-centered redox processes **I**, **II**, **III** and **IV** are observable. The wave labelled **Fc** is that of free ferrocene (1 mmol dm^{-3}) in dichloromethane at 25°C . **Bottom:** Cyclic voltammogram of $(\text{C}_{11}\text{H}_{23})_8\text{-2HPc}$ under the same conditions as for the top CV but in the presence of ferrocene as internal standard. The shape of wave **IV** became distorted compared to the upper CV. This demonstrates *inter alia* the extreme sensitivity of good CV's for these compounds to minor impurities on the surface of the electrode.

The four observed redox processes are associated with the ring-based electron transfer couples $[\text{MPc}]^{2-}/[\text{MPc}]^{\bullet -}$ (wave **I**), $[\text{MPc}]^{\bullet -}/[\text{MPc}]$ (wave **II**), $[\text{MPc}]/[\text{MPc}]^{+ \bullet}$ (wave **III**) and $[\text{MPc}]^{+ \bullet}/[\text{MPc}]^{2+}$ (wave **IV**) with $\text{M} = 2\text{H}$ or Zn as demonstrated in the equation in Figure 3.19.

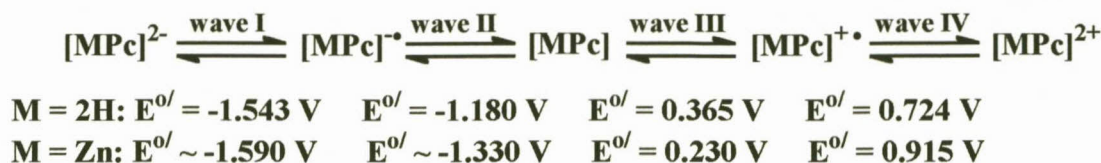


Figure 3.19: Redox couples and average formal reduction potentials, E^0 for $(\text{C}_{11}\text{H}_{23})_8\text{-MPc}$ ($\text{M} = 2\text{H}$ or Zn) at a scan rate of 50 mV s^{-1} vs Ag/Ag^+ .

When free ferrocene is used as internal marker in the presence of the metal-free phthalocyanine (bottom CV, Figure 3.18), slightly better ΔE_p values of 0.062 and 0.089 for the ferrocene and wave **III** signals respectively are observed. The redox wave of the free ferrocene marked as **Fc** is also shown in Figure 3.18 (middle CV). It is important to note that although the position of the free ferrocene cyclic voltammogram does not coincide with that of ferrocene used as internal marker, the closeness of the ferrocene/ferrocenium couple to that of wave **III** of the phthalocyanine has a tendency to distort and/or shift both the **Fc** and phthalocyanine wave **III** peak and alter E^0 . In this example, E^0 for the Fc/Fc^+ couple shifted from 0.221 V to 0.206 V in the presence of the phthalocyanine when free ferrocene is used as internal marker. Data reported and voltammograms shown in this study are therefore referenced to Ag/Ag^+ and not to the ferrocene/ferrocenium couple. An interested reader can convert potentials reported in this section to be referenced against Fc/Fc^+ by subtracting the formal reduction of Fc , 0.221 V vs Ag/Ag^+ (in dichloromethane) from all potential data.

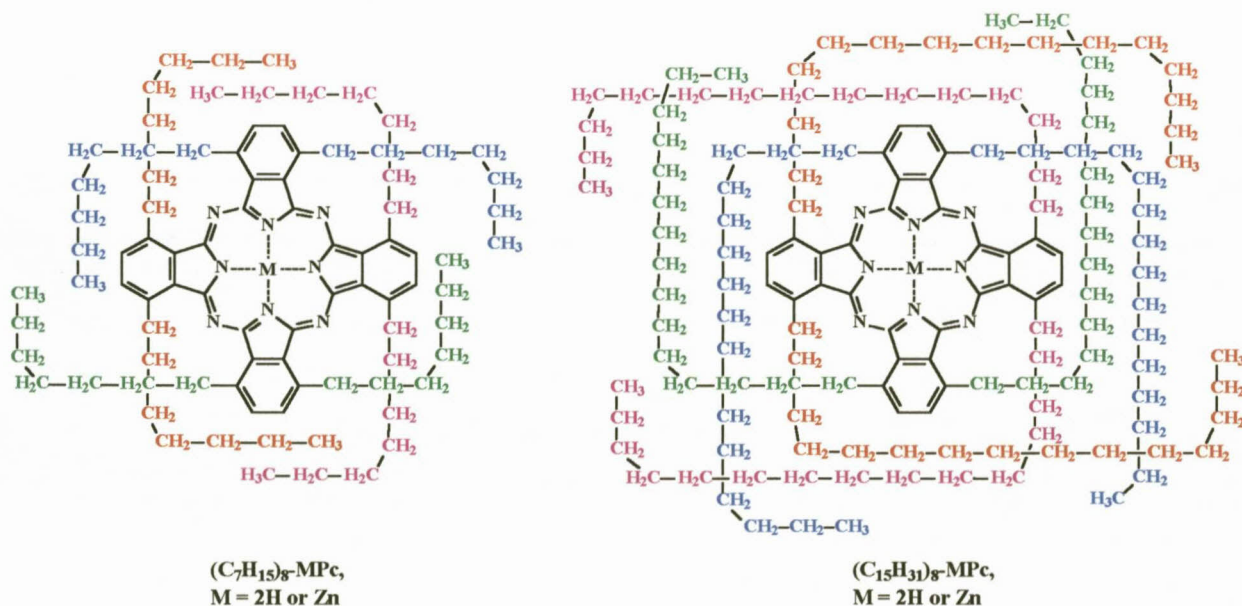


Figure 3.20: Proposed encapsulation of the phthalocyanine core by the alkyl side chains for the C_7 - and C_{15} - derivatives.

Cyclic voltammograms of all the metal-free octa-alkyl substituted phthalocyanines from C_5 through to C_{15} , recorded at a scan rate of 100 mV s^{-1} , are shown in Figure 3.21 and results of the electrochemical parameters are summarised in Table 3.10, page 101.

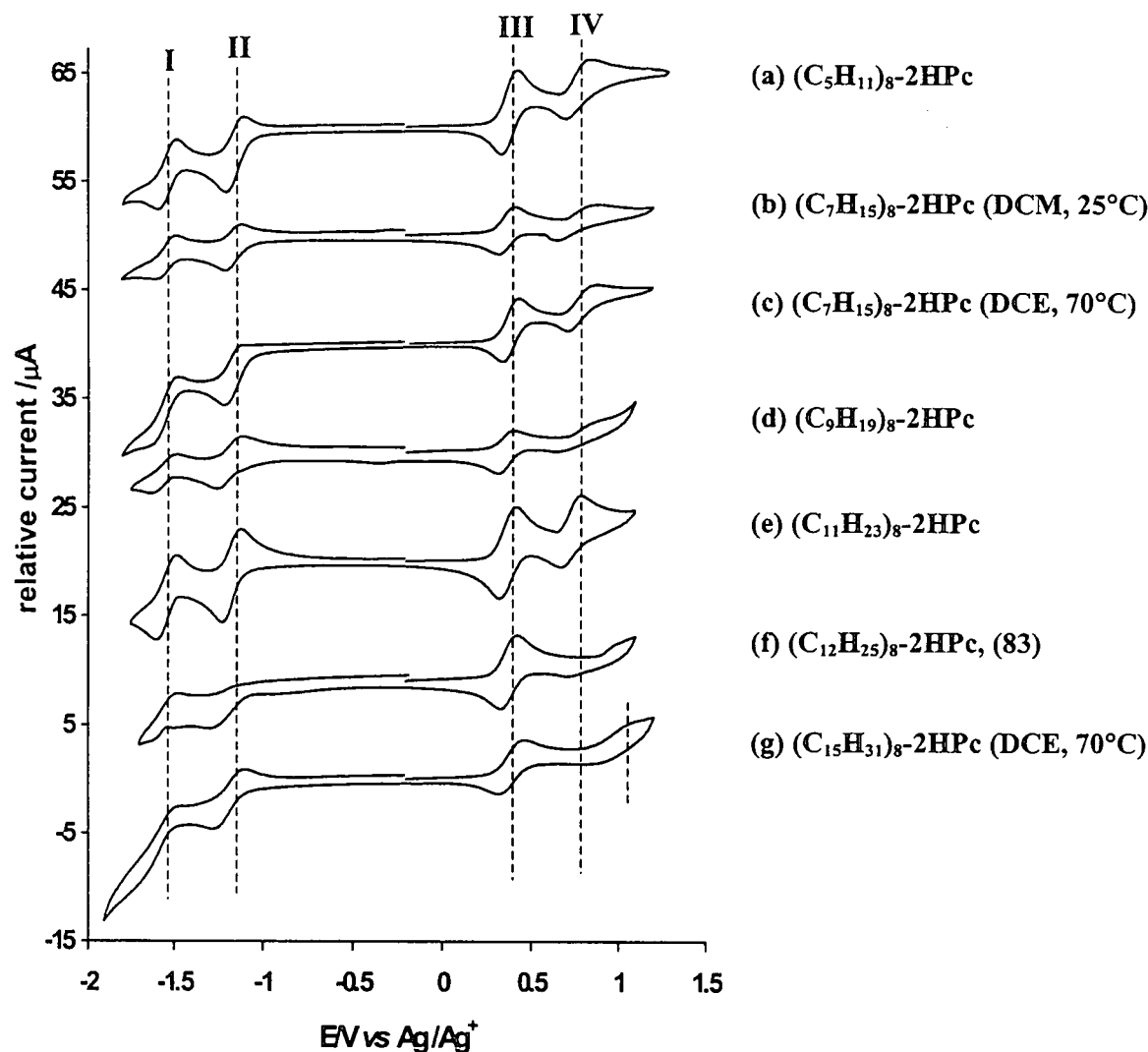


Figure 3.21: Cyclic voltammograms (CV's) of a series of octa-alkyl substituted 2HPc (1 mmol dm^{-3} in DCM at 25°C , unless otherwise stated, with 0.2 mol dm^{-3} $(n\text{Bu})_4^+\text{NPF}_6^-$ as supporting electrolyte) on a platinum working electrode, recorded at a scan rate of 100 mV s^{-1} . Four ring-based centered redox processes I, II, III and IV were observed. The similarity in shape of CV's (b) and (c) shows that temperature and solvent changes do not alter the CV's of the studied compounds. DCM = dichloromethane, DCE = dichloroethane and $n\text{Bu} = n\text{-butyl}$.

Except for waves I and IV of the C_{15} -derivative, well-defined cyclic voltammograms were obtained for all the metal-free phthalocyanines. This result is consistent with the expectation that the very long C_{15} side chains encapsulates the phthalocyanine core much more effective than shorter chain derivatives, for example the C_7 derivative as demonstrated in Figure 3.20, very much in a protein-like fashion. This encapsulation apparently has an enhanced protective effect in the fully reduced (charge 2^-) and fully oxidised (charge 2^+) species which explains the distorted shapes of wave I, and especially wave IV in the C_{15} compound, Figure 3.21.

Table 3.10: Peak cathodic potentials (E_{pc}), difference in peak anodic and peak cathodic potentials (ΔE_p), formal reduction potentials (E°), peak cathodic currents (i_{pc}) and peak current ratios (i_{pc}/i_{pa}) for the indicated 2H- and Zn- phthalocyanines. Potentials are versus Ag/Ag^+ . DCM = dichloromethane and DCE = dichloroethane.

Pc	v/ mV s ⁻¹	Wave I					Wave II					Wave III					Wave IV				
		$E_{pc}/$ V	$\Delta E_p/$ V	$E^\circ/$ V	$i_{pc}/$ μA	i_{pc}/i_{pa}	$E_{pc}/$ V	$\Delta E_p/$ V	$E^\circ/$ V	$i_{pc}/$ μA	i_{pc}/i_{pa}	$E_{pc}/$ V	$\Delta E_p/$ V	$E^\circ/$ V	$i_{pc}/$ μA	i_{pc}/i_{pa}	$E_{pc}/$ V	$\Delta E_p/$ V	E°/V	$i_{pc}/$ μA	i_{pc}/i_{pa}
(C ₅ H ₁₁) ₈ -2HPc at 25°C in DCM	250	-1.592	0.122	-1.531	6.23	1.38	-1.224	0.133	-1.158	7.13	1.00	0.439	0.112	0.383	7.49	0.99	0.873	0.202	0.772	4.94	0.78
	200	-1.591	0.118	-1.532	5.58	1.28	-1.216	0.122	-1.155	6.69	1.01	0.436	0.108	0.382	6.80	1.00	0.865	0.185	0.773	4.83	0.77
	150	-1.588	0.112	-1.532	4.79	1.22	-1.210	0.110	-1.155	6.09	1.01	0.433	0.102	0.382	5.92	1.02	0.850	0.176	0.767	4.31	0.82
	100	-1.585	0.105	-1.533	3.87	1.12	-1.200	0.094	-1.153	5.27	1.00	0.430	0.096	0.382	4.94	1.05	0.835	0.144	0.763	3.74	0.87
	50	-1.583	0.095	-1.536	3.16	1.07	-1.194	0.076	-1.156	4.31	1.01	0.427	0.090	0.382	3.64	1.03	0.819	0.098	0.770	3.24	0.83
	Av.			-1.533					-1.155		1.01			0.382		1.02			0.769		0.81
(C ₇ H ₁₃) ₈ -2HPc at 25°C in DCM	250	-1.610	0.123	-1.549	3.65	1.07	-1.229	0.121	-1.169	4.38	0.98	0.414	0.110	0.359	3.52	1.01	0.929	0.300	0.779	2.31	0.79
	200	-1.605	0.117	-1.547	3.35	1.08	-1.222	0.109	-1.168	3.88	1.00	0.413	0.106	0.360	3.27	1.00	0.916	0.283	0.776	2.08	0.80
	150	-1.600	0.109	-1.546	2.30	1.05	-1.213	0.092	-1.167	3.29	1.01	0.410	0.096	0.362	2.64	0.97	0.888	0.246	0.765	1.63	0.79
	100	-1.595	0.101	-1.545	1.91	1.04	-1.209	0.084	-1.167	2.78	1.02	0.408	0.091	0.363	2.16	0.97	0.862	0.214	0.755	1.34	0.80
	50	-1.589	0.093	-1.543	1.27	1.07	-1.203	0.076	-1.167	1.95	1.01	0.404	0.083	0.363	1.44	1.01	0.834	0.179	0.745	0.87	0.79
	Av.			-1.546		1.06			-1.168		1.00			0.361		0.99			0.764		0.79
(C ₉ H ₁₉) ₈ -2HPc at 25°C in DCM	250	-1.642	0.149	-1.568	2.13	1.25	-1.268	0.162	-1.187	3.76	1.07	0.415	0.099	0.366	2.69	1.06	0.910	0.290	0.765	1.80	0.38
	200	-1.637	0.145	-1.565	1.92	1.18	-1.264	0.154	-1.187	3.45	1.01	0.414	0.097	0.366	2.47	1.03	0.904	0.283	0.763	1.64	0.40
	150	-1.631	0.141	-1.561	1.76	1.14	-1.260	0.145	-1.187	3.02	0.94	0.412	0.093	0.366	2.14	1.13	0.899	0.275	0.762	1.54	0.35
	100	-1.624	0.135	-1.557	1.43	1.07	-1.254	0.135	-1.187	2.59	0.82	0.408	0.087	0.365	1.65	1.28	0.896	0.270	0.761	1.52	0.32
	50	-1.617	0.130	-1.552	1.15	0.95	-1.246	0.120	-1.186	1.48	0.52	0.402	0.082	0.365	1.04	1.49	0.884	0.254	0.758	1.36	0.21
	Av.			-1.561					-1.187					0.366					0.762		
(C ₁₁ H ₂₃) ₈ -2HPc at 25°C in DCM	250	-1.607	0.127	-1.544	5.88	1.61	-1.240	0.120	-1.180	7.00	1.01	0.418	0.106	0.365	7.09	0.98	0.782	0.116	0.724	6.18	0.75
	200	-1.604	0.122	-1.543	5.38	1.54	-1.237	0.115	-1.180	6.50	1.00	0.417	0.104	0.365	6.53	0.99	0.781	0.113	0.724	5.69	0.75
	150	-1.601	0.118	-1.542	4.82	1.64	-1.234	0.109	-1.180	5.90	0.99	0.416	0.102	0.365	5.94	1.00	0.779	0.111	0.724	5.04	0.78
	100	-1.598	0.112	-1.542	4.10	1.61	-1.232	0.104	-1.180	5.04	0.94	0.414	0.098	0.365	4.93	1.00	0.778	0.108	0.724	4.05	0.78
	50	-1.594	0.103	-1.542	3.17	1.61	-1.228	0.098	-1.180	4.00	0.89	0.413	0.096	0.365	3.64	1.00	0.776	0.105	0.724	2.98	0.78
	Av.			-1.543		1.60			-1.180		0.97			0.365		0.99			0.724		0.77
(83) (C ₁₂ H ₂₅) ₈ -2HPc at 25°C in DCM	250	-1.614	0.143	-1.543	2.94	1.50	-1.253	0.132	-1.188	4.26	1.61	0.324	0.103	0.376	5.63	0.97	0.661	0.339	0.831	1.47	0.61
	200	-1.606	0.133	-1.540	2.12	1.24	-1.261	0.132	-1.196	3.73	1.64	0.326	0.098	0.375	5.21	0.99	0.671	0.326	0.834	1.27	0.72
	150	-1.600	0.127	-1.537	1.47	0.95	-1.274	0.135	-1.207	3.31	1.69	0.329	0.092	0.375	4.73	1.04	0.677	0.317	0.836	0.98	0.71
	100	-1.597	0.121	-1.537	0.96	0.74	-1.282	0.138	-1.216	2.82	1.58	0.332	0.087	0.376	3.91	1.04	0.694	0.295	0.842	0.73	0.64
	50	-1.593	0.109	-1.538	0.41	0.50	-1.290	0.145	-1.218	2.36	1.32	0.337	0.079	0.377	3.00	1.10	0.721	0.267	0.852	0.49	0.61
	Av.			-1.539					-1.205					0.376		1.03			0.839		
(C ₁₅ H ₃₁) ₈ -2HPc at 70°C in DCE	250	-1.700	0.241	-1.580	5.60	1.69	-1.264	0.175	-1.177	4.71	1.00	0.458	0.137	0.390	4.56	0.95	1.059	0.230	0.944	2.58	0.60
	200	-1.697	0.234	-1.580	5.09	1.65	-1.263	0.166	-1.180	4.13	1.01	0.455	0.132	0.389	4.19	1.01	1.051	0.218	0.942	2.5	0.58
	150	-1.692	0.213	-1.586	4.42	1.95	-1.261	0.150	-1.186	3.50	1.01	0.453	0.127	0.390	3.12	1.01	1.046	0.194	0.949	2.27	0.42
	100	-1.681	0.200	-1.581	4.33	2.50	-1.257	0.134	-1.190	2.83	0.98	0.451	0.123	0.390	2.70	1.06	1.036	0.172	0.950	1.94	0.34
	50	-1.669	0.185	-1.577	-	-	-1.245	0.130	-1.180	2.24	1.04	0.450	0.120	0.390	2.35	1.08	1.024	0.151	0.949	1.71	0.30
	Av.			-1.581					-1.183		1.01			0.390		1.02			0.947		

Table 3.10 continues on page 101.

Table 3.10 (continued)

Pc	v/ mV s ⁻¹	Wave I					Wave II					Wave III					Wave IV				
		E _{pc} / V	ΔE _p / V	E ^o / V	i _{pc} / μA	i _{pc} /i _{pa}	E _{pc} / V	ΔE _p / V	E ^o / V	i _{pc} / μA	i _{pc} /i _{pa}	E _{pc} / V	ΔE _p / V	E ^o / V	i _{pc} / μA	i _{pc} /i _{pa}	E _{pc} / V	ΔE _p / V	E ^o /V	i _{pc} / μA	i _{pc} /i _{pa}
(C ₁ H ₃) ₈ -ZnPc at 70°C in DCE		To insoluble, the cyclic voltammogram of (C ₁ H ₃) ₈ -ZnPc gave no clear-cut peaks. ^a																			
(C ₅ H ₁₁) ₈ -ZnPc at 70°C in DCE	250	-1.598	0.202 ^c	-1.497 ^c	4.05 ^b	- ^b	-1.327	0.088 ^c	-1.283 ^c	1.87	- ^b	0.314	0.090	0.269	2.38	1.03	0.865	0.106	0.812	2.48	0.83
	200	-1.598	0.202 ^c	-1.497 ^c	4.11 ^b	- ^b	-1.327	0.086 ^c	-1.284 ^c	1.88	- ^b	0.311	0.088	0.267	2.20	1.01	0.863	0.102	0.812	2.38	0.85
	150	-1.600	0.204 ^c	-1.498 ^c	4.18 ^b	- ^b	-1.325	0.082 ^c	-1.284 ^c	1.86	- ^b	0.309	0.088	0.265	2.16	0.99	0.861	0.098	0.812	2.07	0.85
	100	-1.600	0.206 ^c	-1.497 ^c	4.05 ^b	- ^b	-1.321	0.076 ^c	-1.284 ^c	1.63	- ^b	0.304	0.087	0.261	1.82	1.02	0.858	0.092	0.812	1.91	0.71
	50	-1.601	0.207 ^c	-1.498 ^c	3.67 ^b	- ^b	-1.317	0.065 ^c	-1.285 ^c	1.23	- ^b	0.299	0.083	0.258	1.32	1.01	0.851	0.081	0.811	1.44	0.83
	Av.													0.264		1.01			0.812		0.81
(C ₇ H ₁₅) ₈ -ZnPc at 70°C in DCE	250	-1.648	0.227 ^c	-1.535 ^c	4.69 ^b	- ^b	-1.375	No clear-cut oxidation peak observed.		2.22 ^b	- ^b	0.302	0.101	0.252	3.04	1.13	0.891	0.115	0.834	2.98	1.11
	200	-1.648	0.225 ^c	-1.536 ^c	4.63 ^b	- ^b	-1.373			2.21 ^b	- ^b	0.300	0.097	0.252	2.87	1.15	0.888	0.110	0.833	2.85	1.10
	150	-1.645	0.221 ^c	-1.535 ^c	4.56 ^b	- ^b	-1.372			2.03 ^b	- ^b	0.299	0.091	0.254	2.42	1.20	0.882	0.103	0.831	2.49	1.09
	100	-1.642	0.215 ^c	-1.534 ^c	4.23 ^b	- ^b	-1.372	Assume ΔE _p ≈90		2.16 ^b	- ^b	0.297	0.083	0.256	2.07	1.13	0.876	0.093	0.830	1.93	1.08
	50	-1.641	0.211 ^c	-1.536 ^c	3.90 ^b	- ^b	-1.370	imply E ^o ≈-1.325		2.29 ^b	- ^b	0.296	0.078	0.257	1.45	1.08	0.869	0.080	0.829	1.41	1.07
	Av.													0.254		1.14			0.831		1.09
(C ₉ H ₁₉) ₈ -ZnPc at 70°C in DCE	250	Wave I too poorly identified for meaningful measurements.					-1.494	- ^b	- ^b	4.43	- ^b	0.348	0.188	0.254	3.02	0.95	1.061	0.294	0.914	2.33	0.73
	200						-1.450	- ^b	- ^b	3.29	- ^b	0.340	0.175	0.253	2.62	0.99	1.047	0.271	0.912	2.20	0.66
	150						-1.433	- ^b	- ^b	3.07	- ^b	0.331	0.157	0.253	2.37	0.98	1.029	0.239	0.910	1.93	0.60
	100						-1.419	- ^b	- ^b	2.84	- ^b	0.322	0.140	0.252	2.04	1.04	1.019	0.218	0.910	1.70	0.58
	50						-1.412	- ^b	- ^b	2.29	- ^b	0.313	0.124	0.251	1.44	1.17	0.989	0.178	0.900	1.28	0.54
	Av.													0.253		1.03			0.909		
(C ₁₁ H ₂₃) ₈ -ZnPc at 70°C in DCE	250	-1.526	- ^b	- ^b	4.12	- ^b	Wave II too poorly identified for meaningful measurements.					0.289	0.123	0.228	3.83	1.00	1.019	0.207	0.916	2.94	0.35
	200	-1.539	- ^b	- ^b	3.98	- ^b						0.288	0.119	0.229	3.63	0.99	1.016	0.203	0.915	3.14	0.31
	150	-1.542	- ^b	- ^b	4.06	- ^b						0.288	0.114	0.231	3.59	0.99	1.005	0.190	0.910	2.85	0.31
	100	-1.544	- ^b	- ^b	3.91	- ^b						0.285	0.106	0.232	2.98	0.97	1.001	0.174	0.914	2.74	0.28
	50	-1.550	- ^b	- ^b	3.54	- ^b						0.282	0.100	0.232	2.11	1.02	0.985	0.135	0.918	2.05	0.23
	Av.													0.230		0.99			0.915		
(84) (C ₁₂ H ₂₅) ₈ -ZnPc at 70°C in DCE	250	Wave I too poorly identified for meaningful measurements.					-1.479	- ^b	- ^b	5.72	- ^b	0.325	0.144	0.254	4.04	0.90	1.048	0.251	0.923	3.51	0.28
	200						-1.441	- ^b	- ^b	3.97	- ^b	0.324	0.141	0.254	3.89	0.89	1.037	0.233	0.921	3.26	0.29
	150						-1.437	- ^b	- ^b	3.85	- ^b	0.322	0.135	0.255	3.45	0.91	1.021	0.203	0.920	2.84	0.31
	100						-1.423	- ^b	- ^b	3.42	- ^b	0.316	0.126	0.253	2.83	0.94	0.996	0.165	0.914	2.22	0.36
	50						-1.409	- ^b	- ^b	2.94	- ^b	0.311	0.118	0.252	2.08	1.00	0.982	0.134	0.915	1.45	0.42
	Av.													0.254		0.93			0.919		
(C ₁₃ H ₃₁) ₈ -ZnPc at 70°C in DCE	250	Wave I too poorly identified for meaningful measurements.					-1.514	- ^b	- ^b	-	-	0.398	0.213	0.292	1.57	1.03	1.061	0.293	0.915	1.73	0.59
	200						-1.499	- ^b	- ^b	-	-	0.395	0.205	0.293	1.46	1.01	1.044	0.269	0.910	1.37	0.66
	150						-1.466	- ^b	- ^b	-	-	0.384	0.184	0.292	1.31	1.02	1.030	0.239	0.911	1.16	0.64
	100						-1.471	- ^b	- ^b	-	-	0.374	0.161	0.294	1.05	1.07	1.016	0.219	0.907	0.89	0.76
	50						-1.466	0.121	-1.439	0.24	-	0.360	0.139	0.291	0.80	1.13	0.999	0.174	0.912	0.68	0.68
	Av.													0.292		1.05			0.911		

^aPoor solubility and extensive aggregation destroys meaningful CV's, no estimate possible.^bCV quality too poor for meaningful measurements.^cResolution poor, value an estimate.

Temperature and solvent changes from 25 to 70°C and dichloromethane to dichloroethane respectively had no large adverse effect on the peak potentials of the phthalocyanines, as illustrated in the CV's (b) and (c) of the C₇-derivative (Figure 3.21), although wave I in DCE at 70°C is distorted by the solvent decomposition that begins to take place at *ca.* -1.8 V.

ΔE_p for waves I and II of the shorter alkyl chains C₅ and C₇ were below 96 mV at slow scan rates while the longer alkyl chains produced larger ΔE_p values (Table 3.10). Wave IV differs noticeably in shape from that of other waves, in that its ΔE is obviously very large. Larger ΔE_p values are consistent with slower kinetics of electron transfer between the working electrode and analyte, here the [MPc]⁺ and/or [MPc]²⁺ species. At slow scan rates (50 mV s⁻¹) ΔE_p for wave III for all derivatives except C₁₅ phthalocyanine were below 96 mV and borders on the requirements for electrochemical reversibility. Only at faster scan rates do ΔE values become so large that quasi electrochemical reversibility is assigned to the electron transfer process. The increase in ΔE_p values, with an increase in chain length as well as scan rate is an indication that the rate of electron transfer between the electrode and the phthalocyanines are severely hampered by alkyl side chains of increasing length. This implies that electrochemical reversibility becomes poorer with an increase in substituent chain length. The increase in ΔE_p values therefore implies that a non-hindered, efficient route allowing fast electron exchange between the electrode and the phthalocyanine core becomes less and less available as the side chain length increases. This can be quantified by envisaging that longer chain length in the eight alkyl substituents may become more efficient in coiling and wrapping itself around the phthalocyanine core, thereby partially isolating the active redox centre more and more effective from the electrode. This is demonstrated in Figure 3.20 (page 99).

However, the chain length of the alkyl groups on the phthalocyanine macrocycle could not be increased indefinitely, as they become less soluble after fifteen carbon atom side chain lengths. The solubility of the C₁₅-2HPc derivative became so poor at room temperature (25°C) that the electrochemistry had to be performed at 70°C in dichloroethane. Hence the maximum carbon chain length in the side chains of the class of phthalocyanines that this laboratory is concerned with is eighteen.¹³ The chain length of the substituted alkyl groups did not result in changes in the formal reduction potentials, E^o , of more than 36 mV for waves II and III for metal-free phthalocyanines. However the C₁₅-2HPc derivative showed anomalous behaviour in that wave I and IV were poorly defined under our experimental conditions. Further more, the E^o of wave

I (C_{15} -derivative), was 49 mV more positive than that of the C_{11} derivative and $E^{\circ'}$ for wave IV of $(C_{15}H_{31})_8$ -2HPc was 222 mV more positive than that of the C_{11} derivative.

The cyclic voltammograms of the $(C_5H_{11})_8$ -ZnPc in dichloroethane at 70°C is shown in Figure 3.22 as a representative example of the zinc-containing phthalocyanines. The redox wave of ferrocene in dichloroethane at 70°C is also shown. Poor solubility of all ZnPc's in dichloromethane at 25°C prevented us from using it as solvent. The higher temperature, 70°C, was needed to dissolve the ZnPc's. However, a drawback of dichloroethane is that it itself is electrochemically destroyed at -1.8 V vs Ag/Ag^+ . This means that waves I and II of all ZnPc's are to a large extent distorted.

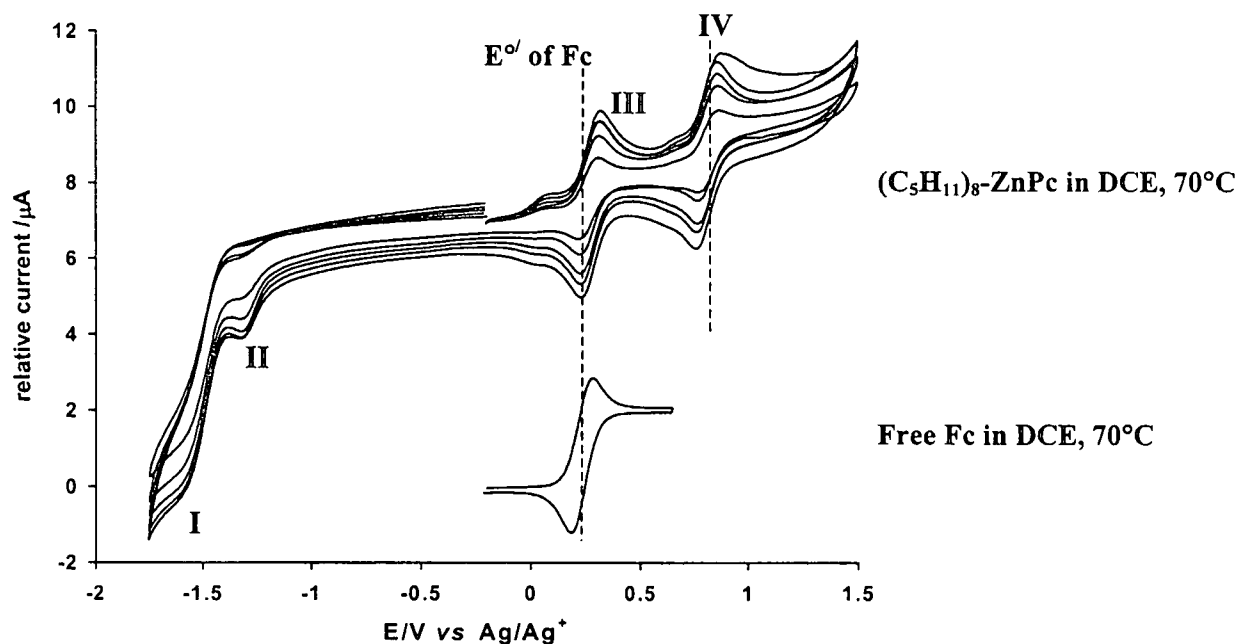


Figure 3.22: Above: Cyclic voltammograms of $(C_5H_{11})_8$ -ZnPc (1 mmol dm^{-3}) in dichloroethane at 70°C with 0.2 mol dm^{-3} $(\text{Bu})_4\text{NPF}_6$ as supporting electrolyte on a platinum working electrode, recorded at scan rates of 50, 100, 150, 200 and 250 mV s^{-1} . Bottom: The redox wave of free ferrocene (1 mmol dm^{-3}) in dichloroethane at 70°C recorded at a scan rate of 100 mV s^{-1} . ($E^{\circ'} = 0.231 \text{ V}$ and $\Delta E_p = 0.097$).

In the CV of $(C_5H_{11})_8$ -ZnPc two well defined ring-centred redox processes III and IV were observed, while waves I and II were poorly defined. Note that the $E^{\circ'}$ of the free ferrocene cyclic voltammogram (bottom CV) coincides with that of wave III of the zinc-containing phthalocyanine. When free ferrocene is used as internal marker in the presence of ZnPcs the $E^{\circ'}$ of wave III and that of the Fc/Fc^+ couple are overlapping so much that peak separation was not observed. Similar type of results as for the C_5 -derivative was obtained for all the other zinc-

containing phthalocyanines in this study. For this reason, the experimentally determined potentials for the zinc phthalocyanines series are also given vs. Ag/Ag^+ as reference electrode. The cyclic voltammetry behaviour of the octa-alkylated ZnPcs from C_1 through to C_{15} , recorded at a scan rate of 100 mV s^{-1} are shown in Figure 3.23 and the electrochemical data summarised in Table 3.10, page 102.

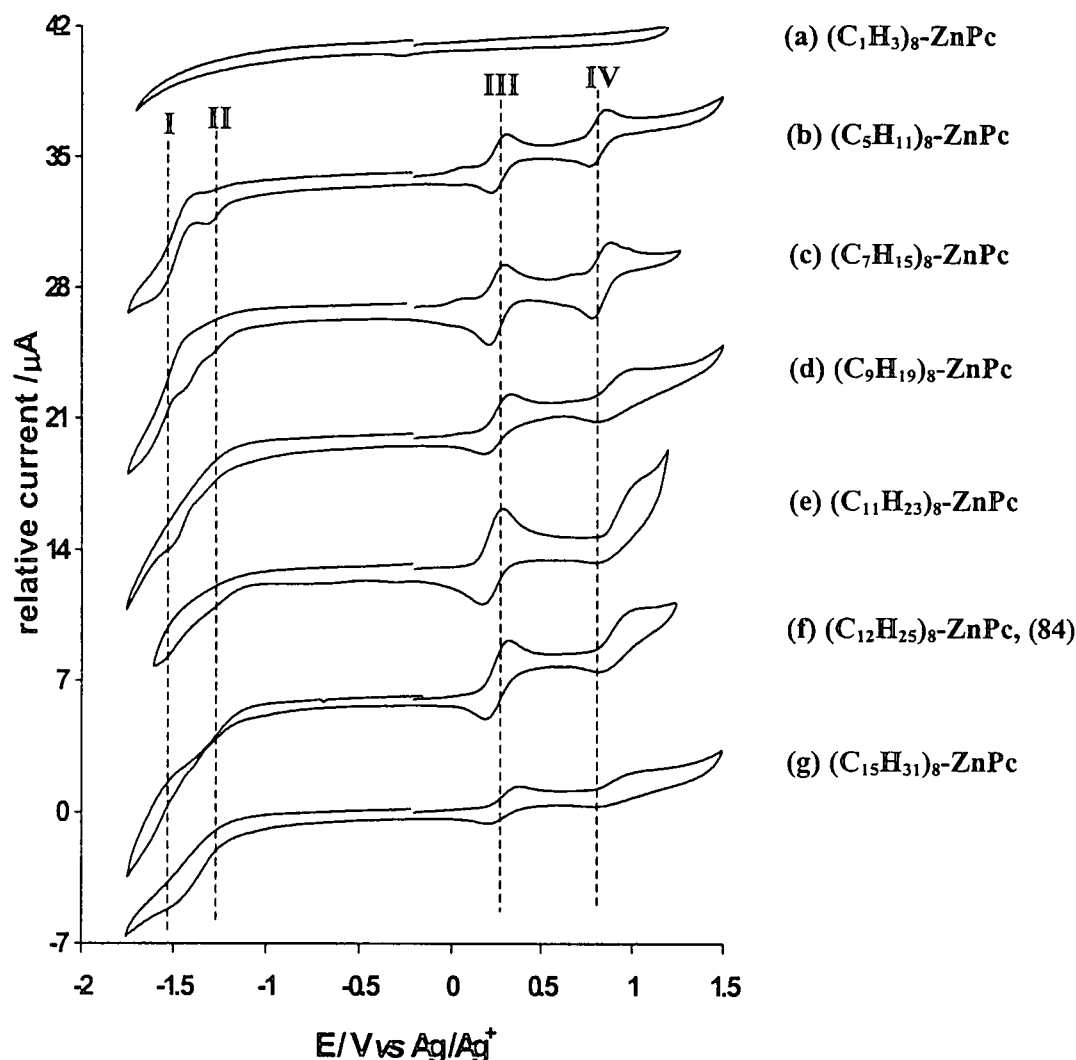


Figure 3.23: Cyclic voltammograms of a series of octa-alkylated zinc phthalocyanines (1 mmol dm^{-3} in dichloroethane at 70°C with 0.2 mol dm^{-3} $(^t\text{Bu})_4\text{NPF}_6$ as supporting electrolyte) on a platinum working electrode, recorded at a scan rate of 100 mV s^{-1} . Poor solubility and extensive aggregation destroys meaningful CV's for (a) $(\text{C}_1\text{H}_3)_8\text{-ZnPc}$. Poorly defined waves I and II are the result of solvent reduction that commences at *ca.* -1.8 V .

Except for the C_1 -derivative, two quasi-reversible ring-centred redox processes, III and IV were observed for all the zinc-containing phthalocyanines under our experimental conditions. The two expected reduction waves, waves I and II were poorly defined for all our ZnPc complexes and became even worse as the chain length of the alkyl substituents increased. No oxidation or

reduction waves were observed for the C₁-ZnPc derivative because it remained insoluble in DCE even at 70°C.

Reduction waves **I** and **II** were so poorly defined that only estimated $E^{o'}$ and ΔE_p values for the shorter alkyl chains, C₅ and C₇ can be given. ΔE_p values for waves **III** and **IV** at slow scan rates for the shorter alkyl chains were below 84 mV while the longer alkyl chains produced larger ΔE_p values.

The $E^{o'}$ of wave **III** (C₁₅-derivative), was 38 mV more positive than for the C₁₂-derivative and 28 mV more positive than the C₅-derivative while $E^{o'}$ of wave **IV** (C₁₂-and C₁₅-derivatives), was *ca.* 100 mV more positive than the shortest alkyl substituted C₅-derivative.

The peak cathodic and peak anodic current ratio, i_{pc}/i_{pa} , at slow scan rates for waves **II** (except the C₉-and C₁₂-derivatives) and **III** (except C₉-derivative) of the metal-free and wave **III** (except the C₁-derivative) of the zinc phthalocyanines (Table 3.10), approached unity, indicating that these electrochemical processes was not accompanied by any other physical or chemical process. Waves **I** (except the shorter C₅ and C₇ alkyl chains) and **IV** of the 2HPc's and wave **IV** of the ZnPc's deviated, however substantially from unity, while no i_{pc}/i_{pa} values for waves **I** and **II** of the ZnPc's could be determined due to very poorly defined waves. However, since no additional electrochemical process apart from the four belonging to the phthalocyanine system could be identified, it was concluded that the deviation from unity is probably not the consequence of a chemical process that accompany these processes either. Rather the lack of suitable solubility of these *in situ* generated [MPc]²⁻, [MPc]^{-•} and [MPc]²⁺ species in the non-polar solvents dichloromethane or 1,2-dichloroethane disallows the generation of a cyclic voltammogram half wave of sufficient intensity during the reverse sweep to maintain i_{pc}/i_{pa} ratios approaching unity. The possibility of these intermediates forming thin coatings by adsorption on the electrode is to a large extent limited in view of the protective layer, or globule, that the long alkyl substituents apparently form around the phthalocyanine core.

By substituting the two protons in the phthalocyanine core with the zinc metal, differences in ΔE_p and shifts in $E^{o'}$ values for some waves were observed. ΔE_p for wave **III** for example, at a slow scan rate for (C₁₂H₂₅)₈-2HPc, (**83**) is 39 mV smaller than the same wave of the (C₁₂H₂₅)₈-ZnPc, (**84**) while ΔE_p of wave **IV** for (**83**) is 133 mV larger than for its zinc-containing analogue (**84**). The $E^{o'}$ of wave **III** for the C₁₂-derivative, shifted to 254 mV, some 122 mV more negative in the presence of the zinc metal inside the phthalocyanine macrocycle,

($C_{12}H_{25}$)₈-ZnPc, (**84**) compared to $E^o = 376$ mV for the ($C_{12}H_{25}$)₈-2HPc, derivative (**83**). In contrast, wave IV for the C_{12} -Zn derivative ($E^o = 919$ mV) moved to a more positive potential by 80 mV compared to the C_{12} -2HPc derivative ($E^o = 839$ mV).

The relationship between ΔE_p and the length of the alkyl chain (n) on the 2H and Zn-containing phthalocyanine macrocycle were explored. Figure 3.24 highlights the relationship graphically for waves I, II and III (2HPc's) and waves III and IV for ZnPc's.

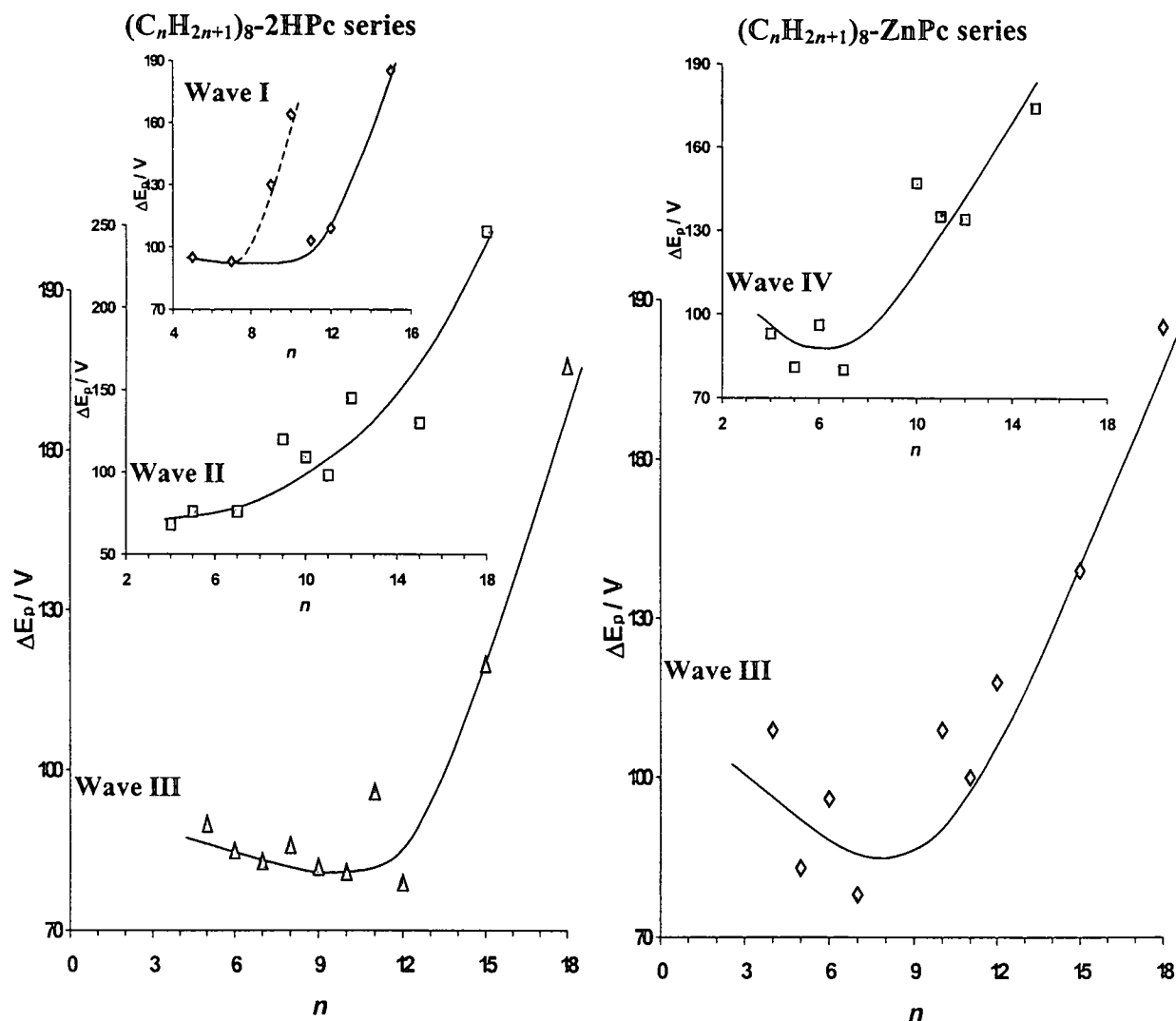


Figure 3.24: Relationship between ΔE_p and length of the alkyl chain (n) on the phthalocyanine macrocycles of general formula (C_nH_{2n+1})₈-MPc, where M = 2H (left) or Zn (right). ΔE_p values for complexes with $n = 4, 6, 8, 10$ and 18 are from reference 14.

The poor definition of waves I and II for the ZnPc's prevented us from considering them in this relationship, while wave IV was ignored in the 2HPc series of compounds because of the obvious slow kinetics (as indicated by extremely large ΔE_p values) of electron transfer for this couple. It was used, however, for the ZnPc series of compounds, because waves I and II

electrochemical data were very poor (see Figure 3.23). All five graphs in Figure 3.24 consisted of two definite regions that could most easily be identified for wave **III**. The first position, representing region with smaller n -values, in general showed a slight decrease in ΔE_p values with increase in n -values. However, at a certain key n -value, all five graphs moved into the second region (or portion) where an increase in n -values caused a dramatic increase in ΔE_p values. For the 2HPc's, this happened with $n = 7$ for wave **I**, $n \approx 9$ for wave **II** and $n = 12$ for wave **III**, while $n = 8$ appear to be the point when ΔE_p for ZnPc's begins to increase rapidly with increase in substituent chain length (waves **III** and **IV**). The first portion of all five graphs (*i.e.* ΔE_p decrease with increasing n) is consistent with an enhancement of phthalocyanine solubility with increasing chain length. It also can be traced to lesser degrees of aggregation of the phthalocyanines with longer chain lengths in Pc-substituents. Lesser degrees of aggregation imply easier (and hence faster) electron transfer between phthalocyanine and working electrode. Hence ΔE_p values are decreasing with increase in side chain n -values (in the first portion of each graph).

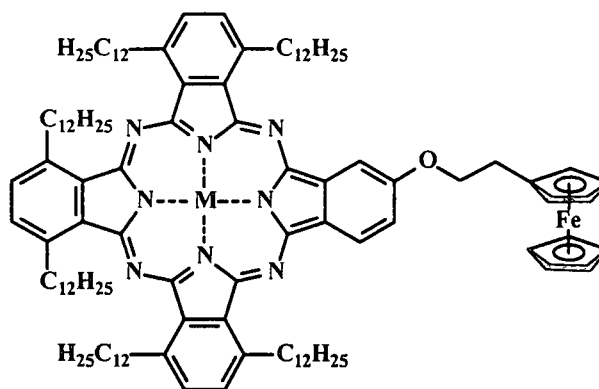
However, when the n -value of the side chains becomes too large, the side chains do not only prevent aggregation of Pc's. By wrapping itself around the phthalocyanine core, the side chain now begin to act as an isolator, and prevents good reaction contact between phthalocyanine macrocycle and electrode. This also explains the sudden fast increase in ΔE_p values for the Pc's with very large substituents (very large n -values) in the second portion of the five graphs.

The plots in Figure 3.24 are regarded as electrochemical proof that encapsulation by the eight alkyl substituents on the Pc macrocycle take place, and that this encapsulation becomes more effective with increase in alkyl chain length. To visualise this, Figure 3.20 (page 99) is once again instructive.

3.4.2.2 Cyclic voltammetry of ferrocenyl-phthalocyanine conjugates

The cyclic voltammetry of the metal-free and zinc-containing ferrocenyl-phthalocyanine conjugates, **(86)** and **(87)** in Figure 3.25, were investigated under the same experimental conditions as for the octa-alkylated phthalocyanines. The metal-free ferrocenyl-phthalocyanine, **(86)** was studied in dichloromethane at 25°C and the zinc-containing derivative, **(87)** in dichloroethane at 70°C. As expected, the presence of the ferrocenylethoxide group on the phthalocyanine macrocycle changed the redox properties of the system as can be seen in Figure 3.26. Five redox signals were observed for the metal-free ferrocenyl-phthalocyanine conjugate,

(86) in the potential range -2.0 to 1.2 V vs Ag/Ag^+ . The electrochemical data for these processes are summarised in Table 3.11, page 111.



(86): $M = 2\text{H}$

(87): $M = \text{Zn}$

Figure 3.25: Metal-free and zinc-containing ferrocenyl-phthalocyanine conjugates (86) and (87) that were studied by means of cyclic voltammetry.

When one considers the average formal reduction potentials, $E^{\circ'}$, tabulated in Table 3.11, it can be deduced that waves **I**, **II**, **III** and **IV** for $(\text{C}_{12}\text{H}_{25})_6\text{-2HPc-O-(CH}_2)_2\text{-Fc}$, (86), correlates to some extent with waves **I**, **II**, **III** and **IV** for $(\text{C}_{12}\text{H}_{25})_8\text{-2HPc}$, (83) respectively. This also happens for $(\text{C}_{12}\text{H}_{25})_6\text{-ZnPc-O-(CH}_2)_2\text{-Fc}$, (87) and $(\text{C}_{12}\text{H}_{25})_8\text{-ZnPc}$, (84). These four redox processes in compound (86) are therefore assigned to the electron transfer processes on the phthalocyanine macrocycle, while the redox couple indicated by FcPc , ($E^{\circ'} = 0.222\text{V}$) in Figure 3.26 is assigned to electron transfer on the ferrocenyl group.

Peak separation between waves **III** and FcPc for the metal-free derivative $(\text{C}_{12}\text{H}_{25})_6\text{-2HPc-O-(CH}_2)_2\text{-Fc}$, (86), is larger than for the zinc-containing derivative (87): approximately 126 and 40 mV respectively. This coalescence of waves FcPc and **III** for the ZnPc (87) came about because $E^{\circ'}$ of wave **III** for the zinc-containing ferrocenyl-phthalocyanine conjugate, (87) shifted by approximately 85 mV to a more negative potential compared to wave **III** for the metal-free derivative (86). This caused poor peak separation for this compound and a broad oxidation wave is observed due to the overlap of wave FcPc for the ferrocene group and wave **III** for this phthalocyanine macrocycle. In contrast, $E^{\circ'}$ of wave **IV** for the ZnPc derivative (87) moved to a slightly more positive potential by *ca.* 20 mV compared to wave **IV** of the 2HPc derivative (86). Wave FcPc for phthalocyanine (86) indicates electrochemical reversibility with $\Delta E_p = 68$ mV at 50 mV s^{-1} , but the poor resolution between wave **III** and the FcPc wave in (87) disallows accurate ΔE_p measurements.

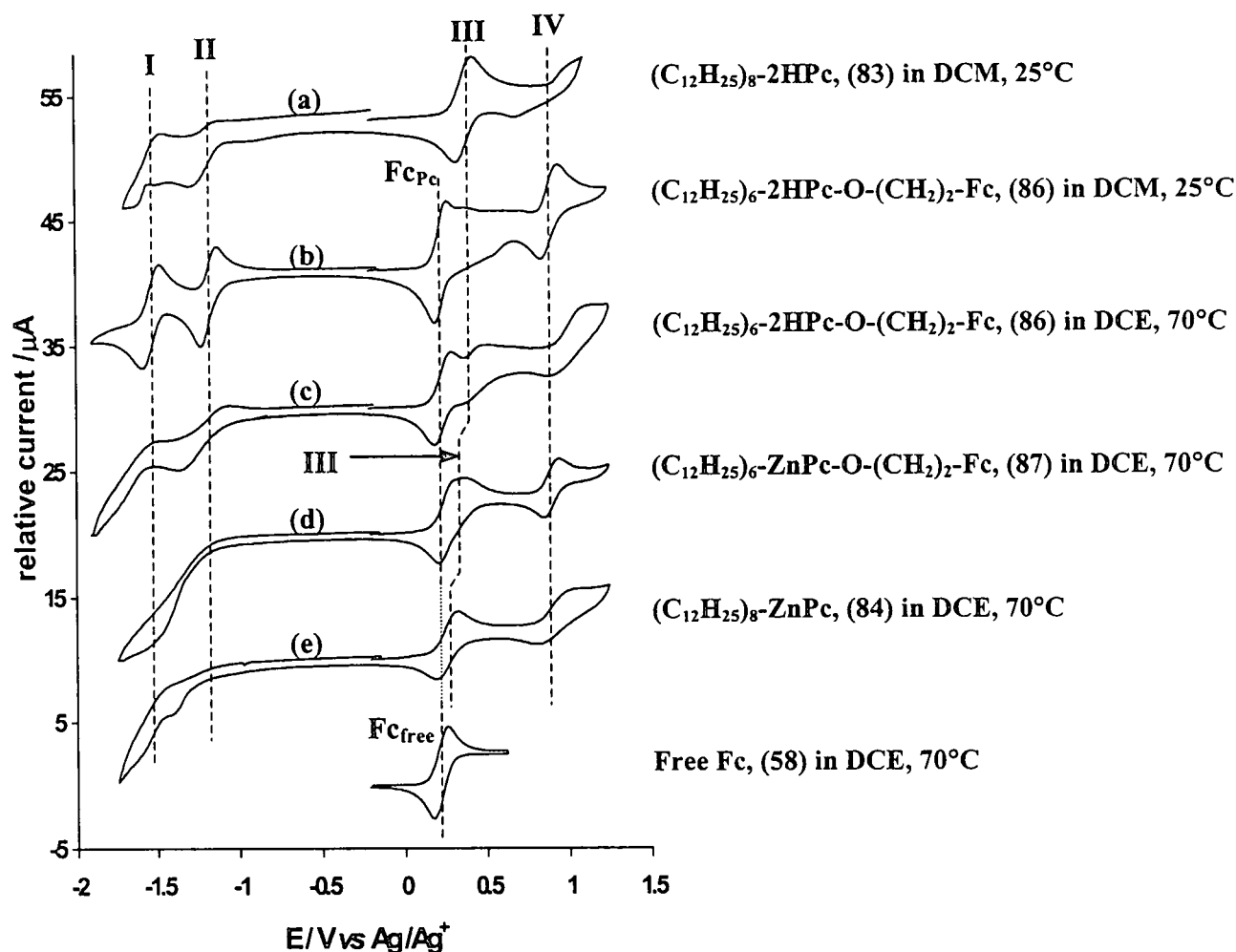


Figure 3.26: Cyclic voltammograms (CV's) of 1 mmol dm⁻³ ferrocenyl-free phthalocyanines (83) and (84) and ferrocenyl-phthalocyanine conjugates (86) and (87) in DCM at 25°C and DCE at 70°C respectively, with 0.2 mol dm⁻³ (tBu)₄⁺NPF₆⁻ as supporting electrolyte on a platinum working electrode, at a scan rate of 150 mV s⁻¹. Four redox processes I, II, III and IV on the phthalocyanine ring system and a fifth redox process Fc_{Pc} at the anchored ferrocenyl group can be identified. The CV of free ferrocene, (58) (at 100 mV s⁻¹) is also shown and is labelled Fc_{free}. DCM = dichloromethane and DCE = dichloroethane.

The reaction sequence for the electrochemical processes associated with (86) and (87) is summarised in Figure 3.27 as:

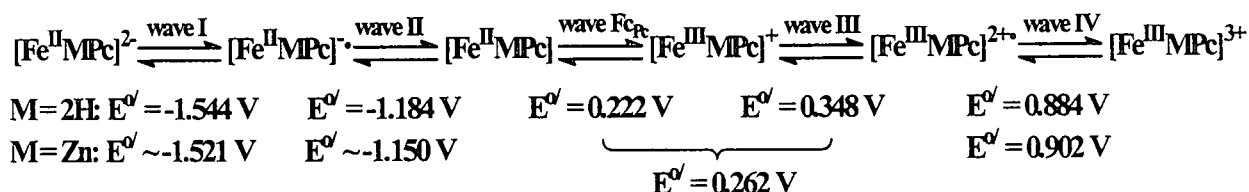


Figure 3.27: Redox couples and average formal reduction potentials, E^o for $(C_{12}H_{25})_6-MPc-O-(CH_2)_2-Fc$, with M = 2H, (86) or Zn, (87) vs Ag/Ag^+ .

Table 3.11: Peak cathodic potentials (E_{pc}), difference in peak anodic and peak cathodic potentials (ΔE_p), formal reduction potentials (E°), peak cathodic currents (i_{pc}) and peak current ratios (i_{pc}/i_{pa}) for phthalocyanines (83), (84), (86) and (87). Potentials are versus Ag/Ag^+ . DCM = dichloromethane and DCE = dichloroethane.

Pc	v/ mV s ⁻¹	Wave I					Wave II					Wave Fc _{Pc}					Wave III					Wave IV				
		$E_{pc}/$ V	$\Delta E_p/$ V	$E^{\circ}/$ V	$i_{pc}/$ μA	i_{pc}/i_{pa}	$E_{pc}/$ V	$\Delta E_p/$ V	$E^{\circ}/$ V	$i_{pc}/$ μA	i_{pc}/i_{pa}	$E_{pc}/$ V	$\Delta E_p/$ V	$E^{\circ}/$ V	$i_{pc}/$ μA	i_{pc}/i_{pa}	$E_{pc}/$ V	$\Delta E_p/$ V	$E^{\circ}/$ V	$i_{pc}/$ μA	i_{pc}/i_{pa}	$E_{pc}/$ V	$\Delta E_p/$ V	$E^{\circ}/$ V	$i_{pc}/$ μA	i_{pc}/i_{pa}
(83) (C ₁₂ H ₂₃) ₈ - 2HPc at 25°C in DCM	250	-1.614	0.143	-1.543	2.94	1.50	-1.253	0.132	-1.188	4.26	1.61	Compound does not have a ferrocene- containing substituent.					0.324	0.103	0.376	5.63	0.97	0.661	0.339	0.831	1.47	0.61
	200	-1.606	0.133	-1.540	2.12	1.24	-1.261	0.132	-1.196	3.73	1.64						0.326	0.098	0.375	5.21	0.99	0.671	0.326	0.834	1.27	0.72
	150	-1.600	0.127	-1.537	1.47	0.95	-1.274	0.135	-1.207	3.31	1.69						0.329	0.092	0.375	4.73	1.04	0.677	0.317	0.836	0.98	0.71
	100	-1.597	0.121	-1.537	0.96	0.74	-1.282	0.138	-1.216	2.82	1.58						0.332	0.087	0.376	3.91	1.04	0.694	0.295	0.842	0.73	0.64
	50	-1.593	0.109	-1.538	0.41	0.50	-1.290	0.145	-1.218	2.36	1.32						0.337	0.079	0.377	3.00	1.10	0.721	0.267	0.852	0.49	0.61
	Av.			-1.539					-1.205										0.376		1.03			0.839		
(86) (C ₁₂ H ₂₃) ₆ - 2HPc-O- (CH ₂) ₂ -Fc, at 25°C in DCM	250	-1.633	0.156	-1.555	5.64	0.99	-1.250	0.125	-1.188	9.78	2.75	0.173	0.094	0.220	6.77	0.84	0.319	0.062	0.350	3.89	1.72	0.816	0.136	0.884	5.02	0.91
	200	-1.623	0.146	-1.550	5.47	1.02	-1.247	0.122	-1.186	8.55	2.42	0.175	0.091	0.221	6.52	0.90	0.320	0.057	0.349	3.46	1.91	0.820	0.124	0.882	4.64	0.92
	150	-1.609	0.131	-1.544	5.14	1.11	-1.241	0.114	-1.184	7.02	2.00	0.180	0.084	0.222	5.82	0.92	0.323	0.051	0.348	3.06	1.82	0.827	0.112	0.883	4.14	0.97
	100	-1.594	0.111	-1.539	4.42	1.09	-1.233	0.106	-1.180	5.27	1.51	0.184	0.079	0.224	5.02	0.98	0.327	0.044	0.349	2.53	2.02	0.831	0.105	0.884	3.21	0.91
	50	-1.575	0.089	-1.531	3.26	1.07	-1.225	0.086	-1.182	3.51	1.08	0.189	0.064	0.221	3.76	1.01	0.328	0.037	0.345	2.00	2.66	0.844	0.086	0.887	2.23	0.85
	Av.			-1.544		1.06			-1.184					0.222		0.93			0.348					0.884		0.91
(87) (C ₁₂ H ₂₃) ₆ - ZnPc-O- (CH ₂) ₂ -Fc, at 70°C in DCE	250	-1.613	- ^a	-	20.5	- ^a	Wave II too poorly identified for meaningful measurements. E° is expected at -1.1 to -1.2 V.					Wave Fc overlaps so much with wave III, that poor resolution is obtained. $E^{\circ}_{Fc} \approx$ ca. 0.222 V and $E^{\circ}_{Wave III} \approx$ ca. 0.262 V. Approximate data for the combined peaks is summarised in Wave III.					0.199 ^b	0.127 ^b	0.263 ^b	8.63 ^b	1.09 ^b	0.853	0.097	0.902	4.64	0.92
	200	-1.566	- ^a	-	13.7	- ^a											0.201	0.124	0.263	8.05	1.09	0.857	0.090	0.902	4.27	0.86
	150	-1.534	- ^a	-	9.01	- ^a											0.202	0.121	0.263	7.16	1.09	0.862	0.082	0.903	3.65	0.81
	100	-1.528	- ^a	-	7.68	- ^a											0.202	0.118	0.261	6.22	1.11	0.864	0.078	0.903	3.10	0.80
	50	-1.512	- ^a	-	5.08	- ^a											0.204	0.108	0.258	4.95	1.18	0.865	0.070	0.900	2.70	0.94
	Av.																		0.262		1.11			0.902		0.87
(84) (C ₁₂ H ₂₃) ₈ - ZnPc at 70°C in DCE	250	Wave I too poorly identified for meaningful measurements.					-1.479	- ^b	- ^b	5.72	-	Compound does not have a ferrocene- containing substituent.					0.325	0.144	0.254	4.04	0.90	1.048	0.251	0.923	3.51	0.28
	200						-1.441	- ^b	- ^b	3.97	-						0.324	0.141	0.254	3.89	0.89	1.037	0.233	0.921	3.26	0.29
	150						-1.437	- ^b	- ^b	3.85	-						0.322	0.135	0.255	3.45	0.91	1.021	0.203	0.920	2.84	0.31
	100						-1.423	- ^b	- ^b	3.42	-						0.316	0.126	0.253	2.83	0.94	0.996	0.165	0.914	2.22	0.36
	50						-1.409	- ^b	- ^b	2.94	-						0.311	0.118	0.252	2.08	1.00	0.982	0.134	0.915	1.45	0.42
	Av.																		0.254		0.93			0.919		

^a CV quality too poor for meaningful measurements.

^b See remark in column for wave Fc_{Pc}, compound (87).

The influence of temperature (and solvent) on the CV of (86) can be seen by comparing CV's (b) and (c) in Figure 3.26. The higher temperature caused better wave definition/resolution for the waves labelled **FcPc** and **III**. The solvent change from DCM to DCE caused peak distortion for waves **I** and **II**, and is considered to be caused by solvent destruction at *ca.* -1.8 V. The presence of the O-(CH₂)₂-Fc group caused wave **IV** to be the fingerprint of a much more ideal and fast electron transfer process in (86) [CV (b)] and (87) [CV (d)] because $\Delta E_p \leq 86$ mV (Table 3.11). The ferrocene-free analogues, (83) and (84), has $\Delta E_p \geq 134$ mV. This is taken as evidence that the ferrocenyl group may act as an electron transfer mediator between the species [MPc]^{•+}/[MPc]²⁺ and the platinum working electrode.

The close approximation of i_{pc}/i_{pa} current ratios to unity at slow scan rates also shows that in both the phthalocyanines (C₁₂H₂₅)₆-2HPc-O-(CH₂)₂-Fc, (86) and (C₁₂H₂₅)₆-ZnPc-O-(CH₂)₂-Fc, (87), electrochemical processes are not followed by a subsequent chemical step. The deviation of measurable i_{pc}/i_{pa} current ratios from unity at slow scan rates for waves **I**, **II** and **IV** of (86) or (87) are regarded as a consequence of experimental conditions in terms of the solvent, DCE and the temperature, 70°C. The deviation of i_{pc}/i_{pa} from unity for wave **III**, especially of (86) is regarded as a consequence of the overlapping of wave **FcPc** for the ferrocene group and wave **III** for this phthalocyanine macrocycle. It is not attributed to any significant chemical process that takes place on the phthalocyanine macrocycle.

3.5 UV/VIS spectroscopy of selected phthalocyanine derivatives

The solution absorption spectra of phthalocyanines give characteristic strong absorption bands in the UV region (Soret band ≈ 345 nm) and very intense absorption bands in the visible region (Q-band ≈ 700 nm). This led to an investigation of the UV-visible spectroscopic properties of the newly synthesised phthalocyanines indicated in Figure 3.28.

The UV-visible absorption spectra between 300 and 800 nm for the phthalocyanine derivatives indicated in Figure 3.28 (except (1), results for this phthalocyanine is from reference 15) were recorded in THF at 25°C and are shown in Figure 3.29.

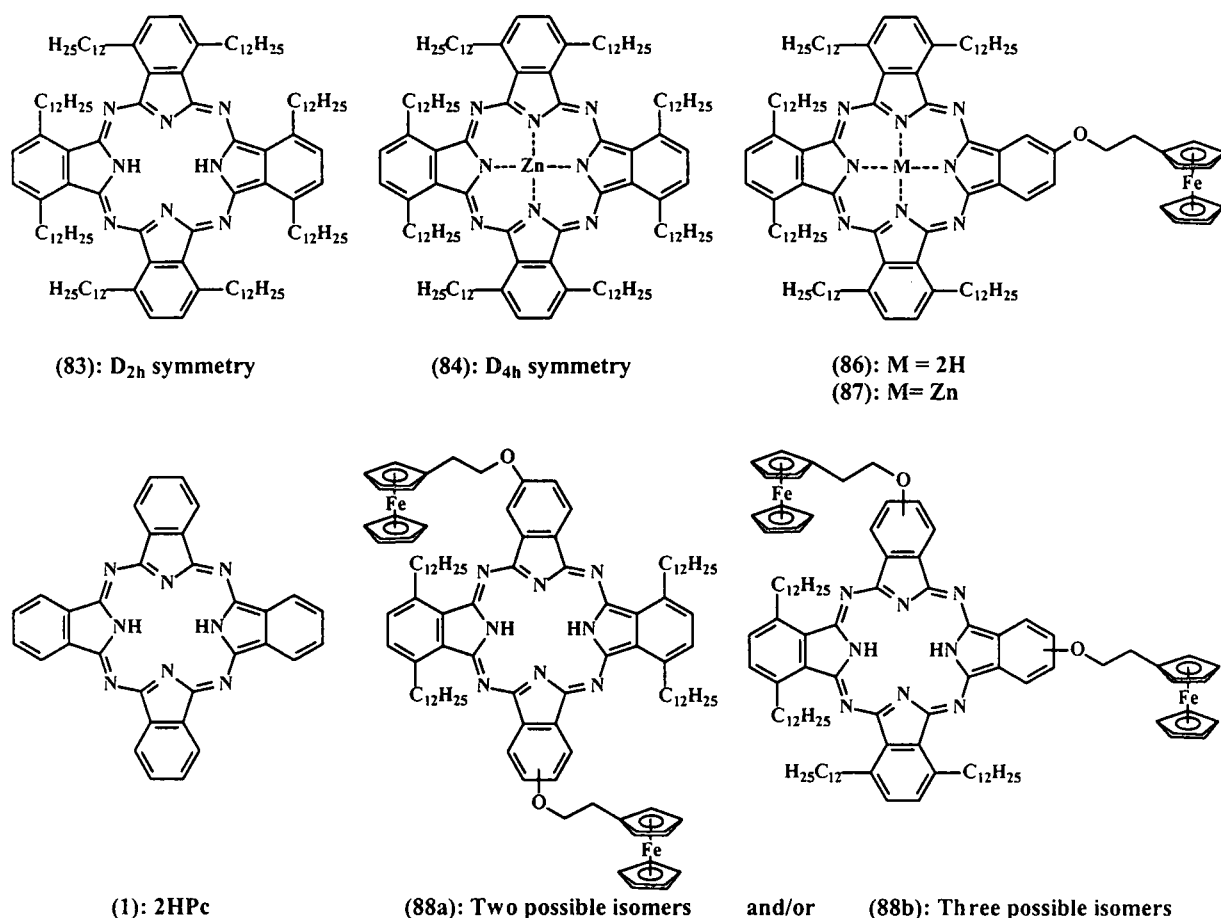


Figure 3.28: Structures of the metal-free and zinc-containing octakis(dodecyl)phthalocyanines and ferrocenyl-phthalocyanine conjugates studied by UV/VIS spectroscopy.

It is important to note that a red shift of the Q-bands absorption peak maxima for the non-peripheral octadodecylated metal-free phthalocyanine, $(C_{12}H_{25})_8$ -2HPc, (83), is observed (the green line in Figure 3.29) at $\lambda_{\max} = 698$ and 729 nm, compared to $\lambda_{\max} = 655$ and 699 nm for the unsubstituted metal-free phthalocyanine, 2HPc, (1), (spectrum not shown).¹⁵ This is mutually consistent with what was found for other non-peripheral octa substituted metal-free phthalocyanines (see section 2.7 on page 39).¹⁶

Metal-free and metal-containing phthalocyanines differ in having D_{2h} and D_{4h} symmetry respectively (see Figure 3.28) and this is manifested in differences especially in the Q-band region. The ZnPcs, (84) and (87) showed a single-peak intense Q-band maximum at 701 and 693 nm respectively. However, degeneracy of the lowest energy singlet state of the metallated derivatives is lifted in the corresponding metal-free analogous. This leads to a splitting of the Q-band into a Q_x and Q_y component at 677 - 698 nm and 711 - 729 nm (see Figure 3.29,

compounds (83), (86) and (88)). The low intensity bands at shorter wavelengths than the Q-band, i.e. at *ca.* 617 and 651 nm, are vibronic in origin.

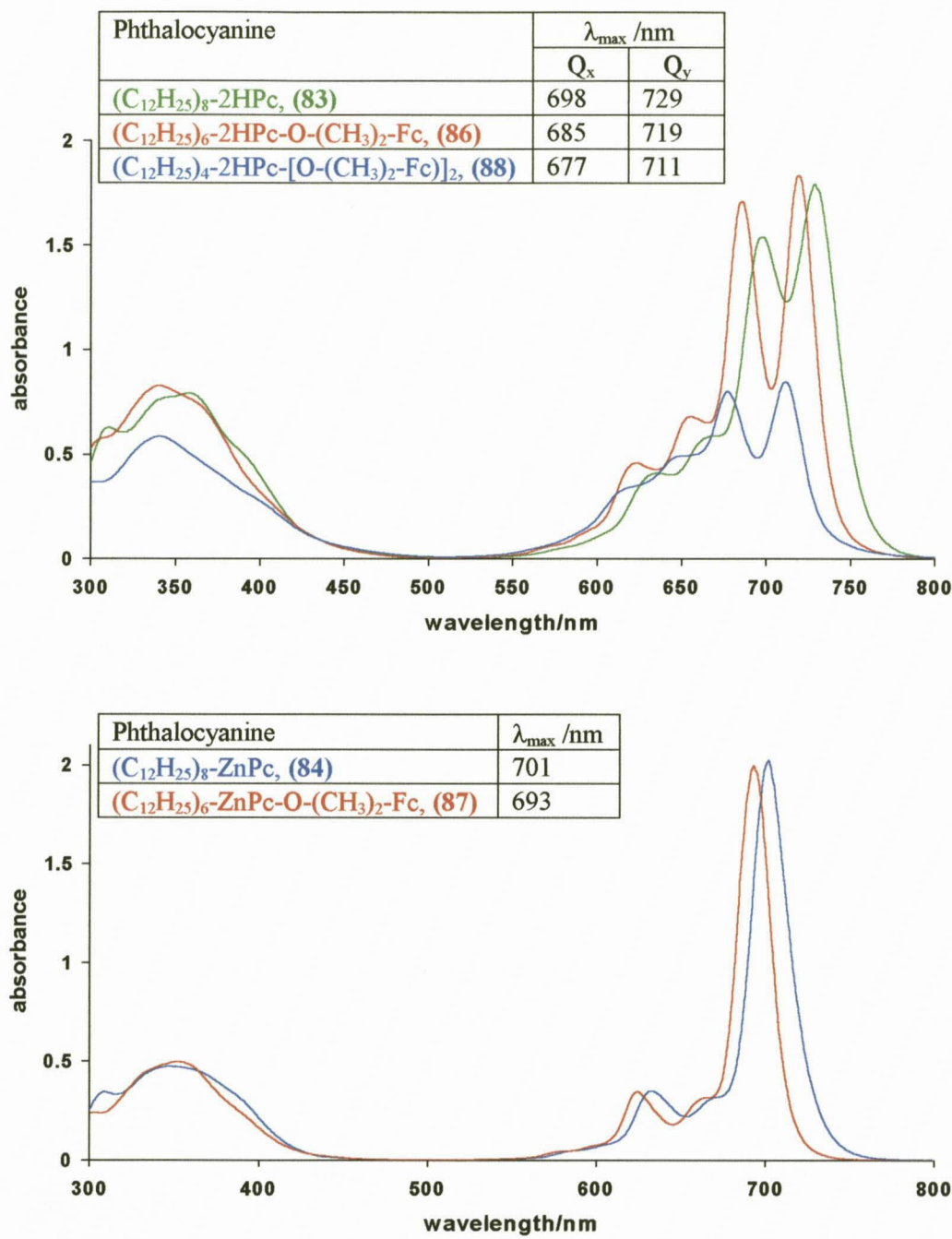


Figure 3.29: UV/VIS absorbance spectra in THF at 25°C for the indicated metal-free and zinc-containing phthalocyanines possessing dodecyl and/or ferrocenylethoxide groups, recorded at a concentration of approximately 80 $\mu\text{mol dm}^{-3}$.

The Q-band maxima for all the compounds under investigation are at longer wavelengths than 680 nm. This is in the near infrared region of the electromagnetic spectrum where tissue penetration by visible light is superior compared to penetration at $\lambda_{\text{max}} = 630\text{ nm}$, the

wavelength where HpD are irradiated during photodynamic cancer therapy. This property imply that the zinc-containing phthalocyanines of this study may be more suitable for irradiation by low cost diode lasers during the photodynamic therapy of cancer than porphyrins. The reason is because porphyrins absorb poorly at these long (>680 nm) wavelengths and because light penetration in body tissue is poor at wavelengths of 630 nm and shorter where porphyrins usually absorb light.

The Beer-Lambert law, $A = \epsilon cl$ [where A = absorbance, c = concentration, ϵ = molar extinction coefficient and l = path length of light in the cell = 1mm used for this study (not the normal 1 cm)] was used to determine to what extend the phthalocyanines under investigation aggregate. It is known that at higher concentrations, phthalocyanine aggregation takes place. Aggregation of phthalocyanines in solution significantly lowers the solution extinction coefficient of these compounds.^{16,17,18} Aggregation of phthalocyanines also leads to a decrease in their photodynamic activity.¹⁹ The extinction coefficient, ϵ , of a compound represents the slope of the linear relationship between absorbance and concentration. Figure 3.30 shows this linear relationship for $(C_{12}H_{25})_8$ -2HPc, **(83)** and $(C_{12}H_{25})_8$ -ZnPc, **(84)**. The Soret-band ϵ -value is relatively insensitive to minute deviations in this relationship for phthalocyanines, but the Q-band is very sensitive to deviations for linearity in this relationship, *inter alia* because of aggregation. From Figure 3.30, using Q-band data, it is clear that no deviation in ϵ is observed for $(C_{12}H_{25})_8$ -2HPc, **(83)** at concentrations up to $163 \mu\text{mol dm}^{-3}$ and for $(C_{12}H_{25})_8$ -ZnPc, **(84)**, at concentrations up to $101 \mu\text{mol dm}^{-3}$. Higher concentrations give rise to $A > 2.5$, which are so high, one cannot read any meaning into. Even 2.5 absorbance values is very high. This result implies that aggregation of **(83)** and **(84)** is not observable within the studied concentration ranges. (In order to take concentrations as high as possible 1 mm path length cells were used, and not the normal 1 cm path length cells.)

Although not shown, the ferrocenyl-phthalocyanine conjugates, **(86)** and **(87)** also showed linear absorbance/concentration relationships up to concentrations of 123 and $78 \mu\text{mol dm}^{-3}$ respectively. Extinction coefficients for **(83)** – **(88)** at peak wavelengths are summarised in Table 3.12.

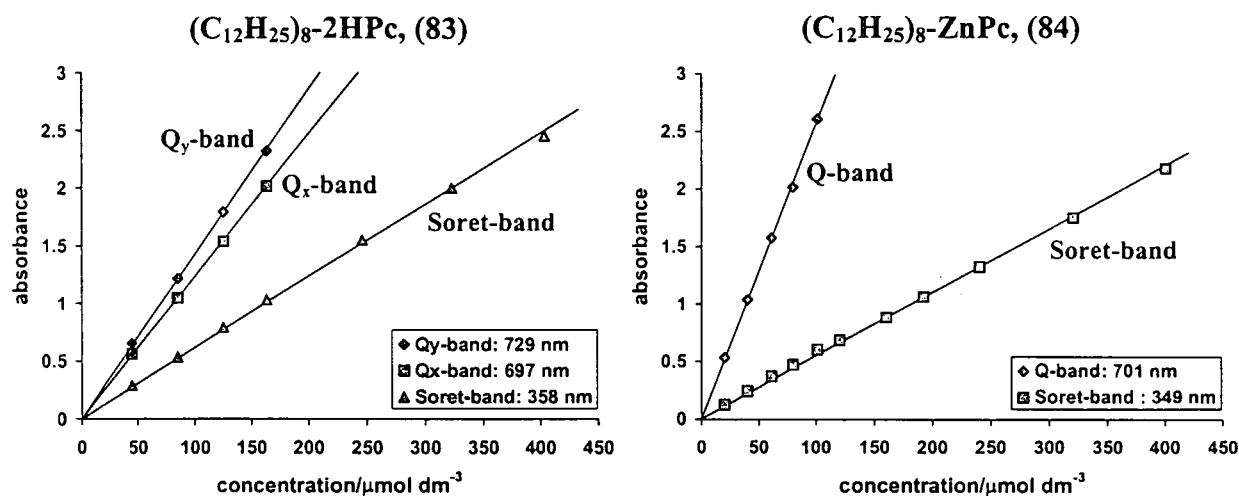


Figure 3.30: Graph of absorbance *versus* concentration for the indicated 2H- and Zn-containing phthalocyanines in THF for the Soret and Q-bands. The graphs show a linear relationship between absorbance and concentration, implying that aggregation is absent in the concentration range studied.

Table 3.12: Extinction coefficients, ϵ for phthalocyanines (83), (84), (86), (87) and (88) at Q-band maximas and Soret band.

Pcs	λ_{max}/nm	ϵ/dm^3 $mol^{-1}\ cm^{-1}$	λ_{max}/nm	ϵ/dm^3 $mol^{-1}\ cm^{-1}$	λ_{max}/nm	ϵ/dm^3 $mol^{-1}\ cm^{-1}$
(83)	729	1.42×10^5	698	1.22×10^5	358	6.16×10^4
(84)	701	2.57×10^5	---	---	349	5.41×10^4
(86)	719	1.43×10^5	685	1.33×10^5	341	6.59×10^4
(87)	693	2.45×10^5	---	---	349	5.93×10^4
(88)	711	6.92×10^5	677	5.75×10^4	340	4.63×10^4

Cook and co-workers¹⁸ showed that the longer-chain octa-alkyl substituted phthalocyanines show little propensity to aggregate up to concentrations of at least $10^{-5}\ mol\ dm^{-3}$. The octadecyl-ZnPc (C_{10} -derivative) is remarkable in remaining unaggregated up to a concentration of $1.5 \times 10^{-4}\ mol\ dm^{-3}$ ($150\ \mu mol\ dm^{-3}$). This provides evidence that encapsulation of the Zn-or 2H-containing macrocyclic phthalocyanine core by the longer-chained alkyl substituents plays an important role in decreasing the tendency towards aggregation for these phthalocyanines.

The concentration range in which the Beer Lambert law from Figure 3.30 is satisfied, is put into perspective when one considers Figure 3.31. Figure 3.31 shows at what concentration aggregation in $(C_nH_{2n+1})_8-ZnPc$, $n = 5$ to 12 takes place (data from reference 18, except for $n = 12$, which is from this study). The smaller the value of n the earlier aggregation takes place.

The C₅-derivative showed aggregation at 10 $\mu\text{mol dm}^{-3}$, the C₁₀ compound at 150 $\mu\text{mol dm}^{-3}$ while for the C₁₂ compound, (**84**) of this study, no aggregation was detected even at 400 $\mu\text{mol dm}^{-3}$ (utilising the Soret band data in Figure 3.30).

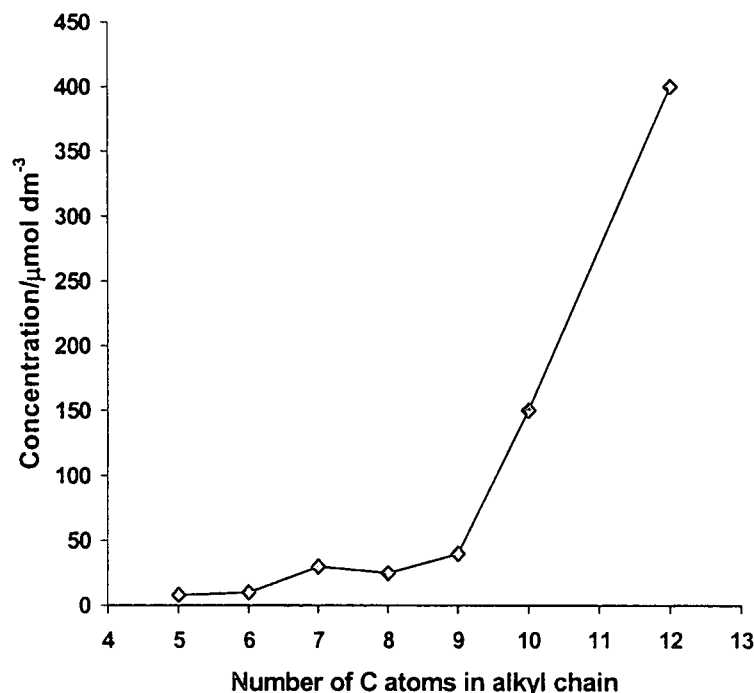


Figure 3.31: Aggregation data for compounds $(\text{C}_n\text{H}_{2n+1})_8\text{-ZnPc}$, $n = 5$ to 12 expressed as the concentration of the sample at which the Beer-Lambert plot for the Q-band absorption deviates from linearity.

This implies that with the long chain octaalkyl substituents, phthalocyanine aggregation is prevented by virtue of the long substituents which prevents phthalocyanine stacking, the reader is again referred to Figure 3. 20, which demonstrates this phenomena. It is concluded that the spectroscopic study that was performed during this research program, which highlighted the aggregation tendency of the new phthalocyanines of this study, is mutually consistent with the proposed encapsulation phenomena described in the electrochemistry section 3.4.2.1, page 99. It appears that the consequence of this potential wrapping of the side chains around the phthalocyanine core to effectively encapsulate it, in certain circumstances proves to be beneficial, while in over cases not. For example, very effective encapsulation with long alkyl substituents minimises aggregation, thereby increasing the maximum concentration at which phthalocyanine can exist in solution as monomeric, unaggregated species (see Figure 3.29), but it also isolates it from reaction partners and slows the rate of chemical or electrochemical electron transfer down (page 106).

Figure 3.32 illustrates how the extinction coefficient, ϵ of compounds (83), (84), (86), (87) and (88) varies with wavelength. One of the reasons why this study was undertaken was to obtain dyes that are more successful in scavenging light energy than porphyrins at wavelengths longer than 630 nm. 630 nm is the minimum cut-off wavelength where light of longer wavelength can penetrate to reasonable depths in body tissue. Light of wavelength shorter than 630 nm has virtually no penetration capability in body tissue. In terms of this goal we were very successful as all our compounds absorbed light in the Q-band region with $\lambda_{\text{max}} > 690$ nm.

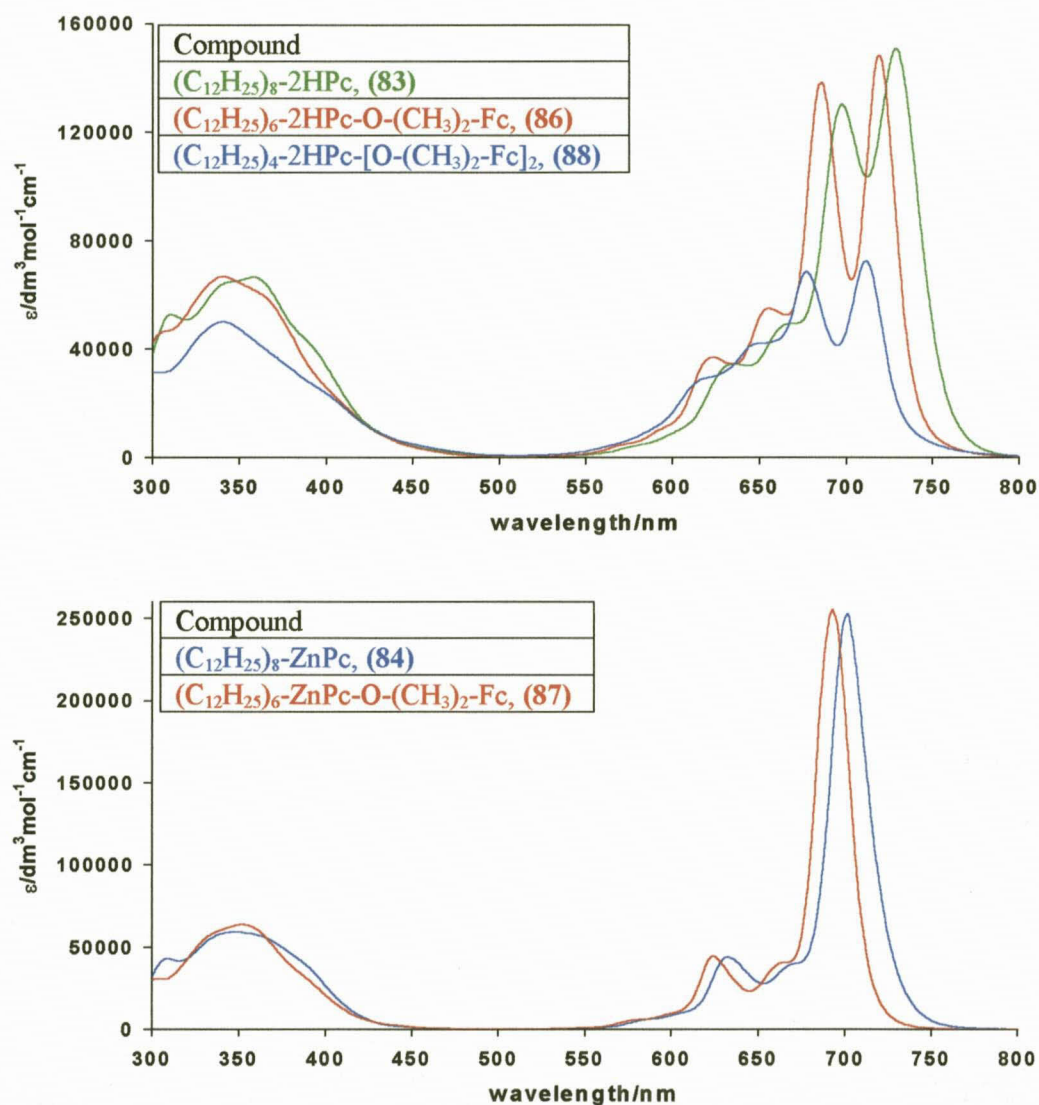


Figure 3.32: Extinction coefficient, ϵ , (in $\text{dm}^3 \text{mol}^{-1} \text{cm}^{-1}$) as a function of wavelength, for the indicated 2H- and Zn-containing phthalocyanines in THF possessing dodecyl and/or ferrocenylethoxide groups. Note ϵ was determined using a 1 mm path length cell, and then converted to units of $\text{dm}^3 \text{mol}^{-1} \text{cm}^{-1}$ by multiplying with 10.

Upon comparing extinction coefficients, ϵ it is also evident that the compounds of this study are more effective scavengers of light in the Q-band region in general than porphyrins. For example, ϵ at $\lambda = 630$ nm for HpD, is approximately $1 \times 10^3 \text{ dm}^3 \text{mol}^{-1} \text{cm}^{-1}$. Our zinc-containing

complexes, (84) and (87) have $\epsilon = 2.8 \times 10^5$ and $2.4 \times 10^5 \text{ dm}^3 \text{ mol}^{-1} \text{ cm}^{-1}$ respectively. This encouraging result implies that the zinc phthalocyanines (84) and (87) may show enhanced activity in photodynamic cancer therapy over, for instance HpD, when tested.

By increasing the number of ferrocenylethoxide groups in the peripheral positions of the phthalocyanine macrocycle, a wavelength shift to shorter λ_{max} values (i.e. blue shift) in only the Q-band region as indicated in Figure 3.32, is observed. This blue shift, relative to λ_{max} of the octadodecylated phthalocyanines (green line graph in Figure 3.32), is the direct result of decreasing the number of alkyl substituents in the non-peripheral positions as the number of ferrocenylethoxide groups in the peripheral positions on the phthalocyanine macrocycle increases. The extent of blue shifting with increase in number of peripheral ferrocenylethoxide substituents is graphically presented in Figure 3.33.

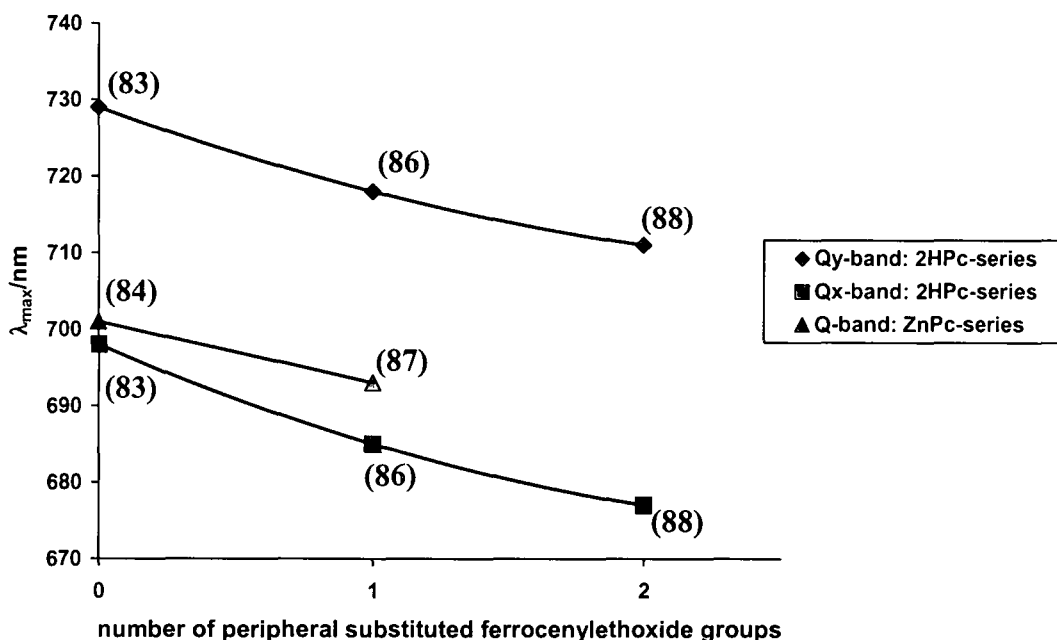


Figure 3.33: Relationship between λ_{max} and the number of ferrocenylethoxide groups in the peripheral positions of the phthalocyanine macrocycle for the indicated dodecylated and ferrocenylethoxide-phthalocyanine conjugates.

The UV-visible spectra of all these phthalocyanine derivatives has shown that, although substitution of the non-peripheral dodecyl side-chains with peripheral ferrocenylethoxide groups caused a marked blue shift of λ_{max} , they still have a maximum absorption peak at wavelengths longer than 680 nm. This, together with the absence of aggregation, suggests that the zinc phthalocyanine derivatives shown in Figure 3.28, could be useful in the photodynamic therapy of cancer.

3.6 Liquid crystalline properties of phthalocyanine derivatives.

Discotic thermotropic liquid crystal behaviour were displayed by both the octadodecyl substituted phthalocyanines, (83) and (84), as well as the ferrocenyl-phthalocyanine conjugates (86) and (87) shown in Figure 3.34. The liquid crystalline phase changes of these compounds were studied using differential scanning calorimetry (DSC) and polarised optical microscopy. The energy changes from one mesophase to another, or from mesophase to isotropic liquid or crystalline solid were often small and observation of phase changes were often depended on whether the DSC was on a heating or cooling cycle. Hence the results described in this section represents the combined insight obtained from DSC studies, physical observation with a polarised light optical microscope, and by recording UV/VIS spectra of thin films of these compounds cast on glass slides at different temperatures.

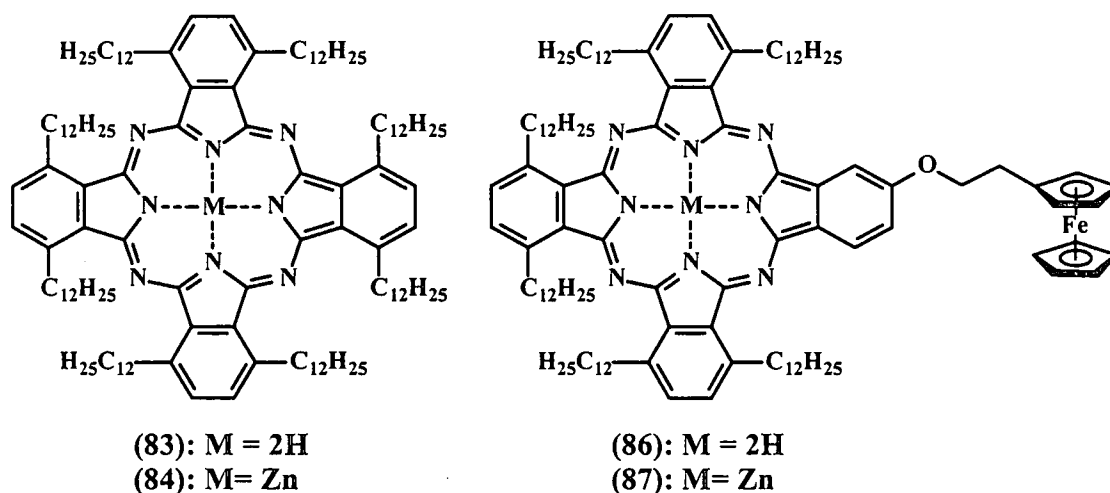


Figure 3.34: Octadodecylated phthalocyanines (83), (84) and ferrocenyl-phthalocyanine conjugates (86), (87) that were investigated for their liquid crystalline properties using differential scanning calorimetry as well as polarized light optical microscopy.

The differential scanning calorimetry (DSC) traces and the variable temperature UV spectra of thin films of phthalocyanines (83) and (84), are shown in Figure 3.36 (page 125) while that of (86) and (87) are found in Figure 3.37 (page 126). Regarding the DSC trace of (C₁₂H₂₅)₈-2HPc, (83), the first oddity is that the DSC trace shows no clear peak for the conversion for the mesophase to isotropic liquid transition, D₁→I. This observation is taken to imply that the energy required for the D₁→I transition is too small to be measurable on a DSC. However, utilising an optical microscope and polarised light, the temperature for this transition was clearly defined as 115.5°C. It is shown by the dotted line on the DSC trace. Relating to (C₁₂H₂₅)₈-ZnPc, (84), (Figure 3.36), (C₁₂H₂₅)₆-2HPc-O-(CH₂)₂-Fc, (86), (Figure 3.37) and (C₁₂H₂₅)₆-ZnPc-O-(CH₂)₂-Fc, (87), (Figure 3.37), the transition from mesophase to an isotropic

liquid, $D_1 \rightarrow I$, was clearly observable. On the optical microscope this transition was identified at 206.5°C for (84), 189.4°C for (86) and 270.3°C for (87). From these transition temperatures, it is clear that the incorporation of zinc metal into the phthalocyanine core allows the phthalocyanines to exist as liquid crystals at 80-90°C higher temperatures than for the 2HPc derivatives. This indicates that zinc has the capability of stabilising mesophases at higher temperatures compared to hydrogen in the metal-free phthalocyanines. The energy for each of these $D_1 \rightarrow I$ transition varied between 9.33 kJ mol⁻¹ (84), 0.43 kJ mol⁻¹ (86) and 0.69 kJ mol⁻¹ (87) while for (83), the energy for this transition could not be detected. The reason why the transition temperature for the $D_1 \rightarrow I$ transition during the heating and cooling cycles of the DSC experiments are not identical on the DSC trace (e.g. 206 vs. 211.6°C for (84)) are vested in the rate of heat flow from the heating block of the DSC apparatus to the phthalocyanine in the sample holder. This heat flow is not an instantaneous transfer of energy. A finite amount of time is required for this flow of energy. As a result $\Delta T = T_{D_1 \rightarrow I, \text{ heating}} - T_{I \rightarrow D_1, \text{ cooling}}$ for this transition vary between 5.6 and 6.7°C for (84), (86) and (87) respectively.

With respect to the transitions between crystalline solid and mesophases, that is $K \rightleftharpoons D_i$, $i = 1, 2$ or 3, the cooling cycle on the DSC provided a clear $D_i \rightarrow K$ transition temperature for all four compounds that coincided with the temperature obtained visually for the microscope utilising polarised light. The heating cycle did not give a clear cut $K \rightarrow D_i$, $i = 1, 2$ or 3 transition temperature. It is concluded that the properties of the crystalline state is so similar to that of the first mesophase next to it (D_3 in Figure 3.36 and D_2 in Figure 3.37) that during the cooling cycle the transition $D_3 \rightarrow K$ is observed, but during the heating cycle the first definite phase change observed is between two mesophases that is $D_3 \rightarrow D_2$ or $D_2 \rightarrow D_1$. We do not consider the peak labelled "A" in Figures 3.36 and 3.37 as a $K \rightarrow D_i$ transition but rather a $D_{i+1} \rightarrow D_i$ transition for the following reasons:

- a) Optical microscopy during a cooling cycle showed for compound (84), that is $(C_{12}H_{25})_8\text{-ZnPc}$, a phase change at 59°C which was identified by a colour change from green to blue. This phase change is regarded as possibly the same as the crystallisation temperature detected by DSC. During a heating cycle, utilising optical microscopy, an additional phase change was observed at 73°C. This phase change is not the same as the peak labelled "A" in the DSC trace. Peak "A" is observed some 17°C warmer for (84), and it was not associated with a colour change, but with a texture change. With the long alkyl C_{12} chains of this compound it is conceivable that, on a heating cycle, energy is needed to overcome a resistance to flow in the phthalocyanine side chains, while on the

cooling cycle the temperatures may actually fall below the crystallisation temperature before the compound actually crystallises. This interim temperature range of 59-73°C (i.e. a span of 14°C) is at present regarded as a region of metastable equilibrium. However, the texture and colour changes in this temperature region are extremely subtle and very difficult to actually identify. The UV spectra of these compounds, cast as thin films on microscope slides at different temperatures, are also shown in Figures 3.36 and 3.37 and highlight this statement. Compound (83) showed a similar texture change at 58.8°C in the heating cycle of the optical microscope some 10°C warmer than the cooling cycle. No similar changes could, however, be identified for (86) and (87). For these two compounds, the $D_i \rightarrow K$ transition temperature was only identified on the cooling cycle by the DSC apparatus.[†]

- b) When one assumes that the peak labelled as "A" in Figures 3.36 and 3.37 actually represents a $K \rightarrow D_i$, $i = 1, 2$ or 3 transition, then $\Delta T = T_{D_i \rightarrow K, \text{ cooling}} - T_{K \rightarrow D_i, \text{ heating}} = 38.4^\circ\text{C}$ for $(C_{12}H_{25})_8\text{-2HPc}$, (83); 31°C for $(C_{12}H_{25})_8\text{-ZnPc}$, (84); 27.9°C for $(C_{12}H_{25})_6\text{-2HPc-O-(CH}_2)_2\text{-Fc}$, (86) and 26.6°C for $(C_{12}H_{25})_6\text{-ZnPc-O-(CH}_2)_2\text{-Fc}$, (87). The values of ΔT are much more scattered over a wide temperature range than was observed for the $D_1 \rightleftharpoons I$ transition ($5.6^\circ\text{C} < \Delta T_{D_1 \rightleftharpoons I} < 6.7^\circ\text{C}$). The ΔT value for the $D_1 \rightarrow K$ transition obtained using the data from optical microscopy measurements as described in paragraph (a) directly above, that is $\Delta T_{K \rightleftharpoons D_1} = 73 - 59 = 14^\circ\text{C}$, is much more within the temperature range for the $\Delta T_{D_i \rightleftharpoons I}$ transition than the $26.6 < \Delta T_{K \rightleftharpoons D_i} < 38.4^\circ\text{C}$ utilising the peak labelled "A" in Figures 3.36 and 3.37.

Arguments against this assignment is mainly vested in the fact that only compound (84) {see paragraph labelled (a) above} showed a hint of a melting temperature (using an optical microscope) different to the DSC peak labelled "A". We had no other means of trying to detect a melting point. To summarise: The peak labelled "A" may represent a $K \rightarrow D_i$, $i = 1, 2$ or 3 transition, but an assignment of $D_{i+1} \rightarrow D_i$ is favoured for peak "A" because of the arguments presented in paragraphs (a) and (b) above. This assignment then also implies that for each of the compounds (83), (84), (86) and (87), a $K \rightarrow D_i$ transition exist at colder temperatures than the peak labelled "A" in Figures 3.36 and 3.37. This transition involves so little energy that, like

[†] The heating and cooling rate for the DSC apparatus was 10°C/min while for the microscope hotstage it was 2 or 5°C/min .

the $D_1 \rightarrow I$ transition for (83), it cannot be detected by DSC measurements. Alternatively it could also mean that due to the long chains of the substituents, here $C_{12}H_{25}$, by crossing the $K \rightarrow D_i$ transition temperature, a metastable equilibrium of the crystalline state might be instated. Only once the transition temperature for the $D_3 \rightarrow D_2$ phase change is reached, is the energy change enough to shock the metastable K phase into a direct conversion to the D_2 liquid crystalline phase, i.e. a $K_{\text{metastable}} \rightarrow D_2$ transition.

A final observation relating to $D_i \rightarrow K$ transition temperatures on the DSC cooling cycle can be made. When one compares the DSC traces of Figure 3.36, with that of Figure 3.37, the effect of the $O-CH_2-CH_2-Fc$ side chain on (86) and (87) can be quantified. In both the metal-free series of (83) and (86), and the zinc-containing series of compounds (84) and (87), the effect of the $O-CH_2-CH_2-Fc$ side chain was to lower the $D_i \rightarrow K$ transition temperature by more than 15°C : $46.8-30.4 = 16.4^\circ\text{C}$ for the metal-free compounds and $62.7-30.9 = 31.8^\circ\text{C}$ for the zinc-containing derivatives. This can be attributed to the fact that the more symmetrical phthalocyanines (83) and (84) should be capable of packing better, i.e. with less distortions, in the crystalline state. If this is indeed the case, it means the amount of energy required to break the intermolecular forces in crystals of (83) and (84) should be larger than the energies required to break intermolecular forces in crystals of (86) and (87). This is easily understood upon recognising the fact, that phthalocyanine molecules tend to stack on top of each other in a columnar fashion, and that the ferrocenyl group will tend to disrupt this tendency as illustrated in Figure 3.35. This will lead to lower melting points and extended temperature ranges in which these phthalocyanines exist in the mesophase.

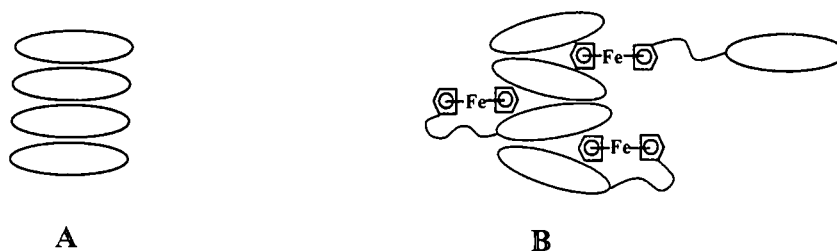


Figure 3.35: Phthalocyanines tend to stack or aggregate on top of each other in a columnar fashion. The columnar stacking of symmetrical phthalocyanines such as (83) and (84) should be near perfect as indicated in the columnar stacking A. The ferrocenyl group in the unsymmetrical phthalocyanines (86) and (87) should impose many flaws on a columnar stacked liquid crystal. This is schematically shown in B. = Phthalocyanine macrocycle.

This result was also mirrored at the $D_1 \rightarrow I$ transition temperature. The replacement of 2 x $C_{12}H_{25}$ groups with one $O-CH_2-CH_2-Fc$ group in $(C_{12}H_{25})_8-2\text{HPc}$, (83), to give $(C_{12}H_{25})_6-2\text{HPc}-$

O-CH₂-CH₂-Fc, (**86**), resulted in an increase in D₁→I transition temperature from 115.5 to 185.3°C i.e. 69.8.9°C while in moving from (C₁₂H₂₅)₈-ZnPc, (**84**), to (C₁₂H₂₅)₆-ZnPc-O-CH₂-CH₂-Fc, (**87**), the D₁→I transition temperature increased from 206.1 to 269.9°C. The latter change represents an increase of 63.8°C. The lower symmetry of (**86**) and (**87**) appears to disorganise the crystal and mesophase states resulting in increases in the temperature range of liquid crystalline behaviour compared to their symmetrically substituted octaalkyl analogues (**83**) and (**84**) respectively. The temperature range in which the new compounds of this study can exist as liquid crystals is therefore:

- (i) 46.8 till 115.5°C, i.e. 68.7°C for (C₁₂H₂₅)₈-2HPc, (**83**)
- (ii) 62.7 till 206.1°C, i.e. 143.4°C for (C₁₂H₂₅)₈-ZnPc, (**84**)
- (iii) 30.4 till 185.3°C, i.e. 154.9°C for (C₁₂H₂₅)₆-2HPc-O-CH₂-CH₂-Fc, (**86**)
- (iv) 30.9 till 269.9°C, i.e. 239°C for (C₁₂H₂₅)₆-ZnPc-O-CH₂-CH₂-Fc, (**87**).

One should take special note of the fact that the inclusion of an oxygen functionality in the peripheral position via the O-CH₂-CH₂-Fc side chain did not inhibit mesophase formation. The new phthalocyanines (**86**) and (**87**) are the first phthalocyanine alkoxide derivatives ever found that possesses liquid crystalline behaviour. Even non-peripheral octa-alkoxide phthalocyanine compounds do not exhibit mesophase behaviour.²⁰

A maximum of three mesophases, D₃, D₂ and D₁ could be identified for (**83**) and (**84**), (Figure 3.36) while (**86**) and (**87**) apparently only had two mesophases (Figure 3.37). D₃ is assigned to the lowest temperature mesophase while D₁ the highest temperature mesophase. Due to the absence of any X-ray diffraction studies of these compounds at this stage, no definite assignments to the two dimensional symmetry or packing modes can be made.

The three observable mesophases, D₁, D₂, and D₃, for (**83**) and (**84**) between the crystalline and isotropic liquid states could only be detected during the heating cycle, not the cooling cycle. At least two factors may have contributed to this observation: Firstly, the energy barrier in the transition from one liquid crystalline mesophase to the other is very small, which implies some mesophase transitions may not be observed by the DSC method. The second reason, as argued before, may be due to the similar properties the mesophase states may have.

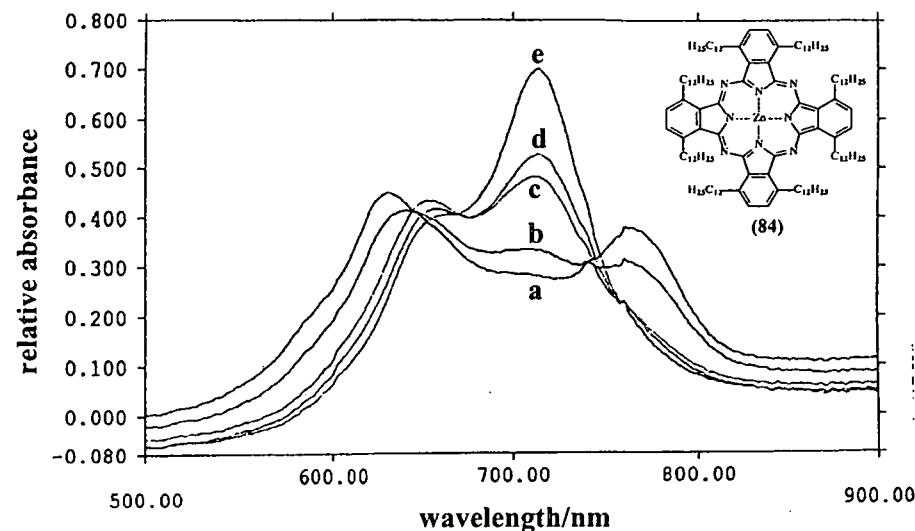
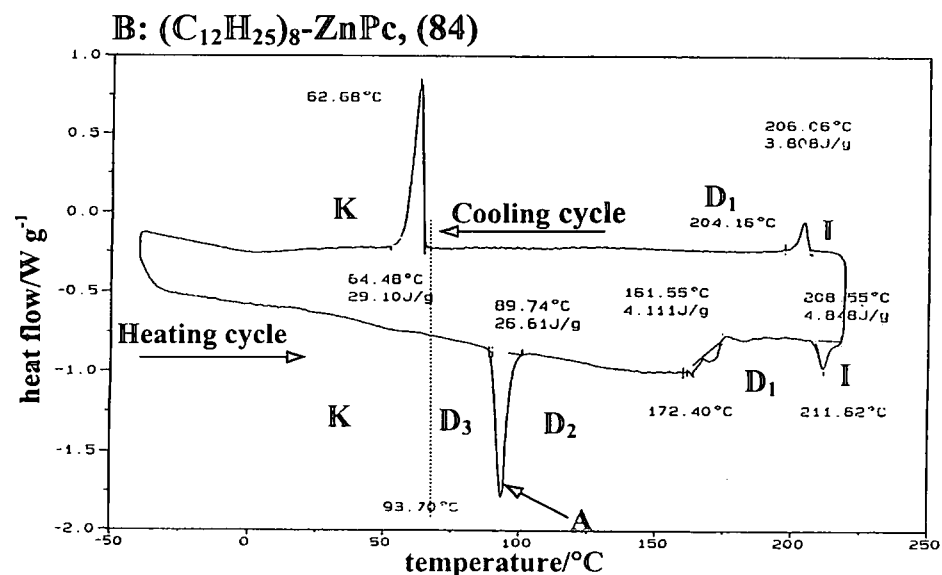
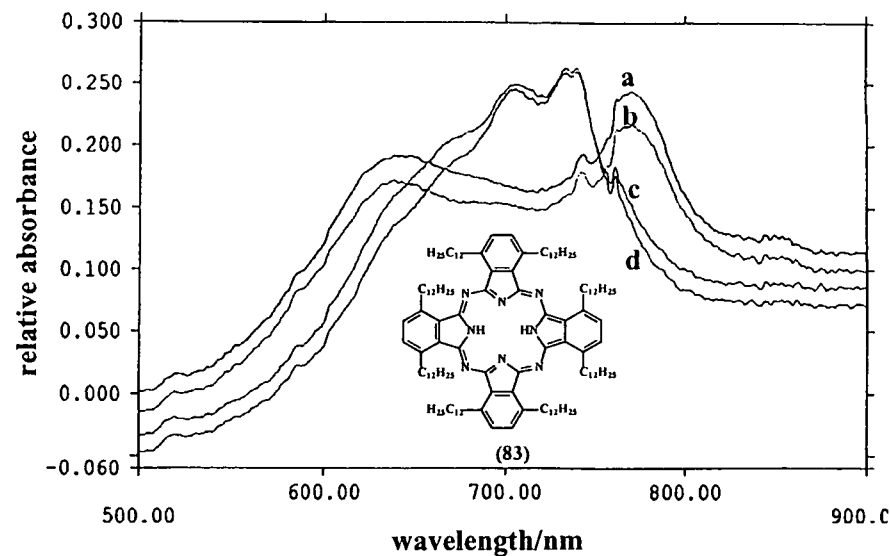
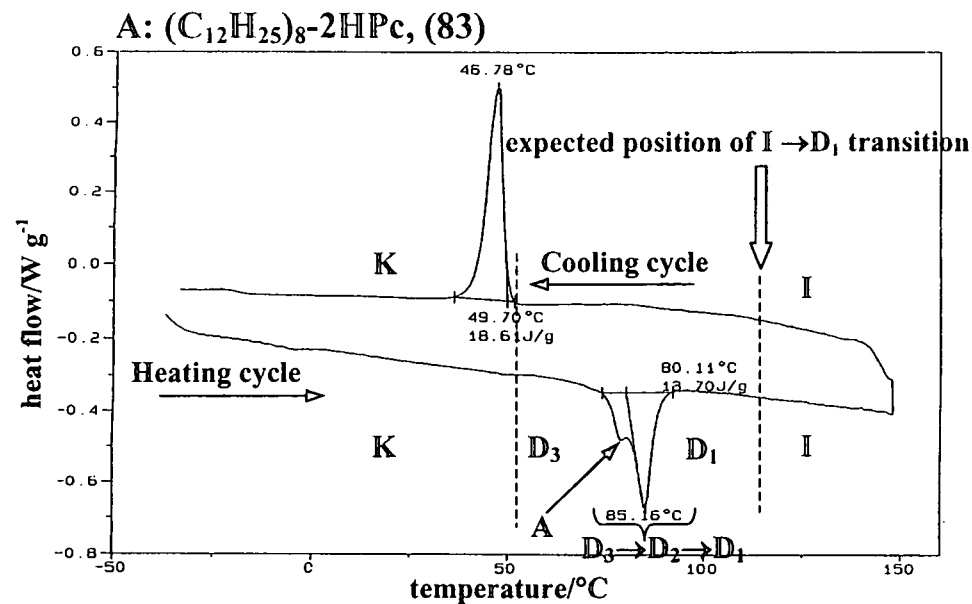


Figure 3.36: Differential scanning calorimetry (DSC) traces of heat flow vs. temperature (left) and variable temperature UV/VIS spectra of spin coated thin films (right) for **A:** metal-free, (83) and **B:** zinc-containing phthalocyanines, (84) respectively. Temperatures corresponding to different phases of the bulk material for (83): (a) 35°C, (b) 60°C, (c) 80°C and (d) 100°C and for (84): (a) 30°C, (b) 80°C, (c) 130°C, (d) 180°C and (e) 230°C. The heating and cooling rate for the DSC apparatus was 10°C/min.

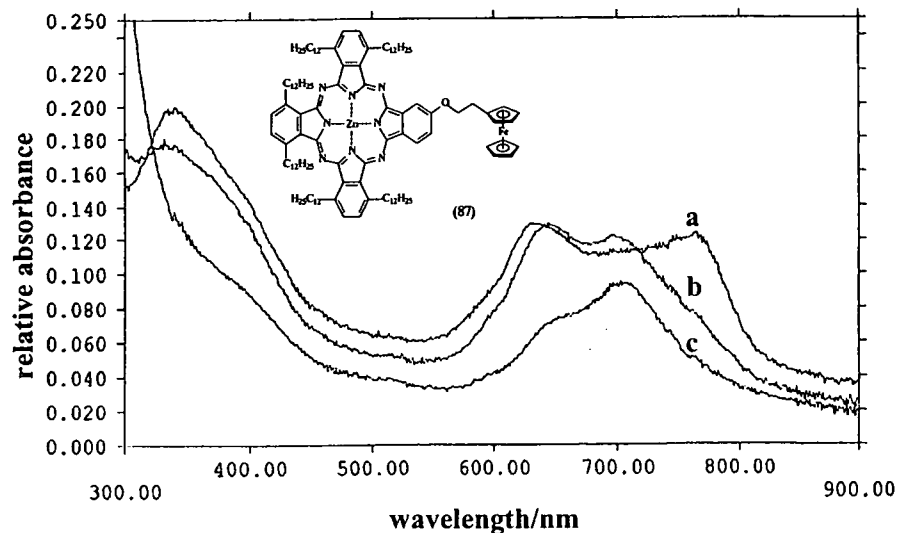
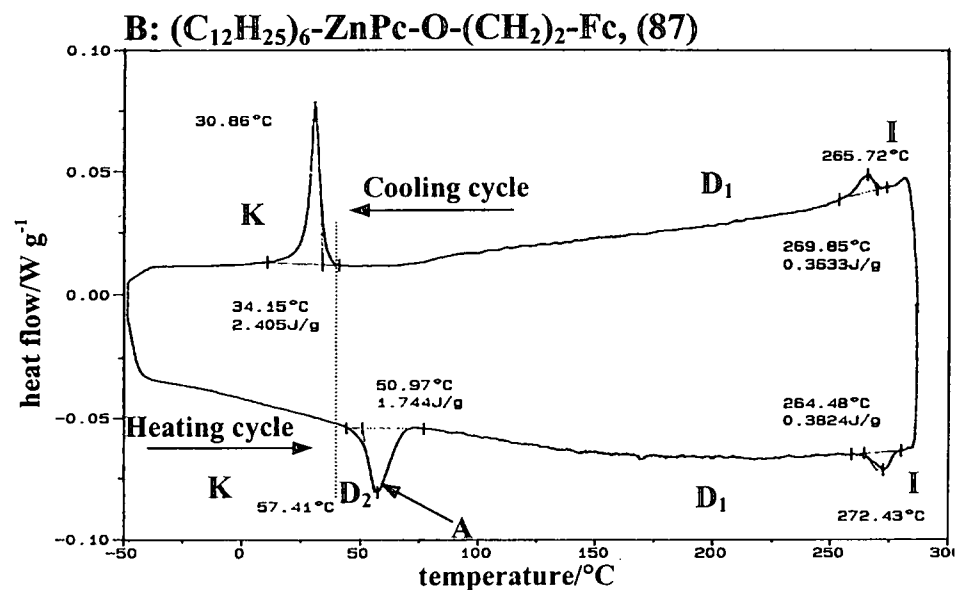
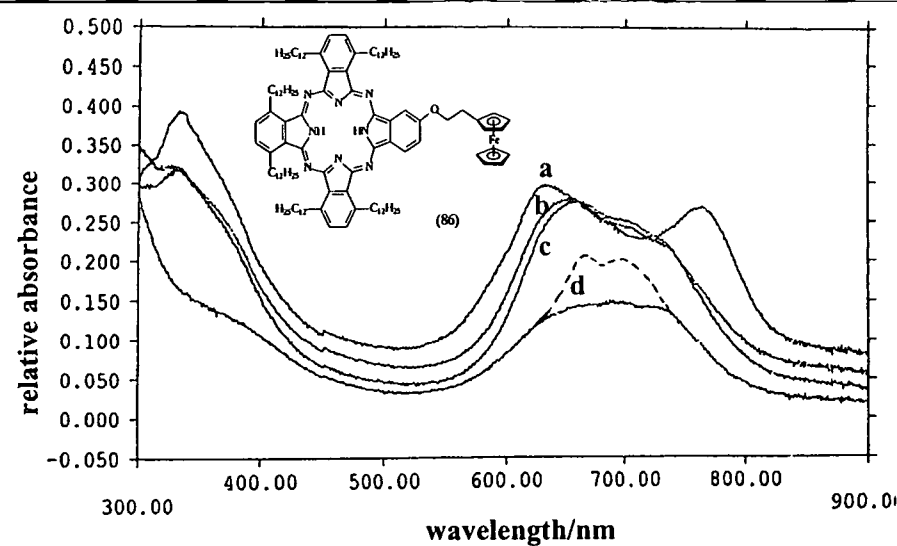
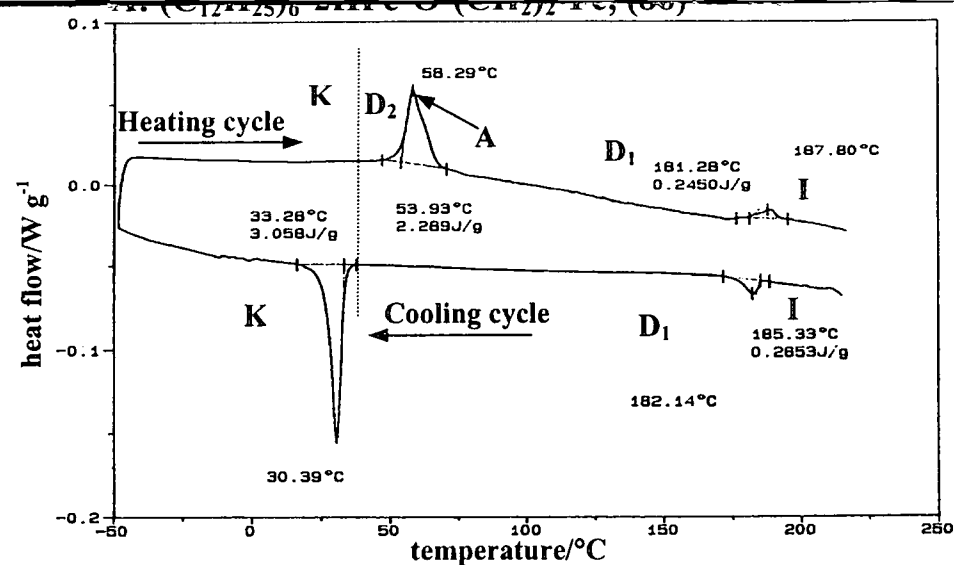


Figure 3.37: Differential scanning calorimetry (DSC) traces of heat flow vs. temperature (left) and variable temperature UV/VIS spectra of spin coated thin films (right) for A: metal-free, (86) and B: zinc-containing ferrocenyl-phthalocyanines, (87) respectively. Temperatures corresponding to different phases of the bulk material for (86): (a) 26°C , (b) 75°C , (c) 150°C and (d) 200°C and for (87): (a) 25°C , (b) 70°C and (c) 280°C . The heating and cooling rate for the DSC apparatus was 10°C/min .

As far as the details of the DSC's are concerned, for $(C_{12}H_{25})_8\text{-ZnPc}$, (**84**), the melting point of 64.5°C was confirmed by polarised optical microscopy between $64.5\text{--}93.7^\circ\text{C}$, on the heating cycle, (**84**) exist either as the low temperature discotic liquid mesophase, D_3 or as a metastable crystalline solid. On heating to above 93°C the D_3 mesophase undergoes a transition to the D_2 mesophase. The next phase conversion at 172.4°C represents the transition temperature for the conversion $D_2 \rightarrow D_1$. At 211.6°C the D_1 mesophase converts to the isotropic liquid, I. During the cooling cycle mesophase D_1 was regenerated at 206.1°C , but transition temperatures to the D_2 and D_3 mesophases could not be detected by DSC measurements. This can be attributed to flow resistance of the liquid crystalline D_1 mesophase state on the time scale of the DSC.

It is not difficult to envisage this flow resistance in view of the bulkiness of the octa dodecyl groups. For the moment the reader has to assume that (**84**) exists between 206.1 and 64.5°C in a metastable D_1 mesophase. Upon cooling to 64.5°C the sample converts from a metastable D_1 mesophase to the crystalline state in one step and all of the combined energies for the conversions $K \rightarrow D_3$, $D_3 \rightarrow D_2$ and $D_2 \rightarrow D_1$ is simultaneously released as crystallisation energy. Proof towards this statement is found when one compares the sum of energies $K \rightarrow D_3$ (the energy for this phase transition is too small to be measured and is taken as 0), $D_3 \rightarrow D_2$ and $D_2 \rightarrow D_1$ during the heating cycle, $0 + 26.61 + 4.11 = 30.72 \text{ J g}^{-1}$ with the $D_{1 \text{ metastable}} \rightarrow K$ energy, 29.1 J g^{-1} . These two values are so close, experimentally they really are the same, that it is mutually consistent with our explanation of the existence of a D_1 metastable mesophase during the cooling cycle between 206.1 and 64.5°C .

The metal-free derivative (**83**) showed three liquid crystalline mesophases between the crystalline and the isotropic liquid states. During the heating cycle, the sample should melt at *ca* 50°C from the crystalline solid to the D_3 mesophase. Alternatively, if D_3 is not actually formed at this temperature, 50°C , the crystalline solid may exist in a metastable crystalline phase. Upon further heating to 85.1°C two mesophase changes are formed in quick succession and it represents the conversions $D_3 \rightarrow D_2 \rightarrow D_1$. The sample then melts at 115.5°C . The cooling cycle showed no clear transition from $I \rightarrow D_1$, $D_1 \rightarrow D_2$ or $D_2 \rightarrow D_3$. Rather it appears that between 115.5 and 46.8°C $(C_{12}H_{25})_8\text{-2HPc}$, (**83**) exists in a metastable mesophase D_1 . The metastable mesophase D_1 description is preferred over super cooled liquid because a mesophase was clearly detected on the optical microscope. However, the $I \rightarrow D_1$ conversion must consume very little energy because upon conversion to the crystalline liquid at 46.8°C , all the mesophase

energies are released in one single step with $\Delta H = 18.6 \text{ J g}^{-1}$. This is for all practical purposes the same as the combined energies for mesophase conversions $D_3 \rightarrow D_2 \rightarrow D_1$, 18.7 J g^{-1} during the heating cycle.

A summary of the mesophase behaviour of (83), (84), (86) and (87) can be found in Table 3.13.

Table 3.13: Phase transition temperatures and transition energies, (ΔH), observed during DSC and variable temperature optical microscopy studies of non-peripherally octadodecyl-substituted phthalocyanines, (83) and (84) as well as the ferrocenylethoxide-phthalocyanine conjugates, (86) and (87). The values in brackets were obtained from cooling cycles, while the others were from the heating cycles of DSC traces.

Compound	Transitions	Transition temperatures /°C	$\Delta H / \text{kJ mol}^{-1}$
$(\text{C}_{12}\text{H}_{25})_8\text{-2HPc}$, (83)	$(D_{1\text{metastable}} \rightarrow K), K \rightarrow D_3$	(46.8), 58.8*	(34.6), — ^b
	$D_3 \rightarrow D_2 \rightarrow D_1$	85.1	25.5
	$D_1 \rightarrow I$	— ^a , 115.5*	— ^b
$(\text{C}_{12}\text{H}_{25})_8\text{-ZnPc}$, (84)	$(D_{1\text{metastable}} \rightarrow K), K \rightarrow D_3$	(62.7), (59*), 73*	(56.0), (— ^b), — ^b
	$D_3 \rightarrow D_2$	93.7	51.2
	$D_2 \rightarrow D_1$	172.4	7.9
	$(I \rightarrow D_1), D_1 \rightarrow I$	(206), 206.5*, 211.6	(7.3), — ^b , 9.3
$(\text{C}_{12}\text{H}_{25})_6\text{-2HPc-}$ $\text{O}-(\text{CH}_2)_2\text{-Fc}$, (86)	$(D_{1\text{metastable}} \rightarrow K)$	(30.4), (48.2*)	(5.4)
	$(D_1 \rightarrow D_2), D_2 \rightarrow D_1$	(98.5*), 58.3, 68.9*	(— ^b), 4.0, — ^b
	$(I \rightarrow D_1), D_1 \rightarrow I$	(185.3), 187.8, 189.4*	(0.50), 0.43, — ^b
$(\text{C}_{12}\text{H}_{25})_6\text{-ZnPc-}$ $\text{O}-(\text{CH}_2)_2\text{-Fc}$, (87)	$(D_{1\text{metastable}} \rightarrow K)$	(30.9)	(4.4)
	$(D_2 \rightarrow D_3), D_3 \rightarrow D_2$	(68.8*), 50.9	(— ^b), 3.1
	$(D_1 \rightarrow D_2)$	(105.3*)	(— ^b)
	$(I \rightarrow D_1), D_1 \rightarrow I$	(269.8), 270.3*, 272.4	(0.66) — ^b , 0.70

*From optical microscopy. ^a ΔH was too small to measure on DSC. ^b ΔH not obtainable on the optical microscope.

The DSC traces of both the metal-free and zinc containing ferrocenyl-phthalocyanine conjugates, (86) and (87) respectively showed two liquid crystalline phases (denoted as D_1 and D_2) between the crystalline and isotropic liquid states. The absence of an observable third or more mesophase for both (86) and (87) does not preclude its existence, but it was not observable by the measuring methods at our disposal. Towards this notion it is instructive to observe that texture changes in the samples could be observed visually by optical microscopy at 48.2 and 98.5°C during the cooling cycle and at 68.9°C during the heating cycle for (86).

Compound (**87**) showed texture changes at 68.8 and 105.3°C during the cooling cycle. None of these changes could be quantified in terms of energy transfer on the DSC.

In previous reports on the C₄ and C₈ derivatives,²¹ different mesophases were tentatively assigned by comparing the optical textures observed under the polarised microscope with those whose packing symmetries were previously determined from X-ray diffraction studies. These designations were D_{hd}, a discotic disordered mesophase phase showing a fan-like texture and comprised of columns of cofacially stacked molecules arranged within a two-dimensional lattice symmetry, a second disordered hexagonal mesophase, D_{hd}, with a needle-like texture and a third disordered mesophase possessing rectangular symmetry, D_{rd}, which is characterised by a mosaic texture. In the cases reported hitherto, the fan texture of the D_{hd} mesophase was observed at the first transition upon cooling from the isotropic liquid, *i.e.* in the D₁ mesophase. The needle texture was infrequently observed upon further cooling and the mosaic texture was associated with the mesophase just prior to conversion to a solid crystal.

In this study, we found that the texture under the microscope was very much a function of the rate of cooling or heating. The photograph in Figure 3.38 (left) shows both the needle-like bundles stacked together to create the appearance of fibres and the fan-like texture observed during this transition. Further cooling produces a clear colour change from greenish to bluish when crystallisation (D→K transition) sets in. In many heating and cooling cycles subtle changes from an apparent mosaic to a fan-like texture was also observed as shown in Figure 3.38 (right).

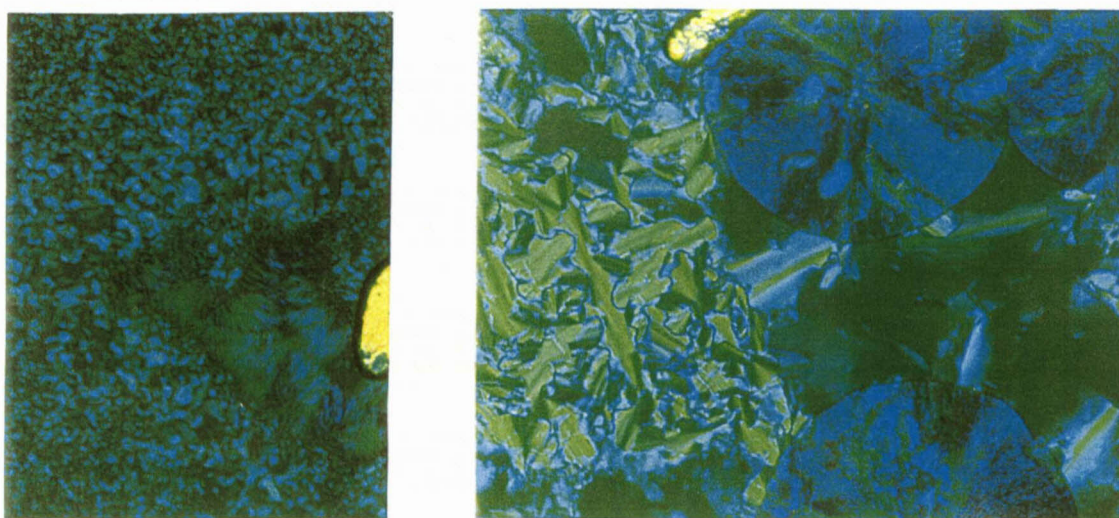


Figure 3.38: **Left:** Photograph showing simultaneously the fan (D₁, majority of graph) and needle (D₂, next to the yellow spot, needles are bundled together in the form of fibres) texture for (C₁₂H₂₅)₈-2HPc, (**83**). **Right:** Photograph showing simultaneously the blue crystalline solid (K) and the green D₂ mesophase with a mosaic pattern.

Accordingly, although by comparison to previous studies the observed phases D_1 , D_2 and D_3 are expected to confirm to the D_{hd} , fan, D_{hd} , needle, and D_{rd} , mosaic, two dimensional symmetry or packing modes. However, in the absence of X-ray diffraction studies, no definite assignment to this effect can be made. A possible explanation for the less than distinct mesophase transitions observed in the present study may arise from the length of the side chains of $(C_{12}H_{25})_8-2HPc$, (83). It is quite conceivable that the long chain length of the substituents on (83) interfere with the ease by which any semi-ordered liquid crystalline packing may be achieved. This interference will result in a slower formation of any order in the packing of the liquid crystalline phase and it may lead to pronounced distortions in molecular packing.

3.7 Visible region spectroscopy of spin-coated thin films of selected phthalocyanines.

As all of the synthesised phthalocyanines (83), (84), (86) and (87) exhibit thermotropic liquid crystal behaviour, it is to be expected that the molecular assemblies within thin films might undergo molecular reorganisations on heating. This is indeed the case. Variable temperature UV/VIS spectra of the title compounds, cast as thin films on glass undergoes sharp changes at or close to the mesophase transition temperatures of the bulk material. Spectra of spin-coated films of the metal-free and zinc-containing phthalocyanines (83), (84), (86) and (87), at temperature corresponding to different phases, are shown in Figures 3.36 and 3.37 (pages 125 and 126) next to each DSC trace.

The UV/VIS spectra of $(C_{12}H_{25})_8-ZnPc$, (84), at 30°, 80°, 130°, 180° and 230°C are given in Figure 3.39 to facilitate easier discussion. The spectrum at 30°C {*i.e.* of the compound in the crystalline form, line labelled (a)} shows two peaks at 632 and 765 nm respectively. The spectrum at 80°C {line (b)} is of the compound in the low temperature mesophase, D_3 . The peak at 632 nm was shifted to 642 nm, but the 765 nm peak was not moved. The appearance of a new peak at 714 nm is, however, just noticeable. At the top end of the second, high temperature (D_1), mesophase temperature range, at 180°C, the spectrum {line (d)} shows a distinct new peak at 714 nm while the peak at 765 nm has disappeared. A weaker peak is also observed at 657 nm. A spectrum of the compound at 230°C {*i.e.* in the isotropic liquid state, line (e)} shows an intense Q-band maximum at 714 nm together with a shoulder at 662 nm. The appearance of the spectrum of the isotropic liquid is very similar to that of the compound in solution, which showed a Q_{max} at $\lambda = 701$ nm and shoulders at 664 and 630 nm. The above spectra can easily be correlated with each mesophase in the DSC (Figure 3.36, page 125).

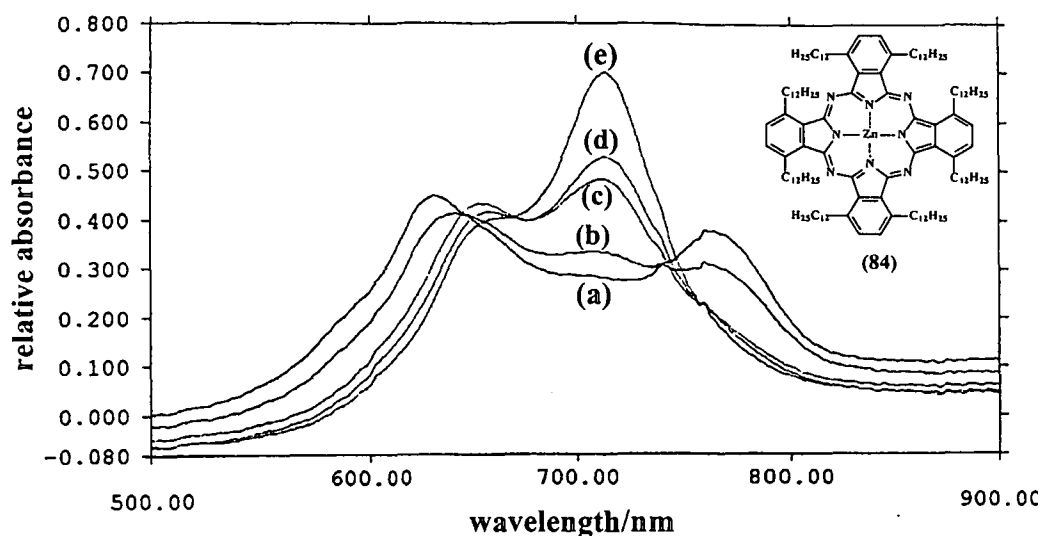


Figure 3.39: Variable temperature UV/VIS spectra of spin-coated films (*ca.* 1000 Å thick) of zinc-containing non-peripherally octadodecyl substituted phthalocyanine, **(84)** on a glass slide at temperatures which correspond to different phases of the bulk material: (a) 30°C, crystalline solid phase K, (b) 80°C, mesophase D₃, (c) 130°C, mesophase D₂, (d) 180°C, mesophase D₁ and (e) 230°C, isotropic liquid phase I.

The spectrum of spin coated films of the metal-free derivative, **(83)** at 35°C {line (a), Figure 3.36, page 124} also showed two peaks this time at $\lambda = 639$ and 770 nm in the crystalline solid state. The spectrum at 60°C {the compound in the low temperature mesophase D₃, line (b)} shows that these two peaks becomes less intense/smaller and the appearance of a new peak at 704 nm is, however faintly apparent. The spectrum at 80°C {line (c)} shows that the two peaks at 639 and 770 nm had collapsed to form the Q_x and Q_y bands with $\lambda_{\text{max}} = 737$ and 704 nm because of the D_{2h} symmetry of **(83)**. Weaker peaks are also observed at 638 and 667 nm. A spectrum at 100°C {i.e. of the compound in the high temperature mesophase D₁, line (d)} gave the same results as for the compound at 80°C. No spectrum could be obtained for the compound in the isotropic liquid state (above 115°C) because of the flowing motion of the thin film of **(83)** in the isotropic liquid state.

The spectrum of the zinc-containing ferrocenyl-phthalocyanine, **(87)** at 25°C {compound in the crystalline solid state, line (a), Figure 3.37, page 126} shows two peaks at 630 and 764 nm respectively. The spectrum at 70°C {line (b)} is of the compound in the mesophase D₂. The peaks at 630 and 764 nm have shifted to 647 and 704 nm respectively. A spectrum of the compound at 280°C {i.e. in the isotropic liquid state, line (c)} shows a Q-band maximum at 704 nm while the peak at 647 nm became very much weaker. The spectrum is also very similar to the solution phase UV/VIS spectra (see page 114). The higher intensity of the shoulder at 647

nm compared to that observed for the solution phase study is indicative of strong aggregation of these complexes in the molten liquid state.

For the metal-free ferrocenyl-phthalocyanine conjugate, (86) two peaks at 634 and 764 nm were observed in the spectrum at 25°C {crystalline state, line (a), Figure 3.37}. The spectrums at 70 {line (b)} and 150°C {line (c)} are of the compound in the high temperature mesophase D_1 . The peak at 634 nm shifted to 652 nm while the peak at 764 nm disappeared. The appearance of a new peak at 703 nm is, however faintly apparent. The dotted line shows the expected two peaks at 666 and 702 nm of the compound in the isotropic liquid state at 200°C {line (d)}. In practise these two peaks were not observed in the spectrum due to decomposition of the compound and the flow of the film down the glass slide at 200°C.

It can clearly be seen from Figures 3.36, 3.37 and 3.39 that the spectra varied as the temperature of the films were changed to be representative from one phase to another. On the basis of these results a wavelengths of 714 nm for (84), 780 nm for (83) (Figure 3.40), 701 nm for (86) and 690 nm for (87) (Figure 3.41) was chosen to spectroscopically monitor phase changes.

The transition at 90°C leading to an increase in absorbance during the heating cycle of (84) (Figure 3.40), corresponds to the $D_3 \rightarrow D_2$ (or $K_{\text{metastable}} \rightarrow D_2$) transition observed for the bulk material on the DSC (Figure 3.36, page 124). A subtle absorbance change was also detected at 145°C. The energy of this phase change, was however, so small that the DSC could not measure it. Just prior to 180°C a phase change was beginning to be observable. However, as the sample persistently decomposed in air at this temperature (our apparatus does not make provision for an inert atmosphere), we cannot comment on this slight increase other than saying it may be associated with the onset of the $D_1 \rightarrow I$ transition. The second half of the graph, from 180-30°C, represents the cooling cycle, which was obtained after the film was heated to 180°C and then cooled. This cycle showed two transitions leading to a decrease in absorbance at 118°C and 98°C respectively. Neither of these could directly be associated with the cooling curve DSC results, but the higher temperature transition (118°C) may correspond to the $D_1 \rightarrow D_2$ transition while the lower-temperature transition probably corresponds to the $D_2 \rightarrow D_3$ transition. These absorbance changes are assigned to molecular reorganisations within the films, which arise because of the mesogenic behaviour of the compound. Because the latter 2 transitions were only observable in the thin film studies (film thickness $\approx 1000 \text{ \AA}$ thick), and not in the DSC experiments when the material was investigated in the bulk form, we conclude that molecular

packing changes during phase transitions in thin films are easier detected than in the bulk where the macroscopic size of the sample may well retard the kinetics of phase transitions due to molecular reorganisation.

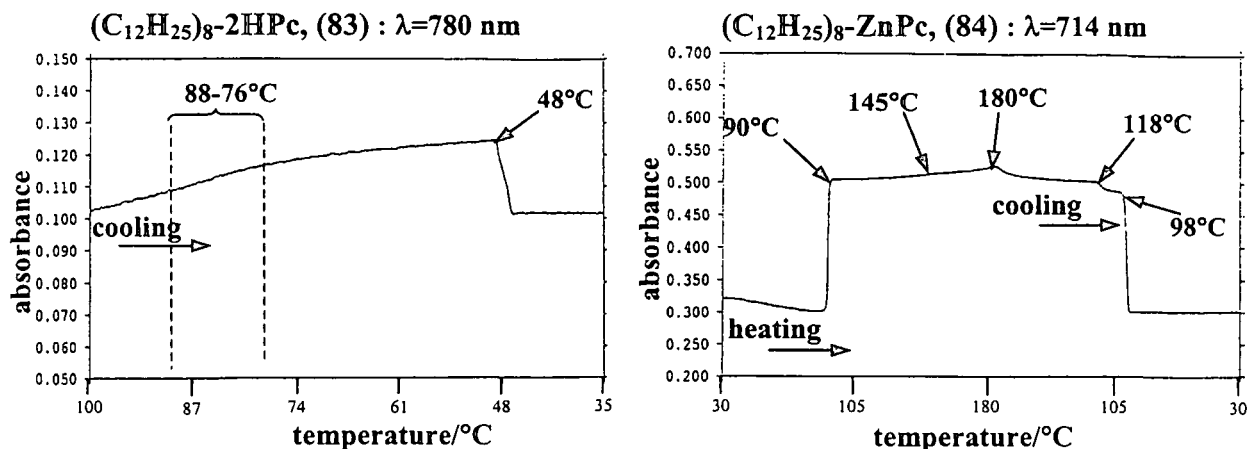


Figure 3.40: Absorbance/Temperature profiles showing phase transitions as a function of absorbance changes at 780 nm for a spin coated film of (83), left and at 714 nm for a spin coated film of (84), right. The heating and cooling rates were 5°C/min.

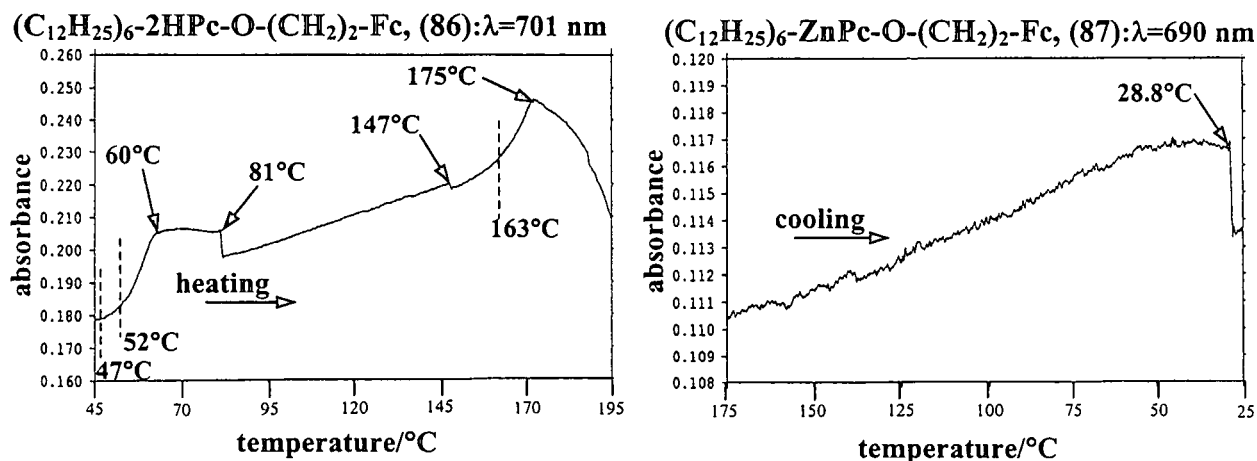


Figure 3.41: Absorbance/Temperature profiles showing phase transitions as a function of absorbance changes at 701 nm for a spin coated film of (86), left and at 690 nm for a spin coated film of (87), right. The heating and cooling rates were 5°C/min.

Only the cooling cycle of the metal-free derivative, (83) was studied (Figure 3.40). Attempts to obtain the I→D₁ transition failed because the compound melted above 100°C and flow down the sides of the glass slide. A gradually intensifying absorbance change was detected between 88-76°C. This phase change was not observed during the cooling cycle on the DSC trace (Figure 3.36, page 125), but may correspond to the D₁→D₂→D₃ transition equivalent of the

$D_3 \rightarrow D_2 \rightarrow D_1$ transition observed on the DSC heating cycle. The transition at 48°C leading to a decrease in absorbance, corresponds to the $D_3 \rightarrow K$ (or D_1 metastable $\rightarrow K$) transition observed for the bulk material on the DSC.

During the heating cycle of (86) (Figure 3.41), an increase in absorbance between 47-52°C was observed that may correspond to the $K \rightarrow D_2$ transition which was not observed during the heating cycle on the DSC trace (Figure 3.37, page 126). The transition from 52-60°C leading to an increase in absorbance is assigned to the $D_2 \rightarrow D_1$ transition observed for the compound on the DSC. The transition at 81°C leading to a decrease in absorbance is then observed on the thin film slide. Evidence on the DSC of (86) shows that there may be two transitions at 54-58°C overlapping because of a broad peak observed at this temperature range. An extra phase change at 147°C leading to a decrease in absorbance was then detected that could not directly be associated with the heating cycle DSC results. The increase in absorbance between 163-175°C and thereafter decrease in absorbance is thought to be a mesophase phase change that is immediately followed by melting. It corresponds to the broad peak observed on the DSC of the compound at 181°C. The Absorbance/Temperature profile of (86) shows more than two liquid crystal phase transitions with a variation in absorbance being observed while only two mesophases were detected on the DSC trace of this compound. The compound melted and flowed down the glass slide at 175°C.

Compound (87) is very unstable under our non-inert conditions and decomposed at high temperatures. Only the cooling cycle of the compound was studied (Figure 3.41) with the initial temperature colder than the melting point of the compound to try and prevent decomposition or flow of the compound down the glass slides. This meant that no phase change was obtained corresponding to the $I \rightarrow D_1$ transition. Only one transition at 28.8°C leading to a decrease in absorbance during the cooling cycle could be observed. This transition corresponds to the D_1 metastable $\rightarrow K$ transition observed for the bulk material on its DSC trace (Figure 3.37, page 126).

- ¹ A. McKillop and J.A. Tarbin, *Tetrahedron*, 1990, **31**, 5955.
- ² (a) R. Curci, A. Giovine and G. Modena, *Tetrahedron*, 1966, **22**, 1235; (b) D.J. Brown and P.W. Ford, *J. Chem. Soc. (C)*, 1969, 2720; (c) G.A. Russel and L.A. Ochrymowycz, *J. Org. Chem.*, 1970, **35**, 2106.
- ³ (a) R.W. Murray and R. Jeyaraman, *J. Org. Chem.*, 1985, **50**, 2847; (b) P.F. Corey and F.E. Ward, *J. Org. Chem.*, 1986, **51**, 1925; (c) R.W. Murray, R. Jeyaraman and M.K. Pillay, *J. Org. Chem.*, 1987, **52**, 746; (d) W. Adam, Y-Y. Chan, D. Cremer, J. Gauss, D. Scheutzow and M. Schindler, *J. Org. Chem.*, 1987, **52**, 2800.
- ⁴ Y. Miyahara and T. Inazu, *Tetrahedron Lett.*, 1990, **31**, 5955.
- ⁵ M.J. Cook, A.J. Dunn, S.D. Howe and A.J. Thomson, *J. Chem. Soc., Perkin Trans. 1*, 1988, 2453.
- ⁶ N.B. McKeown, I. Chambrier and M.J. Cook, *J. Chem. Soc., Perkin Trans. 1*, 1990, 1169.
- ⁷ R.R. Gagne, C.A. Koval and G.C. Licensky, *Inorg. Chem.*, 1980, **19**, 2854.
- ⁸ W.C. (Ina) du Plessis, J.J.C. Erasmus, G.J. Lamprecht, J. Conradie, T.S. Cameron, M.A.S. Aquino and J.C. Swarts, *Can. J. Chem.*, 1999, **77**, 378.
- ⁹ P.T. Nonjola, M.Sc. Thesis, University of the Free State, Bloemfontein, South Africa, 2001, p. 67.
- ¹⁰ T.J. Curphey, J.O. Santer, M. Rosenblum and J.H. Richards, *J. Am. Chem. Soc.*, 1960, **82**, 5249.
- ¹¹ P.J. Swarts, M. Immelman, G.J. Lamprecht, S.E. Greyling and J.C. Swarts, *S. Afr. J. Chem.*, 1997, **50**(4), 208.
- ¹² (a) S.E. Maree, M.Sc. Thesis, University of the Free State, Bloemfontein, South Africa, 1998, p. 104; (b) J.C. Swarts, *Unpublished results*.
- ¹³ J.C. Swarts, E.H.G. Langner, N. Krokeide-Hove and M.J. Cook, *J. Mater. Chem.*, 2001, **11**, 434.
- ¹⁴ J.C. Swarts and E.H.G. Langner, *Unpublished results*.
- ¹⁵ J.H. Sharp and M. Lardon, *J. Phys. Chem.*, 1968, **72**, 3230.
- ¹⁶ N.B. McKeown, I. Chambrier and M.J. Cook, *J. Chem. Soc., Perkin Trans. 1*, 1990, 1169.
- ¹⁷ I. Chambrier, M.J. Cook, S.J. Cracknell and J. McMurdo, *J. Mater. Chem.*, 1993, **3**, 841.
- ¹⁸ M.J. Cook, I. Chambrier, S.J. Cracknell, D.A. Mayes and D.A. Russell, *Photochem. Photobiol.*, 1995, **62**, 542.
- ¹⁹ (a) N. Ishikawa, O. Ohno, Y. Kaizu and H. Kobayashi, *J. Phys. Chem.*, 1992, **96**, 8832; (b) D. Wöhrle, A. Wendt, A. Weitemeyer, J. Stark, W. Spiller, S. Müller, U. Michelsen, H. Kliesch, A. Heuermann and A. Ardeschirpur, *Russ. Chem. Bull.*, 1994, **43**, 1953.
- ²⁰ M.J. Cook and J.C. Swarts, *Personal communication*, June 2000.
- ²¹ (a) A.S. Cherodian, A.N. Davies, R.M. Richardson, M.J. Cook, N.B. McKeown, A.J. Thompson, J. Feijoo, G. Ungar and K.J. Harrison, *Mol. Cryst. Liq. Cryst.*, 1991, **196**, 103; (b) M.J. Cook, *J. Mater. Sci., Materials in Electronics*, 1994, **5**, 117.

CHAPTER 4

EXPERIMENTAL

4. Equipment and Chemicals

4.1 Chemicals

Chemicals from Merck, Sigma and Aldrich were used without further purification. Organic solvents used were distilled prior to use and water was double distilled. THF was dried by refluxing over sodium metal and distilled just prior to use. Merck silica gel 60 (grain size 0.040-0.063 mm) was used for column chromatography. TLC was performed using Merck silica gel 60 F₂₅₄ on aluminium sheets. Melting points are uncorrected and were determined with a Reichert Thermopan microscope equipped with a Koffler hotstage.

4.2 Techniques and apparatus

4.2.1 Spectroscopy

¹H NMR-spectra at 298 K were recorded on a Bruker Advanced DPX 300 instrument. Chemical shifts are reported as δ -values (ppm) relative to SiMe₄ at 0.00 ppm. IR spectra were recorded on a Hitachi spectrophotometer, model 270-50. For liquids, thin films between NaCl plates were used, while a KBr matrix was used for solids. Stretching frequencies are expressed as cm^{-1} . Electronic absorbance spectra of Pcs (1 mM) in THF were recorded on a Cary-50 UV/VIS dual beam spectrophotometer at 298 K. MALDI-tof mass spectra were obtained using a Kratos Kompact MALDI 3 with a dithranol matrix at the University of Manchester. Thin film variable temperature visible spectra were recorded on a Hitachi U-3000 spectrophotometer fitted with a near-infrared sensitive detector and polaroid polarisers. The film-bearing substrate was located in a Mettler FP82 hotstage orientated orthogonally to the incident beam and controlled by a FP80 Mettler Processor.

4.2.2 Electrochemistry

Electrochemical measurements of phthalocyanine solutions (1 mmol dm⁻³) in dichloromethane at 25°C or in 1,2-dichloroethane at 70°C and ferrocenyl compounds (1 mmol dm⁻³) in acetonitrile at 25°C, with tetra-*n*-butylammonium hexafluorophosphate, (tBu)₄⁺NPF₆ (0.20 mol dm⁻³) as supporting electrolyte, were conducted under a blanket of argon using a computer controlled BAS voltammograph,¹ model CV-27. A three-electrode cell which utilised a Pt-auxiliary electrode, a Pt-working electrode and a Ag/Ag⁺ (0.01 mol dm⁻³ AgNO₃ in acetonitrile)

reference electrode,² mounted on a Luggin capillary³ filled with the supporting electrolyte (0.20 mol dm⁻³ (nBu)₄⁺NPF₆ in acetonitrile) was employed. Uncorrected data for junction potentials was collected with an Adalab-PCTM and AdaptTM data acquisition kit with locally developed software, and analysed with Hyperplot (JHM International Inc).

4.2.3 Differential scanning calorimetry (DSC)

Transitions between crystal, liquid crystal and isotropic liquid states were monitored by DSC (for enthalpy changes, *ca.* 7 mg samples at a heating and cooling rate of 10°C min⁻¹ between -70°C and a convenient maximum temperature at least 30°C higher than the melting point of the compounds). A TA Instruments DSC 10 thermal analyser fitted with a DuPont Instruments mechanical cooling accessory and a TA Instruments Thermal Analyst 2000 data processing unit were used.

4.2.4 Variable temperature microscope studies

Visual measurements to obtain transition temperatures were performed on an Olympus BH-2 polarising microscope in conjunction with a Linkam TMS 92 thermal analyser with a Linkam THM 600 cell. The heating and cooling rates used were either 5°C min⁻¹ or 2°C min⁻¹.

4.2.5 Thin film preparations

Spin-coated films were prepared from solutions of phthalocyanines in THF (*ca.* 2.5 mg in 0.1 ml) dropped onto a thoroughly cleaned (described under 4.2.6) microscope glass slide rotating at 2000 rpm using a spinner (Headway Research, Inc.). Spinning was continued for 20 s by which the solvent had evaporated. It has been established from previous measurements of film thickness using mechanical stylus equipment that films formed under these conditions are *ca.* 1000 Å thick.⁴

4.2.6 Microscope glass slide cleaning

Microscope glass slides (BDH, 71 mm x 25.5 mm x 1mm) were first washed with water, wiped clean with soft paper that does not leave fluff or threads, and subsequently washed with acetone and methanol. Hereafter the slides were only handled with tweezers. It was then placed on a

fritted glass (no. 3) inside a tube container. Isopropanol was boiled and the vapours allowed to pass through the fritted glass to clean the glass slide surface (Figure 4.1).

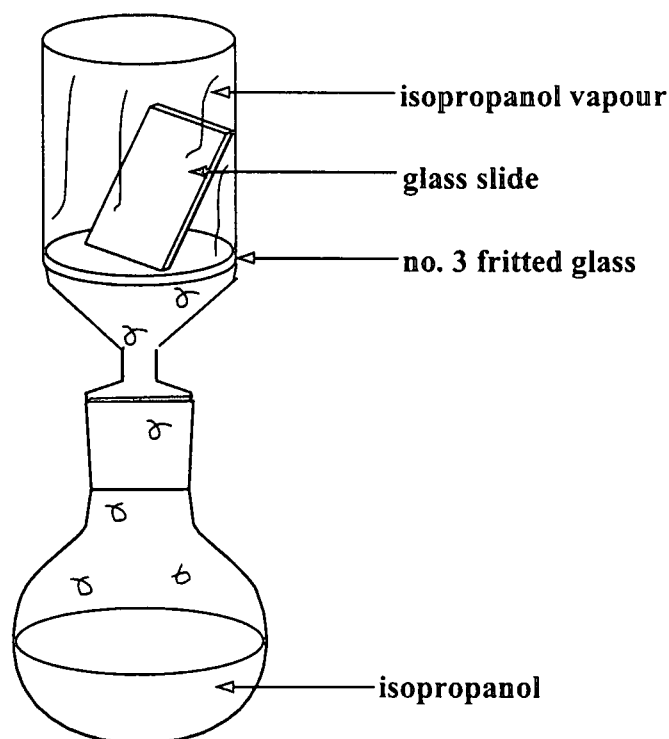


Figure 4.1: Cleaning of glass slides used for thin film preparations.

This treatment was maintained for 10 minutes on each side of the glass slide before it was removed and stored in a dust free slide container till usage.

4.3 Synthesis of 3,6-bis(dodecyl)phthalonitrile, (79)

4.3.1 2,5-Bis(dodecyl)thiophene^{5,6}, (76) [Scheme 3.1, page 62]

A stirred solution of thiophene, (37) (8.4 g, 0.1 mol) in dry THF (50 cm³), precooled to -80°C in a $\text{CO}_2(\text{s})$ /acetone bath, was treated under nitrogen with *n*-butyllithium (0.25 mol, 105 cm³ of a 2.5 mol dm⁻³ solution in hexane, 2.5 equivalents) for 30 min. The reaction mixture was allowed to warm slowly to room temperature and stirring continued for 24 h. The mixture was then cooled to -80°C and the formed dilithiated specie (75) treated under nitrogen with an excess of 1-bromododecane (62.3 g, 0.25 mol) over a period of 30 min. The resultant mixture was allowed to warm slowly to room temperature while stirring for 24 h, poured onto crushed ice and the crude product extracted with diethyl ether (3 x 150 cm³). The combined ethereal

fractions were dried over MgSO_4 , filtered and the solvent evaporated under reduced pressure at 80°C to afford dark brown oil, (58.8 g) as crude product. The residue was fractionally distilled under reduced pressure (1-1.5 mmHg) and the third fraction between $175\text{--}190^\circ\text{C}$ collected to afford 2,5-bis(dodecyl)thiophene, (**76**) (32.2 g, 76.5%) as a light brown oil, b.p. $175^\circ\text{C}/1\text{--}1.5$ mmHg; Anal. (Found: C, 79.9; H, 12.4; S, 7.6%. $\text{C}_{28}\text{H}_{52}\text{S}$ requires C, 79.9; H, 12.5; S, 7.6%); $\delta_{\text{H}}(\text{CDCl}_3, \text{ spectrum } 1)$ 0.90 (6H, t, 2 x $-\text{CH}_3$), 1.30 (36H, s, 2 x $(-\text{CH}_2-)_9$), 1.65 (4H, m, 2 x $-\text{CH}_2-$), 2.75 (4H, t, 2 x $-\text{CH}_2-$), and 6.57 (2H, s, $\text{C}_4\text{H}_2\text{S}$). $\nu_{\text{max}}/\text{cm}^{-1}$ (NaCl discs) 2860 (C-H) and 1464 ($-\text{CH}_3$).

4.3.2 2,5-Bis(dodecyl)thiophene-1,1-dioxide, (**77**), [Scheme 3.1, page 62]

4.3.2.1 Method 1: Dimethyldioxirane⁷

To a solution of 2,5-bis(dodecyl)thiophene, (**76**) (6.31 g, 15 mmol) in dichloromethane (270 cm^3) was added a mixture of H_2O (330 cm^3), acetone (240 cm^3), and NaHCO_3 (180 g) in a 2 litre 2-neck flask, equipped with an efficient stirrer and a large CO_2 /acetone condenser. The resulting heterogeneous mixture was cooled in an ice bath before solid oxone (300 g) was carefully added over 30 min while stirring. To the reaction mixture stirred for 16 h at room temperature, water (1.5 l) was added (to dissolve most of the inorganic salts) and decanted. The decanted aqueous layer with the remaining solids was extracted with dichloromethane (1 l), the combined organic phases washed with water (1.5 l), dried over MgSO_4 and the solvent evaporated under reduced pressure to afford a crude brownish product. The residue was recrystallised from ethanol to afford 2,5-bis(dodecyl)thiophene-1,1-dioxide, (**77**) (5.63 g, 82.8%) as white needle-like crystals, m.p. 72°C ; Anal. (Found: C, 73.8; H, 11.5; S, 6.8%. $\text{C}_{28}\text{H}_{52}\text{SO}_2$ requires C, 74.3; H, 11.6; S, 7.1%); $\delta_{\text{H}}(\text{CDCl}_3, \text{ spectrum } 2)$ 0.90 (6H, t, 2 x $-\text{CH}_3$), 1.30 (36H, s, 2 x $(-\text{CH}_2-)_9$), 1.67 (4H, m, 2 x $-\text{CH}_2-$), 2.48 (4H, t, 2 x $-\text{CH}_2-$) and 6.28 (2H, s, $\text{C}_4\text{H}_2\text{SO}_2$). $\nu_{\text{max}}/\text{cm}^{-1}$ (KBr) 1284 and 1137 ($-\text{SO}_2$).

4.3.2.2 Method 2: *m*-Chloroperoxybenzoic acid⁵

A solution of 2,5 bis(dodecyl)thiophene, (**76**) (6.31 g, 15 mmol) in dichloromethane (190 cm^3) was treated with *m*-chloroperoxybenzoic acid (50-60% tech. grade, 9.38 g, ~ 22.5 mmol) at 0°C for 3 h with stirring in the presence of an excess of NaHCO_3 (37.5 g, 57.8 mmol). The mixture was then left to stand for 16 h at 5°C before the precipitate was filtered and washed with

dichloromethane ($2 \times 100 \text{ cm}^3$). The combined organic phases were subsequently washed with 20% aqueous NaOH ($2 \times 100 \text{ cm}^3$) and water ($2 \times 100 \text{ cm}^3$), dried over MgSO_4 , the solvent evaporated and the crude product recrystallised from warm ethanol to yield 2,5-bis(dodecyl)thiophene-1,1-dioxide, (**77**) (2.77g, 40.7%), m.p. 72°C .

4.3.2.3 Method 3: Sodium perborate⁶

Sodium perborate monohydrate (17.309 g, 0.112 mol) was added in small portions over *ca.* 5 min to a stirred solution of 2,5-bis(dodecyl)thiophene, (**76**) (6.31 g, 15 mmol) in glacial acetic acid (65 cm^3). The reaction mixture was heated to 50°C while stirred for 5 h, allowed to cool to room temperature and left to stand overnight. Acetic acid was removed under reduced pressure and water (60 cm^3) added. The resultant mixture was stirred for 30 min, filtered and the remaining solid dissolved in diethyl ether (75 cm^3). The ethereal solution was washed with water (75 cm^3), saturated NaCl (75 cm^3), dried over MgSO_4 and filtered. The solvent was removed under reduced pressure and the crude product recrystallised from hexane to afford 2,5-bis(dodecyl)thiophene-1,1-dioxide, (**77**) (1.17 g, 17.2%), m.p. 72°C .

4.3.3 3,6-Bis(dodecyl)phthalonitrile^{5,7}, (**79**) [Scheme 3.1, page 62]

2,5-Bis(dodecyl)thiophene-1,1-dioxide, (**77**) (4.5 g, 9.94 mmol) and fumaronitrile (0.776g, 9.94 mmol) were washed with a minimum volume of chloroform (*ca.* 1.5 cm^3) into a glass tube. The tube was sealed and heated at 160°C for 16 h[†]. The contents of the tube were dissolved in chloroform and the solvent removed under reduced pressure at 90°C until the residue stopped liberating bubbles (*ca.* 20-30 min). The remaining residue was chromatographed over silica (with toluene as eluent) and the second band collected. The solvent was evaporated under reduced pressure yielding a brown crude product which was recrystallised from ethanol, filtered and the precipitate washed with ethanol until the filtrate was clear to afford off white 3,6-bis(dodecyl)phthalonitrile, (**79**) (2.03 g, 44%), m.p. 73.5°C , $R_f = 0.82$; Anal. (Found: C, 82.8; H, 11.1; N, 6.1%. $\text{C}_{32}\text{H}_{52}\text{N}_2$ requires C, 82.7; H, 11.3; N, 6.0%); δ_{H} (CDCl_3 , spectrum 3) 0.87 (6H, t, $2 \times -\text{CH}_3$), 1.28 (36H, s, $2 \times (-\text{CH}_2-)_9$), 1.65 (4H, m, $2 \times -\text{CH}_2-$), 2.83 (4H, t, $2 \times -\text{CH}_2-$) and 7.44 (2H, s, C_6H_2). $\nu_{\text{max}}/\text{cm}^{-1}$ (KBr) 2228 ($\text{C}\equiv\text{N}$).

[†] The sealed glass tube was put into a steel pipe and filled with sand to protect the oven against an explosion.

4.4 Synthesis of 4-(2'-ferrocenylethoxy)phthalonitrile, (81)

4.4.1 Dimethylaminomethylferrocene^{8,9}, (61) [Scheme 3.3, page 67]

Bis(dimethylamino)methane[†] (43.2 g, 0.422 mol) was added drop wise, with cooling in an ice bath to a stirring solution of phosphoric acid (43.2 g, 0.44 mol, 26.45 cm³) in acetic acid (400 cm³) in a 2 litre 3-neck round-bottomed flask equipped with a condenser. Ferrocene, (58) (46.4 g, 0.25 mol) was added under nitrogen and the resulting suspension refluxed for 5 h at 105°C. The reaction mixture, a dark-amber solution, was allowed to cool to room temperature, diluted with water (550 cm³) and the unreacted ferrocene removed by extracting the solution with diethyl ether (3 x 325 cm³). The aqueous solution was cooled in ice water and made alkaline by the addition of sodium hydroxide solution [NaOH pellets (245 g) dissolved in water (200 cm³)]. The tertiary amine separates from the alkaline solution as oil in the presence of some black tar. The mixture was extracted with diethyl ether (3 x 500 cm³) and the organic layer washed with water, dried over MgSO₄ and filtered. On evaporation of the solution, the crude dimethylaminomethylferrocene, (61) (45.59 g, 75%) was obtained as a dark-red liquid, b.p. 118-121°C/5-6 mmHg. δ_{H} (CDCl₃, spectrum 4) 2.18 (6H, s, 2 x -CH₃), 3.29 (2H, s, -CH₂-), 4.12 (7H, s, -C₅H₄ and C₅H₅) and 4.18 (2H, t, -C₅H₄).

4.4.2 *N,N*-Dimethylaminomethylferrocene methiodide^{8,9}, (62) [Scheme 3.3, page 67]

To a gently swirled solution of the amine (61) (0.25 mol) in methanol (54 cm³) methyl iodide (54 cm³, 0.87 mol) was added and the solution heated on a Buchi at 80°C for 5 min, cooled to room temperature and diethyl ether (500 cm³) added. The ammonium salt, (62), which separates as an oil and crystallises on being scratched was filtered on a Büchner funnel, washed with diethyl ether and dried under reduced pressure at room temperature to yield *N,N*-dimethylaminomethylferrocene methiodide, (62) (75.68 g, 78.6%) as an orange powder, m.p. 185-195°C[†]. δ_{H} (CDCl₃, spectrum 5) 3.32 and 3.24* (9H, s, 3 x -CH₃), 4.34 and 4.34* (5H, s, C₅H₅), 4.38 and 4.47* (2H, t, -C₅H₄) and 4.57, 4.88* (2H, t, -C₅H₄) and 4.92, 5.64* (2H, s, -CH₂-).

[‡] Is a potent lachrymator, and should be handled only in a hood.

[†] The melting point is ill-defined because of darkening and shrinking of the product that starts at 173°C.

* Integrals of a second specie of (62) in approximately 14% population percentage as per integral ratios.

4.4.3 Ferrocenylacetonitrile¹⁰, (63) [Scheme 3.3, page 67]

A solution of *N,N*-dimethylaminomethylferrocene methiodide, (62) (21.1 g, 0.055 mol) and potassium cyanide (21.5 g, 0.325 mol) in water (215 cm³) was refluxed for 2,5 h at 105°C. The resulting dark brown reaction mixture with a fine precipitate was cooled to room temperature, decanted and the aqueous layer subsequently extracted with diethyl ether (3 x 200 cm³) and benzene (2 x 200 cm³). The fine precipitate was dissolved in benzene and the benzene fractions combined, washed with water, dried over MgSO₄, filtered and the solvent evaporated. The combined ethereal solution was washed with water, dried over MgSO₄, filtered and evaporated to dryness. All solid residues were combined, dissolved in boiling hexane (200 cm³), filtered, allowed to cool to room temperature, placed in a refrigerator (4°C) for 5 h and in freezer overnight to afford ferrocenylacetonitrile, (63) (7.26 g, 58.8%) as yellow crystals, m.p. 76-79°C. δ_{H} (CDCl₃, spectrum 6) 3.45 (2H, s, -CH₂-), 4.19 (2H, t, -C₅H₄), 4.25 (5H, s, C₅H₅) and 4.27 (2H, t, -C₅H₄). ν_{max} /cm⁻¹ (KBr) 2248 (C≡N) and 1414 (-CH₂-).

4.4.4 Ferrocenylacetic acid¹⁰, (64) [Scheme 3.3, page 67]

To a solution of potassium hydroxide (15.1 g) in water (150 cm³), a suspension of the nitrile (63) (6.0 g, 0.026 mol) in ethanol (80 cm³) was added, refluxed until evolution of ammonia had ceased (5 h) and excess ethanol was removed under reduced pressure to ca. 50 cm³. The residual suspension was dissolved in water (300 cm³), extracted with diethyl ether (2 x 400 cm³) and filtered. Acidification of the alkaline solution with 85% phosphoric acid afforded flaky golden crystals. The product was filtered, dissolved in diethyl ether, washed with water, dried over MgSO₄, filtered and the solvent removed to yield ferrocenylacetic acid, (64) (5.65 g, 86.8%) as orange-brown crystals, m.p. 151-155°C. δ_{H} (CDCl₃, spectrum 7) 3.42 (2H, s, -CH₂-), 4.16 (7H, s, -C₅H₄ and C₅H₅) and 4.24 (2H, s, -C₅H₄). ν_{max} /cm⁻¹ (KBr) 3088 (-OH), 1710 (C=O), 1401 (-CH₂-) and 1227 (C-O).

4.4.5 2-Ferrocenylethanol¹⁰, (80) [Scheme 3.3, page 67]

Ferrocenylacetic acid, (64) (2,0 g, 8.19 mmol) in dry diethyl ether (100 cm³) was added to a flask containing a stirred refluxing suspension of lithium aluminium hydride (2.48 g, 65,55 mmol) in dry diethyl ether (30 cm³). The reaction mixture was stirred at room temperature for 30 min, refluxed for 3 h, ice cooled, treated with water (30 cm³), 6 mol dm⁻³ H₂SO₄ (10 cm³)

and the aqueous layer quickly decanted. The ethereal layer was topped to 250 cm³, washed with 5% sodium hydroxide solution (200 cm³), ice water (2 x 250 cm³), dried over MgSO₄, and filtered. The solvent was then removed under reduced pressure to afford 2-ferrocenylethanol, (80) (1.76 g, 93.5%) as a red-brown viscous oil, m.p. 32-33°C. δ_{H} (CDCl₃, spectrum 8) 2.62 (2H, t, Fc-CH₂-), 3.75 (2H, m, -CH₂-OH) and 4.13 (9H, m, -C₅H₄ and C₅H₅). ν_{max} /cm⁻¹ (NaCl discs) 3408 (-OH) and 1038 (C-O).

4.4.6 4-(2'-Ferrocenylethoxy)phthalonitrile¹¹, (81) [Scheme 3.2, page 66]

4-Nitrophthalonitrile, (52) (0.76 g, 4.40 mmol) and 2-ferrocenylethanol, (80) (2.02 g, 8.80 mmol) were stirred in the presence of potassium carbonate (3.65 g, 26.4 mmol) in dry DMF (15 cm³) under a slow nitrogen stream at room temperature for 10 days. The mixture was then poured into ice water (100 cm³), extracted with ethyl acetate (3 x 80 cm³) and combined ethyl acetate fractions washed with cold water (2 x 150 cm³), followed by a saturated sodium hydroxide solution (100 cm³), dried over MgSO₄ and filtered. The solvent was evaporated under reduced pressure and the residue dissolved in a minimum ethyl acetate before adding 4 times as much hexane to the solution. Purification by column chromatography over silica with ethyl acetate:hexane (1:4) as eluent, gave unreacted 2-ferrocenylethanol as the third fraction, which could be reused. The second fraction, after solvent removal, afforded 4-(2'-ferrocenylethoxy)phthalonitrile, (81) as orange crystals (0.84 g, 86.1%), mp. 137-139°C, R_{f} = 0.34. δ_{H} (CDCl₃, spectrum 9) 2.85 (2H, t, Fc-CH₂-), 4.12 (11H, m, -CH₂-O-, -C₅H₄ and C₅H₅), 7.13 (1H, dd, Ar-H), 7.21 (1H, d, Ar-H) and 7.67 (1H, d, Ar-H). ν_{max} /cm⁻¹ (KBr) 2228 (C≡N) and 1254 (Ar-O-R).

4.5 Synthesis of substituted phthalocyanines

4.5.1 1,4,8,11,15,18,22,25-Octakis(dodecyl)phthalocyanine, (83)^{5,7} [Scheme 3.4, page 71]

To 3,6-bis(dodecyl)phthalonitrile, (79) (0.20 g, 0.43 mmol) dissolved in warm (80°C) pentanol (5 cm³), an excess of freshly cleaned lithium metal (0.07–0.10 g, 10.1–14.4 mmol) was added in small portions and the mixture refluxed at 110°C for 16 h. The cooled, deep green coloured suspension was stirred with acetone (25 cm³), the solution filtered and the solids washed with acetone (25 cm³) before the combined acetone solutions were concentrated to ca. 12.5 cm³. Glacial acetic acid (25 cm³) was added, the heterogeneous mixture stirred for 30 min, filtered

and the precipitate collected to afford after recrystallisation, from THF/methanol 1,4,8,11,15,18,22,25-otakis(dodecyl)phthalocyanine, (**83**) (39.1 mg, 19.5%); Anal. (Found: C, 82.19; H, 11.21; N, 5.61%. $C_{128}H_{210}N_8$ requires C, 82.61; H, 11.37; N, 6.02%); δ_H (CDCl₃, spectrum 10) 0.86 (24H, t, 8 x -CH₃), 1.21 (128H, m, 8 x (-CH₂-)₈), 1.35 (16H, m, 8 x -CH₂-), 2.06 (16H, m, 8 x -CH₂-), 4.41 (16H, t, 8 x Ar-CH₂-) and 7.82 (8H, s, 4 x C₆H₂).

4.5.2 2,9,16,23-Tetrakis(2'-ferrocenylethoxy)phthalocyanine, (**85**) [Scheme 3.6, page 73]

To 4-(2'-ferrocenylethoxy)phthalonitrile, (**81**) (0.20 g, 0.56 mmol) dissolved in warm (80°C) pentanol (5 cm³), an excess of cleaned lithium metal (0.10 g, 14.4 mmol) in small portions was added. The reaction mixture was refluxed at 110°C for 16 h in the dark. On cooling, the suspension was stirred with acetone (150 cm³), filtered and the solids washed with acetone (200 cm³). The combined acetone solutions were concentrated to *ca.* 40 cm³, acetic acid (150 cm³) added and stirred for 30 min. Water (1.8 l) was added and the mixture extracted with chloroform (3 x 80 cm³). The combined chloroform fractions were washed with water (2 x 200 cm³) and the organic solvent evaporated under reduced pressure. The residue was purified by column chromatography over silica with toluene-THF (20:1) as eluent, to afford after recrystallisation from THF/methanol 2,9,16,23-tetrakis(2'-ferrocenylethoxy)phthalocyanine, (**85**) (10.2 mg, 5.1%); R_f = 0.45 in toluene; δ_H (CDCl₃, spectrum 12) 3.16 (8H, m, 4 x Fc-CH₂-), 4.36 (36H, m, 4 x C₅H₅, 4 x -C₅H₄), 4.52 (8H, m, 4 x -CH₂-O-) and 7.05-8.60 (12H, m, 4 x Ar-H₃). A second fraction (4.2 mg) was washed out of the silica using THF as eluent, but could not be identified due to unsatisfactory ¹H NMR spectra.

4.5.3 Statistical condensation of 3,6-bis(dodecyl)phthalonitrile and 4-(2'-ferrocenylethoxy)phthalonitrile (3:1 mole ratio) with lithium in pentanol [Scheme 3.7, page 74]

3,6-Bis(dodecyl)phthalonitrile, (**79**) (0.929 g, 2.00 mmol) and 4-(2'-ferrocenylethoxy)phthalonitrile, (**81**) (0.237 g, 0.66 mmol) were dissolved in pentanol (14 cm³) at 80°C. An excess of clean lithium metal (0.666 g, 95.9 mmol) was added in small portions and the mixture refluxed at 110°C for 16 h in the dark. The cooled suspension was stirred with acetone (350 cm³), filtered, the solids washed with acetone (2 x 200 cm³) and the combined acetone fractions concentrated to *ca.* 150 cm³. Acetic acid (300 cm³) was added and the mixture stirred for 30

min followed by filtration.[†] Water (1.8 l) was added and the mixture extracted with chloroform (2 x 150 cm³). The combined chloroform fractions were washed with water (2 x 300 cm³) and the organic solvent removed under reduced pressure to afford after recrystallisation from THF/methanol the crude product. The residue was chromatographed over silica with hexane-toluene (20:1 volume ratio) as eluent. Five fractions were isolated and recrystallised from THF/methanol. During the collection of the second fraction, the toluene gradient was increased to hexane-toluene (4:1), for the third (1:2) and the fourth hexane-THF (9:1). The last fraction was washed out of the silica with THF.

Fraction 1:

1,4,8,11,15,18,22,25-Octakis(dodecyl)phthalocyanine (87.1 mg, 17.6 %); $R_f = 0.97$.

Fraction 2:

8,11,15,18,22,25-Hexakis(dodecyl)-2-(2'-ferrocenylethoxy)phthalocyanine (59.7 mg, 12.8 %); $R_f = 0.59$; δ_H (CDCl₃, spectrum 13) 0.85 (18H, m, 6 x -CH₃), 1.13-1.48 (96H, m, 6 x (-CH₂)₈), 1.60 (12H, m, Ar-CH₂-CH₂-CH₂-), 2.18 (12H, m, 6 x Ar-CH₂-CH₂-), 3.15 (2H, t, Fc-CH₂-), 4.15-4.68 (23H, m, 6 x Ar-CH₂-, -O-CH₂-, C₅H₅-, -C₅H₄) and 7.66-9.14 (9H, m, 3 x Ar-H₂ and Ar-H₃); ms(MALDI-tof) m/z calcd. for (C₁₁₆H₁₇₄N₈OFe) 1752.3, found 1752.5.

Fraction 3:

15,18,22,25-Tetrakis(dodecyl)-2,9-bis(2'-ferrocenylethoxy)phthalocyanine and/or 8,11,22,25-tetrakis(dodecyl)-2,16-bis(2'-ferrocenylethoxy)phthalocyanine isomer (27.1 mg, 6.2 %); $R_f = 0.11$; δ_H (CDCl₃, spectrum 14); ms(MALDI-tof) m/z calcd. for (C₁₀₄H₁₃₈N₈O₂Fe₂) 1644, found 1644.1.

Fraction 4:

Mixture of 15,18,22,25-tetrakis(dodecyl)-2,9-bis(2'-ferrocenylethoxy)phthalocyanine and/or 8,11,22,25-tetrakis(dodecyl)-2,16-bis(2'-ferrocenylethoxy)phthalocyanine isomer and 22,25-bis(dodecyl)-2,9,16-tris(2'-ferrocenylethoxy)phthalocyanine (22.3 mg, 5.1%); $R_f = 0.06$; See δ_H (CDCl₃, spectrum 14); ms(MALDI-tof) m/z calcd. for (C₁₀₄H₁₃₈N₈O₂Fe₂) 1644, found 1644.1 and calcd. for (C₉₂H₁₀₂N₈O₃Fe₃) 1535.8, found 1535.4.

Fraction 5:

The fifth fraction could not be identified due to unsatisfactory ¹H NMR spectra (3.7 mg); $R_f = 0$ (spot at the origin).

[†] The precipitate was too fine and went through with the filtrate.

Low yield of fractions two to four may be attributed to a failure of recovering all possible products from the column because not all the crude product could be retrieved from the silica column.

4.5.4 Statistical condensation of 3,6-bis(dodecyl)phthalonitrile and 4-(2'-ferrocenylethoxy)phthalonitrile (9:1 mole ratio) with lithium in pentanol^{5,6} [Scheme 3.7, page 74]

To 3,6-bis(dodecyl)phthalonitrile, (**79**) (0.957 mg, 2.06 mmol) and 4-(2'-ferrocenylethoxy)-phthalonitrile, (**81**) (0.082 mg, 0.23 mmol) dissolved in pentanol (18.0 cm³) at 80°C, an excess of cleaned lithium metal (0.229 g, 32.93 mmol) in small portions was added. The reaction mixture was refluxed at 110°C for 16 h in the dark. The cooled suspension was stirred with acetone (350 cm³), filtered, the solids washed with acetone (2 x 200 cm³) and the combined acetone fractions concentrated to *ca.* 150 cm³. Acetic acid (300 cm³) was added, the heterogeneous mixture stirred for 30 min., filtered and the precipitate collected to afford on recrystallisation from THF/methanol the crude product (0.450 g). The residue was subjected to column chromatography over silica with hexane-toluene (20:1) as eluent. Four fractions were isolated and recrystallised from THF/methanol. During the collection of the third band, the toluene gradient was increased to hexane-toluene (1:1) and for the fourth band THF was used.

Fraction 1:

1,4,8,11,15,18,22,25-Octakis(dodecyl)phthalocyanine (212.6 mg, 49.9 %); $R_f = 0.96$.

Fraction 2:

8,11,15,18,22,25-Hexakis(dodecyl)-2-(2'-ferrocenylethoxy)phthalocyanine (50.4 mg, 9.6%); $R_f = 0.58$.

Fraction 3:

15,18,22,25-Tetrakis(dodecyl)-2,9-bis(2'-ferrocenylethoxy)phthalocyanine and/or 8,11,22,25-tetrakis(dodecyl)-2,16-bis(2'-ferrocenylethoxy)phthalocyanine isomer (13.1 mg, 3.5%); $R_f = 0.10$.

Fraction 4:

Mixture of 15,18,22,25-tetrakis(dodecyl)-2,9-bis(2'-ferrocenylethoxy)phthalocyanine and/or 8,11,22,25-tetrakis(dodecyl)-2,16-bis(2'-ferrocenylethoxy)phthalocyanine isomer and 22,25-bis(dodecyl)-2,9,16-tris(2'-ferrocenylethoxy)phthalocyanine (7.9 mg, 2.1%); $R_f = 0$ (spot at the origin).

4.5.5 Statistical condensation of 3,6-bis(dodecyl)phthalonitrile and 4-(2'-ferrocenylethoxy)phthalonitrile (3:1 mole ratio) with zinc acetate dihydrate in dimethylaminoethanol [Scheme 3.7, page 74]

To 3,6-bis(dodecyl)phthalonitrile, (**79**) (0.697 mg, 1.5 mmol) and 4-(2'-ferrocenylethoxy)phthalonitrile, (**81**) (0.178 mg, 0.5 mmol) dissolved in dimethylaminoethanol (3 cm³), an excess of zinc acetate dihydrate (0.439 g, 2.0 mmol) was added. The reaction mixture was refluxed at 130°C for 16 h under nitrogen. To the cooled mixture, acetone (50 cm³) was added and the precipitated formed on addition of methanol (10 cm³), filtered and washed until the filtrate was clear. The crude product obtained was chromatographed on silica with hexane-toluene (2:1) as eluent. Three fractions were isolated and recrystallised from THF/methanol. During the collection of the second fraction, the toluene gradient was increased to hexane-toluene (1:1) and the third fraction washed out with toluene.

Fraction 1:

[1,4,8,11,15,22,25-octakis(dodecyl)phthalocyaninato]zinc(II) (27.4 mg, 7.2%), $R_f = 0.97$; Anal. Found: C, 79.92; H, 10.71; N, 5.49%. $C_{128}H_{208}N_8$ requires C, 79.88; H, 10.89; N, 5.82%; δ_H (CDCl₃, spectrum 11) 0.85 (24H, t, 8 x -CH₃), 1.12-1.40 (144H, m, 8 x (-CH₂-)₉), 2.04 (16H, m, 8 x -CH₂-), 4.28 (16H, t, 8 x Ar-CH₂-) and 7.64 (8H, s, 4 x C₆H₂). ms (MALDI-tof) m/z calcd. for ($C_{128}H_{208}N_8OZn$) 1924.5, found 1924.

Fraction 2:

[8,11,15,18,22,25-hexakis(dodecyl)-2-(2'-ferrocenylethoxy)phthalocyaninato]zinc(II) (21.1 mg, 5.8%); $R_f = 0.81$; δ_H (CDCl₃, spectrum 16) 0.86 (18H, t, 6 x -CH₃), 1.15-1.53 (96H, m, 6 x (-CH₂-)₈), 1.65 (12H m, 6 x Ar-CH₂-CH₂-CH₂-), 2.18 (12H, m, 6 x Ar-CH₂-CH₂-), 3.10 (2H, t, -CH₂-Fc), 3.89-4.50 (23H, m, 6 x Ar-CH₂-, C₅H₅-, -C₅H₄-, -O-CH₂-), and 7.33-8.58 (9H, m, 3 x Ar-H₂ and Ar-H₃); ms (MALDI-tof) m/z calcd. for ($C_{116}H_{172}N_8OFeZn$) 1815.9, found 1815.

Fraction 3:

The third fraction could not be identified due to unsatisfactory ¹H NMR spectra (3.9 mg); $R_f = 0$ (spot at the origin).

Low yields are attributed to the fact that approximately 30% of the crude product could not be retrieved from the silica column.

4.5.6 Complexation of Zn^{2+} with metal-free phthalocyanines⁷

The general procedure was as follows:

4.5.6.1 For [1,4,8,11,15,22,25-octakis(dodecyl)phthalocyaninato]zinc(II), (**84**) [Scheme 3.5, page 71] a stirred mixture of the metal-free 1,4,8,11,15,18,22,25-octakis(dodecyl)-phthalocyanine, (**83**) (150 mg, 0.081 mmol), zinc acetate dihydrate (73.3 mg, 0.334 mmol) and pentanol (6 cm³) was refluxed at 130°C for 16 h. To the cooled mixture, methanol (12 cm³) was added, the precipitate filtered and washed with excess methanol, followed by recrystallisation from THF/methanol to afford the blue [1,4,8,11,15,22,25-octakis(dodecyl)phthalocyaninato]zinc(II), (**84**) (129.6 mg, 83.1%).

4.5.6.2 For [8,11,15,18,22,25-hexakis(dodecyl)-2-(2'-ferrocenylethoxy)phthalocyaninato]zinc (II), (**87**) [Scheme 3.8, page 80] a stirred mixture of the metal-free 8,11,15,18,22,25-hexakis(dodecyl)-2-(2'-ferrocenylethoxy)phthalocyanine, (**86**) (57.7 mg, 0.033 mmol), zinc acetate dihydrate (28.8 mg, 0.132 mmol) and pentanol (2 cm³) was refluxed at 130°C for 16 h. To the cooled mixture, methanol (4 cm³) was added, the precipitate filtered and washed with excess methanol, followed by recrystallisation from THF/methanol to afford the blue [8,11,15,18,22,25-hexakis(dodecyl)-2-(2'-ferrocenylethoxy)phthalocyaninato]zinc(II), (**87**) (51.6 mg, 86.43%).

- ¹ BAS CV-27 Voltammograph Instruction Manual, Bioanalytical Systems Inc., West Lafayette: Indiana, 1994.
- ² D.T. Sawyer and J.L. Roberts Jr., *Experimental Electrochemistry for Chemists*, Wiley: New York, 1974, p. 54.
- ³ G.A. Mabbott, *J. Chem. Educ.*, 1983, **60**, 697.
- ⁴ G.C. Bryant, M.J. Cook, C. Ruggiero, T.J. Ryan, A.J. Thorne, S.D. Haslam and R.M. Richardson, *Thin Solid Films*, 1994, **243**, 316.
- ⁵ N.B. McKeown, I. Chambrier and M.J. Cook, *J. Chem. Soc., Perkin Trans. 1*, 1990, 1176.
- ⁶ I. Chambrier, M.J. Cook, S.J. Cracknell and J. McMurdo, *J. Mater. Chem.*, 1993, **3**, 845.
- ⁷ J.C. Swarts, E. Langner, N. Krokeide-Hove and M.J. Cook, *J. Mater. Chem.*, 2000, **10**, 8.
- ⁸ D. Lednicer and C.R. Hauser, *Org. Synth.*, 1961, **40**, 31.
- ⁹ J.K. Lindsay and C.R. Hauser, *J. Org. Chem.*, 1957, **22**, 355.
- ¹⁰ D. Lednicer, J.K. Lindsay and C.R. Hauser, *J. Org. Chem.*, 1958, **23**, 653.
- ¹¹ (a) T.M. Keller, T.R. Price and J.R. Griffith, *Synlett.*, 1980, 613; (b) C.C. Leznoff, S. Greenberg, P.C. Minor, P. Seymour and A.B.P. Lever, *Inorg. Chim. Acta*, 1984, **89**, L35. (c) D.M. Drew and C.C. Leznoff, *Synlett.*, 1994, 623.

CHAPTER 5

CONCLUSIONS

AND

FUTURE PERSPECTIVES

In this study the author has shown that a possible route towards the synthesis of unsymmetrically multidodecylated phthalocyanine-ferrocenylethoxide conjugates is the lithium alkoxide-catalysed statistical condensation of 3,6-bis(dodecyl)phthalonitrile and 4-(2'-ferrocenylethoxy)-phthalonitrile in a 9:1 or 3:1 ratio. The multiple step synthetic routes to obtain the correct phthalonitrile precursors were also developed. In spite of the poor solubility of the products of the statistical condensation they could, to a satisfactory extent, be separated by column chromatography that greatly enhanced the viability of this synthetic approach. A multidodecylated phthalocyanine-ferrocenylethoxide conjugate containing 3 ferrocenyl groups could not be successfully isolated during this research program, but it may be possible to synthesise such a conjugate by switching the ratio of the two precursors to 1:9 for 3,6-bis(dodecyl)phthalonitrile and 4-(2'-ferrocenylethoxy)phthalonitrile. In future, attempts to synthesise these multidodecylated phthalocyanine-ferrocenylethoxide conjugates via other routes, e. g. the ring expansion of subphthalocyanines and the polymer support route should be investigated. The possibility of using similarly substituted diiminoisoindolines as precursors should also be investigated. It will also be important to attempt the synthesis of an unsymmetrically substituted phthalocyanine containing six alkyl chains and a nitro group. This will provide an extremely useful mononitro-functionalised phthalocyanine that could be replaced by many different nucleophiles including alcohols, amines and mercapto groups to liberate a variety of phthalocyanines with different properties.

The complexations of zinc with the metal-free ferrocenyl-phthalocyanine conjugates were very efficient, high yielding reactions. The insertion of other metals, *e.g.* molybdenum, silicon and iridium, into the central cavity of the phthalocyanines of these conjugates should in future be researched.

Although only 4-(2'-ferrocenylethoxy)phthalonitrile, with 2 carbon atoms in the alkoxide linking chain between the ferrocene and phthalonitrile moieties was used as a precursor in the synthesis of the ferrocenyl-phthalocyanine conjugates during this study, future studies may be designed to include a variation of the length of the alkoxide linking group. Variation in the position of the ferrocenylalkoxide moiety on the phthalonitrile precursor and ultimately on the phthalocyanine macrocycle should also be researched in future. The central metallocene may also be changed from iron to ruthenium, cobalt, titanium or osmium.

In a second aspect of this research program, the electrochemistry of ten ferrocenyl compounds substituted with groups possessing different electron withdrawing capacities were investigated in acetonitrile using cyclic voltammetry. Most compounds showed one-electron reversible electrochemical behaviour. Two redox processes were however, observed for ferrocenylmethanol and *N,N*-dimethylaminomethylferrocene methiodide.

Fourteen new phthalocyanines were also investigated electrochemically. Four ring-based electron transfer processes were observed for the octa-alkylated phthalocyanines, whereas the hexadecylated phthalocyanine-ferrocenylethoxide conjugates showed an additional, fifth, redox couple associated with the ferrocenyl moiety. Electrochemical evidence was presented that proved encapsulation of the phthalocyanine macrocycle by long-chain alkyl substituents ultimately slow down the rate of electron exchange with the working electrode. It also limits aggregation.

In the third aspect of this research program, the position of λ_{\max} of the Q-band in the red or near infrared region of the electronic spectrum of the phthalocyanines synthesised in this study, was found to be sufficiently red shifted to be favourable for photodynamic therapy of cancer. The substitution of two non-peripheral alkyl substituents on the phthalocyanine macrocycle with one peripheral ferrocenylethoxide group caused a systematic blue shift of the position of the Q-band λ_{\max} values by *ca.* 10 nm from 729 to 719 nm. In future, clinical studies should be performed on the new zinc-containing compounds of this study to establish their viability as agents for the photodynamic treatment of cancer, because the red shift in Q_{\max} of these compounds imply light absorption by body tissue will not minimise PDT activity as much as it does in, for example hematoporphyrin (Hp). It will also be important to determine if a synergistic effect between the chemotherapeutic ferrocenyl moiety and the photodynamic phthalocyanine moiety exists. In future the insertion of other photoactive metals, *e.g.* aluminium and gallium or chemotherapeutic metals such as platinum may also be researched.

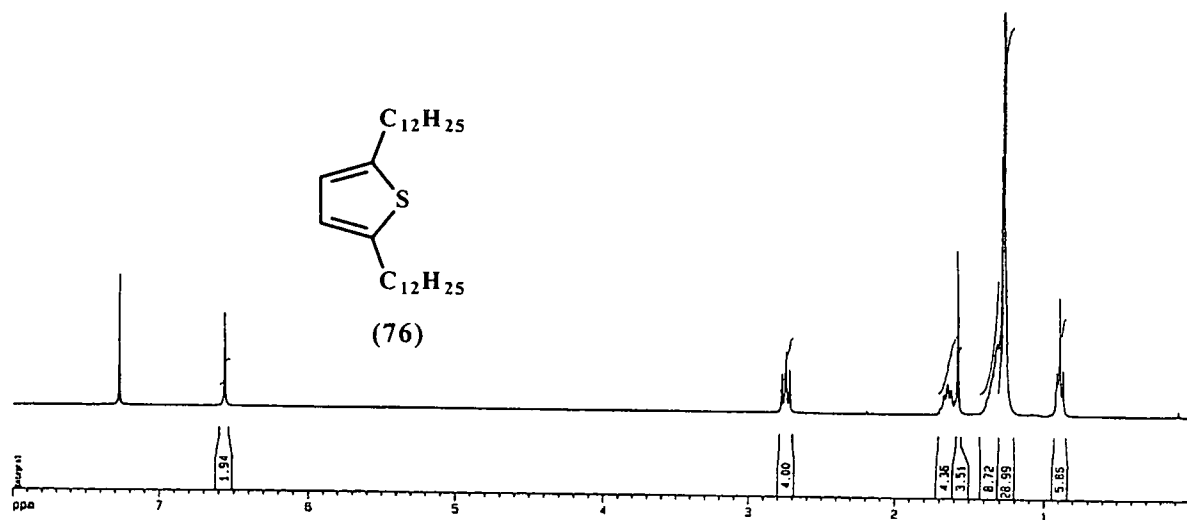
The fourth aspect researched in this study program centred around determining the liquid crystalline properties of the new phthalocyanines of this study. It was found that conversion of a metal-free phthalocyanine to a zinc-containing phthalocyanine caused a substantial increase in temperature range in which the phthalocyanine macrocycles displayed liquid crystalline properties. Incorporation of a ferrocenyl fragment in the phthalocyanine macrocycle caused the liquid crystalline temperature range to increase from 68.7°C for (C₁₂H₂₅)₈-2HPc derivative to

239°C for $(C_{12}H_{25})_6-2HPc-O(CH_2)_2Fc$. The thermodynamic properties of each mesophase were probed by DSC, polarised light optical microscopy and variable temperature UV/VIS spectroscopy of thin layers of the phthalocyanines cast on glass. Up to four mesophases could be detected and the enthalpy associated with each phase change was determined.

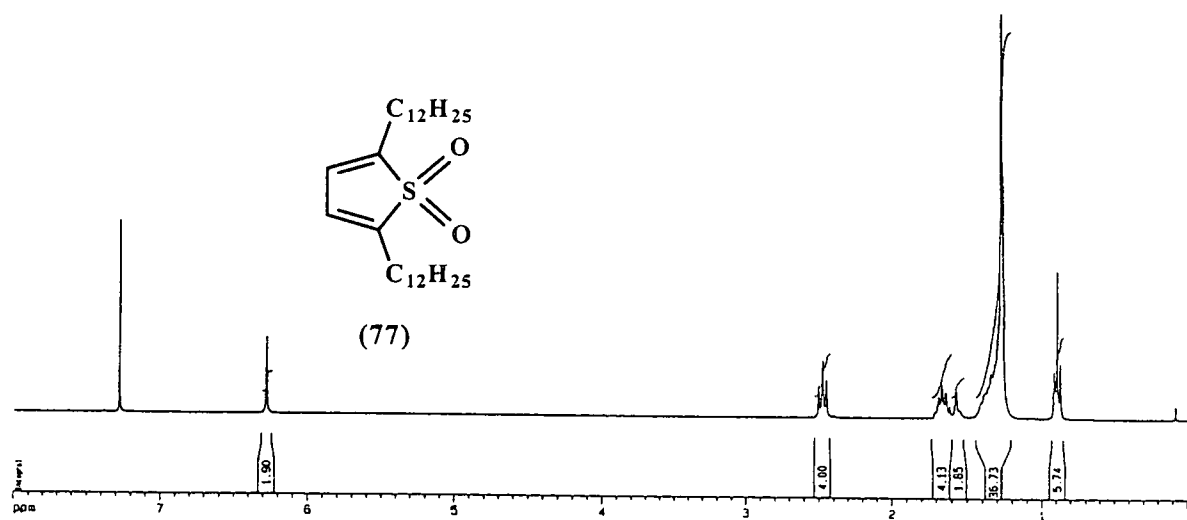
Future thermodynamic studies on liquid crystals could include determining the effects of various metals coordinated into the phthalocyanine core on the mesophase behaviour of these new phthalocyanines as well as the influence of different metallocene-containing alkyl, alkoxide, amide or mercapto side chains of different chain lengths on the liquid crystal properties of these compounds. Some of the cited future research possibilities mentioned in this concluding chapter are already under investigation in this laboratory.

^1H NMR SPECTRA

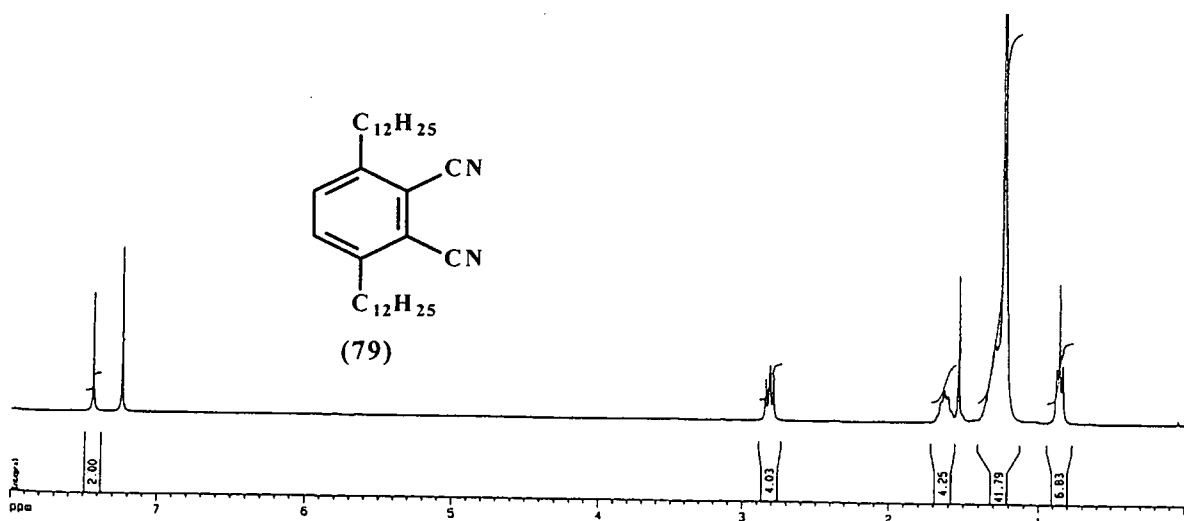
¹H NMR



Spectrum 1: 2,5-Bis(dodecyl)thiophene, (76)

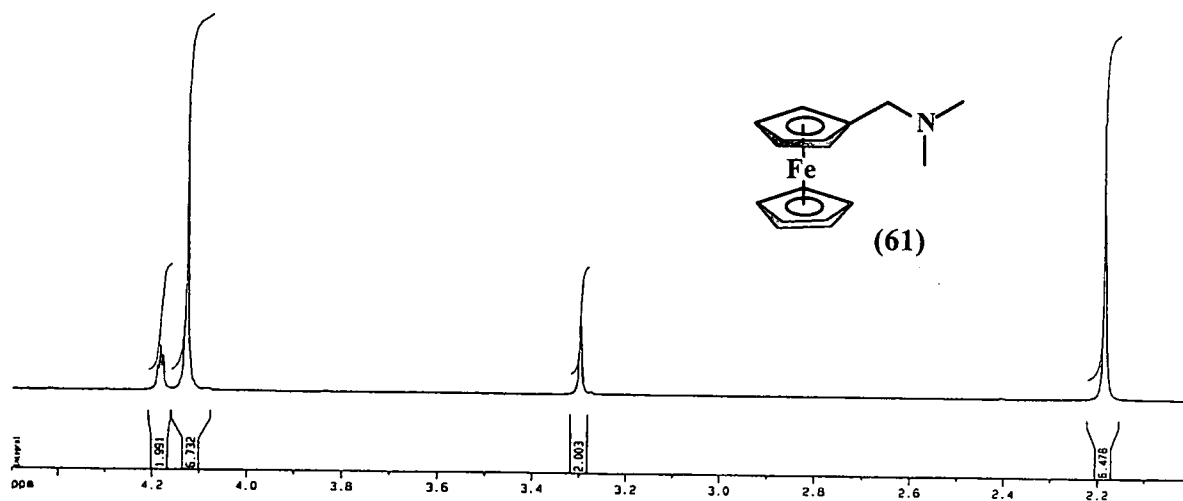


Spectrum 2: 2,5-Bis(dodecyl)thiophene-1,1-dioxide, (77)

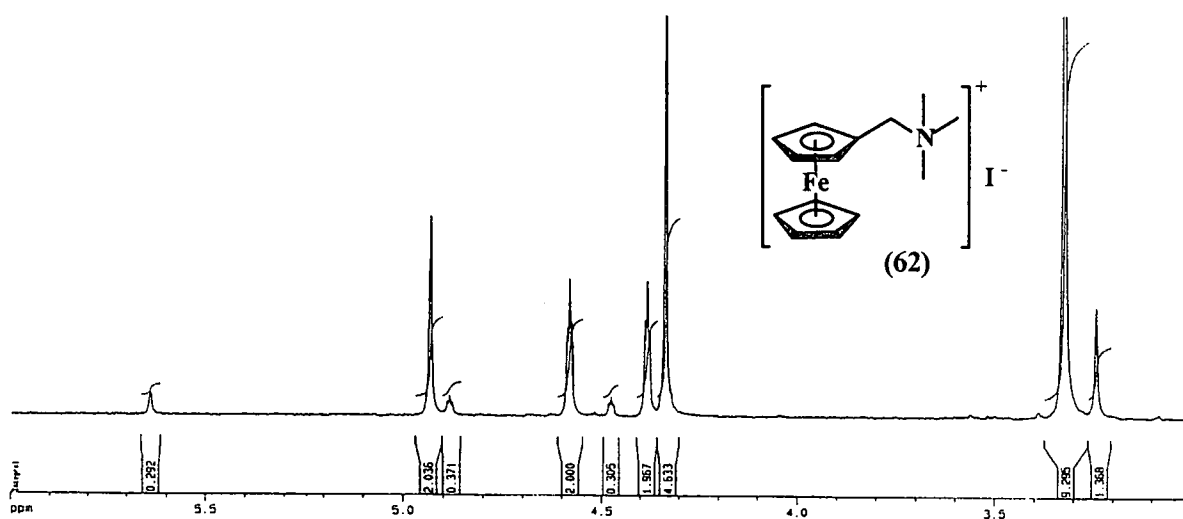


Spectrum 3: 3,6-Bis(dodecyl)phthalonitrile, (79)

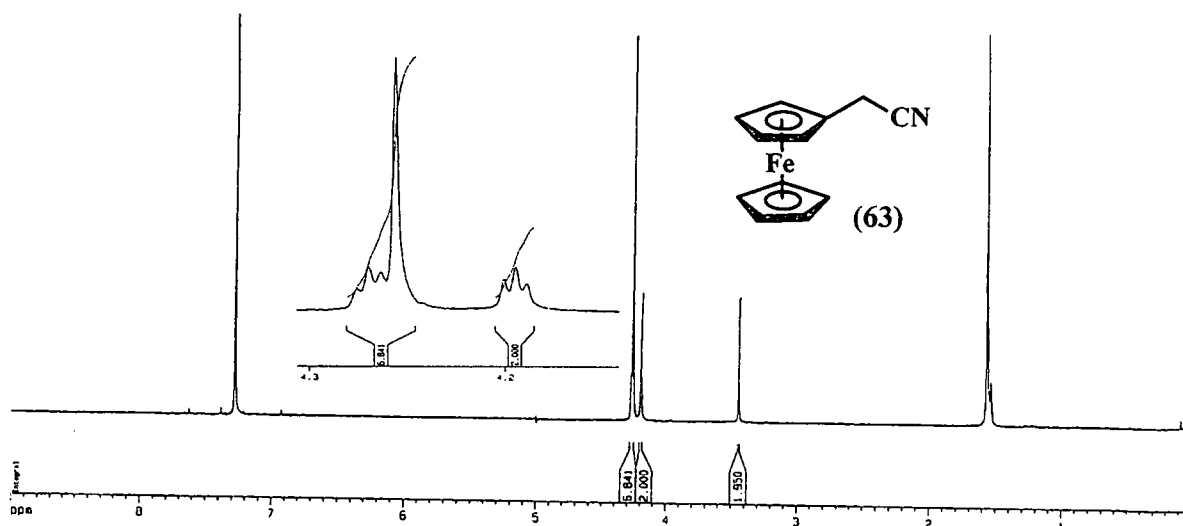
¹H NMR



Spectrum 4: Dimethylaminomethylferrocene, (61)

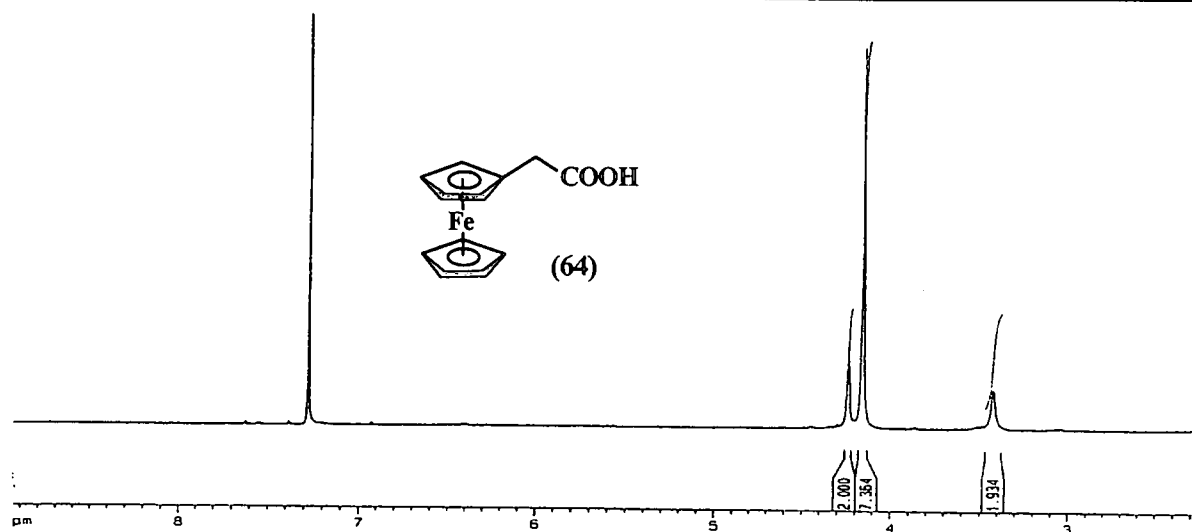


Spectrum 5: *N,N*-dimethylferrocene methiodide, (62)

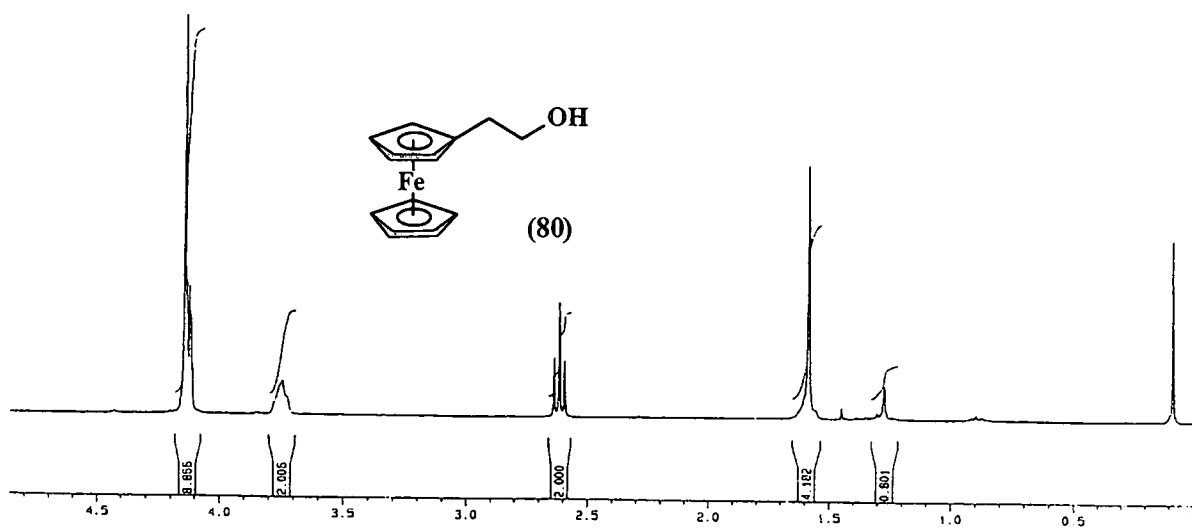


Spectrum 6: Ferrocenylacetonitrile, (63)

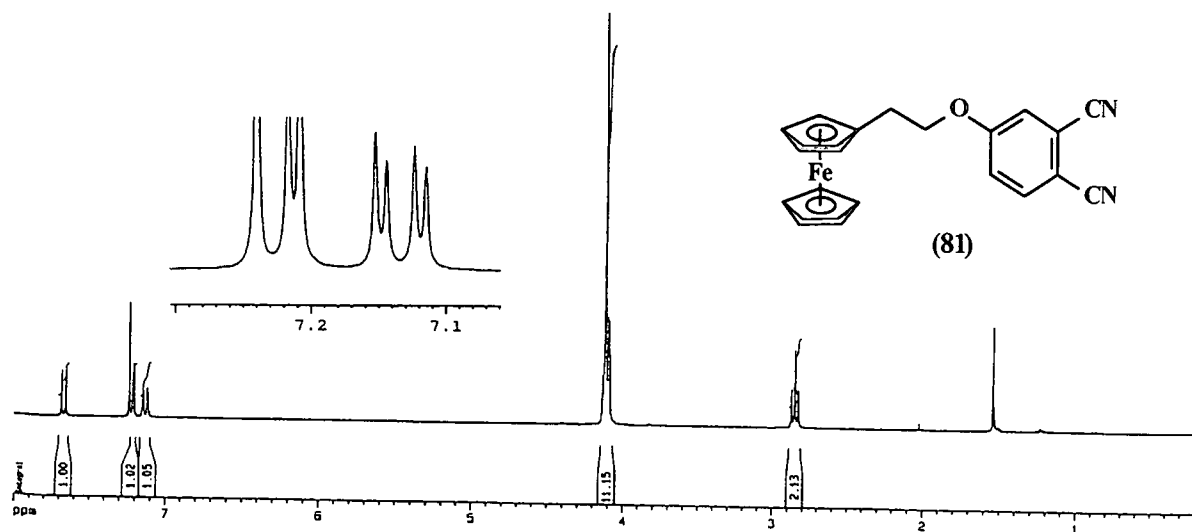
¹H NMR



Spectrum 7: Ferrocenylacetic acid, (64)

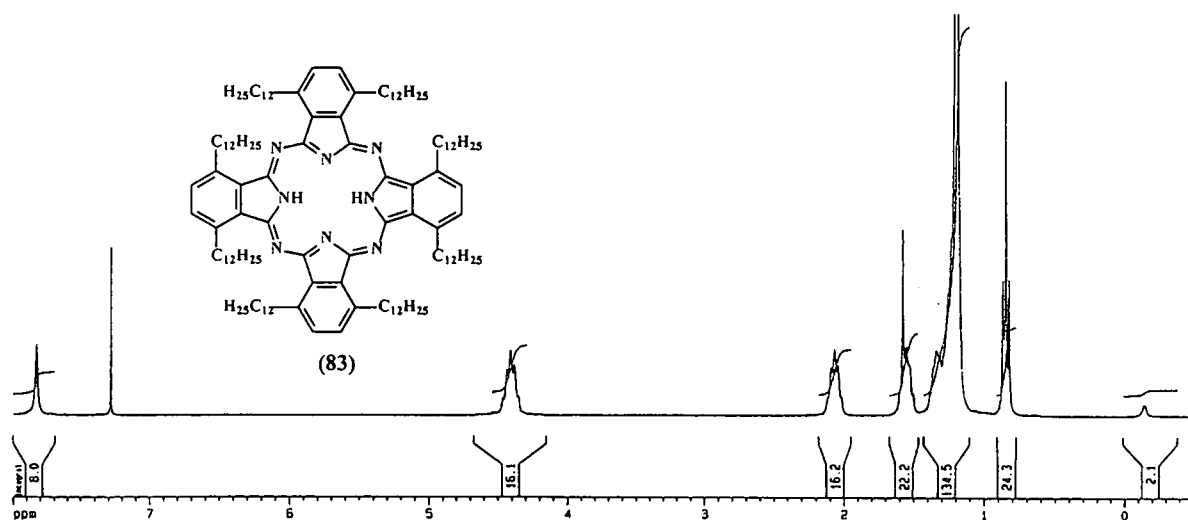


Spectrum 8: 2-Ferrocenylethanol, (80)

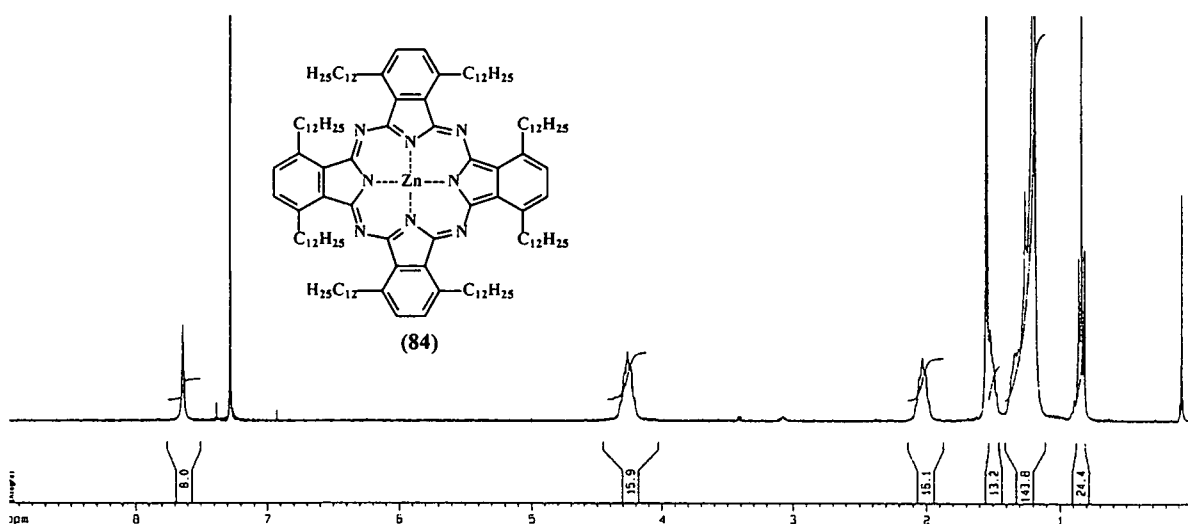


Spectrum 9: 4-(2'-Ferrocenylethoxy)phthalonitrile, (81)

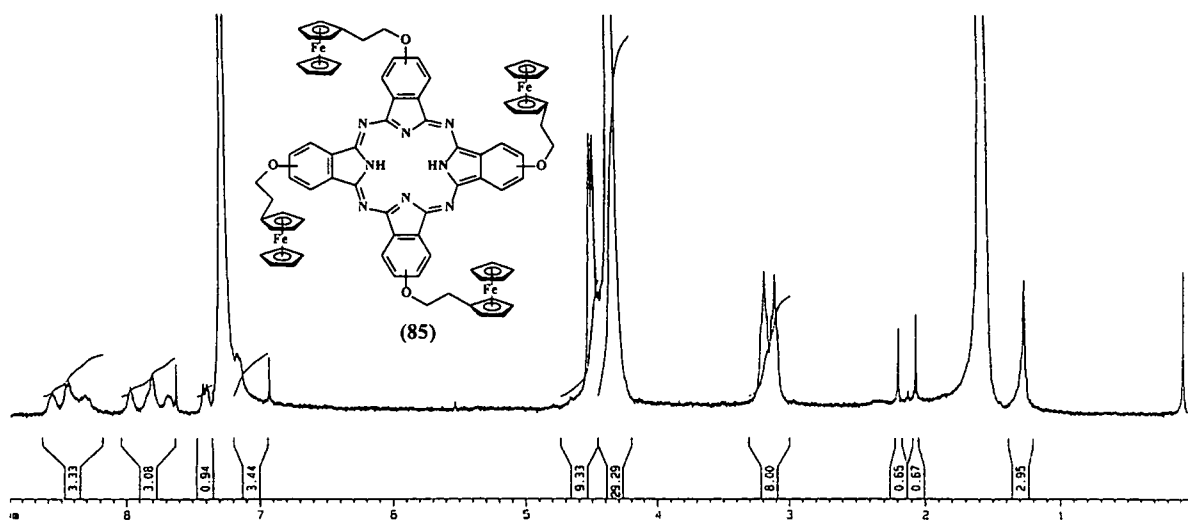
¹H NMR



Spectrum 10: (C₁₂H₂₅)₈-2HPC, (83)

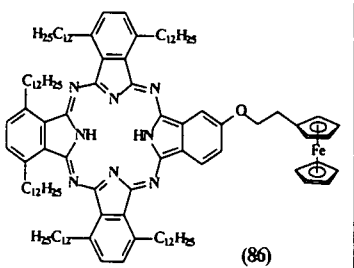


Spectrum 11: (C₁₂H₂₅)₈-ZnPc, (84)

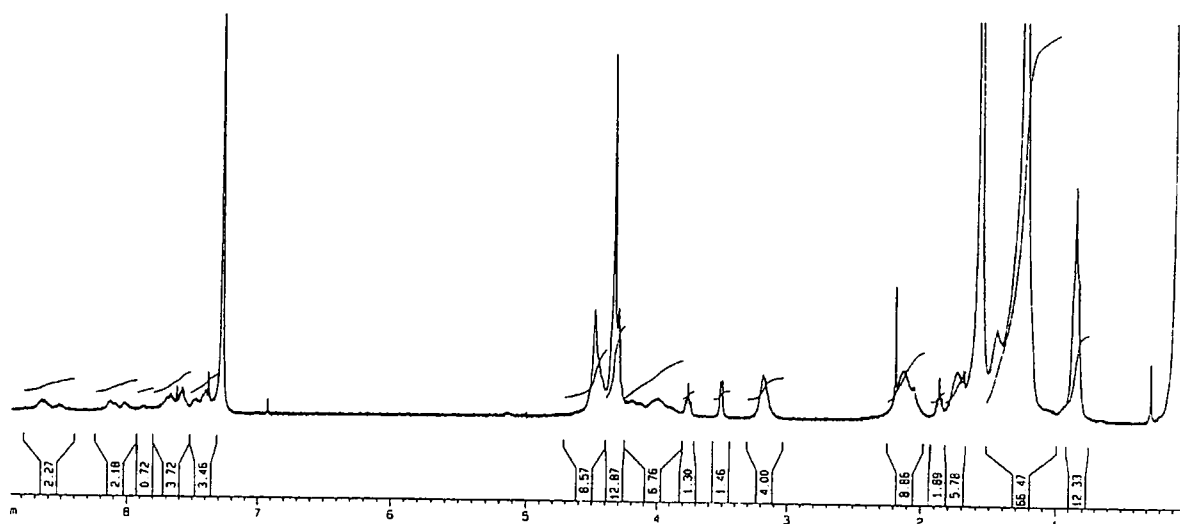


Spectrum 12: 2HPC-[O-(CH₂)₂-Fc]₄, (85)

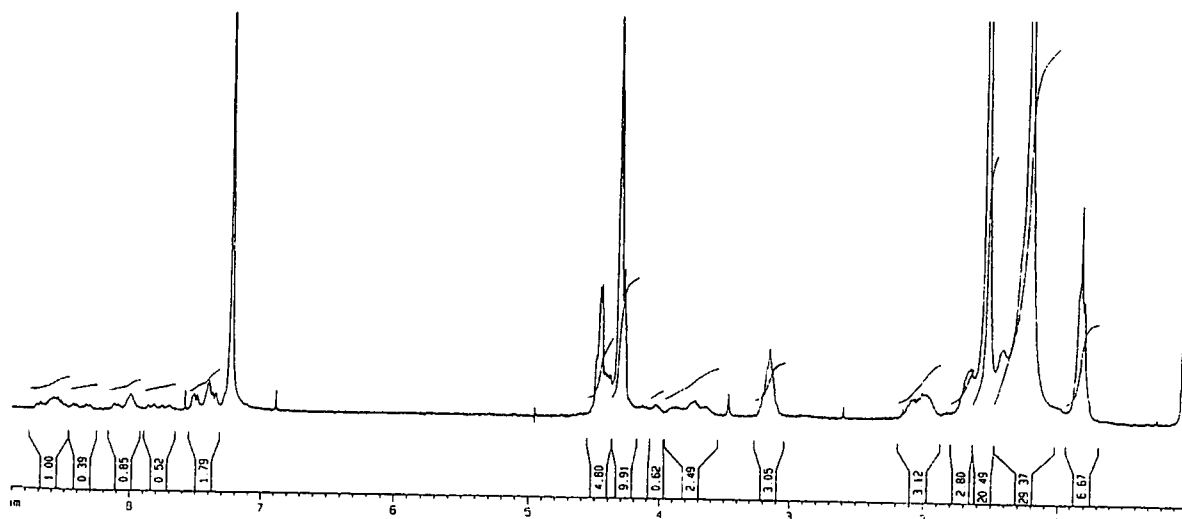
¹H NMR



Spectrum 13: $(C_{12}H_{25})_6-2HPc-O-(CH_2)_2-Fc$, (86)

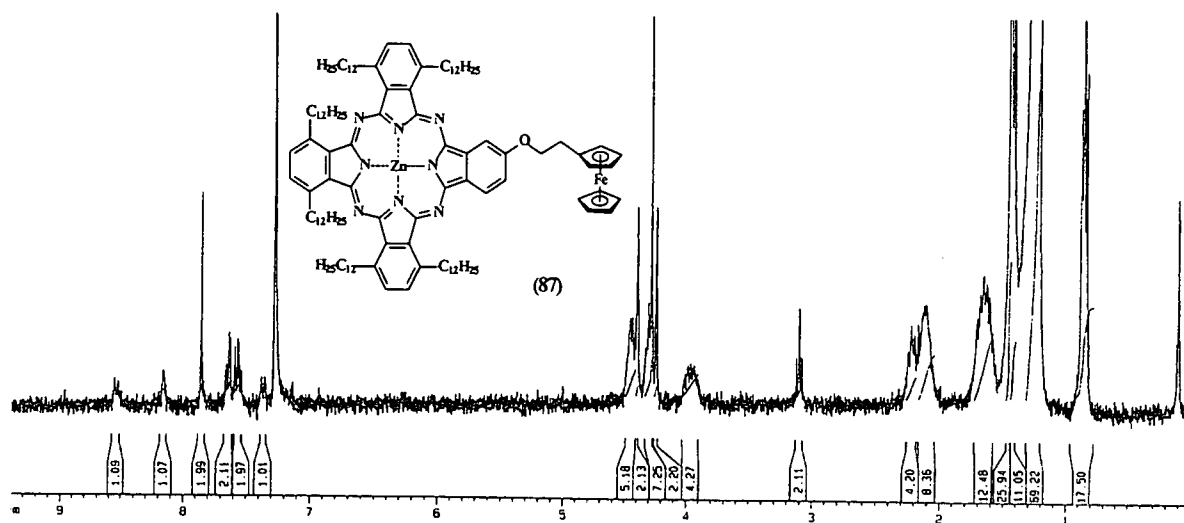


Spectrum 14: (C₁₂H₂₅)₄-2HPc-[O-(CH₂)₂-Fc]₂, (88), AABB and/or ABAB



Spectrum 15: Mixture of $(C_{12}H_{25})_4-2HPC-[O-(CH_2)_2-Fc]_2$ and $(C_{12}H_{25})_2-2HPC-[O-(CH_2)_2-Fc]_3$

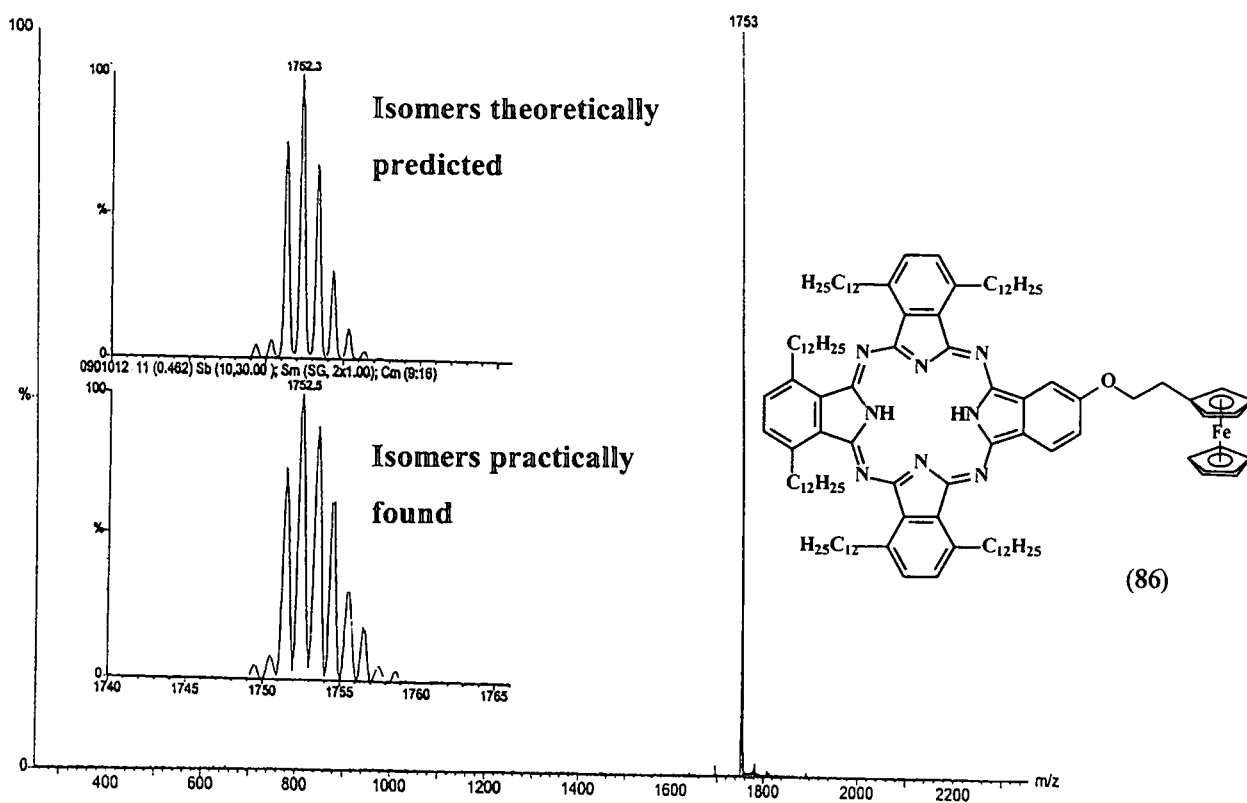
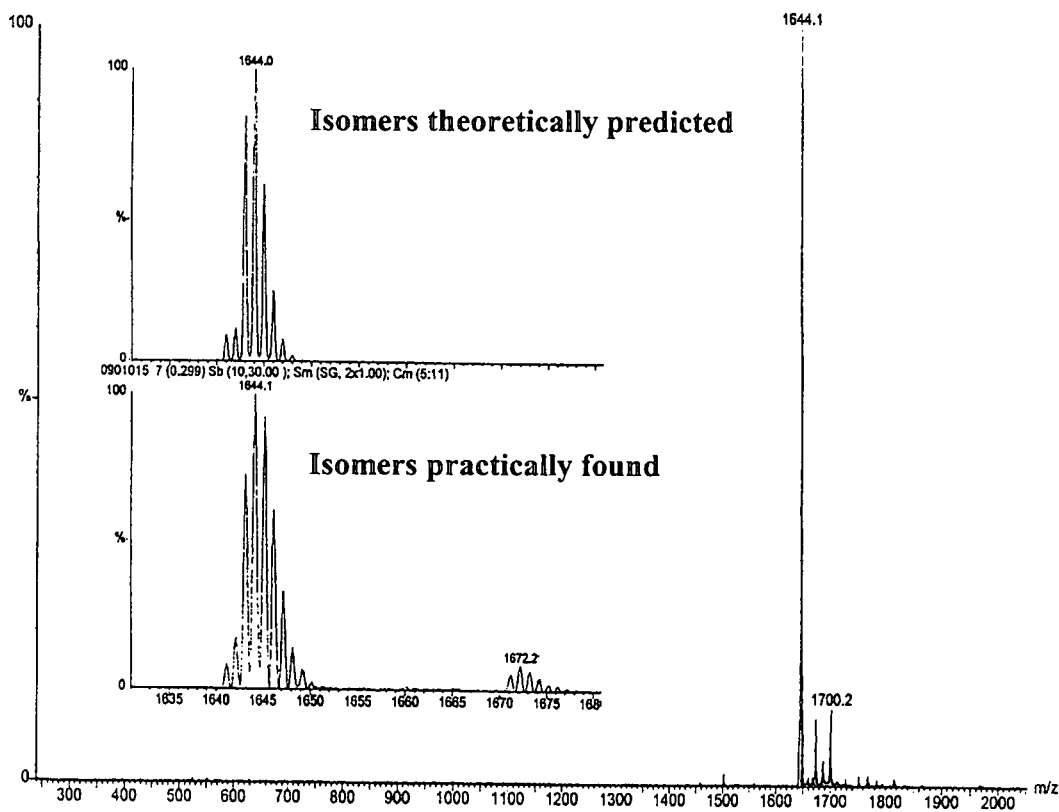
¹H NMR



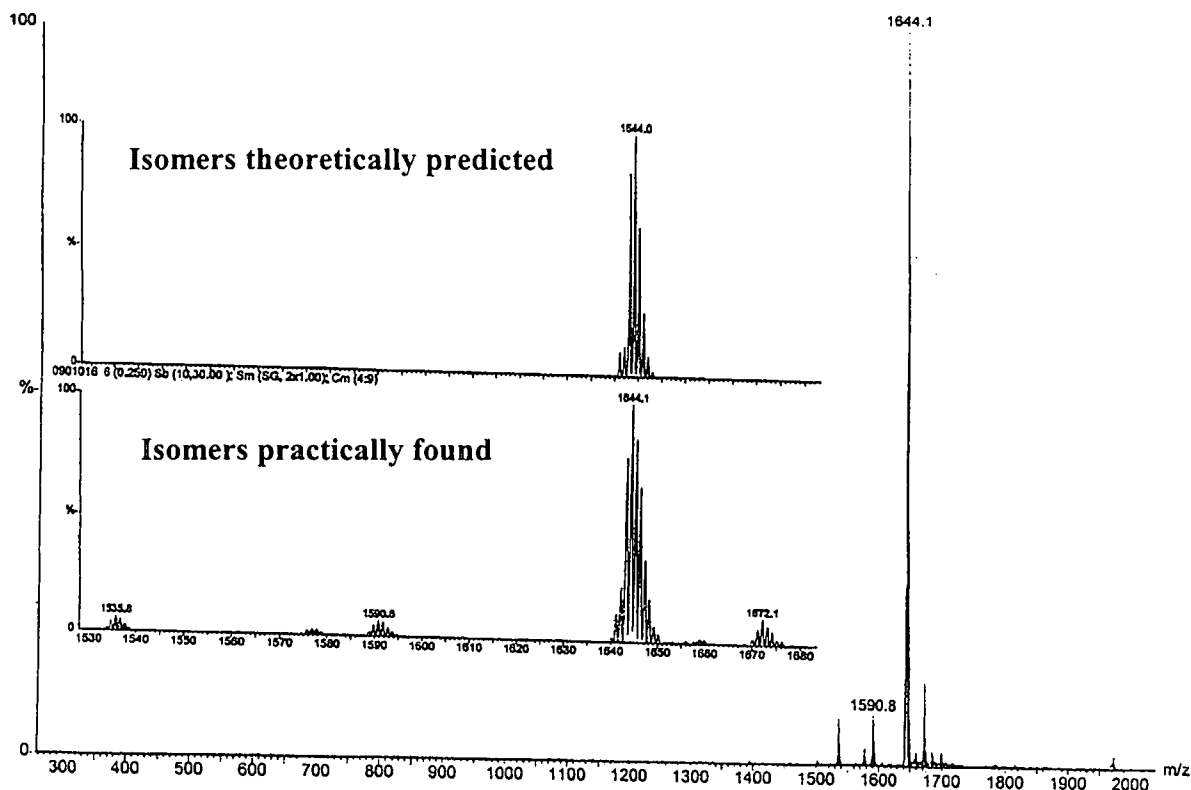
Spectrum 16: (C₁₂H₂₅)₆-ZnPc-O-(CH₂)₂-Fc, (87)

MALDI-tof SPECTRA

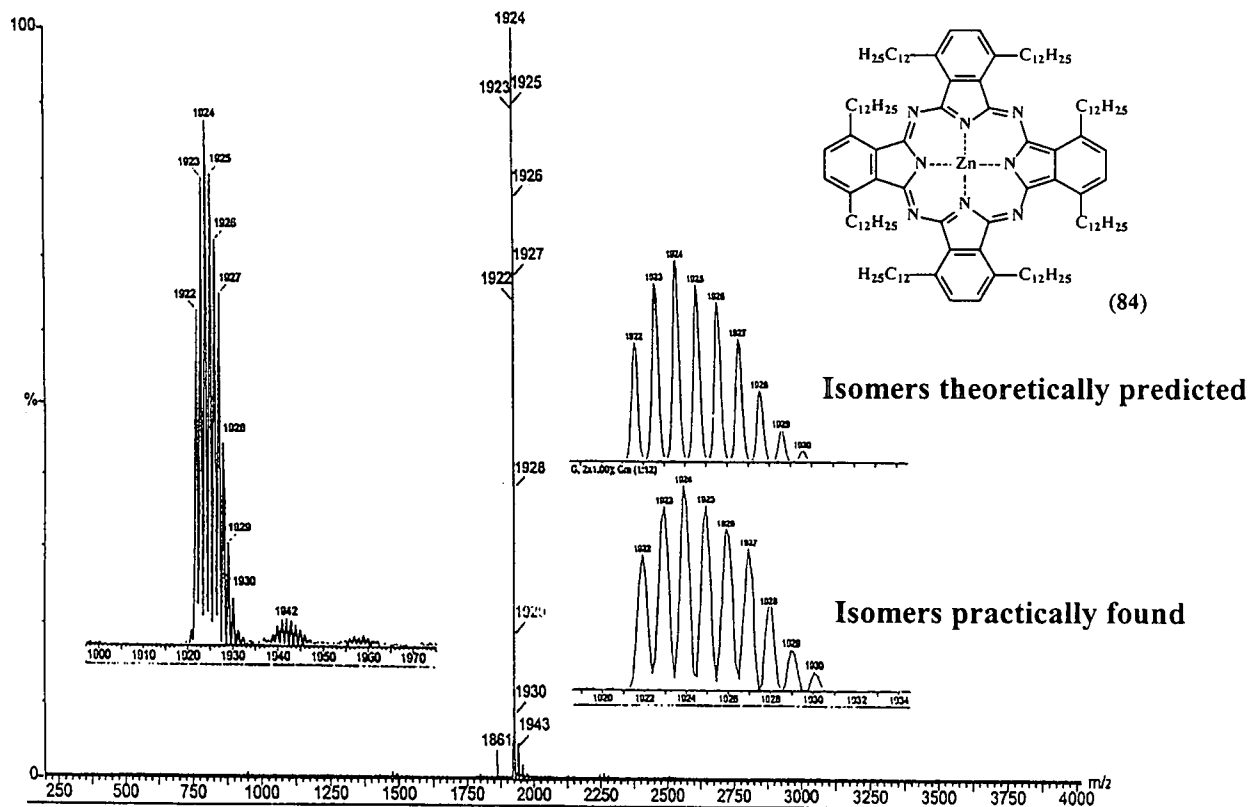
MALDI-tof

Spectrum 17: $(C_{12}H_{25})_6-2HPC-O-(CH_2)_2-Fe$, (86)Spectrum 18: $(C_{12}H_{25})_4-2HPC-[O-(CH_2)_2-Fe]_2$, (88), AABB and/or ABAB

MALDI-tof

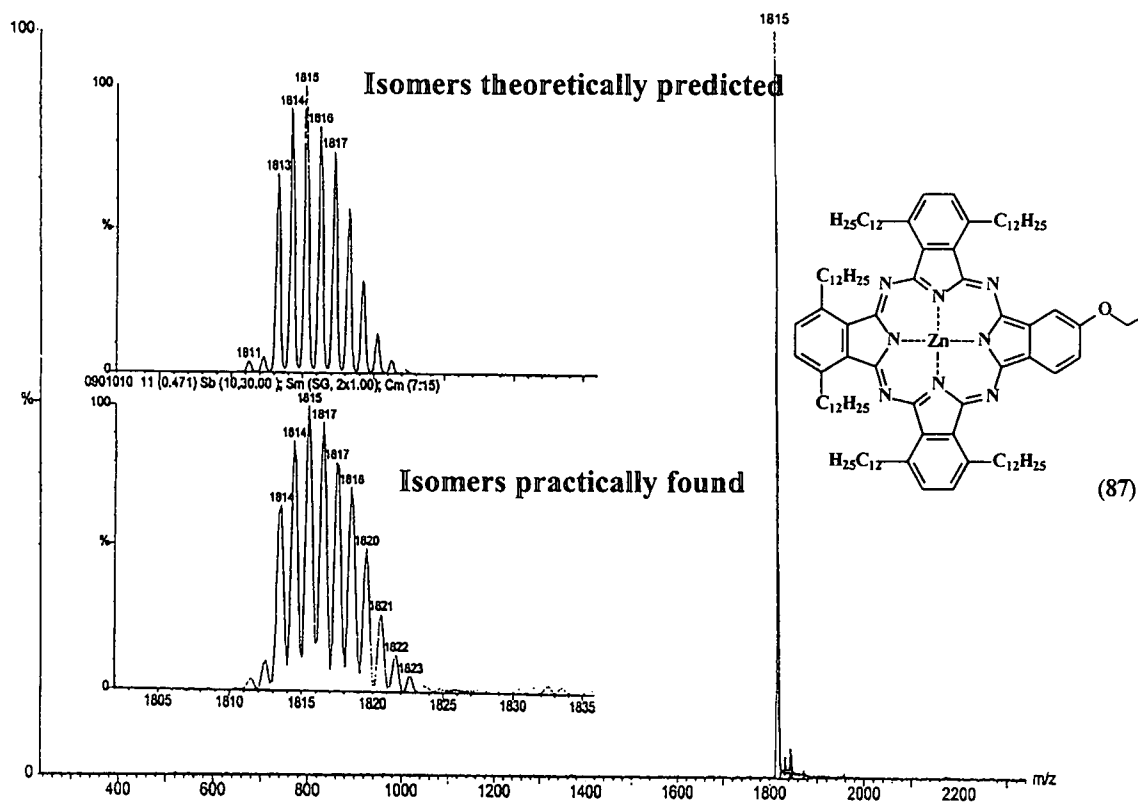


Spectrum 19: Mixture of $(C_{12}H_{25})_4\text{-2HPc-[O-(CH}_2)_2\text{-Fc]}_2$ and $(C_{12}H_{25})_2\text{-2HPc-[O-(CH}_2)_2\text{-Fc]}_3$



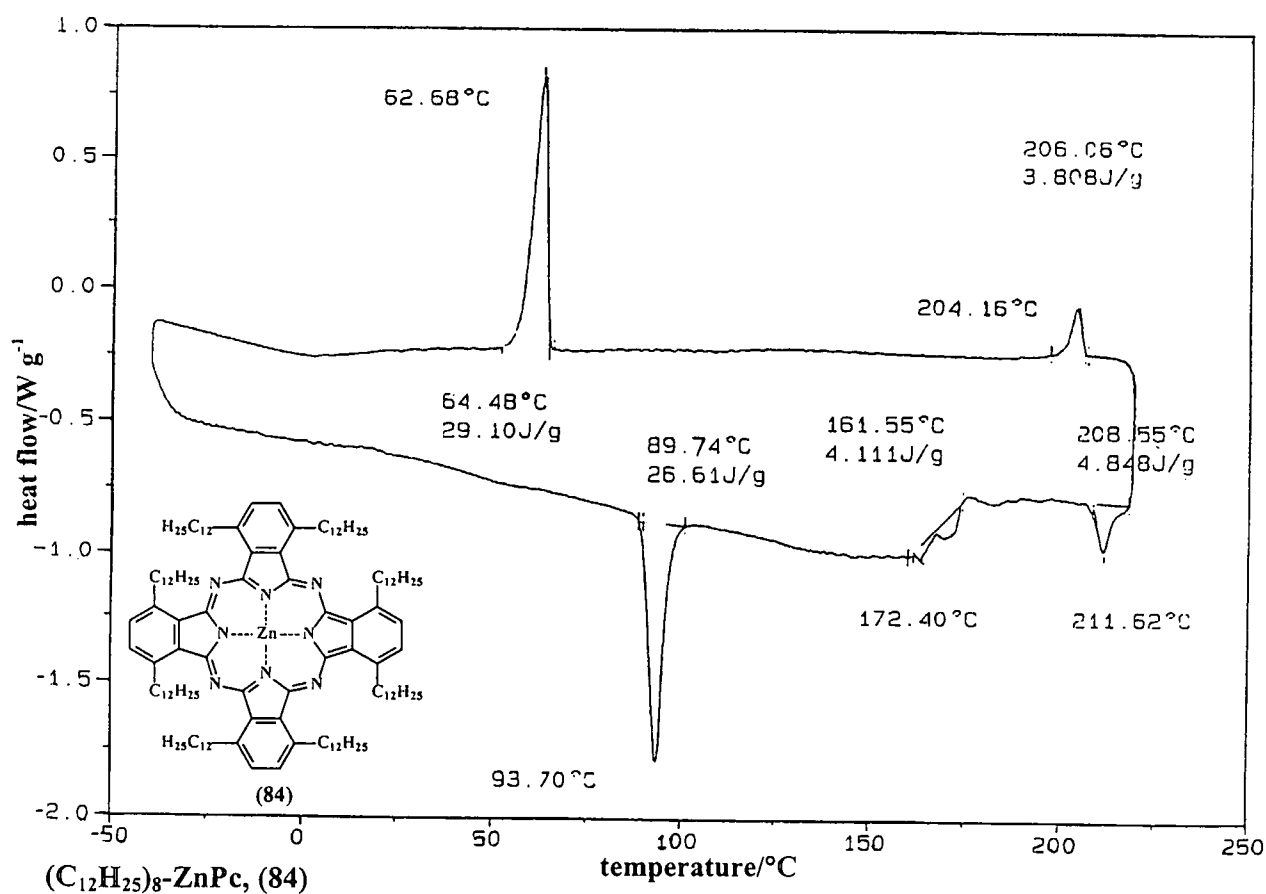
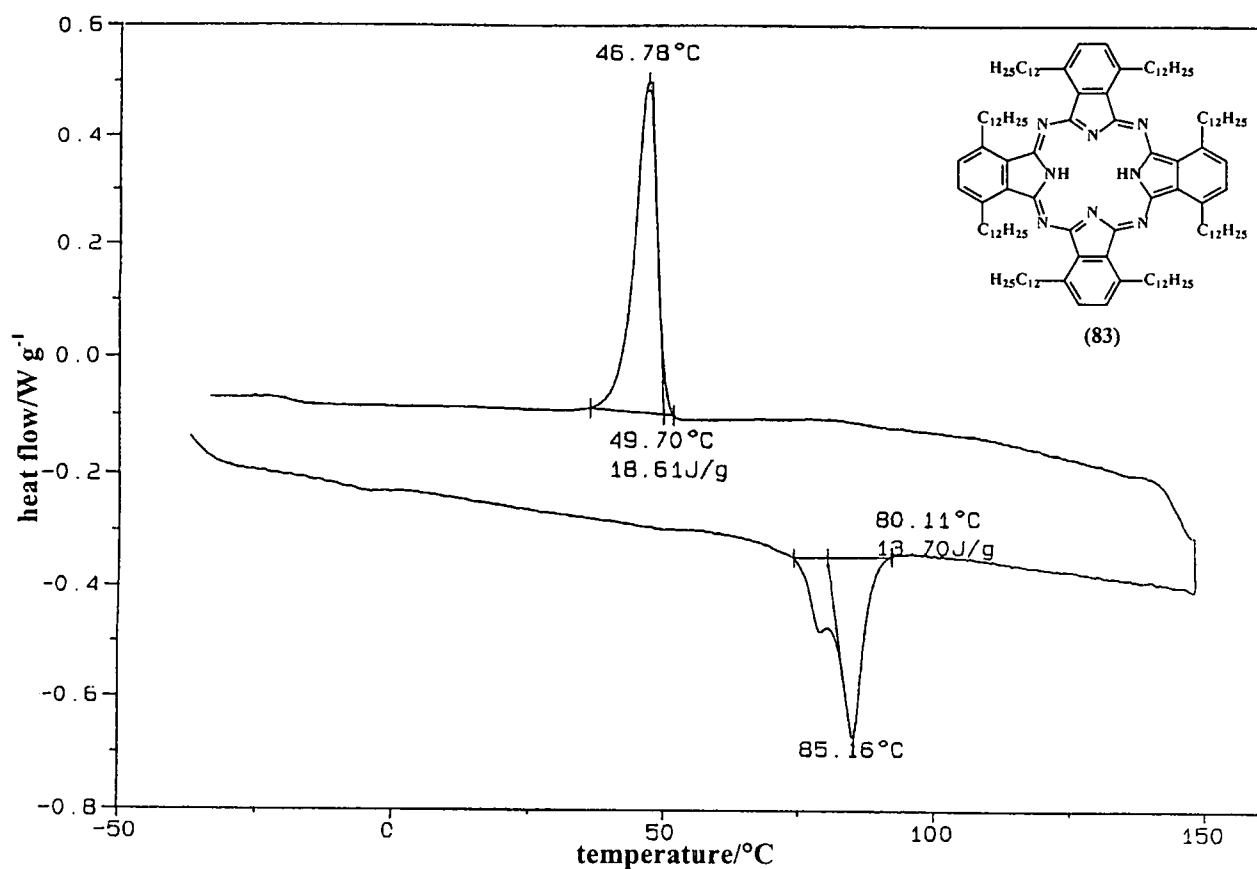
Spectrum 20: $(C_{12}H_{25})_8\text{-ZnPc, (84)}$

MALDI-tof

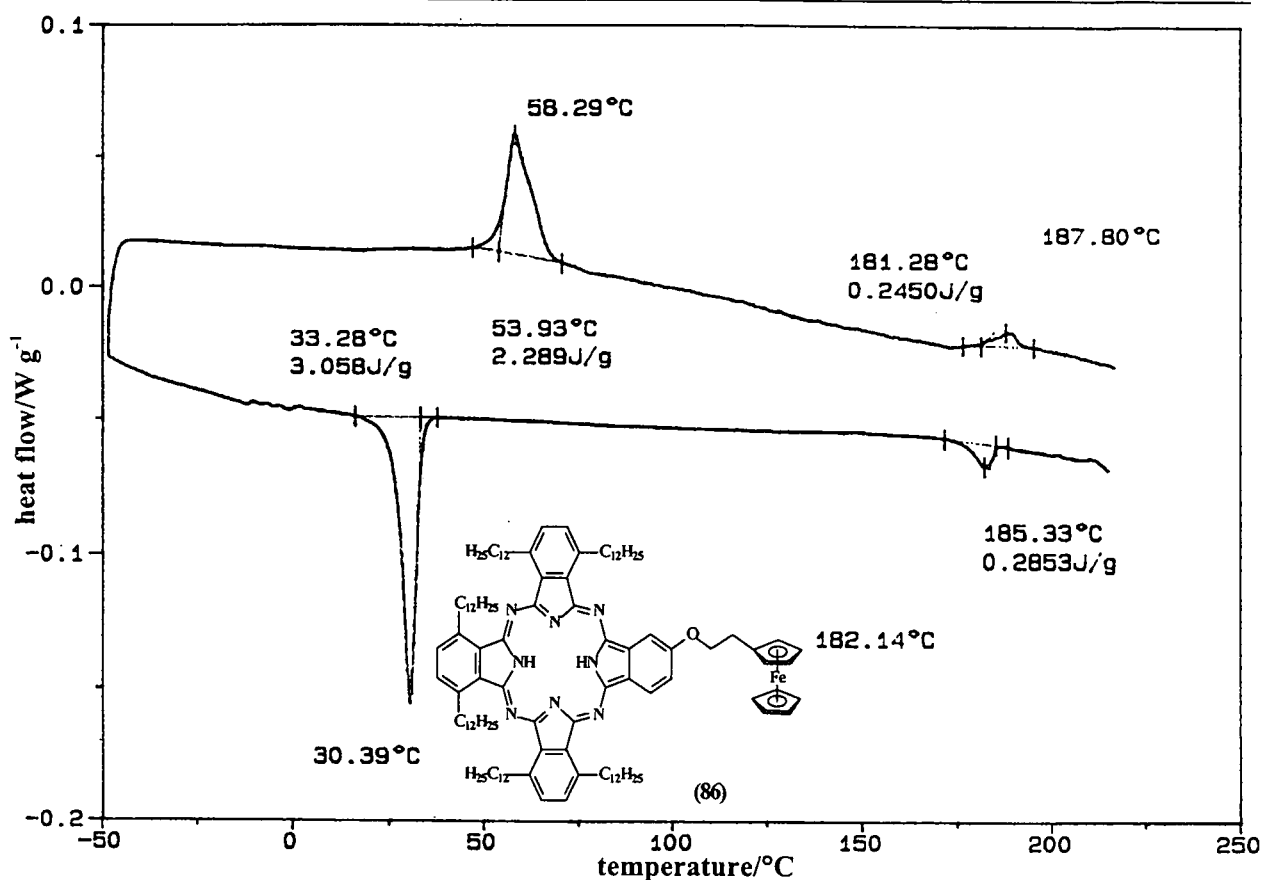
Spectrum 21: $(\text{C}_{12}\text{H}_{25})_6\text{-ZnPc-O}-(\text{CH}_2)_2\text{-Fc}$, (87)

DSC SCANS

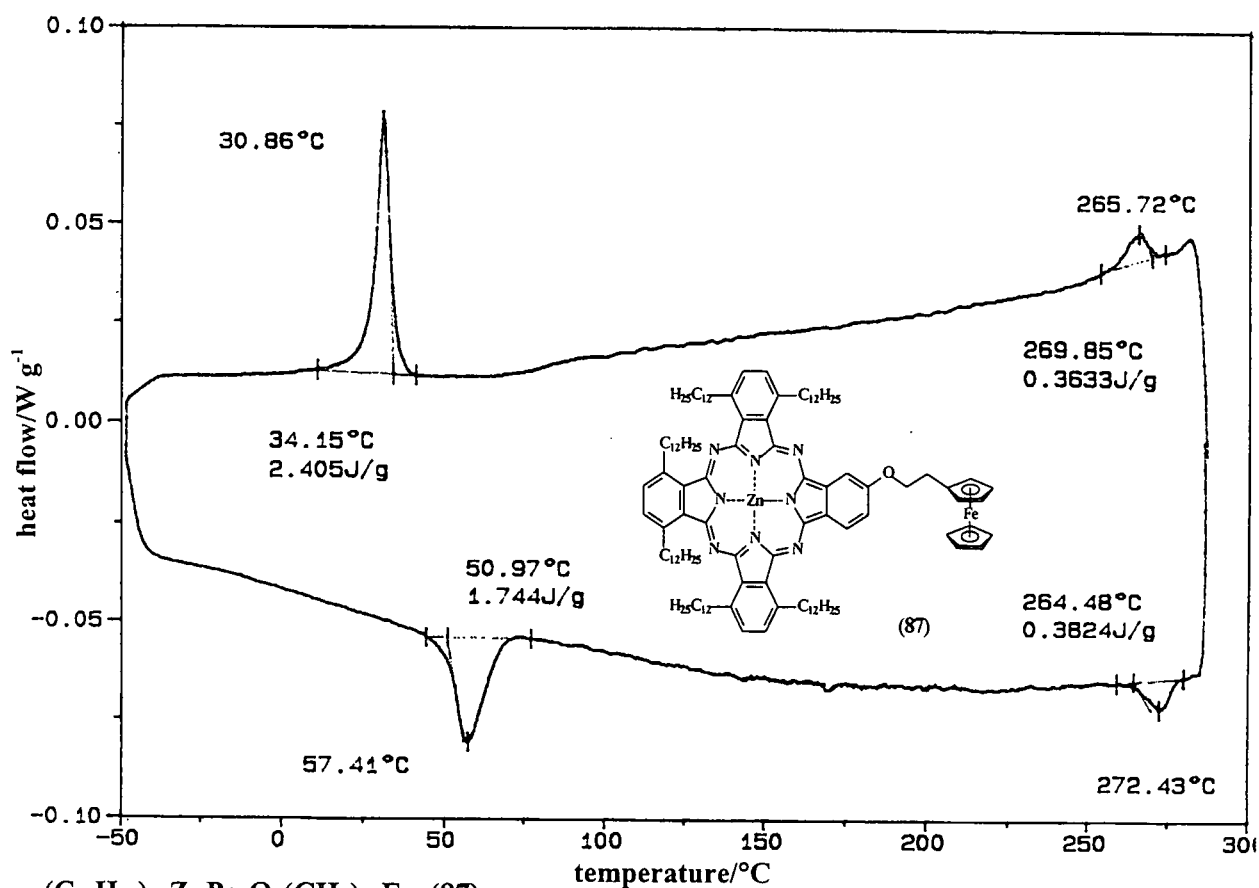
DSC



DSC



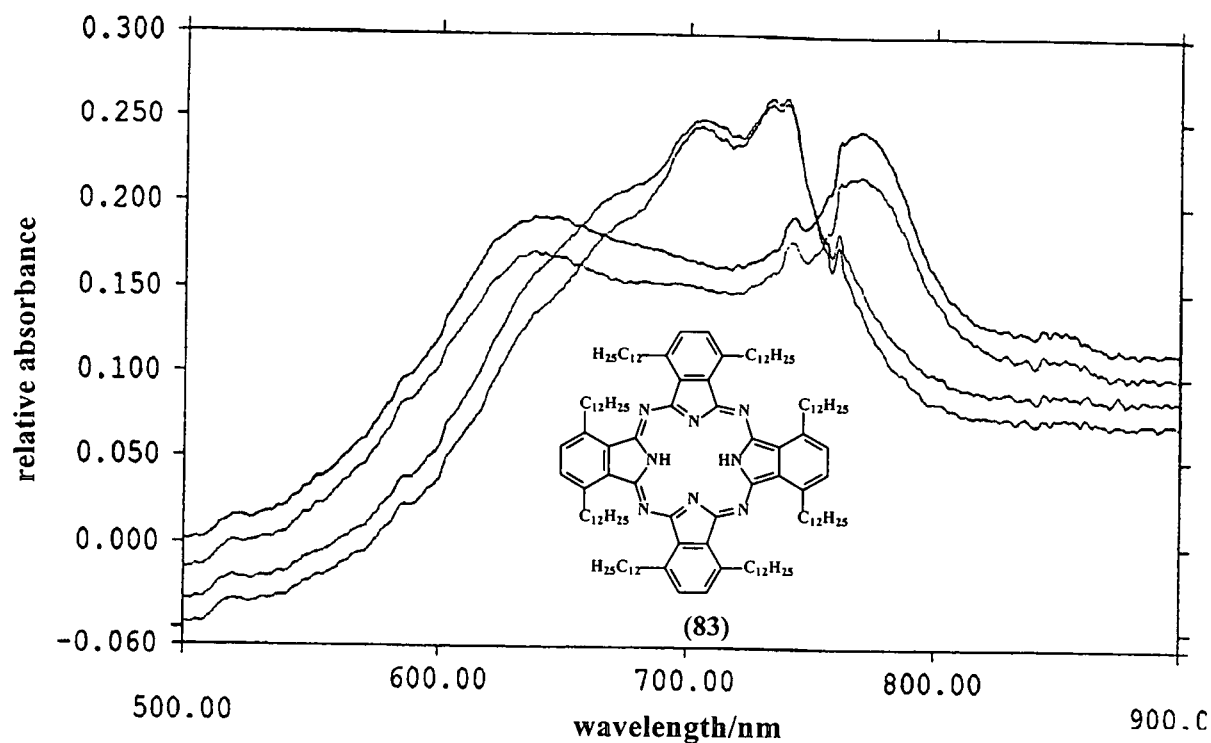
$(C_{12}H_{25})_6\text{-2HPc-O-(CH}_2)_2\text{-Fc}$, (86)



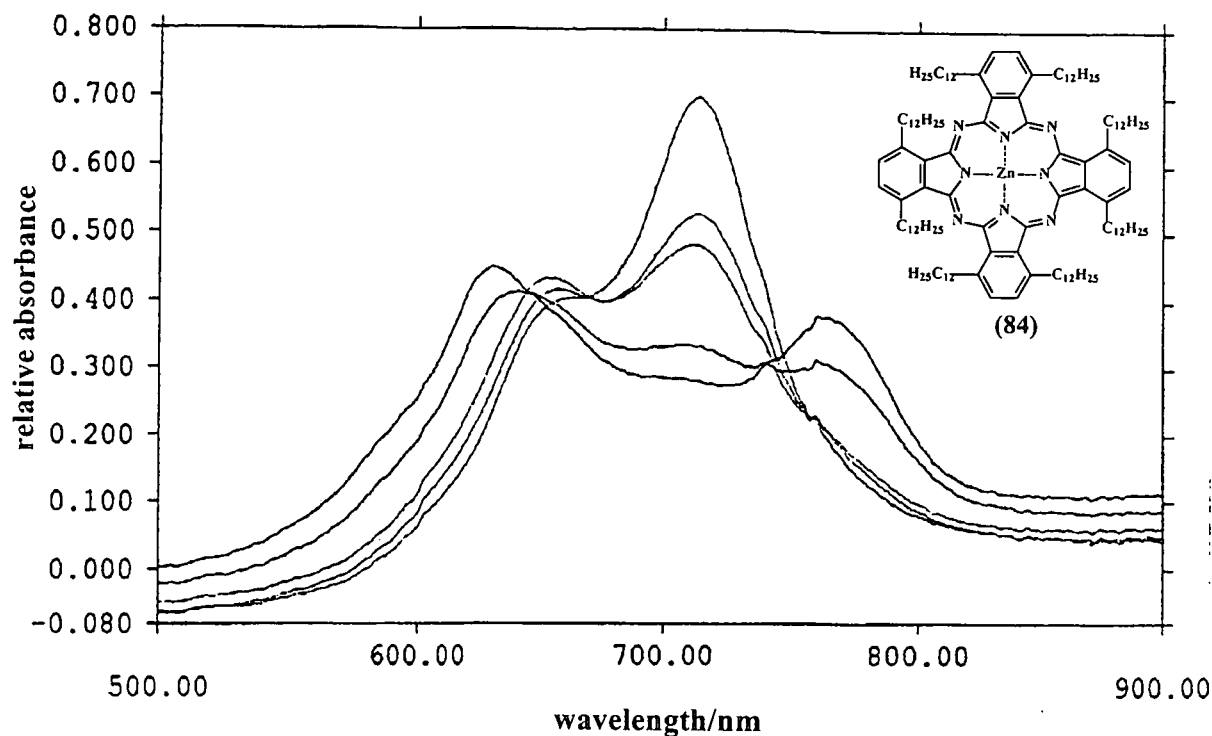
$(C_{12}H_{25})_6\text{-ZnPc-O-(CH}_2)_2\text{-Fc}$, (87)

UV/VIS SPECTRA

UV/VIS spectra

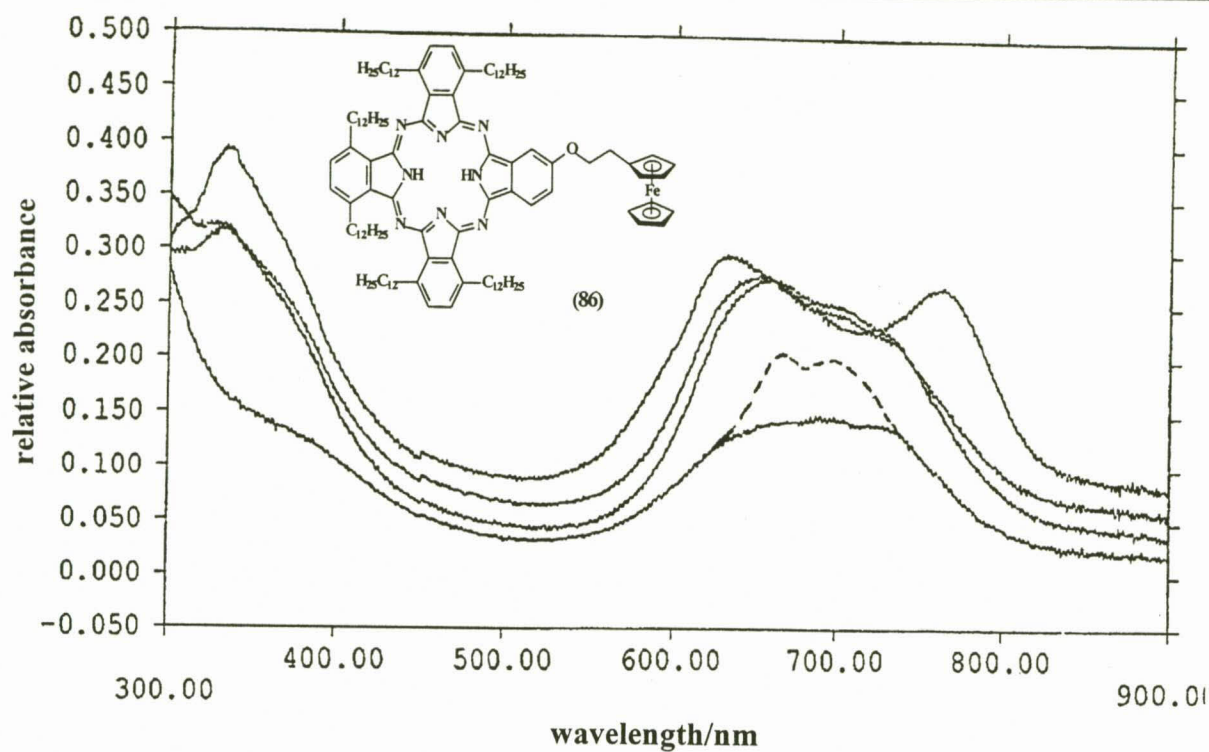


Variable temperature UV/VIS spectra of spin coated thin films of (83)

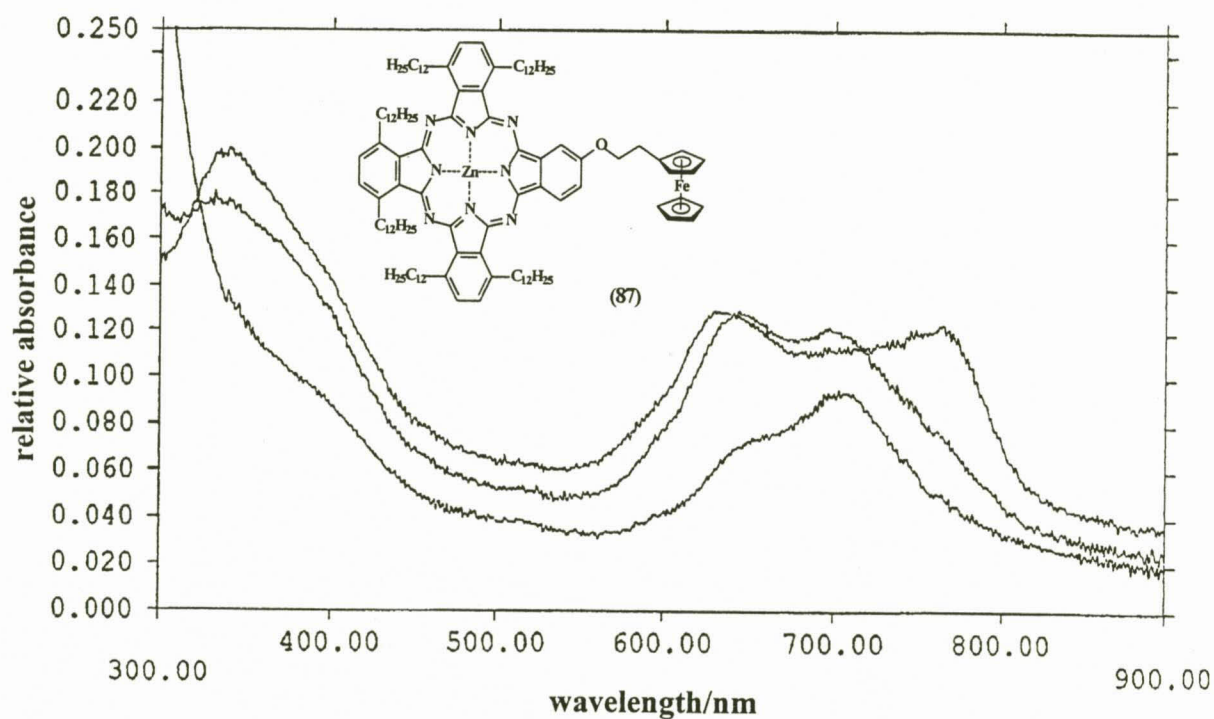


Variable temperature UV/VIS spectra of spin coated thin films of (84)

UV/VIS spectra



Variable temperature UV/VIS spectra of spin coated thin films of (86)



Variable temperature UV/VIS spectra of spin coated thin films of (87)

Ek, verklaar dat die verhandeling wat hierby vir die graad M. Sc. aan die Universiteit van die Vrystaat deur my ingedien word, my selfstandige werk is en nie voorheen deur my vir 'n graad aan 'n ander universiteit/fakulteit ingedien is nie. Ek doen voorts afstand van outeursreg in die verhandeling ten gunste van die Universiteit van die Vrystaat.

Wade Luke Davis

Geteken: 10 Februarie 2003